University of Alberta

Scaling of Effervescent Atomization and Industrial Two-Phase Flow

by

Mohammad Azizur Rahman

A thesis submitted to the Faculty of Graduate Studies and Research
in partial fulfillment of the requirements for the degree of

Doctor of Philosophy

Department of Mechanical Engineering

©Mohammad Azizur Rahman

Spring 2011
Edmonton, Alberta

Permission is hereby granted to the University of Alberta Libraries to reproduce single copies of this thesis and to lend or sell such copies for private, scholarly or scientific research purposes only. Where the thesis is converted to, or otherwise made available in digital form, the University of Alberta will advise potential users of the thesis of these terms.

The author reserves all other publication and other rights in association with the copyright in the thesis and, except as herein before provided, neither the thesis nor any substantial portion thereof may be printed or otherwise reproduced in any material form whatsoever without the author's prior written permission.

ABSTRACT

The objective of this thesis was to develop a novel understanding of the mechanics of two phase gas-liquid flows and sprays injected through industrial effervescent nozzles. This was done using detailed experimental investigations and scaling for two-phase flows and sprays. This study helps to quantify near-field liquid and gas phase statistics that are challenging and impossible to measure in the reactors due to inaccessibility restrictions. The development of nozzles is generally performed on air-water systems. My plan was to begin with the study of small-scale sprays (air and water) to compare to full scale industrial conditions at pilot operation (air-water) or at commercial operation (steam-bitumen), to determine size scaling relationships. The relationship between the lab scale air-water experiments and real industrial scale steam-bitumen has never been fully examined. Knowledge from this thesis will make the development of future nozzles with much less dependent on trial and error. This thesis was an attempt to establish fundamental scaling relationships for the prediction of two-phase spray behavior that can be applied directly to full scale industrial size nozzles that would be of very significant value to industries and to the scientific community in general. Understanding the performance of two phase nozzles through established scaling laws will aid in optimizing the two phase nozzle flow conditions and will serve as a major tool in nozzle design and development for future generation nozzles for many industrial applications.

Acknowledgements

I express heartfelt thanks to my supervisors Dr. Brian A. Fleck and Dr. Ted Heidrick for their unique supervision and excellent guidance throughout my PhD thesis work. Their vigorous pursuit of excellence in research, mentorship, advising and every other aspect of their work is truly inspiring. They have always actively encouraged me to broaden my research interests and develop professionalism. I am deeply appreciative for many helpful discussions and all the work they have done on my behalf.

I thank my supervisory committee, for the helpful advice and critical feedback. Additionally, I am grateful to Professor André G. McDonald for his productive feedback. The expertise of the machine shop staff, Greg, Berny, Roger, and Tuula, was of great help in the laboratory.

I would like to extend my thanks to my colleagues at the University of Alberta and at the Syncrude research facility in Edmonton. Dr. Jennifer McMillan and Dr. Edward Chan have provided me exemplary motivation in my research endeavours. I thank NSERC and Alberta Innovates-Technology Futures for providing financial support.

I would like to thank my mother, my late father, my wife, my son, my daughter, and my family for their extraordinary support in my PhD research endeavour. For their commendable encouragement, mental support, inspiration and cooperation, I was able to complete my thesis smoothly and productively. Finally, my greatest thanks go to Almighty Allah for all of His blessings.

To my parents and family:

To my wife, my daughter, Rodela and my son, Abeer

TABLE OF CONTENTS

LIST OF FIGURES

List of Tables

Nomenclature for Chapter 1

1.1. Abbreviations

ALR	air to liquid ratio by mass
FC	feeding conduit
HSVS	high-speed video shadowgraphy
IS	impulse sensor
PDA	particle dynamics analyzer
PDPA	Phase Doppler Particle Anemometer
PA	primary atomization
QCV	quick closing valve
SA	secondary atomization
SMD	Sauter mean diameter
SBSI	stroboscopic back scattered imagery
SPT	static pressure transducers

1.2. Symbols

A	cross-sectional area of the pipe (m^2)
A_g	area occupied by the gas phase (m^2)
D_n	nozzle diameter (m)
D_{10}	arithmetic mean diameter (m)
D_{32}	Sauter mean diameter (m)
d_1	major axis lengths of a ellipsoid (m)
d_2	minor axis lengths of a ellipsoid (m)
d	droplet/bubble diameter (m)
d_d	droplet diameter (m)
d_b	bubble diameter (m)
F_{km}	interfacial forces (N)
$\mathbf{g}$	gravity (m/s^2)
i	i-th object
l_c	closing length between the two valves (m)
L	characteristic length scale (m)
m_g	mass flow rates of the gas phase (kg/sec)
m_l	mass flow rates of the liquid phase (kg/sec)
N	total number (-)
P	pressure (Pa)
P	pressure (Pa)
Q_g	volume flow rate of the gas phase (m^3/sec)
Q_l	volume flow rate of the liquid phase (m^3/sec)
R	universal gas constant (8.3144×10^{-3} kJ/mol.K)
T	absolute temperature (293 K)
t_{ac}	asynchronization closing time (s)

u_m	mixture velocity in the conduit (m/sec)
u_{rel}	relative velocity between the gas and liquid phase (m/sec)
u	velocity (m/sec)
u_{gs}	superficial velocity of the gas phase phases (m/sec)
u_{ls}	superficial velocity of the liquid phases (m/sec)

1.3. Greek Letters

ϕ	scattering angle (^{o})
α	void fraction (%)
α_H	homogeneous void fraction (%)
α_e	entrance void fraction (%)
β	air to liquid ratio by mass (%)
ρ	density (kg/m^3)
ρ_l	density of liquid phase (20°C pure water, 998 kg/m^3)
ρ_g	density of gas phase (20°C air, 1.205 kg/m^3)
μ	viscosity ($kg/m.s$)
μ_c	viscosity of the carrier fluid (20°C pure water, 1.00×10^{-3} kg/m.s)
μ_g	viscosity of the gas phase (20°C air, 1.82×10^{-5} kg/m.s)
σ	Surface tension (20°C pure water, 72.8 N/m)
τ_p	particle momentum response time (s)
τ_c	flow system time (s)

1.4. Subscripts

c, l, w	continuous/liquid/water phase
p ,d, g, a	particle/dispersed/gas/air phase
d	droplet
b	bubble
k	phase (-)
m	mixture

1.5. Dimensionless Numbers

Oh	Ohnesorge number
St	Stokes number
Re	Reynolds number
We	Weber number
We_{crit}	Critical Weber number
Lp	Laplace number

Nomenclature for Chapter 2

2.1. Abbreviations

GLR	gas to liquid ratio

QCV	quick closing valve

2.2. Symbols

A_{pipe}	cross sectional area of feeding conduit or pipe (m^2)
A_g	area of the gas phase (m^2)
C_D	drag coefficient
d_p	particle diameter (m)
D	diameter of the pipe (m)
f	wave frequency (Hz)
F	modified Froude number (-)
f_m	mixture friction factor (-)
g	gravity (m/s^2)
G_s	mass flux of gas phase ($kg/m^2.s$)
G_l	mass flux of liquid phase ($kg/m^2.s$)
K_f	friction coefficient (-)
L	characteristic system length (m)
l_c	closing length between the two valves (m)
m_d	mass flow rate of the dispersed phase (kg/s)
m_c	mass flow rate of the continuous phase (kg/s)
P	pressure (Pa)
P_p	pressure in the dispersed phase (pa)
P_c	pressure in the continuous phase(pa)
Q	volume flow rate (m^3/sec)
Q_d	volume flow rate of the dispersed phases (m^3/sec)
Q_c	volume flow rate of the continuous phases (m^3/sec)
R	universal gas constant (8.3144×10^{-3} kJ/mol.K)
T	absolute temperature (293 K)
t_{ac}	asynchronization closing time (s)
u_c	velocity of the continuous phase (m/s)
u_p	velocity of the dispersed phase (m/s)
u_d	velocity of the dispersed phase (m/s)
u_m	total or mixture velocity ($=u_{ds}+u_{cs}$) (m/s)
u_{ds}	superficial velocity of the dispersed phase (m/s)
u_{cs}	superficial velocity of the continuous phase (m/s)
V	total volume / characteristics volume (m^3)
X	Martinelli parameter (-)

x	axial direction (m)
x_q	quality (-)

2.3. Greek letters

α	void fraction [-]
α_H	homogeneous void fraction [-]
τ_p	particle momentum response time (s)
τ_c	characteristic flow system time (s)
τ_m	momentum response time (s)
ρ_p	particle density (kg/m^3)
ρ_d	particle density (kg/m^3)
ρ_c	continuous phase density(kg/m^3)
ρ_m	mixture density
μ_c	viscosity of the continuous phase (kg/m.s)
μ_d	viscosity of the dispersed phase (kg/m.s)
μ_m	mixture viscosity (kg/m.s)
ν	kinematic viscosity (m^2/s)
ν_c	kinematic viscosity of the continuous phase (m^2/s)
ν_d	kinematic viscosity of the dispersed phase (m^2/s)
σ	surface tension (N/m)
ϕ	velocity ratio
λ	flow rate fraction (-)
θ	angle of inclination

2.4. Subscripts

c	continuous phase
p or *d*	article or dispersed phase
h	homogeneous
s	superficial
l	liquid
g	gas
m	mixture
sl	liquid superficial
sg	gas superficial

2.5. Dimensionless groups

Fr	Froude number
F	modified Froude number
St	Stokes number

Ga	Galileo number
St	Strouhal number
Re	Reynolds number
We	Weber Number
Eo	Eotvos number
Mo	Morton Number
Oh	Ohnesorge number
Lp	Laplace number

Nomenclature for Chapter 3

3.1. Abbreviations

GLR	Gas-to-liquid ratio
EAA	Electrical Aerosol Analyzer
PDA	Particle Dynamic Analyzer
PDPA	Phase Doppler Particle Analyzer
ILIDS	Interferometric laser imaging for droplet sizing
LIF	Laser-induced Fluorescence
LDV	Laser Doppler velocimeterry
MMD	Mass median diameter
PIV	Particle Image Velocimetry

3.2. Symbols

A	Area of space associated with the measurement (m^2)
A	Projected area drop ($\pi/4D_{20}^2$)(m^2)
A_p	Probe area (m^2)
A_{pi}	Projected probe volume surface area (m^2)
c_i^{cor}	Probe volume corrected count (-)
D	Characteristics diameter (m)
D_N	Nozzle diameter (m)
D_{ab}	Mean drop size (m)
D_{10}	Arithmetic mean diameter (m)
D_{20}	Surface area diameter (m)
D_{21}	Surface area- length diameter (m)
$D_{30,i}$	Volume mean diameter at location i (m)
D_{31}	Volume- length diameter (m)
D_{32}	Sauter mean diameter (SMD) (m)
D_{43}	De Brouckere or Herdan diameter (m)

$D_{0.1}$	Drop diameter such that 10% of the total liquid volume is in drops of smaller diameter (m)
$D_{0.5}$	Drop diameter such that 50% of the total liquid volume is in drops of smaller diameter. This is the mass median diameter (m)
$D_{0.9}$	Drop diameter such that 90% of the total liquid volume is in drops of smaller diameter (m)
$D_{0.999}$	Drop diameter such that 99.9% of the total liquid volume is in drops of smaller diameter (m)
D_{peak}	Value of D corresponding to peak of drop size frequency distribution curve (m)
$D(d_{\max})_{\max}$	Effective diameter of the laser beam where the light intensity is sufficient for the largest droplets to be detected (m)
E	Energy required for an atomization process
E_s	Surface energy of the liquid
E_k	Kinetic energy
E_l	Energy loss due to friction in the atomizer
$f(D)$	size-probability function
L	characteristic length scale (m)
L_s	Width of the image of the spatial filter in the receiving optics (m)
M	Momentum ratio (-)
m	mass flow rate (kg/s)
N_i	Number of droplets measured at a location i
N_{cor}	Probe volume corrected number density
n	Total number of measurements over the plane
N	Total number of measurements over the plane
P	Pressure (kPa)
PA_i	Probe volume cross sectional area at the location i (m)
T	total measurement time (sec)
T_i	Run time at location i (s)
t_{acq}	Acquisition time (s)
T_{acq}	Acquisition time (s)
T_{at}	Summation of all of the interarrival times (s)
$T = \sum \Delta t$	Total measurement time for total number samples (N)(s)
t_{trans}	Transit time of the droplets (s)
t_i	Runtime at location i (s)
u	velocity (m/s)
v_i	Effective probe volume for the i th size class (m^3)

$v_{\max}$	Effective probe volume for the largest size class.
V	Liquid volumetric flow rate at particular jet cross section (m^3/s)

3.3. Greek letters

α	Void fraction [-]
α_H	Homogeneous void fraction [-]
β	gas to liquid mass ratio
τ_d	Droplet time scale (s)
τ_f	Fluid time scale (s)
$\delta = w/2$	Jet half-width (m)
μ	Viscosity $(kg/m.s)$
ρ	Density (kg/m^3)
ρ_c	Density of the carrier fluid (kg/m^3)
ρ_p	Particle density (kg/m^3)
ρ_d	Particle density (kg/m^3)
ρ_m	Mixture density (kg/m^3)
ρ_r	Density ratio (-)
ω_{slit}	Projected image length of the slit aperture (m)
θ	Scattering angle measured from the direction of propagation (-)
Δ	Relative span factor (-)
Δ_B	Dispersion boundary factor (-)
Δt	Interarrival time
μ_c	Viscosity of the continuous phase $(kg/m.s)$
μ_d	Viscosity of the dispersed phase $(kg/m.s)$
μ_m	Mixture viscosity $(kg/m.s)$
μ_r	Viscosity ratio (-)
σ	Surface tension (N/m)
λ	Wavelength (m)
φ	Off-axis angle (-)
γ	Pulsation parameter (-)
η	Efficiency of atomization (-)
ψ	Droplet uniformity index (-)
Δ	Relative span factor (-)
Δ_B	Dispersion boundary factor (-)

3.4. Subscripts

c	Continuous phase
p or d	Particle or dispersed phase
l	Liquid phase
g	Gas phase
rel	Relative
m	Mixture
x	Axial axis
i	*i*-th size class
j	*j*-th size class
i	*i*-th location
j	*j*-th location

3.5. Dimensionless Numbers

Oh	Ohnesorge number
PIV	Particle Image Velocimetry
Lp	Laplace number
SMD	Sauter mean diameter
SNR	Signal to noise ratio
St	Stokes number
Re	Reynolds number
Re_l	Liquid Reynolds number
We_{crit}	Critical Weber number
We_g	Aerodynamic/gas Weber number
We_l	Liquid Weber number:
Eu	Euler number

Nomenclature for Chapter 4

4.1. Abbreviations

GLR	air to liquid mass ratio (-)
PDPA	Phase Doppler Particle Anemometer

4.2. Symbols

D_n	nozzle diameter (m)
D_{10}	mean droplet diameter (μm)
D_{32}	Sauter Mean Diameter (μm)
Di	*i* th droplet size (μm)
N	total number of samples (-)
P_m	mixing pressure (kPa)
r	radial distance (m)
R	radius of the spray (m)
u	velocity (m/s)

4.3. Greek Letters

α	void fraction (-)
ϕ	scattering angle (°)
x	axial axis

Nomenclature for Chapter 5

5.1 Abbreviations

GLR	gas to liquid ratio by mass
FC	feeding conduit
PDPA	Phase-Doppler-Particle-Analyzer
PA	primary atomization
SA	secondary atomization
TPGL	two-phase gas/liquid flow

5.2. Symbols

D_n	nozzle diameter (m)
D_{ab}	mean drop size (m)
D_{10}	arithmetic mean diameter (m)
D_{20}	surface area diameter (m)
D_{21}	surface area- length diameter (m)
$D_{30,i}$	volume mean diameter at location i (m)
D_{31}	volume- length diameter (m)
D_{32}	Sauter mean diameter (SMD) (m)
D_{43}	De Brouckere or Herdan diameter (m)
D_{max}	maximum diameter (m)
D	diameter (m)
d	diameter (m)
d_d	droplet diameter (m)
d_b	bubble diameter (m)
L	characteristic length (m)
m_g	mass flow rates of the gas phase (kg/sec)
m_l	mass flow rates of the liquid phase (kg/sec)
N	number of samples (-)
P_m	mixing pressure (Pa)
Q_g	volume flow rate of the gas phase (m^3/sec)
Q_l	volume flow rate of the liquid phase (m^3/sec)
r	radial position (m)
R	radius of the spray (m)
u	velocity (m/sec)

U_g	velocity of the gas phase phases (m/sec)
U_l	velocity of the liquid phases (m/sec)
U_d	velocity of the droplet (m/sec)
x	axial distance (m)

5.3. Greek Letters

ϕ	scattering angle (^{o})
α	void fraction (-)
β	gas to liquid ratio by mass (%)
ρ	density (kg/m^3)
ρ_l	density of liquid phase (20°C pure water, 998 kg/m^3)
μ	viscosity ($kg / m.s$)
μ_l	viscosity of the carrier fluid (kg/m.s)
μ_g	viscosity of the gas phase (kg/m.s)
σ	surface tension (N/m)
τ_p	particle momentum response time (s)
τ_c	flow system time (s)

5.4 Subscripts

c, l, w	continuous/liquid/water phase
p ,d, g, a	particle/dispersed/gas/air phase
d	droplet
x	*x*-axis
y	*y*-axis
rel	relative

5.5. Dimensionless numbers

Oh	Ohnesorge number
St	Stokes number
Re	Reynolds number
We	Weber number
We_{crit}	Critical Weber number
Lp	Laplace number

Nomenclature for Chapter 6

6.1. Abbreviations

PDPA	Phase Doppler Particle Anemometer

6.2. Symbols

D_{32}	Sauter mean diameter (m)
D_n	nozzle diameter (m)

F	force (N)
M	mass flux
P	pressure (kPa)
x	axial positions (m)
r	radial distance (m)
R	radius of the spray (m)
U	velocity (m/s)

6.3. Greek Letters

β	gas to liquid mass ratio (-)

6.4. Suffix

c	continuous phase
d	dispersed phase
L	liquid phase
l	liquid phase
G	gas phase
g	gas phase
x	axial direction
y	radial direction
m	mixing
U	upstream
S	stagnation

Nomenclature for Chapter 7

7.1. List of Abbreviations

PDPA	Phase Doppler Particle Anemometer
PDA	Particle dynamics analyzer
2D	Two dimensional

7.2. Symbols

D_d	Drop diameter (μm)
D_N	Nozzle Drop (μm)
D	Characteristic diameter (μm)
D_{i}	Diameter of the *i*th drop (μm)
D_t	Internal diameter of the nozzle orifice (m)
D_{32}	Sauter mean diameter (μm)
$D_{32(gb)}$	Global Sauter mean diameter (μm)
D_{max}	Maximum droplet diameter (μm)
D_{min}	Minimum droplet diameter (μm)
d_i	Diameter of the *i*th drop (μm)
d	Diameter of the droplet (μm)

m_G or m_g or $\dot{m}_g$	Mass flow rate of gas (kg/s)
m_L or m_l or $\dot{m}_l$	Mass flow rate of liquid (kg/s)
L	jet break-up length (m)
N	total number of droplet
P_m	Mixing or injection pressure (Pa)
p	number (-)
q	number (-)
q_L	Volume of liquid per unit area per unit time (m/s)
Q_G	Gas volume flow rate (m^3/s or L/s)
Q_L	Liquid volume flow rate (m^3/s or L/s)
R	radial distance where velocity is zero (m)
r	radial coordinate (m)
U_d	Drop velocity (m/s)
U	Velocity (m/s)
U_i	Velocity of the *i*th drop (m/s)
U1	Beam system 1
U2	Beam system 2
x	Axial distance from nozzle exit (m)
y	radial distance (m)

7.3. Subscripts

l or L	liquid phase
g or G	gas phase
LS	superficial liquid
GS	superficial Gas

7.4. Greek Letters

β	gas to liquid ratio by mass or GLR (-)
ϕ	Scattering (or off-axis) angle (°)
Φ_{12}	Detector pairs 1 and 2
Φ_{13}	Detector pairs 1 and 3
γ	Liquid surface tension (mN/m)
μ_G	Gas absolute (or dynamic) viscosity (mPa-s)
μ_L	Liquid absolute (or dynamic) viscosity (mPa-s)
ρ_d	Drop density (kg/m^3)
ρ_g	Ambient gas density (kg/m^3)
ρ_A	Atomizing air density (kg/m^3)
ρ_G	Atomizing gas density (kg/m^3)
ρ_L	Liquid density (kg/m^3)

7.5. Dimensionless Numbers

Fr_L	Froude number = $\left(\frac{16Q_L^2}{\pi^2 g D_t^5}\right)$
Re_L	Reynolds number = $\left(\frac{4\rho_L Q_L}{\pi \mu_L D_t}\right)$
We	Weber number = $\left(\frac{16\rho_L Q_L^2}{\pi^2 \gamma D_t^3}\right)$
ρ_r	Density Ratio=$\left(\frac{\rho_g}{\rho_l}\right)$

Nomenclature for Chapter 8

8.1. Abbreviations

A	annular
ALR	air-to-liquid mass ratio (-)
DDPIV	defocusing digital particle image velocimetry
DB	dispersed bubble
GLR	gas-to-liquid mass ratio (-)
HSVS	high speed video shadowgraphy
He	nelium
I	intermittent
JBI	jet bed interaction
N_2	nitrogen
PDPA	phase doppler particle anemometer
PDA	particle dynamics analyzer
PIV	particle image velocimetry
QCV	quick closing valve
SBCI	stroboscopic back scattered imagery
SLR	single lens reflex
SS	stratified smooth
SW	stratified wavy

8.2. Symbols

A_L	area of liquid phase (m^2)
a	major axis of an ellipse (m)
A	area (m^2)
B	constant
b	major axis of an ellipse (m)
$C_{L\text{-}V}$	London-van der Waals constant (J.m)
d_b	bubble diameter (m)
d_{cr}	critical Brodkey bubble (m)
d_d	droplet diameter (m)

d_1	major length of the bubble (m)
d_2	minor length of the bubble (m)
d_f	length scale factor (-)
d_{max}	maximum bubble size (m)
d_{min}	minimum bubble size (m)
D	conduct diameter (m)
D_b	bubble diameter (μm)
D_c	conduct internal diameter (m)
D_d	droplet diameter (μm)
D_h	hydraulic diameter (m)
D_n	nozzle exit or orifice diameter (m)
D_{32}	Sauter mean diameter (μm)
f_{moody}	Moody friction factor (-)
$(dP/dx)_{fr}$	frictional pressure gradient (kPa/m)
g	gravitational acceleration (m/s^2)
h	film thickness (μm)
K	constant
L	length of the feeding conduit (m)
L_e	entrainment zone (m)
L_r	redistribution zone (m)
L_f	front zone (m)
L_b	length of body (m)
L_t	length of tail (m)
m_G	gas mass flow rate (kg/s)
m_L	liquid mass flow rate (kg/s)
m_d	dispersed phase mass flow rate (kg/s)
m_c	continuous phase mass flow rate (kg/s)
N_B	number of bubbles (-)
P	pressure (Pa)
P_G	gas phase pressure (kPa)
P_m	mixing pressure (kPa)
Q_L	liquid volumetric flow rate (m^3/s)
Q_G	gas volumetric flow rate (m^3/s)
R_G	characteristics gas constant (kJ/kg.K)
r	radial direction (m)
S	perimeter of a pipe (m)
T_{abs}	absolute temperature (K)
u	velocity (m/s)
u_{LS}	superficial liquid velocity (m/s)
u_L^S	superficial liquid velocity (m/s)
u_{GS}	superficial gas velocity (m/s)
u_G^S	superficial gas velocity (m/s)
u_m	mixture velocity (m/s)= $u_{LS} + u_{GS}$
x	axial direction (m)

X_L	constant (-)

8.3. Greek letters

α	volumetric void fraction of the gas (-)
β	gas-to-liquid mass ratio (-)
$\Delta\rho$	density difference (kg/m^3)
ε	turbulent energy density (m^2/s^3 or watt/kg)
ρ	density (kg/m^3)
ρ_C	density of continuous phase (kg/m^3)
ρ_D	density of dispersed phase (kg/m^3)
ρ_G	density of gas phase (kg/m^3)
ρ_L	density of liquid phase (kg/m^3)
μ	absolute viscosity (Pa.s)
μ_G	gas absolute viscosity (Pa.s)
μ_L	liquid absolute viscosity (Pa.s)
γ	surface tension (N/m)
γ_C	critical surface tension (N/m)
υ	kinematic viscosity (m^2/s)
υ_L	kinematic viscosity (m^2/s)
ρ_m	mixture density (kg/m^3) = $\alpha\,\rho_G + (1-\alpha)\,\rho_L$
μ_m	mixture viscosity (Pa.s) = $\alpha\,\mu_G + (1-\alpha)\,\mu_L$

8.4. Subscripts

c	critical
c	continuous
d	dispersed
G	gas
L	liquid
m	mixture
S	superficial

8.5. Dimensionless Bumber

Re	Reynolds number
We	Weber number
We_c	critical Weber critical number
Eu	Euler number
Fr	Froude number

Nomenclature for Chapter 9

9.1. Abbreviations

PDPA	Phase Doppler Particle Anemometer
CMFD	Computational Multi-Fluid Dynamics
LES	Large Eddy Simulations

9.2. Symbols

D_{32}	Sauter Mean Diameter (m)

CHAPTER 1

INTRODUCTION

In the effervescent atomization, gas and liquid mix upstream of the nozzles and after mixing the two phases, fluids are injected through nozzles where the mixture is atomized to form a spray. One of the drawbacks found with the effervescent atomization is the development of instabilities in the spray caused by the two-phase gas/liquid flow patterns formed inside or upstream of the nozzle at the higher gas to liquid mass ratio (β) [1, 2]. On the contrary, at the lower gas to liquid mass ratio (β) the effervescent atomization forms bigger droplets. A stable spray is demonstrated by a good dispersion of the liquid phase. It is desirable to produce a stable spray with minimum Sauter Mean Diameter (SMD or D_{32}) and well-dispersed liquid droplets. On the other hand, an unstable spray is characterized by intermittency/pulsation in its flow regime with the random formation of fine and coarse droplets in the spray. These pulsations are attributed to the two-phase gas/liquid fluid conditions, such as air-to-liquid mass ratio, β, void fraction, α, mixing pressure, P_m, the design of the mixing chamber and the geometry of nozzle [3]. Previous studies [4, 5] showed that as the β is increased, for a constant operating pressure at a certain transition point (e.g. β >1.5% in the large-scale nozzle), the spray becomes unstable. A homogeneous mixture of the gas-liquid entering the nozzle would maximize the effect of the decompression of the gas phase, resulting in a stable spray. On the other hand, a heterogeneous flow entering into the nozzle causes an unstable spray formation [6].

At the Syncrude research laboratory, the replicated pilot system (at room temperature) has similar dimensions compared to the commercial system (at 345-350^{O}C). At the University of Alberta, we have developed a quarter-scale fluid

coking nozzle assembly that replicates the large-scale assembly installed at Syncrude. This quarter-scale assembly was used for scaling purposes. Measurement techniques of the two-phase gas/liquid flows or sprays are a challenge. Due to highly non-uniform volumetric flow distribution and intermittency in the flow, it is extremely difficult to predict the accurate bubble and droplet size (d_b and d_d) and flow pattern distribution in this type of flow. Thus, uncertainty of the d_b or d_d prediction is exaggerated if the nozzle feeding conduit length is short as in the present study (36.8 cm); since the two-phase gas/liquid flow cannot be fully developed within this short pipe length.

In the heavy oil process industry, the preheated bitumen and steam are mixed upstream of the feed nozzle and subsequently injected into fluidized bed coker reactors via feed nozzles. To achieve high liquid product yields, the bitumen should contact with a large number of fluidized coke particles quickly and uniformly [7]. Excessively large bitumen droplets in conjunction with inadequate mixing momentum provides poor liquid product yield and operability in the in the heavy oil upgrading process. Due to the inaccessibility of the interior of the industrial reactor it is not possible to determine the influence of all critical operating conditions influence the upgrading process. The overall goal of this thesis is to establish multiphase scaling laws. These laws will be the fundamental means of understanding the performance of commercial two phase nozzles. This thesis will aid in optimizing the two phase nozzle flow conditions and will serve as a major tool in nozzle design and development for future generation nozzles for many industrial applications.

1.1. Background

A two-phase gas/liquid flow is the flow of a mixture of two phases such as gas (bubbles) in a liquid, or liquid (droplets) in a gas [8]. The continuity equation for each phase (k) is described as:

$$\frac{\partial}{\partial t}(\rho_k \alpha_k) + \nabla.(\rho_k \alpha_k \mathbf{u_k}) = 0 \quad (1)$$

The momentum equation for each phase is described as:

$$\frac{\partial}{\partial t}(\rho_k \alpha_k \mathbf{u_k}) + \nabla.(\rho_k \alpha_k \mathbf{u_k} \mathbf{u_k}) = -\alpha_k \nabla P + \rho_k \mathbf{g} + \alpha_k \mu_k \nabla^2 \mathbf{u}_k + \mathbf{F_{km}} \quad (2)$$

The first term in the right hand side of the equation indicates the pressure force, the second term indicates the gravity force, the third term indicates viscous force, and the fourth term indicates the summation of all interfacial forces. The symbol 'α' in Equations (1) and (2) indicate the void fraction. The void fraction is the portion of the pipe cross sectional area by the gas phase (A_g/A). When the no-slip condition exists between the phases, the α is termed as a homogeneous void fraction (α_H). The α_H in the two-phase gas/liquid flow system can be defined as:

$$\alpha_H = \frac{u_{gs}}{u_{gs} + u_{ls}} \quad (3)$$

Equation (3) is valid for the dispersed bubbly flow [9-11]. However, due to slip between the phases, the homogeneous void fraction is little bit lower than the no-slip condition (α_H/1.2) [10]. Superficial velocity is the velocity that either of the phases would flow alone occupying the entire cross-section of the pipe. Gas-phase superficial velocity (u_{gs}) is described as: Q_g/A and liquid-phase superficial velocity (u_{ls}) is described as: Q_l/A. Once the α of the two-phase gas/liquid flow is known, the actual velocity of the liquid-phase ($u_g=Q_g/A_g=u_{gs}/\alpha$) and gas-phase ($u_l=Q_l/A_l=u_{ls}/(1-\alpha)$) can be calculated easily. The 'β ' is another important parameter in the two-phase gas/liquid flow. The β can be defined as the ratio of the mass flow rates of the gas-phase and the mass flow rates of the liquid-phase ($\beta = m_g/m_l$). The relationship between the α_H and β is straightforward and can be obtained as follows:

$$\alpha_H = \frac{Q_g}{Q_g + Q_l} = \frac{1}{1 + \frac{Q_l}{Q_g}} = \frac{1}{1 + \frac{\dot{m}_l \rho_g}{\dot{m}_g \rho_l}} = \frac{1}{1 + \frac{P}{\beta \rho_l RT}} \quad (4)$$

In the case of equal phase velocities, or no-slip conditions, both the liquid and gas would flow at the mixture velocity defined as:

$$u_m = \frac{Q_l + Q_g}{A} = u_{ls} + u_{gs} \quad (5)$$

From several studies [4, 12, 13] in the literature it is evident that the liquid atomization depends on the upstream two-phase gas/liquid flow regime in the nozzle feeding conduit and at the nozzle exit. There are very few studies [14-18] that have been conducted for reliable estimation of upstream d_b and α in the two-phase gas/liquid horizontal flows. There are also few studies [9, 19-30] found on the transport of the two-phase gas/liquid flows through pipelines. Several correlations to predict the d_{min} and d_{max} in two-phase gas/liquid flow can also be found in the literature [31-33]. Different flow regime descriptions can also be obtained in the literature as [34]:

a) the stratified flow regime is characterized by a complete separation of the liquid and gas phases,

b) in the intermittent flow regime discontinuities in the liquid and gas flow are observed,

c) in the annular flow regime the liquid coats the tube wall completely and the gas flows through the core of the tube,

d) dispersed flow occurs when the gas-phase forms uniform, tiny bubbles suspended in the liquid medium.

Several studies dealing with the two-phase gas/liquid flow maps are also found in the literature [34-46]. However, these flow maps cannot accurately predict all the two-phase gas/liquid flow classes and transitions between the flow regimes. In a recent study, images of droplets or particles produced by shadowgraph and back-illumination using an infrared diode laser were investigated with a digital image analysis technique [47]. Another study [48] implemented a digital-based image analysis system for the determination of size and distribution of particles suspended in any clear fluid flow. The suitability of the above studies was for

relatively larger particles (some *mm* in diameter). A study [43] was conducted with air and water in a large circulating rig with a 0.105m diameter test section. The bubble diameter, d_b was expressed as [43]:

$$d_b = \sqrt[3]{d_1^2 d_2} \tag{6}$$

In the literature different types of techniques were implemented to measure the α in the two-phase gas/liquid flow. One of the recent techniques is the microwave flow sensor [49]. Several studies on implementing gamma-ray densitometers showed that multi-beam gamma-ray densitometers can analyze the α with high accuracy [50, 51]. One of the disadvantages of the gamma-ray densitometers is the shielding requirement for the gamma-ray. Capacitance sensors for the instantaneous α in air-oil, two-phase flow was developed [52-54]. The α of the two-phase gas/liquid flow is often measured by isolating a section in the nozzle feeding conduit [55-60], named as the quick closing valve (QCV) technique. However, most of the studies were conducted in the vertical bubble column [61]. It is very crucial to commence the closing of both valves simultaneously. Error in the α measurements by the QCV due to asynchronization of the valves can be expressed as [61]:

$$\%\ \ Error = \frac{u_m t_{ac}(1-\alpha)}{l_c \alpha} \times 100 \tag{7}$$

In the atomization process, a liquid jet is atomized by the interaction of the liquid jet with a high-velocity gas. The significant properties of the liquid-phase, which plays an important role in the atomization process, are (in order of significance): viscosity, surface tension, and density [8]. In the atomization process, it is convenient to deal with the mean drop size distributions:

$$\text{e.g. } D_{10} = \sum N_i d_i / \sum N_i \text{ and } D_{32} = \sum N_i d_i^3 / \sum N_i d_i^2 \text{ [62, 63]} \tag{8}$$

In the droplet/bubble motion, the Stokes number (*St*) is a very important parameter. The '*St*' is defined as the ratio of the particle momentum response time over a flow system time, defined as:

$$St = \tau_p / \tau_c = \rho_p d_p^2 u_c / 18 \mu_c L \tag{9}$$

Two types of situations can be observed for particles (bubbles/droplets) suspended in fluid, namely [8]:

a) if the $St<<1$, the particles will have ample time to respond to changes in flow velocity,

b) if $St>>1$, then the particle will have essentially no time to respond to the fluid velocity changes and the particle velocity will be little affected by fluid velocity change. A spray breaks up further downstream from the tip of a nozzle. A typical two-phase gas/liquid atomization process involves a) primary atomization (PA), b) secondary atomization process (SA). The dominant forces involved in the atomization process are [64]:

a) hydrodynamic or inertial force attributed to undulations/perturbations.

b) aerodynamic force attributed to drag/shearing effect.

c) viscous force attributed to opposing a change in liquid geometry, and

d) surface tension forces attributed to a minimum surface energy.

The first two forces are disruptive in nature and the second two forces are cohesive in nature. The interaction of internal forces such as: a) turbulence, b) inertial effects, c) momentum transfer between transverse layers of a jet are mainly responsible for the PA [65]. At this stage the disruptive forces exceed the consolidating forces resulting in oscillations on the liquid surface; and subsequently disintegration of the bulk liquid into drops [66, 67]. The SA in a spray occurs when larger droplets or liquid ligaments break down into smaller droplets. The breakup of a single droplet in a gas is caused by either greater relative velocity, or turbulence [8]. The SA occurs due to two force ratios acting on the drop [68]. Firstly, if the aerodynamic forces overcome the forces due to the surface tension, the droplet will further deform [69]. The ratio of these two forces can be represented by the Weber number (*We*), which can be defined as: i) aerodynamic/gas Weber number:

$$We_g = \rho_g u_{rel}^2 d_d / \sigma \tag{10}$$

or ii) liquid *Weber number*:

$$We_l = \rho_l u_l^2 d_d / \sigma \tag{11}$$

Secondly, the Ohnesorge number (*Oh*)/Laplace number (*Lp*), denoted by:

$$Oh = \sqrt{We_l} / \mathrm{Re}_l = \mu_l / \sqrt{\rho_l d_d \sigma} = 1/\sqrt{Lp} \quad (12)$$

The Ohnesorge number is the ratio of liquid viscous force to surface tension force on the drop, which also plays an important role in the SA. Here Re_l is the liquid *Reynolds number* defined: $Re_l = \rho_l u_l d_d / \mu_l$. Mathematically, if the We_g exceeds the We_{crit}, the SA occurs. For low-viscosity liquids, $We_{crit} = 6$ to 13 for $Oh < 0.1$, $We_{crit} \approx Oh^2$ for $Oh > 0.1$ [70]. In the two-phase gas/liquid spray characteristics measurement, the Phase-Doppler-Particle-Anemometer (PDPA) or Particle-Dynamics-Analyzer (PDA) system and digital image analysis techniques have been used as advanced experimental techniques. The PDPA measurement techniques to measure the two-phase gas/liquid spray can be found in the literature [71-75]. Recently developed digital image analysis techniques are also potentially capable of sizing particles of arbitrary shape and size and with a wide dynamic range [1, 47, 76]. Most of the measurements of the two-phase gas/liquid spray characteristics were conducted by the PDPA and a few of the d_d measurements were conducted by image analysis. The success of two-phase gas/liquid flow or spray measurements largely depends on the respective flow regime; whether it is dispersed, slug, or stratified flow. Most of the α measurements were intrusive in nature. Other methods have safety issues and accuracy challenges. However, the mechanical QCV technique has been proven to be a more reliable and easy-to-implement method if the synchronization of the two closing valves can be assured. High-speed video and photonics measurements are also very reliable, non-intrusive volume fraction and flow pattern estimation techniques. Information obtained from these photonics measurements could be coordinated with the flow transition maps and correlations provided by several researchers. However, most of the flow maps and correlations are designed for round, vertical and large diameter tubes in equilibrium conditions. The current study will identify the applicability of the photonics and coupled PDPA and impulse probe measurements in a non-equilibrium horizontal nozzle assembly.

This will also assist to accurately identify the flow patterns, bubble size, droplet size and mass flux in effervescent atomization.

1.2. Commercial Fluid Coker

The commercial full-scale fluid coker schematic diagram is presented in Fig. 1.1 (left). In the upper right of Fig. 1.1 the nozzle assembly is zoomed and in the lower right of Fig. 1.1 the internal design of the nozzle is zoomed.

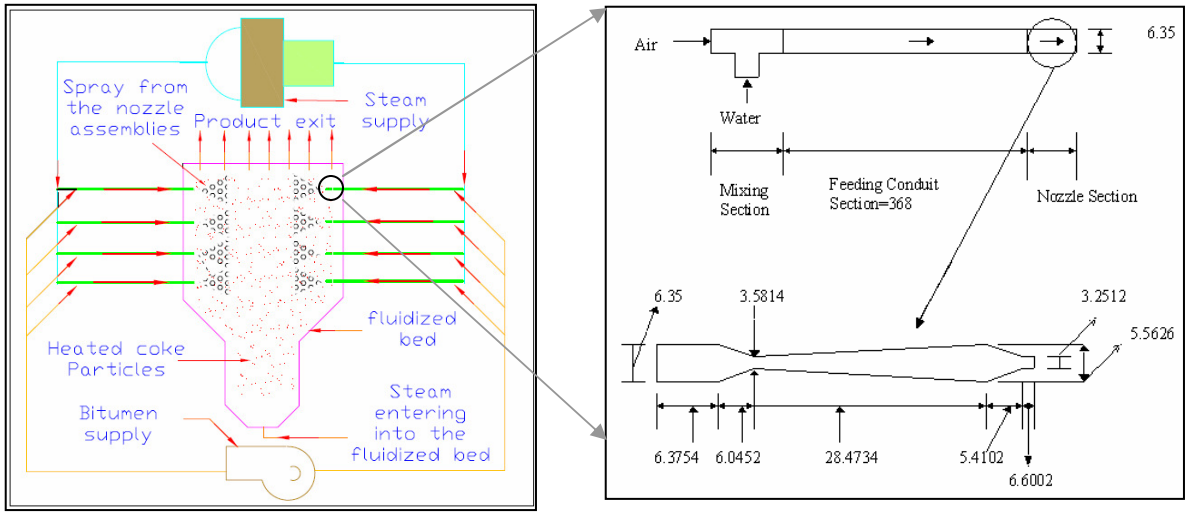

Fig. 1.1. Schematic of the full-scale reactor and nozzle assembly.

1.3. Research Outline

The flow chart in Fig. 1.2 illustrates the outline of this research highlighting the relevant sequence of tasks and measurement techniques. Gas assisted liquid atomization is employed in several industrial processes such as in fluid coking to upgrade bitumen to synthetic crude oil. In a fluid coker a mixture of bitumen and steam is injected as a spray into a fluidized bed of coke particles via nozzles. A class of this type of nozzles requires mixing the gas and liquid well upstream prior to feeding the mixture through the nozzles using a nozzle feeding conduit. The objective of this research is to establish scaling laws for effervescent atomization. The proposed study will contribute to the fundamental knowledge of the two-phase gas/liquid flows or sprays and make concrete headway in the scaling of an industrial nozzle used in a large-scale high impact operation.

Fig. 1.2. Flow chart depicting the experimental program for establishing the scaling laws.

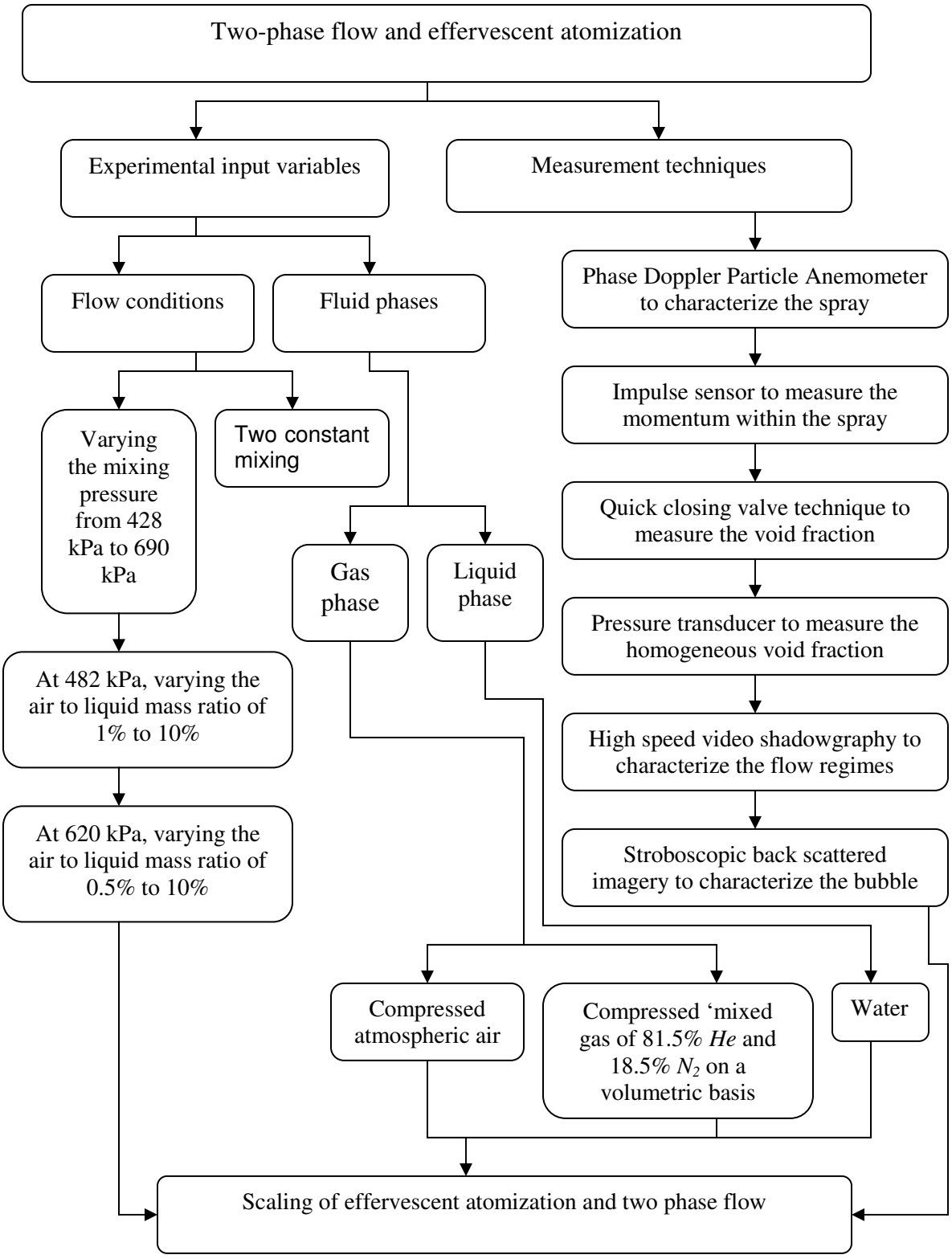

1.4. Thesis Objectives

The objectives of this thesis are as follows:

i) To establish two-phase scaling laws for effervescent atomization.

ii) To improve the similitude of the atomization in 'cold' flow conditions with the actual 'hot' commercial nozzle operation.

iii) To predict correlations between the spray disintegration process and the upstream nozzle feeding conduit flow characteristics.

vi) To understand the fundamentals of the two-phase gas/liquid flow patterns, void fractions, and spray characteristics.

v) To better estimate the mass flux throughout the entire spray.

1.5. Conclusions

The fundamental knowledge of the two-phase gas/liquid flow or atomization process in effervescent nozzles is important for many industrial and chemical reactions. The outcome of this research will help in optimization of commercial process conditions and provide a comprehensive means of improving the design conditions of the two-phase gas/liquid flow or atomization process. Specifically, this thesis will assist to optimize the operating range of the existing effervescent nozzles used in many industrial applications.

1.6. Original Contributions in Effervescent Atomization Study

The outcome of this research can be used in the optimization of industrial processes and will provide a comprehensive means of improving the design of two-phase flow and effervescent atomization. The knowledge base developed in this project is fundamental in nature and can be transferred to a wide range of physical applications ranging from efficient snow production in winter sports to a cost-saving agricultural spray innovation. This study is a milestone toward this energy efficient technology development for the ultimate benefit of industrial needs. This novel research is a breakthrough in establishing the scaling laws of

effervescent atomization. The novel contributions in this current two-phase gas/liquid flow and spray scaling study will be as follows:

a) To the best of my knowledge there has been no study on the effects of gas properties on the atomization behavior of the two-phase gas/liquid flow or spray. The simulation of the 'hot' commercial fluid coking operation with the 'cold' laboratory scale fluid coking operation is first matched by introducing the 'mixed-gas' experiment.

b) This study is the first attempt to establish the scaling laws for the effervescent atomization.

c) The spray force measurement by the impulse sensor (IS) is a novel study in the evaluation of the mass flux in the two-phase gas/liquid spray. The coupled PDPA and impulse probe technique is a breakthrough measurement technique that can reliably measure the mass flux in the multiphase dense spray.

d) This study is the first for the two-phase gas/liquid spray that has examined the profile of the spray in different axial positions and radial locations. This is in contrast to the use of point/peripheral/centerline spray profile measurements, which is common in literature related to this type of study. In addition to the global measurement technique, in this study a global droplet size concept is also incorporated.

e) The attempt to find out the correlations between the upstream two-phase gas/liquid flow conditions in the nozzle feeding conduit and the downstream spray characteristics as a function of the fluid properties (atmospheric air and 'mixed-gas' as the gas-phase) and flow conditions (changing β, α, P_m) would be a breakthrough related to this type of study.

f) The SBSI, HSVS and QCV experiments would be the first kind to evaluate the two-phase gas/liquid flow characteristics in the non-equilibrium condition exits in this study.

1.7. Thesis Scope

An overview of the effervescent atomization and an outline of the thesis are presented in Chapter 1. A critical literature review on the two-phase gas/liquid flow theory and advanced two-phase flow measurement techniques are outlined in Chapter 2. A critical literature review on the two-phase gas/liquid spray theory and advanced two-phase spray measurement techniques are outlined in Chapter 3. Chapter 4 briefly discusses the atomization characteristics, measurement techniques and results. Chapter 5 presents more insights about the two-phase gas/liquid spray break-up mechanism and results. Chapter 6 presents a novel measurement technique to estimate the effervescent atomization mass flux. The effervescent atomization scaling based on the liquid properties (surface tension and liquid viscosity) and geometry (nozzle throat) are presented in Chapter 7. The effervescent atomization scaling based on the gas properties (molecular weight, flow regime, and bubble size) are presented in Chapter 8. Finally, the conclusions and recommendations for continued work on the effervescent atomization scaling are discussed in Chapter 9.

1.7. References

[1] Ariyapadi, S., Berruti, F., Briens, C., Knapper, B., Skwarok, R. and Chan, E. (2005) Stability of horizontal gas–liquid sprays in open-air and in a gas–solid fluidized bed. Powder Technology. 155 161 – 174.

[2] Maldonado, S. (2006) Improving the Stability of Gas-Liquid Sprays by Modifying the Two-Phase Flow Entering The Nozzle, MASc. , MASc. Thesis, University of Alberta.

[3] Tafreshi, Z.M., Kirpalani, D., Bennett, A. and McCracken, T.W. (2002) Improving the efficiency of fluid cokers by altering two-phase feed characteristics. Powder Technology. 125 234– 241.

[4] Roesler, T.C. and Lefebvre, A.H. (1989) Studies on aerated-liquid atomization. International Journal of Turbo Jet Engines. 6: 221-230.

[5] Whitlow, J.D. and Lefebvre, A.H. (1993) Effervescent atomizer operation and spray characteristics. Atomizations and Sprays. 3: 137–155.

[6] Barker, C.L., Cody, G.D., Joseph, C.A. and Sela, U. (1991) Acoustic Monitoring of Two-Phase Feed Nozzles. US Patent 5 004 152.

[7] Ejim, C.E. (2008) Effect of Liquid Viscosity, Surface Tension and Nozzle Size on Atomization in Two-Phase Nozzles, PhD Thesis, Mechanical Engineering, University of Alberta.

[8] Crowe, C.T. (2006) Multiphase flow handbook Boca Raton, FL CRC: Taylor & Francis.

[9] Andreussi, P., Paglianti, A. and Silva, F.S. (1999) Dispersed bubble flow in horizontal pipes. Chemical Engineering Science. 54 (8): 1101-1107.

[10] Chen, X.T., Cai, X.D. and Brill, J.P. (1997) A general model for transition to dispersed bubble flow. Chemical Engineering Science. 52 (23): 4373-4380.

[11] Gomez, L.E., Shoham, O., Schmidt, Z., Chokshi, R.N., Brown, A. and Northug, T. (1999) Unified Mechanicstic Model for Steady-State Two-Phase Flow in Wellbores and Pipelines. In proceedings-SPE Annual Technical Conference, 3–6 October, Houston.

[12] Lefebvre, A.H., Wang, X.F. and Martin, C.A. (1988) Spray characteristics of aerated-liquid pressure atomizers. AIAA Journal of Propulsion and Power. 4 (6): 293-298.

[13] Sovania, S.D., Choua, E., Sojkaa, P.E., Gorea, J.P., Eckerleb, W.A. and Crofts, J.D. (2001) High pressure effervescent atomization: effect of ambient pressure on spray cone angle. Fuel. 80: 427-435.

[14] Hesketh, R.P., Etchells, A.W. and Russell, T.W.F. (1991) Experimental observations of bubble breakage in turbulent flow. Ind. Eng. Chem. Res. 30 (5): 835–841.

[15] Hesketh, R.P., Etchells, A.W. and Russell, T.W.F. (1991) Bubble breakage in pipeline flow. Chem. Eng. Sci. 46: 1–9.

[16] Hesketh, R.P., Russell, T.W.F. and Etchells, A.W. (1987) Bubble size in horizontal pipelines. AIChE J. 33: 663–667.

[17] Walter, J.F. and Blanch, H.W. (1986) Bubble break-up in gas–liquid bioreactors: break-up in turbulent flows. Chem. Eng. J. 32: B7–B17.

[18] Bratukhin, Y.K., Kostarev, K.G., Viviani, A. and Zuev, A.L. (2005) Experimental study of Marangoni bubble migration in normal gravity. Experiments in Fluids. 38 (5): 594-605.

[19] Simmons, M.J.H. and Azzopardi, B.J. (2001) Drop size distributions in dispersed liquid–liquid pipe flow. Int. J. Multiphase Flow. 27: 843–859.

[20] Angeli, P. (2001) Droplet size in two-phase liquid dispersed pipeline flows. Chem. Eng. Technol. 24: 431–434.

[21] Angeli, P. and Hewitt, G.F. (2000) Drop size distributions in horizontal oil–water dispersed flows. Chem. Eng. Sci. 55: 3133–3143.

[22] Kostoglou, M. and Karabelas, A.J. (1998) On the attainment of steady state in turbulent pipe flow of dilute dispersions. Chem. Eng. Sci. 53: 505–513.

[23] Parthasarathy, R., Jameson, G.J. and Ahmed, N. (1991) Bubble breakup in stirred vessels-prediction of the Sauter mean diameter. Trans. IChemE. 69 (Part A): 295–301.

[24] Karabelas, A.J. (1978) Droplet size spectra generated in turbulent pipe flow of dilute liquid/liquid dispersions. AIChE J. 24: 170–180.

[25] Kubie, J. and Gardner, G.C. (1977) Drop sizes and drop dispersion in straight horizontal tubes and in helical coils. Chem. Eng. Sci. 32: 195–202.

[26] Holmes, T.L. (1973) Fluid mechanics of horizontal bubble flow, Ph.D. Thesis, University of Delaware.

[27] Swartz, J.E. and Kessler, D.P. (1970) Single drop breakup in developing turbulent pipe flow. AIChE J. 16: 254–260.

[28] Collins, S.B. and Knudsen, J.G. (1970) Drop-size distributions produced by turbulent pipe flow of immiscible liquids. AIChE J. 16: 1072-1080.

[29] Ward, J.P. and Knudsen, J.G. (1967) Turbulent flow of unstable liquid–liquid dispersions: drop sizes and velocity distributions. AIChE J. 13: 356–365.

[30] Kolmogoroff, A.N. (1949) On the breaking of drops in turbulent flow. Dokl. Akad. Nauk SSSR. 66: 825–828.

[31] Liu, S. and Li, D. (1999) Drop coalescence in turbulent dispersions. Chem. Eng. Sci. 54: 5667–5675.

[32] Razzaque, M.M., Afacan, A., Liu, S., Nandakumar, K., Masliyah, J.H. and Sanders, R.S. (2003) Bubble size in coalescence dominant regime of turbulent air–water flow through horizontal pipes. International Journal of Multiphase Flow. 29 1451–1471.

[33] Shinnar, R. (1961) On the behaviour of liquid dispersions in mixing vessels. J. Fluid Mech. 10: 259–275.

[34] Coleman, J.W. and Garimella, S. (1999) Characterization of two-phase fow patterns in small diameter round and rectangular tubes International Journal of Heat and Mass Transfer. 42 (15): 2869-2881.

[35] Baker, O. (1954) Simultaneous Flow of Oil and gas. The Oil and gas Journal. 53: 185-195.

[36] Breber, G., Palen, J. and Taborek, J. (1980) Prediction of horizontal tubeside condensation of pure components using flow regime criteria. Journal of Heat Transfer. 102: 471-476.

[37] Damianides, C. and Westwater, J.W. (1988) Two phase flow patterns in a compact heat exchanger and in small tubes. Proceedings of Second U.K. National Conference On Heat Transfer, vol II, Glasgow, Scotland.

[38] Ewing, M.E., Weinandy, J.J. and Christensen, R.N. (1999) Observation of Two-phase Flow Patterns in a Horizontal Circular Channel. Heat Transfer Engineering. 20 (1): 9-13.

[39] Hibiki, T., Goda, H., Kim, S., Ishii, M. and Uhle, J. (2004) Structure of vertical downward bubbly flow. International Journal of Heat and Mass Transfer. 47 1847–1862.

[40] Jeffreys, H. (1925) On the formation of water waves by wind. Proc. Royal Soc. A107: 189-206.

[41] Lambrechts, A. (2005) Heat transfer performance during in-tube condensation in horizontal smooth, micro-fin and herringbone tubes, MIng, Mechanical and Manufacturing Engineering, University of Johannesburg.

[42] Mandhane, J.M., Gregory, G.A. and Aziz, A. (1974) A flow pattern map for gas-liquid flow in horizontal pipes. Int. J. Multiphase Flow. 1: 537-553.

[43] Sotiriadis, A.A., Thorpe, R.B. and Smith, J.M. (2005) Bubble size and mass transfer characteristics of sparged downwards two-phase flow. Chemical Engineering Science. 60: 5917 – 5929.

[44] Taitel, Y. and Dukler, A.E. (1976) A model for predicting flow regime transitions in horizontal and near horizontal gas-liquid flow AIChE J. 22 (2): 47-55.

[45] Thomas, R.M. (1981) Bubble coalescence in turbulent flows. Int. J. Multiphase Flow. 7: 709–717.

[46] Whalley, P.B. (1987) Boiling, Condensation and Gas-Liquid Flow, Oxford, New York.

[47] Kashdan, J.T., Shrimpton, J.S. and Whybrew, A. (2003) Two-Phase Flow Characterization by Automated Digital Image Analysis. Part 1: Fundamental Principles and Calibration ofthe Technique. Part. Part. Syst. Charact. 20 387-397.

[48] Lecuona, A., Sosa, P.A., Rodriguez, P.A. and Zequeira, R.I. (2000) Volumetric characterization of dispersed two-phase flows by digital image analysis. Meas. Sci. Technol. 11: 1152–1161.

[49] Everson, J. (2005) Foster-Miller, Inc. See also:http://www.foster-miller.com/projectexamples/cc_icd_sensor_development/microwave_flow_sensor.htm.

[50] Abro, E., Khoryakov, V.A., Johansen, G.A. and Kocbach, L. (1999) Determination of void fraction and flow regime using a neural network trained on simulated data based on gamma-ray densitometry. Measurement Science & Technology. 10 (7): 619-630.

[51] Jiang, Y.J. and Rezkallah, K.S. (1993) An Experimental-Study of the Suitability of Using a Gamma Densitometer for Void Fraction Measurements in Gas-Liquid Flow in a Small Diameter Tube. Measurement Science & Technology. 4 (4): 496-505.

[52] Ahmed, W.H. (2006) Capacitance sensorsor void-fraction measurements and flow-pattern identification in air-oil two-phase flow Ieee Sensors Journal. 6 (5): 1153-1163.

[53] Pawloski, J.L., Ching, C.Y. and Shoukri, M. (2004) Measurement of void fraction and pressure drop of air-oil two-phase flow in horizontal pipes. Journal of Engineering for Gas Turbines and Power-Transactions of the Asme. 126 (1): 107-118.

[54] Elkow, K.J. and Rezkallah, K.S. (1996) Void fraction measurements in gas-liquid flows using capacitance sensors. Measurement Science & Technology. 7 (8): 1153-1163.

[55] Koyama, S., Lee, J. and Yonemoto, R. (2004) An investigation on void fraction of vapor-liquid two-phase flow for smooth and microfin tubes with R134a at adiabatic condition. International Journal of Multiphase Flow. 30 (3): 291-310.

[56] Kim, H.Y., Koyama, S. and Matsumoto, W. (2001) Flow pattern and flow characteristics for counter-current two-phase flow in a vertical round tube with wire-coil inserts. International Journal of Multiphase Flow. 27 (12): 2063-2081.

[57] Spedding, P.L., Woods, G.S., Raghunathan, R.S. and Watterson, J.K. (1998) Vertical two-phase flow - Part II: Experimental semi-annular flow and hold-up. Chemical Engineering Research & Design. 76 (A5): 620-627.

[58] Lemonnier, H., Nakach, R., Favreau, C. and Selmerolsen, S. (1991) Sensitivity Analysis of an Impedance Void Meter to the Void Distribution in Annular-Flow - a Theoretical-Study. Nuclear Engineering and Design. 126 (1): 105-112.

[59] Bjork, E. (2005) A simple technique for refrigerant mass measurement. Applied Thermal Engineering. 25: 1115–1125.

[60] Chien, K.-H., Lin, W.-K. and Tsai, Y.-C. (1997) Effect of the side-tube configuration on the void fraction measurement. Nuclear Technology. 120 (2): 171-178.

[61] Flemmer, R.L.C. and Clark, N. (1984) A technique for synchronizing valves and determining bubble rise velocities in two-phase flow. Fluid engineering winter annual meeting, ASME, December 9-14, New Orleans, LA.

[62] Lefebvre, A.H. (1989) Atomizations and Sprays, New York, Hemisphere.

[63] Mugele, R. and Evans, H.D. (1951) Drop size distributions is sprays. Ind. Eng. Chem. 43 (6): 1317-1324.

[64] Nasr, G.G., Yule, A.J. and Bendig, L. (2002) Industrial sprays and atomization: design, analysis and applications, Springer-Verlag London Limited.

[65] McCarthy, M.J. and Molloy, N.A. (1974) Review of stability of liquid jets and influence of nozzle design. Chemical Engineering Journal. 7: 1-20.

[66] Liu, H. (1999) Science and Engineering of droplets - Fundamentals and Applications, William Andrew Inc./Noyes Publications.

[67] Shavit, U. and Chigier, N. (1996) Development and evaluation of a new turbulence generator for atomization research. Experiments in Fluids. 20 (4): 291-301.

[68] Pilch, M. and Erdmann, C.A. (1987) Use of breakup time data and velocity history data to predict the maximum size of stable fragments for acceleration-induced breakup of a liquid drop. Int. J. Multiphase Flow. 13: 741–757.

[69] Low, T.B. and List, R. (1982) Collision, coalescence and breakup of raindrops. J. Atmos. Sci. 39: 1591–1618.

[70] Faeth, G.M. (1990) Structure and atomization properties of dense turbulent sprays. 23rd Symposium on Combustion, The Combustion Institute, Pittsburgh.

[71] Ariyapadi, S., Balachandar, R. and Berruti, F. (2001) Characterizing Spray Pulsations Using a Phase-Doppler Particle Analyzer. Ind. Eng. Chem. Res. 40: 5282-5290.

[72] Ariyapadi, S., Berruti, F. and Ram, B. (2003) Effect of Crossflow on the Spray Characteristics of an industrial Feed Nozzle. Chem. Eng. Comm. 190: 1: 681-1704.

[73] Copan, J., Balachandar, R. and Berruti, F. (2001) Droplet size-velocity characteristics of sprays generated by two-phase feed nozzles. Chemical Engineering Communications. 184: 105-124.

[74] Ziesenis, J. and Bauckhage, K. (2002) Absorption and Scattering of Light by Highly Concentrated Two-phase Flows. Part. Part. Syst. Charact. 19 195-202.

[75] Ariyapadi, S., Balachandar, R. and Berruti, F. (2000) Effect of Cross-Flow on the Spray Characteristics of an Industrial Feed Nozzle. AIChE Spring Annual meeting, Atlanta, GA.

[76] Zama, Y., Kawahashi, M. and Hirahara, H. (2004) Simultaneous Measurement of Droplet Size and Three-Components of Velocity in Spray. Optical Review. 11 (6): 358–364.

[77] Ejim, C.E., Fleck, B.A. and Amirfazli, A. (2005) A Scaling Study of the Atomization of a Two-Phase Industrial Nozzle: Part 1 - Effect of Surface Tension and Viscosity on Mean Drop Size Profiles. Proceedings of the 20th ILASS - Europe Meeting Sept. 5-7, Orléans, France.

CHAPTER 2

Literature: Two-phase Flow[1]

2.1. Introduction

Two-phase gas/liquid flows are quite complicated transport phenomena. There are still fundamental aspects of the two-phase gas/liquid flow whose physical descriptions are still unknown and whose modeling results are questionable. Experimental observations are difficult in this case, as the migration of dispersed bubbles towards the top of the pipe due to buoyancy and complicated turbulence interaction, causes a highly non-symmetric volume distribution in the pipe cross-section. Lack of solid and comprehensive theories for predicting and calculating the pressure and void fraction variations in two-phase gas/liquid flow situations has left engineers without information essential for the proper design of two-phase gas/liquid systems [1]. Often, existing theoretical solutions do not agree with the experimental results. Accurate measurement techniques of two-phase gas/liquid flow are a ubiquitous challenge. Often, existing measurement techniques cannot explain important physical properties and parameters needed to model the two-phase flow phenomena. There is the utmost need to explore novel experimental techniques in order to obtain better insight into fundamental phenomena associated with two-phase gas/liquid fluid dynamics.

A phase refers to the solid, liquid or vapour state of matter. A two-phase flow is the flow of a mixture of two phases such as gas (bubbles) in a liquid, or liquid (droplets) in gas. In this paper, special emphasis is given to the horizontal two-phase gas/liquid flow condition. Horizontal two-phase gas/liquid flow can be classified into two major categories a) dispersed flow or b) separated flow. Dispersed phase flows are flows in which one phase consists of discrete elements,

[1] A version of this chapter has been published. Rahman *et al.* (2009) The Open Fuels & Energy Science Journal, 2: 54-70.

such as droplets in a gas or bubbles in a liquid and the discrete elements are not connected. In a separated flow, a line of contact separates the two phases. An annular flow is a separated flow in which there is a liquid layer on the pipe wall and a gaseous core [2]. Thus, the accumulated air in a conduit can evolve into different flow patterns, from stratified, annular to dispersed flow patterns.

In this chapter, basic theories and advanced experimental techniques of two-phase gas/liquid flows are reviewed extensively. In the first two sections of this chapter basic theories and several useful non-dimensional numbers for the two-phase gas/liquid flow are explained. Subsequently, the advanced pressure measurement techniques, void fraction measurement techniques and photonics and image analysis techniques used in the two-phase gas/liquid flows are reviewed. Finally, several useful correlations to characterize the bubble size in two-phase gas/liquid horizontal flows are reviewed. This review is a benchmark of the state-of-the-art experimental tools and analysis techniques of the two-phase gas/liquid flows.

2.2. Basic Concepts and Definitions

The basic theory of two-phase, two-component flow is described in this section. The superficial velocity, which is the velocity that either of the phases would flow alone occupying the entire cross-section of the pipe ($u_{ds} = 4Q_d/\pi D^2$ or $u_{cs} = 4Q_c/\pi D^2$), is an important parameter in the gas-liquid flow system [3]. The void fraction, which is the portion of the pipe cross sectional area occupied by the gas phase, is another important parameter in the gas-liquid flow system. When the velocity of the phases is the same (no-slip), the void fraction is termed the homogeneous void fraction, ($\alpha_H = A_g / A_{pipe} = u_{ds} / u_{ds}+u_{cs}$). This definition of the void fraction is valid for the dispersed bubbly flow [4-6]. However, due to slip between the phases, the actual void fraction is a bit lower (approximately 1/1.2 times lower) than the non-slip condition [7]. Air (gas) to liquid ratio or ALR (GLR) ratio can be defined as the ratio of the mass flow rate of the gas phase to the mass flow rate of the liquid phase ($\beta = m_d/m_c$). The relationship between the

homogeneous void fraction and GLR is straightforward and can be obtained as follows:

$$\alpha_H = \frac{Q_d}{Q_d + Q_c} = \frac{1}{1 + \frac{Q_c}{Q_d}} = \frac{1}{1 + \frac{\dot{m}_c \rho_d}{\dot{m}_d \rho_c}} = \frac{1}{1 + \frac{P}{(\beta)\rho_c R T}} \quad (1)$$

where R represents the Universal Gas Constant = 8.3144×10^{-3} kJ/mol.K, ρ_c is the density of liquid (kg/m^3), β is the gas to liquid mass ratio (-), and T represents absolute temperature (K). The response time of a bubble or droplet to change in flow velocity or temperature is important in establishing non-dimensional parameters to characterize the two-phase gas/liquid flow [2]. The momentum response time and the flow field response time comprise the Stokes number ($St = \tau_m/\tau_f$). The Stokes number can be further related to the velocity ratio as follows:

$$\phi = \frac{u_d}{u_c} \approx \frac{1}{1 + St} \quad (2)$$

If the Stokes number tends to be zero, there would be no-slip between the two phases. In two-phase flow, commonly employed averaging techniques are time, volume and mass averaging [3]. Various forms of averaging have been used in the literature: a) time averaging [8, 9], b) volume averaging [10-12], c) flow-area averaging [8, 13, 14], and d) ensemble averaging [3]. A detailed literature review on averaging techniques of two-phase flows can also be found in the literature [15-18]. Two-phase flow modeling is a ubiquitous challenge due to complex interaction between the phases. However, several simplified two-phase flow models can be found in the literature. Two basic assumptions required to consider a flow homogeneous are [3]: a) The time scale for the transport between phases is much shorter than the overall characteristic or system time scale, and b) two phases are in thermodynamic equilibrium, i.e. V_p=V_c, P_p=P_c, and T_p=T_c. Under this situation one can consider the mixture as a single-phase flow. The mixture, or effective, density can be written as [2]:

$$\rho_m = \alpha\rho_d + (1-\alpha)\rho_c \quad (3)$$

here, α is the void fraction (V_d/V). Several suggestions have been proposed for the mixture viscosity as follows: a) For suspension of fluid spheres at low concentration ($\alpha \le 0.05$) [11, 19, 20], b) For suspension of solid spheres at low concentration ($\alpha \le 0.05$) [21], c) For suspension of low-viscosity gas bubbles at low concentration ($\alpha \le 0.05$) [3]. In the case of gas-liquid flows with large void fractions ($\alpha \ge 0.05$) several suggestions have also been provided [22-24]. Due to their simplicity, the mixture models are quite advantageous for use in the computational analysis. The drift flux model is based on the concept of analyzing the mixture as a whole rather than in separated phases. However, this model accounts for the relative motion between the phases [3]. The 1-D drift flux model is described in detail for vertical pipe flow [25], vertical rectangular ducts [26] and vertical annular two-phase flow conditions [27]. Separated flow models indicate the physical separation of two immiscible fluids flowing in layers. Either Eulerian-Lagrangian (particle trajectory models) or Eulerian-Eulerian models are employed to solve separated flow problems [28-32].

2.3. Dimensionless Numbers in Two-Phase Flows

In two-phase flow, the use of traditional dimensionless numbers is very limited in correlating data sets [3]. However, there are several important dimensionless numbers found in the literature. In liquid-particle motion and particle dynamics, the Stokes number is a very important parameter where particles are suspended in a fluid flow. The Stokes number is defined as the ratio of the particle momentum response time over a flow system time. Mathematically:

$$St = \frac{\tau_p}{\tau_c} = \frac{\rho_p d_p^2 / 18\mu_c}{L / u_c} \tag{4}$$

Three types of situations can be observed for particles (bubbles/droplets) suspended in fluid, namely: Case a) If $St<<1$, the response time of the particles is much less than the characteristic time associated with the flow field. In this case the particles will have ample time to respond to changes in flow velocity. Case b) $St \to 0$, where the two phases are in thermodynamic or velocity equilibrium.

Case c) If *St*>>1, then the particle will have essentially no time to respond to the fluid velocity changes and the particle velocity will be little affected by fluid velocity change [2]. The Reynolds number quantifies the relative importance of the inertial forces to viscous forces for given flow conditions. In many industrial applications with small droplets/bubbles in two-phase two component flows, the relative Reynolds number is an important parameter as this number determines whether the flow falls into the category of the Stokes flow or not. This number is also a benchmark to determine the appropriate drag coefficient (C_D). The particle or relative Reynolds number can be defined as follows:

$$\mathrm{Re}_p = \frac{\rho_c d_p \left| u_c - u_p \right|}{\mu_c} \tag{5}$$

If *Re*<<1, the two-phase flow would be termed the Stokes flow. In the Stokes flow regime viscous bubbles or drops remain spherical, regardless of the value of the Eötvös number [$Eo=gd_p^2(\rho_p-\rho_c)/\sigma$]. The Eötvös number can be used to characterize the shape of bubbles or drops moving in a surrounding fluid. Even at low relative Reynolds numbers, a wake is formed behind the sphere. This is a steady-state wake that becomes stronger as the Reynolds number increases and the inertia of the flow around the bubbles/droplets overcomes the viscosity effects on the surface of the bubbles/droplets [2]. The Froude number is another important number in two-phase gas/liquid horizontal flows, which is the ratio of inertial forces to gravitational forces. The Froude number is given by [33]:

$$Fr = \frac{u_m^2}{gD} \tag{6}$$

Total, or mixture, velocity can be defined as:

$$u_m = \frac{Q_c + Q_d}{A_d} = u_{cs} + u_{ds} \tag{7}$$

If there were no slip between phases, both the liquid and gas would flow at the mixture velocity. When $Fr < 1$, small surface waves can move upstream; when $Fr > 1$, they will be carried downstream; and when $Fr = 1$ (said to be the critical Froude number), the velocity of flow is equal to the velocity of surface

waves. The Weber number is a measure of the relative importance of the fluid's inertia compared to its surface tension. This quantity is useful in analyzing the formation of droplets and bubbles. If the surface tension of the fluid decreases, bubbles/droplets will have the tendency to decrease due to higher momentum transfer between the phases. The Weber number can be defined as:

$$We = \frac{Inertia}{Surface} = \frac{\rho_c u_c^2 L}{\sigma} = \mathrm{Re}^2 \left(\frac{Mo}{Eo} \right)^{-\frac{1}{2}} \tag{8}$$

here, *Re* is the Reynolds number, *Eo* is the Eotvos number, and *Mo* is the Morton Number [$g\mu_c^4(\rho_c-\rho_d)/\rho_c^2\sigma^3=We^3/FrRe^4$]. In addition to the above dimensionless numbers, the Ohnesorge number/Laplace number [$Oh=\sqrt{We}/Re=\mu/\sqrt{(\rho\sigma D)}=1/\sqrt{Lp}$] and Galileo number are [$Ga = gd_p^3(\rho_p-\rho_c)/v_c^2\rho_c^3$] are also two important numbers in two-phase gas/liquid flow in determining the critical Weber number and the motion of a bubble/droplet under the action of gravity in the gravity-driven viscous flow, respectively.

2.4. Advanced Pressure Measurement Techniques

In two-phase gas-liquid flow, accurate pressure predictions assist to evaluate design criteria to prevent rupture and pulsation [34]. Since the slug flow is a periodic phenomenon, if the frequency of the wave is near to the frequency of the structure, then it can lead to resonance and can increase damage risk to the conduit [1]. In two-phase gas-liquid flow, average density, flow velocity and flow regime prediction; in combination with transient void fractions can be extracted from the pressure pulse data [1, 35]. Pressure fluctuations can also be used to discover and locate leaks in long water tunnels and offshore pipelines [36]. In addition, studies show that the velocity and attenuation of the pressure waves are a function of the frequency and bubble radius [37]. Accurate prediction of the pressure drop in horizontal conduits is of great interest in many industries, especially in the oil industry.

A study [38] provided two-phase friction factor correlations based on 2,435 pieces of data from gas–liquid flow experiments in horizontal pipelines. They proposed several analytical expressions for the friction factor covering both laminar and turbulent two-phase gas-liquid flows, which were obtained by fitting the transition region between laminar and turbulent flows. However, in the aforementioned study the Reynolds number was based on the mixture velocity and the liquid kinematic viscosity. It will be more appropriate to calculate the Reynolds number and the friction factor for gas-liquid flow based on mixture kinematic viscosity rather liquid kinematic viscosity. The mixture properties are useful to predict a preliminary idea about the flow conditions. It also helps to use the single phase established correlations assuming two phases are acting as a mixture of one with no-slip between the phases. In two-phase gas/liquid flows, the mixture density and kinematic viscosity is lower than the single-phase liquid properties.

Dimensionless pressure gradients are usually expressed as friction factors. For a single-phase flow the Moody chart provides this friction factor reliably. The pipe roughness is an important factor in the Moody diagram. In a two-phase flow, the friction factor increases with 0.25 power of Reynolds number for turbulent flows [38]. In this study, novel Moody diagrams for gas-liquid flows in horizontal pipelines in terms of a mixture Fanning friction factor and mixture Reynolds number are proposed. The aforementioned study pointed out that pipe roughness does not have a major effect on turbulent gas-liquid, two-phase flow. However, the effects of interacting phases appear to dominate the effects of wall roughness. Previous studies [22, 39] used various combinations of dimensionless parameters to find out the relative error between the correlated and experimental values. The dimensionless parameters introduced by a study [38] are presented below. The mixture Fanning friction factor for the gas-liquid mixture, f_m, is defined as:

$$f_m = \frac{(\Delta P / L)D}{2\rho_m u_m^2} \tag{9}$$

where the pressure drop per unit length ($\Delta P/L$) in (N/m^3) is related to the wall shear stress ($\tau_w=D\Delta P/4L$) in (N/m^3), D is the pipe diameter (m), u_m ($=u_{sg}+u_{sl}$) is the mixture velocity (m/s), which is defined in terms of the superficial gas velocity ($u_{sg}=Q_g/\pi D^2$) and the superficial liquid velocity ($u_{sl} = Q_l/\pi D^2$). Q_g and Q_l are the gas and liquid volumetric flow rates; respectively. The mixture Fanning friction factor, f_m, was correlated with a mixture Reynolds number ($Re_m=u_m D/\upsilon_l$). In the aforementioned study it was thought that the frictional resistance of the mixture was mainly due to the liquid phase. A single composite equation that can be used to predict the mixture friction factors for a wide range of gas/liquid flow rates, viscosity values and different flow patterns was obtained by Beattie *et al.* and Patankar *et al.* [40, 41]. The equation was given by ($1\times10^3 \le \mathrm{Re} \le 1\times10^6$):

$$f_m = 0.0925\,\mathrm{Re}^{-0.2534} + \frac{13.98\,\mathrm{Re}^{-0.9501} - 0.0925\,\mathrm{Re}^{-0.2534}}{\left(1+\left(\frac{\mathrm{Re}}{293}\right)^{4.864}\right)^{0.1972}} \qquad (10)$$

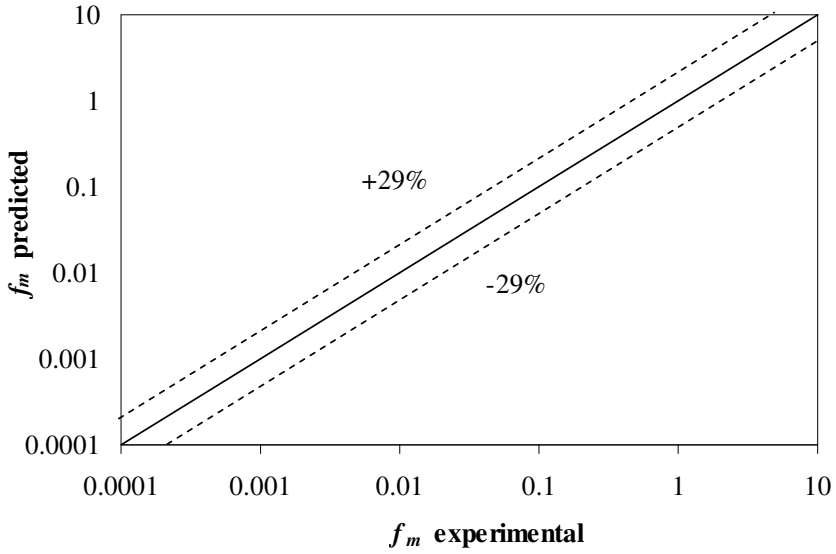

Fig. 2.1. Predicted mixture Fanning friction factor vs. experimental mixture Fanning friction factor for the universal composite correlation, adapted from [38]. Experiments were conducted for annular, dispersed bubble, slug, stratified smooth and stratified wavy flow.

The spread of the experimental data around the composite friction factor correlation is shown in Fig. 2.1. In this study, it was pointed out that the correlation had an average error of -4.27% and an average absolute error of 20.27%. The best agreements were obtained for slug and dispersed bubble flow data, with an average absolute error of 12.41% and 8.98%, respectively. The worst agreements were obtained for annular and stratified flow data, with an average absolute error of 38.65% and 34.57%, respectively. Garcia *et al.* [42] proposed the liquid holdup correlation in the following form:

$$h_L = e\,\mathrm{Re}^r (1-\lambda)^{l\,\mathrm{Re}^s} \tag{11}$$

where λ is the flow rate fraction ($\lambda = Q_l/[Q_g+Q_l]$). The friction factor correlations are in the form [42]:

$$f_m = h_L^p\ (1-\lambda)^n 16/\mathrm{Re}^m \tag{12}$$

Values of the parameters *e*, *r*, *l*, *s*, *p*, *n*, and *m* are 0.59, 0.1, 0.16, 0.17, -0.10, 1.12 and 0.96, respectively. The presence of the liquid holdup in the correlations shows that the friction factor is a function of the void fraction. It was pointed out that two flows with the same Reynolds number would give rise to different friction factors if the void fractions are different. Kabiri-Samani *et al.* [1] showed that more intensive phase interactions initiate stronger fluctuations. It was suggested that the maximum pressure inside the pipe would reach up to 10 times the upstream hydrostatic pressure. The experimental set-up used in the experiment [1] is depicted in Fig. 2.2. Zielinski *et al.* [43] showed that when the Reynolds number was greater than 10^4, the effects of viscosity could be neglected; in which case the dimensionless pressure head can be written as:

$$\frac{P}{h} = f(f_m, \alpha, Fr, St, We) \tag{13}$$

where, *P* is the pressure inside the pipe (Pa), *h* is the headwater ($ku_l^2/2g$ in m), K_f is the friction coefficient [$K_f = (f_m L)/D$, here, *L* is the characteristic slug wavelength].

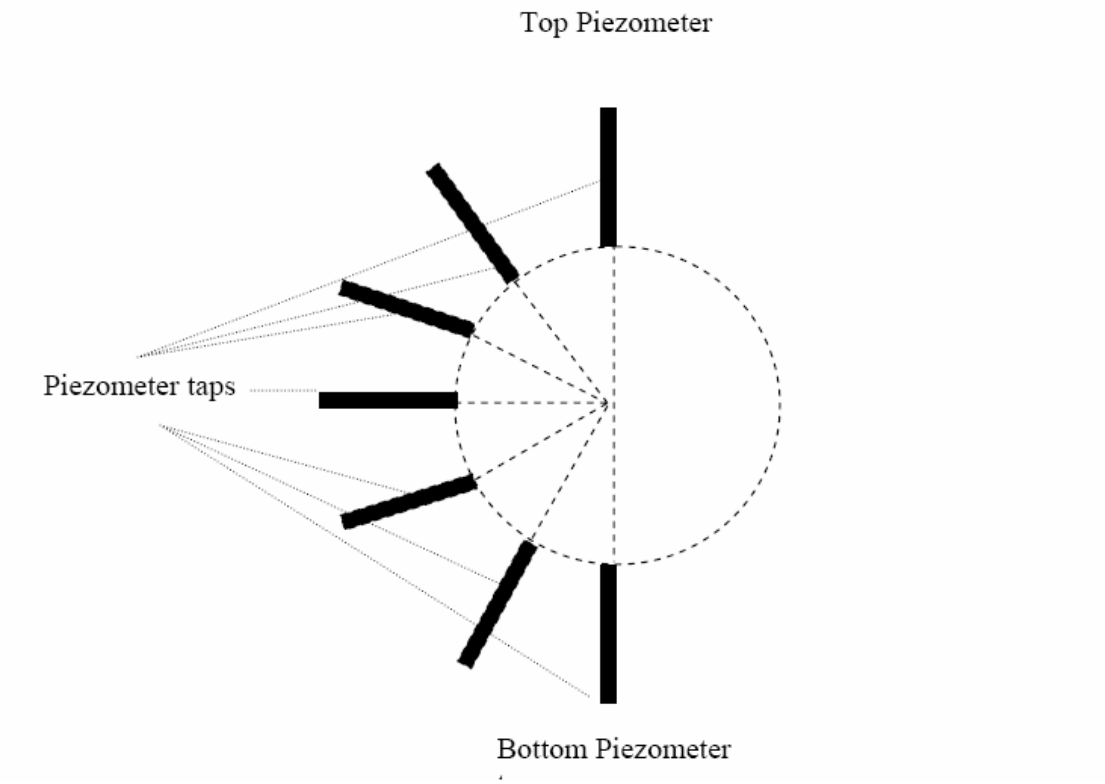

Fig. 2.2. The arrangement of pressure sensors at a pipe section. Adapted from [1].

The parameter f_m is the two-phase gas/liquid flow mixture friction factor can be expressed as [44]:

$$f_m = 0.08\left(\frac{u_m D}{x_m \mu_g + (1-x_m)\mu_l}\right)^{-0.25} \tag{14}$$

where u_m is the mixture velocity (m/s). D is the pipe diameter, α is the void fraction, Fr is the Froude number, St is the Strouhal number [$St=(2Df)/u_m$, f is the wave frequency), and We is the Weber number. In this study, a proposed equation for predicting the mean pressure in the air-water two-phase flow was introduced as below:

$$\frac{P}{h} = \frac{0.26 Fr^{1.43} K_f^{0.81} \alpha^{0.03}}{Sh^{0..19} C^{0.2} W^{0.26}} + 1.2 \tag{15}$$

Shedd *et al.* [45] used U-tube water manometers to measure pressure drops. In addition, an optical measurement was used to measure local liquid film thickness [46, 47]. The flow characteristics were: annular, horizontal two-phase flow, air and water as working fluid, a round (12.7 mm and 25.4 mm ID), and a square (15.2×22.7 mm) tube were used, both 6.5 m long. Ribeiro *et al.* [48] measured pressure drop using Validyne differential pressure transducers operating in the range of 225-500 mm H_2O. The pressure taps were 0.825 m apart. The pressure drop signal was recorded at a frequency of 250Hz for a period of 5 min. The flow characteristics were: two-phase, gas-liquid flow in horizontal conduits, air and water as working fluid, square cross-section channel (a height of 0.02425m and a length of 2.3m). Liquid flow rates of 2.77×10^{-2} kg/s to 2.88×10^{-2} kg/s and gas flow rates of 7.73×10^{-3} kg/s to 1.49×10^{-2} kg/s were used.

In addition to the above experimental techniques, there are several studies found in the literature that attempt to obtain a two-phase experimental pressure drop. Oscillatory characteristics and pressure drop in vertical two-phase churn flows were experimentally investigated [49]. In the aforementioned study, the vertical test tube was made from acrylic resin and the inner diameter was 25.8 mm. Wavy stratified two-phase, gas-liquid flow in the horizontal Plexiglas pipes of 0.024 m and 0.0508 m ID, superficial velocity of 510-25 m/s for air and 50-0.05 m/s for the liquid (electro-chemical solution) was investigated [50]. An analytical solution of gas wall, liquid wall and interfacial friction factors for two-phase horizontal co-current pipe flow was proposed and verified with reliable experimental data [51]. Two equations were proposed in attempt to predict liquid wall friction factors:

$$f_l = 0.263[(1-\alpha)\,\mathrm{Re}_{sl}]^{-.05} \tag{16}$$

$$f_l = 0.0262[(1-\alpha)\,\mathrm{Re}_{sl}]^{-.0.139} \tag{17}$$

here α is the void fraction and Re_{sl} is the Reynolds number based on liquid superficial velocity. The first equation can be used in small diameter pipes and the second equation can be used in large diameter pipes. However, in this study the dimension of the smaller and larger diameter pipes was indicted clearly.

2.5. Advanced Void Fraction Measurement Techniques

Void fraction or volume fraction, α, (as defined earlier) is an important parameter in two-phase gas-liquid flow. It has always been a challenge to measure volume fraction of the phases, due to the highly non-symmetric nature of two-phase gas-liquid horizontal flow, e.g. bubbles can coalesce, break-up, or interact with the conduit wall; which makes the flow extremely unstable. In the literature different types of techniques were implemented to measure the void fraction in two-phase, gas-liquid closed flow. Some of these are described in this section.

In several literature sources, particular emphasis is given to the Electrical Process Tomography methods, due to their inherent suitability for widespread online use [52]. A review article by Beck *et al.* [53] broadly explains the tomographic technique and the selection criteria of the sensors, which is listed in the following paragraph. As defined in the literature, the tomographic technology involves the acquisition of measurement signals from sensors located on the periphery of an object, such as a process vessel or pipeline. A tomographic system can measure the ratios of two phases within a resolved image element, even though the individual particles cannot be resolved. Optical, X-ray, γ-ray, and position emission tomography methods use electromagnetic radiation with approximate spatial resolution of 1% (percentage of diameter of cross section). The X-ray and γ-ray method are slow and radiation safety assurance is required. The position emission tomography method needs a labeled particle and the process is not on-line. Nuclear magnetic resonance uses electromagnetic resonance with an approximate spatial resolution of 1%. This is a fast and expensive method. Another complex to use method is the ultrasonic measurement, which uses acoustics with an approximate spatial resolution of 3%. Finally, the capacitive, conductive and inductive methods work through the measurement of electrical properties of different phases with an approximate spatial resolution of 5%. This method is fast, low cost and suitable for either a small or large scale experimental set-up. When greater temporal resolution is required (up to 100 frames per

second), the electrical tomographic measurement is beneficial. Whereas when greater spatial resolution is required (0.4 mm), the X-ray tomography is beneficial [54]. Electrical capacitance tomography (ECT) to image multiphase flows for inner diameter exceeding 1m was conducted with good performance in regard to resolution, linearity and stability [55]. An online and rapid direct flow-pattern identification method using electrical capacitance tomography was also proposed without the need for imaging [56].

The void fractions in bubbly flows were investigated by several researchers using optical probes [57-59]. A fiber optics method was implemented to measure the void fraction. It was found that the rise time of the signal pulses were created when bubbles crossed the probe tip and were closely correlated with the bubble velocities. Therefore, bubble velocities and hence bubble sizes could be estimated using a single probe. It was observed that the correlation between the rise time and the bubble velocity varied significantly between probes, but was only a weak function of water type (i.e., freshwater or seawater) and the bubble impaction angle. This method provided high accuracy and stable measurements. The size and velocity of each bubble were measured with this method. This method was also applicable for non-conductive fluid. However, the use of fiber optic probes to measure very small void fractions was not recommended because of the large errors that were anticipated [57]. The effect of bubble deflection is expected to be more pronounced as the bubble radius and velocity decrease and as the liquid viscosity increases [58]. In the aforementioned study the bubble diameters ranged from approximately 1 to 6 mm and the bubble velocities ranged from 5 to 120 cm/s, while the water velocity varied from 45 to 92 cm/s. Changa *et al.* [60] used an optical signal derived from a diode laser driven by a constant current then launched into a single-mode optical fiber and transmitted, through a fiber coupler, to the signal fiber (125 μm in diameter) inserted into the test fluid. By analyzing the signal, the velocity and void fraction ratio of each phase could be obtained. However, there is intrusion to the fluid by the tiny fiber probe. Pettigrew *et al.*

[61] developed a fiber-optic probe to measure local void fraction. Each probe has a conical tip and is made from an optical fiber of 170 μm diameter. Application of a dual optical probe for local volume fraction, drop velocity and drop size measurements in a kerosene-water, liquid-liquid, two-phase flow was also investigated [62]. In the experiment, measurements were carried out in a large-scale vertical two-phase facility, mainly at the pipe center-line, to demonstrate the advantages of using optical fibers with normal cut ends in a kerosene-water, two-phase flow. High reliability of this measurement technique for detailed studies of the drop component of liquid-liquid, two-phase flow could be possible. Other previously used fiber optic techniques can be found in the literature [63-66].

Several researchers conducted void fraction determination by means of multibeam gamma-ray densitometers. Several studies on implementing gamma-ray densitometers showed that multi-beam gamma-ray densitometers with detector responses examined by neural networks can analyze a two-phase flow void fraction with high accuracy [67, 68]. Void fraction and flow regime in oil/gas pipes could be measured with an error of 3% for all of the flow regimes. Oil-water two-phase flow experiments were conducted in a 15m long, 8.28 cm diameter, inclinable steel pipe using mineral oil (density of 830 kg/m^3 and viscosity of 7.5 mPa.s) and brine (density of 1060 kg/m^3 and viscosity of 0.8 mPa.s) [69]. In addition, other research results showed that mixture densities obtained with gamma-ray densitometers agree well with the direct measurements made by using quick-closing valves [70]. One of the disadvantages of the gamma-ray densitometers is the shielding requirement of the gamma-ray.

Various attempts have been made in the past to measure the void fraction of two-phase bubbly liquid flows using capacitive sensors. Capacitance sensors for instantaneous void fraction in air-oil, two-phase flow were developed [71-73]. This method could effectively identify the different flow regimes although it was not effective while there was high water loading. In addition, synchrotron X-rays

[74], pulsed neutron technique [75], conductance probes [76], ultrasonic technique [77] and ring impedance probes [78] have been used successfully to measure the void fraction in two-phase flow systems.

One of the more recent techniques is the microwave flow sensor [79]. Using radio frequency signals, the non-invasive meter will measure the mass-flow, quality and void fraction of any non-conducting vapor-liquid mixture. This method can identify the quality and void fraction. These sensors are good for cryogens, refrigerants and low flow rate two-phase, gas-liquid flow. Since these instruments are entirely data-driven, the results depend heavily on the amount and quality of the data that is acquired for a given application. The probe however, cannot measure mixtures with significant water content.

Quick-closing valves provide an exact void fraction measurement and are useful for calibrating or comparing against other methods. Void fraction of two-phase flow is often measured by isolating a section in the conduit [80-85] termed the quick-closing-valve (QCV) technique. However, most of the studies were conducted in a vertical bubble column. A technique for synchronizing valves and determining bubble rise velocities in two-phase flow is presented in a study by [86]. It is very crucial to commence the closing of both valves simultaneously. Error in void fraction measurements by the QCV method due to asynchronization of the valves can be expressed as [86]:

$$\% \qquad Error = \frac{100 u_m t_{ac} (1-\alpha)}{\alpha \, l_c} \tag{18}$$

here, u_m is the mixture velocity in the conduit, α is the void fraction, t_{ac} is the asynchronization closing time, and l_c is the closing length between the two valves. Previous studies showed that for a two-phase bubble flow at low flow rates and a closing length of 5m, for each millisecond of delay there would be 1% error.

2.6. Advanced Photonics and Image Analysis Techniques

The flow regime description obtained by the photonics measurement [87] is described in this section. Description of the different flow patterns is depicted in Fig 2.3. The stratified flow regime is characterized by a complete separation of the liquid and gas phases. When both of the liquid and gas flows are laminar and no fluctuations at the flow interface can be detected, the flow pattern is called stratified (stratified smooth). As the gas mass flow rate is increased, instabilities form at the liquid-gas interface due to the interfacial velocity differential (termed as Kelvin-Helmholtz instability). This flow pattern is called wavy flow (stratified wavy) and is characterized by the formation of small interfacial waves. In larger diameter tubes these waves can amplify, producing a crest. These waves are easier to detect in large diameter tubes and the wave height can be large enough to allow the waves to break up. In small diameter tubes [87] large breaking waves were typically not observed. The intermittent flow regime is characterized by discontinuities in the liquid and gas flow. Elongated bubble flow (plug flow) is characterized by a continuous stream of gas plugs flowing in the liquid. A thin film of liquid coats the tube wall and surrounds the gas plug. Small disturbances may exist fore and aft of the bubbles, but as a whole the plugs remain intact and uniform. As the gas mass flow rate is increased, these disturbances amplify until the aft portion of the plug breaks apart into smaller bubbles. At this point, the flow pattern becomes slug flow.

The annular flow regime consists of a nearly complete separation of liquid and gas along the circumference of the tube wall. The first form of annular flow occurs when the surfaces of waves in wavy flow amplify to the extent that they touch the top of the tube wall. This flow pattern is known as wavy-annular flow (pseudo slug flow). As the gas mass flow rate is increased, the liquid is pushed up around the circumference of the tube wall by the increase in the gas momentum and falls downward under gravity in the form of annular waves. When the liquid coats the tube wall completely (forming an annular ring of the liquid phase) and

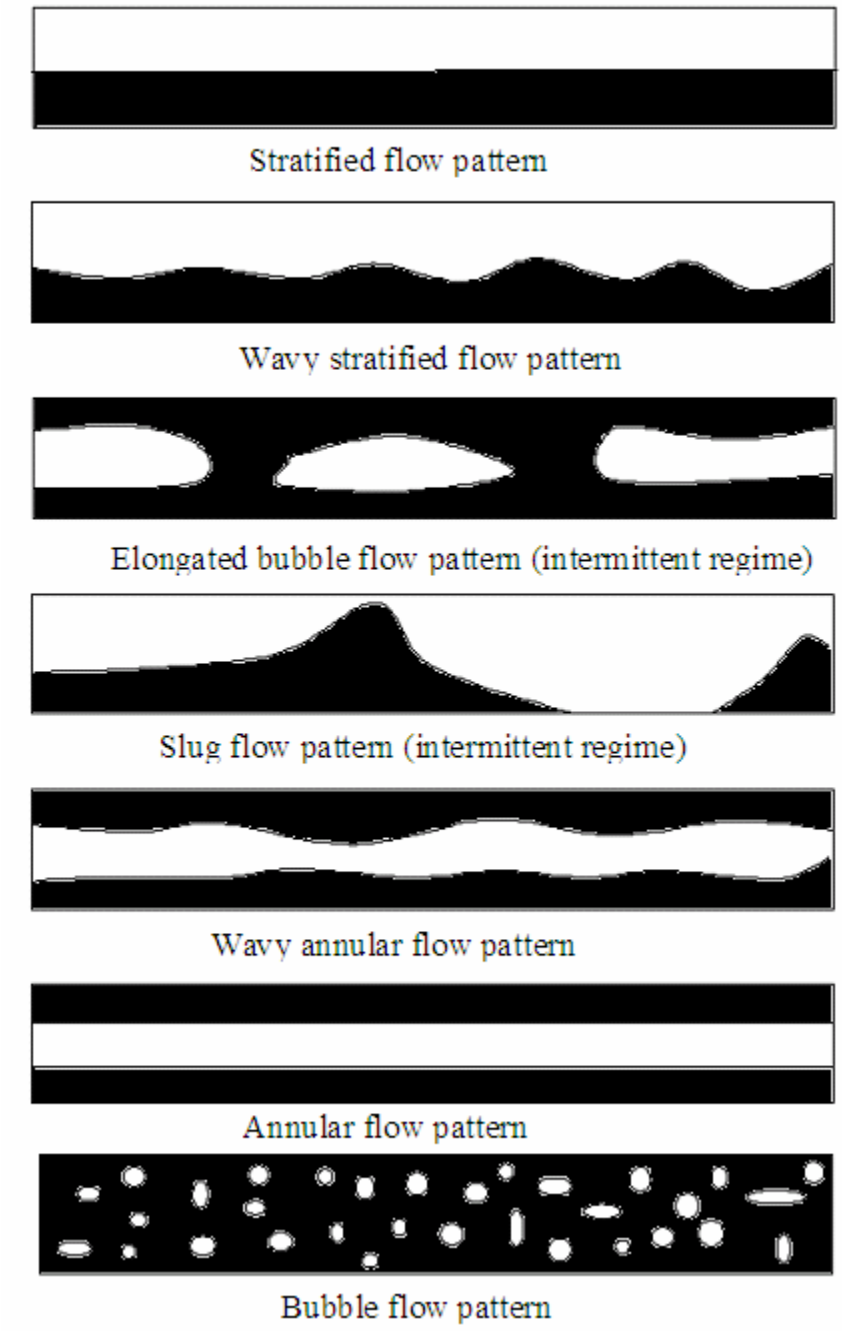

Fig. 2.3. Description of flow regimes and patterns. Adapted from [87]. The black part indicates liquid phase and white part indicates gas phase.

the gas flows through the core of the tube, the flow pattern is known as annular flow. Dispersed flow occurs when the liquid flow is turbulent and the gas phase is in laminar or turbulent flow. When the gas flow is laminar, small bubbles are driven by buoyant forces and flow primarily in the top half of the tube. This pattern is known as bubble flow. As the Reynolds number of the gas increases, keeping other variables constant, the bubble size decreases and the bubbles begin to disperse across the entire tube cross section. This flow pattern is known as dispersed bubble or dispersed flow.

Flow patterns for concurrent air-water mixtures in horizontal round and rectangular tubes were determined by high-speed video analysis to develop flow regime maps and the transitions between these flow regimes [87]. In this study, gas and liquid superficial velocities ranged from 0.10 to 100 m/s, respectively. The test sections for the round tubes were made of Pyrex glass. Liquid and gas flow rates ranged from 0.013 to 8.331 m^3/s and 0.002 to 1.18 m^3/s, respectively. The uncertainties in the flow rate measurements were estimated to be $\pm 4\,\%$. The recording equipment used was a Canon ES5000 8 mm video camera with a zoom range of 40X. A shutter speed of 0.0001s and a frame speed of 0.003 s were used. Four different types of round tubes were examined in this study at: 5.5 mm, 2.6 mm, 1.75 mm and 1.30 mm. They observed several flow patterns such as bubbly, dispersed, elongated bubble, slug, stratified, wavy, wavy annular and annular flow patterns. Further studies on advanced photonics measurements can be found in the literature [45, 88-102].

In the literature, different flow pattern maps were proposed to predict the two-phase gas/liquid flow regimes. Although in the literature these flow maps were investigated for larger length scale experimental set-ups, the applicability of these maps to a smaller length scale set-up was not conducted extensively. In this context, in the present study the different flow maps were tested for different flow input conditions in order to determine the best flow map for the present nozzle

assembly. A brief theory behind the different flow maps are described in this section.

2.6.1. Taitel and Dukler Flow Maps [87, 103]

Taitel and Dukler attempted to predict the flow regimes for concurrent gas-liquid flow in pipes using a momentum balance (Fig 2.4). The momentum balance was non-dimensionalized with respect to D for length, D^2 for area, u_{sg} for gas velocities, and u_{sl} for liquid velocities. Flow regime transition was defined by a set of non-dimensional parameters, such as X, F, K and T.

$$X = \left[\frac{(dP/dx)_l}{(dP/dx)_g} \right]^{1/2} \tag{19}$$

$$Fr = \frac{\rho_g u_{gs}}{\sqrt{\rho_g (\rho_l - \rho_g) Dg}} \quad \text{or} \quad F = \sqrt{\frac{\rho_g}{(\rho_l - \rho_g)}} \frac{u_{gs}}{\sqrt{Dg\cos\theta}} = \sqrt{\frac{\rho_g}{(\rho_l - \rho_g)}} Fr^{1/2} \tag{20}$$

here, X is the Martinelli parameter, F is modified Froude number, θ is the angle of inclination, D is the diameter of the tube, x is the axial direction, and P is the pressure inside the conduit.

$$K = \left[\frac{\rho_g \rho_l u_{sg}^2 u_{sl}}{(\rho_l - \rho_g) g \mu_l \cos\theta} \right]^{1/2} \tag{21}$$

$$T = \left[\frac{(dP/dx)_l}{(\rho_l - \rho_g) g \mu_l \cos\theta} \right]^{1/2} \tag{22}$$

here, g is the gravity, and μ is the dynamic viscosity.

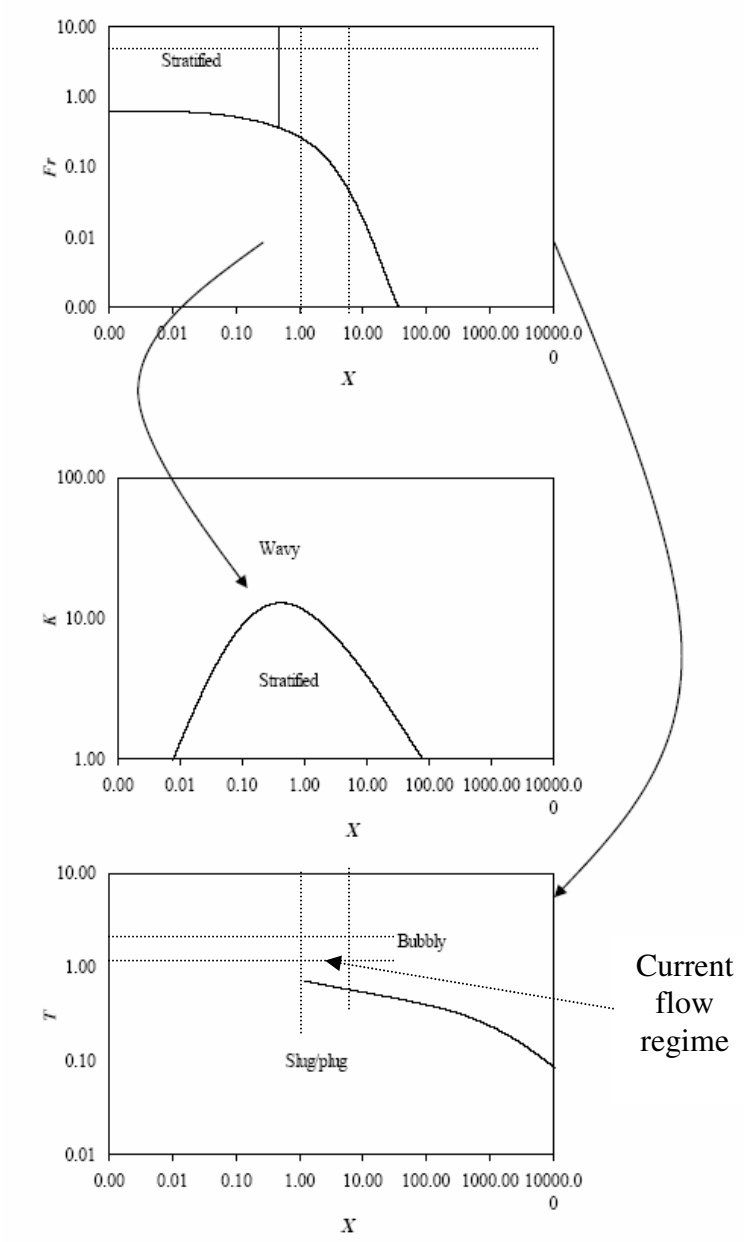

Fig. 2.4. Taitel and Dukler [103] map for flow pattern determination in a horizontal tube. Here, *X* is the Martinelli parameter, *Fr* is the Froude number, *K* and *T* are another two dimensionless numbers. Based on the value of *X* and *Fr* number the flow pattern is either stratified or bubbly or slug flow. More explanation on the flow pattern identification for the current experiment (for 6-15 m/s and 20-50 m/s liquid flow rate and gas flow rate, respectively) by the author can be found in Fig. 8.6.

2.6.2. Breber Map [104]

A Breber map is depicted in Fig. 2.5. This map is divided into square regions, which is easier to implement. This map makes use of the Martinelli number and the Wallis factor as axes. The Wallis factor is defined as:

$$j_g = \frac{\rho_l u_{sl} x_q}{\sqrt{D\, g \rho_g (\rho_l - \rho_g)}} \tag{23}$$

whereas the Martinelli number is defined as:

$$X = \left(\frac{1-x_q}{x_q}\right)^{0.9} \left(\frac{\rho_g}{\rho_l}\right)^{0.5} \left(\frac{\mu_l}{\mu_g}\right)^{0.1} \tag{24}$$

here x_q is the quality. A study [105] conducted an experiment to investigate the validity of the Breber map and found out that there was a good consistency between the experimental result and the Breber map.

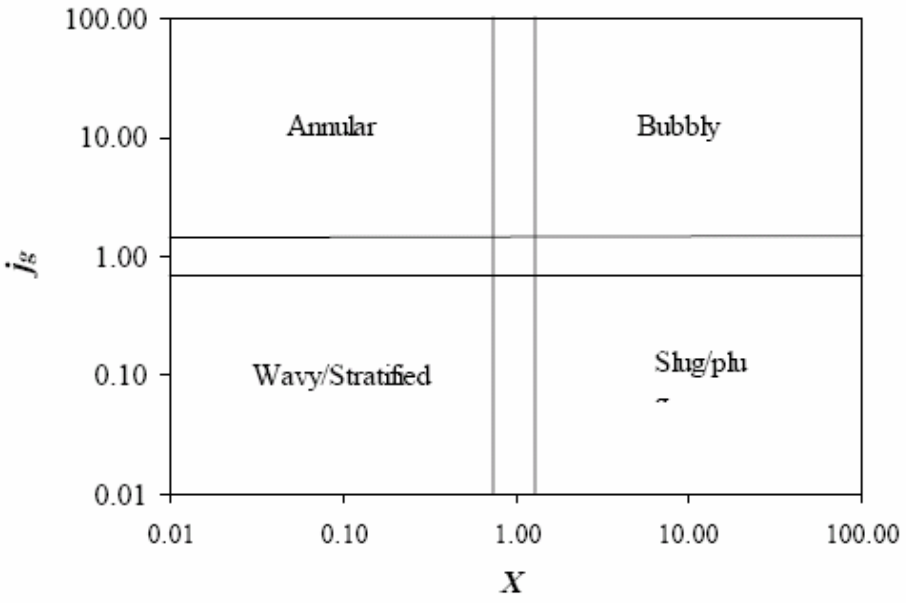

Fig. 2.5. Breber [106] flow transition map for determining the flow pattern in two-phase flow in a horizontal tube. For the current flow conditions the flow regime is out of the graph.

2.6.3. Baker Map [104]

The Baker [107] map for air-water flow is depicted in Fig. 2.6. The axes are defined in terms of $u_{sg}\,\rho_g/\zeta$ and $u_{sl}\,\rho_l/\zeta$, where, $u_{sg}\rho_g = G_s$ =mass flux of gas phase (kg/m^{2}s) = (gas mass flow rate/tube cross-sectional area) and $u_{sl}\rho_l = G_L$ =mass flux of liquid phase (kg/m^{2}s) = (liquid mass flow rate/tube cross-sectional area). The parameter λ and ψ are defined as follows:

$$\lambda = \left(\frac{\rho_g \rho_l}{\rho_{air} \rho_{water}} \right)^{1/2} \tag{25}$$

$$\psi = \frac{\sigma_{water}}{\sigma} \left(\frac{\mu_l}{\mu_{water}} \left[\frac{\rho_{water}}{\rho_l} \right] \right)^{1/3} \tag{26}$$

where, ρ_l is the liquid density (kg/m^3), ρ_g is the gas density (kg/m^3), ρ_{water} =1000 kg/m^3 is the density of water, ρ_{air} = 1.23 kg/m^3 is the density of air; μ_l is the liquid viscosity (N.s/m^2), μ_{water} = 10x10^{-3} N.s/m^2 is the viscosity of water; σ is the surface tension (N/m) and σ_{water} = 0.072 N/m is the surface tension of air-water. The Baker map works well for water/air and oil/gas mixtures in tubes with smaller diameters, not bigger than 50 mm [108].

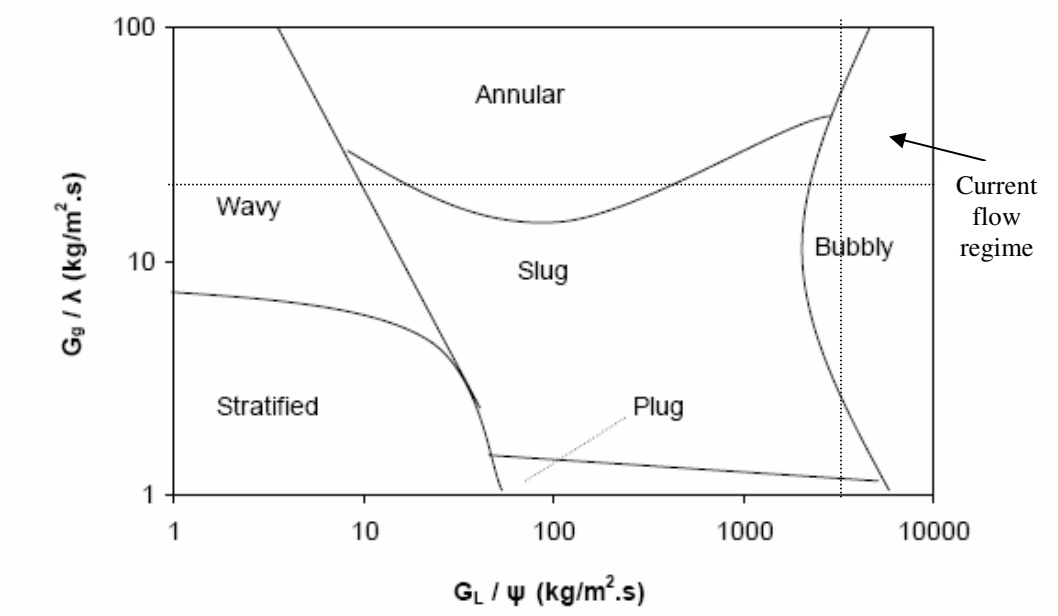

Fig. 2.6. Baker [107] flow pattern map for horizontal flow in a tube. The flow regime for the current experiment can be found in Table 8.4.

Data obtained from Mandhane *et al.* [109] was consistent with the Taitel and Dukler map for a 25 mm diameter tube. For smaller tubes, a large deviation from the Taitel and Dukler map was reported [110]. Visual identification of the flow regimes was plotted on the flow regime map, which has been proposed [106] for condensation application. The results indicated consistency between the observations and the trends predicted by the Breber map.

2.7. Bubble Size in Two-Phase, Air-Water Horizontal Flows

Effective prediction of bubble size, density and distribution is crucial in two-phase, two-component flows. Due to highly non-uniform volumetric flow distribution and intermittency in the flow, it is extremely difficult to predict accurate bubble size distribution in this type of flow. Thus, a fairly reliable statistical tool is required to find out the uncertainty level in the bubble size estimation. In petro-chemical process industries most of the light crude oil upgrading processes is associated with two-phase, two-component flows in the feeding conduit of the nozzles. Atomization from the nozzle strongly depends on bubble size in the feeding conduit. Thus, it is essential to have a good understanding and a reasonable estimate of the effect of turbulent two-phase, two-component gas (steam/air) and liquid (bitumen/water) flow on bubble size distribution. This knowledge would assist in the design and operation of a system that can achieve high product yield. To the author's knowledge, there are very few studies that have been conducted for the prediction of bubble size in two-phase, air-water horizontal flows [111-114]. There are also several studies found in the literature on the transport phenomena of two-phase, two-component gas and liquid flows through pipelines [4, 115-126].

A backscatter technique was used to examine drop size distributions in a 0.063 m pipe (both horizontal and vertical alignment) for a two-phase mixture of kerosene and aqueous potassium carbonate solution. In a recent study, images of droplets or

particles produced by shadowgraph via back-illumination using an infrared diode laser were investigated with a digital image analysis technique [127]. This technique was potentially capable of sizing particles of arbitrary shape and size and with a wide dynamic range. Yule *et al.* [128] observed biasing effects for a given depth-of-field, with small droplets being less detectable. Measured image diameters were also found to increasingly underestimate the true diameter with increasing defocus distance [128]. Lecuona *et al.* [129] implemented a digital-based image analysis system for the experimental determination of size, spatial distribution and two components of velocity for particles suspended in any clear fluid flow.

2.8. Conclusions

In this chapter, several advanced two-phase, gas-liquid measurement techniques with greater emphasis in the horizontal flow cases were examined. I focused on two-phase pressure, void fraction and bubble size distribution measurement techniques. Due to the highly non-symmetric nature of two-phase gas-liquid horizontal flow systems, it has always been a challenge to obtain accurate data in this type of flow. In addition, the success of pressure and void fraction measurements in gas/liquid horizontal flow largely depends on the respective flow regime; whether it is dispersed, slug or stratified flow. Measurement accuracy and characteristics depend on the phase velocity and air-to-liquid ratio. In the literature, most of the studies were conduced on vertical bubble columns rather than in a horizontal alignment. Based on pressure and photonics measurements in two-phase gas/liquid flow, several empirical equations have been developed.

High performance dynamic and static pressure transducers would be reliable instruments in two-phase gas/liquid pressure measurements. Most of the void fraction measurements were intrusive in nature. Other methods have safety issues and accuracy challenges. However, the mechanical quick-closing-valve technique has been proven to be a more reliable and easy-to-implement method if the

synchronization of the two closing valves can be assured. Also the online electrical process tomography method would be a valuable measurement tool in future to evaluate void fractions in multiphase flows. High-speed video and photonics measurements are also very reliable, non-intrusive volume fraction and flow pattern estimation techniques; especially if one wants to measure unclosed multiphase flow behaviour (e.g. in spray). Generally, there are three kinds of methods used to identify two-phase flow regimes. The first one is the direct method. This method includes the direct identification of the flow regimes as to flow forms, such as the high-speed photography method. The second is the indirect method. This method includes the statistical analysis of measured signals, which reflect the fluctuant characteristic of two-phase flows and the flow regimes. The third is the intrusive method. This method includes the placement of high performance sensing probes inserted inside the conduit, which provide a time varying signal. This method disturbs the local flow field significantly and in some cases could provide erroneous information. To the author's knowledge, these different types of photonics measurements (high-speed photography, shadowgraphy, stroboscopic back scattered imagery, high power pulsed laser) would be able to accurately provide the flow structure of two-phase gas/liquid flow. Information obtained from these photonics measurements could be coordinated with the flow transition maps and correlations provided by several researchers. However, most of the flow maps and correlations are designed for rectangular, vertical and large diameter tubes.

2.9. References

[1] Kabiri-Samani, A.R., Borghei, S.M. and Saidi, M.H. (2007) Fluctuation of air-water two-phase flow in horizontal and inclined water pipelines. Journal of Fluids Engineering-Transactions of the Asme. 129 (1): 1-14.

[2] Crowe, C.T. (2006) Multiphase flow handbook Boca Raton, FL CRC: Taylor & Francis.

[3] Kleinstreuer, C. (2003) Two-phase flow: theory and applications, New York, NY, Taylor & Francis.

[4] Andreussi, P., Paglianti, A. and Silva, F.S. (1999) Dispersed bubble flow in horizontal pipes. Chemical Engineering Science. 54 (8): 1101-1107.

[5] Chen, X.T., Cai, X.D. and Brill, J.P. (1997) A general model for transition to dispersed bubble flow. Chemical Engineering Science. 52 (23): 4373-4380.

[6] Gomez, L.E., Shoham, O., Schmidt, Z., Chokshi, R.N., Brown, A. and Northug, T. (1999) Unified Mechanicstic Model for Steady-State Two-Phase Flow in Wellbores and Pipelines. In proceedings-SPE Annual Technical Conference, 3–6 October, Houston.

[7] Daniels, L. (1995) Dealing with two-phase flows. Chemical Engineering. 102 (6): 70-78.

[8] Delhaye, J.M. (1981) Two-phase flow patterns: Thermohydraulics of Two-Phase Systems for Industrial Design and Nuclear Engineering, New York, NY, McGraw-Hill.

[9] Ishii, M. and Hibiki, T. (2005) Thermo-fluid Dynamics of Two-Phase Flow US, Springer.

[10] Ni, J. and Beckermann, C. (1991) A Volume-Averaged 2-Phase Model for Transport Phenomena During Solidification. Metallurgical Transactions B-Process Metallurgy. 22 (3): 349-361.

[11] Soo, S. (1990) Multiphase Fluid Dynamics, Beijing, P.R.C. and Gower Technical, Brookfield, MA, Science Press.

[12] Whitaker, S. (2006) The Method of Volume Averaging, US, Springer.

[13] Boure, J.A. and Delhaye, J.M. (1982) General equations and two-phase flow modeling, handbook of multiphase system, New York, NY, McGraw-Hill.

[14] Yadigaroglub, G. and JrLahey, R.T. (1976) On the various forms of the conservation equations in two-phase flow. International Journal of Multiphase Flow. 2 (5-6): 477-494.

[15] Banerjee, S. and Chan, A.M.C. (1980) Separated Flow Models .1. Analysis of the Averaged and Local Instantaneous Formulations. International Journal of Multiphase Flow. 6 (1-2): 1-24.

[16] Drew, D.A. (1991) Two-fluid modeling, Troy, NY, Renseelaer Polytecnic Institute.

[17] Lahey, R.T.J. and Drew, D.A. (1988) The three-dimensional time and volume averaged conservation equations of two-phase flow, New York, NY, Plenum Press.

[18] Ransom, V.H. and Ramshaw, J.D. (1992) Discrete modeling considerations in multiphase fluid dynamics Coca Raton, FL, CRC press.

[19] Taylor, G.I. (1932) The viscosity of a fluid containing small drops of another fluid. Proceedings of the Royal Society of London Series. 138 (834): 41-48.

[20] Wallis, G.B. (1969) One-Dimensional Two-Phase Flow, New York, NY, McGraw-Hill.

[21] Brady, J.F. (1984) The Einstein Viscosity Correction in N-Dimensions. International Journal of Multiphase Flow. 10 (1): 113-114.

[22] Dukler, A.E., Wicks, M. and Cleveland, R.G. (1964) Frictional Pressure Drop in Two-Phase Flow: An Approach Through Similarity Analysis. AIChE.J. 10: 44-51.

[23] McAdams, W., Wood, W. and Bryan, R. (1942) Vaporization inside Horizontal Tubes-II-Benzene-Oil Mixtures. Trans. ASME. 64: 193.

[24] Cicchitt, A.L.C. and Silvestri, M. (1960) Two-Phase Cooling Experiments Pressure Drop,Heat Transfer and Burnout Measurement. Energia Nuclear. 7 (6): 407-425.

[25] Zuber, N. and Findlay, J.A. (1965) Average volumetric concentration in two-phase flow systems. Journal of Heat Transfer. 87: 453-468.

[26] Kroeger, P.G. and Zuber, N. (1968) An Analysis of Effects of Various Parameters on Average Void Fractions in Subcooled Boiling. International Journal of Heat and Mass Transfer. 11 (2): 211-233.

[27] Ishii, M. (1976) Drift flux model and derivation of kinematic constitutive laws: two-phase flow and heat transfer, Washington DC, Hemisphere Publication Corporation.

[28] Li, A. and Ahmadi, G. (1995) Computer-Simulation of Particle Deposition in the Upper Tracheobronchial Tree. Aerosol Science and Technology. 23 (2): 201-223.

[29] Kim, C. and Iglesias, A. (1989) Deposition of inhaled particles in bifurcating airway models: I. Inspiratory deposition. Journal of aerosol medicine. 2: 1-14.

[30] Li, A. and Ahmadi, G. (1992) Dispersion and Deposition of Spherical-Particles from Point Sources in a Turbulent Channel Flow. Aerosol Science and Technology. 16 (4): 209-226.

[31] Patankar, N.A. and Joseph, D.D. (2001) Modeling and numerical simulation of particulate flows by the Eulerian-Lagrangian approach. International Journal of Multiphase Flow. 27 (10): 1659-1684.

[32] Snider, D.M., O'Rourke, P.J. and Andrews, M.J. (1998) Sediment flow in inclined vessels calculated using a multiphase particle-in-cell model for dense particle flows. International Journal of Multiphase Flow. 24 (8): 1359-1382.

[33] Brill, J.P. and Mukherjee, H. (1999) Multiphase Flow in Wells, Henry L. Doherty Series, Society of Petroleum Engineers, Richardson, TX, Henry L. Doherty Series, Society of Petroleum Engineers.

[34] Baruna, S., Shamara, Y. and Brosius, M.G. (1990) Two-Phase Flow Model Aids Flare Network Design. Oil & Gas J. 90 (4): 90–94.

[35] Gudmundsson, J.S. (1994) Method for Determination of Flow Rate Especially Two-Phase Flow, Norwegian Patent, No. 944264, 1994.

[36] Erickson, D. and Twaite, D. (1996) Pipeline Integrity Monitoring System for Leak Detection, Control, Optimization of Wet Gas Pipelines. SPE-36607, Brown and Root, eds., Multi-Phase Solutions, Denver.

[37] Lahey, R.T. (1991) Void wave propagation phenomena in two-phase flow. A.I.Ch.E. Journal. 37 (1): 123–173.

[38] Garcia, F., Garcia, R., Padrino, J.C., Mata, C., Trallero, J.L. and Joseph, D.D. (2003) Power law and composite power law friction factor correlations for laminar and turbulent gas-liquid flow in horizontal pipelines. International Journal of Multiphase Flow. 29 (10): 1605-1624.

[39] Beggs, H. and Brill, J. (1973) A study of two-phase flow in inclined pipes. J. Pet. Technol. 25: 607–617.

[40] Beattie, D. and Whalley, P. (1982) A simple two-phase frictional pressure drop calculation method. Int. J. Multiphase Flow. 83–87.

[41] Patankar, N.A., Joseph, D.D., Wang, J., Barree, R.D., Conway, M. and Asadi, M. (2002) Power law correlations for sediment transport in pressure driven channel flows. International Journal of Multiphase Flow. 28 (8): 1269-1292.

[42] Garcia, F., Garcia, R., Padrino, J.C., Mata, C., Trallero, J.L. and Joseph, D.D. (2003) Power law correlations for gas/liquid flow in a flexible pipeline simulating terrain variation. Int. J. Multiphase Flow. 29 1605–1624.

[43] Zielinski, P.B. and Willemonte, J.R. (1968) Effect of Viscosity on Vortex-Orifice Flow. J. Hydr. Div., ASCE. 94 (3): 195–205.

[44] Levy, S. (1999) Two-Phase Flow in Complex Systems, New York, Wiley.

[45] Shedd, T.A. and Newell, T.A. (2004) Characteristics of the liquid film and pressure drop in horizontal, annular, two-phase flow through round, square and triangular tubes. Journal of Fluids Engineering-Transactions of the Asme. 126 (5): 807-817.

[46] Hurlburt, E.T. and Newell, T.A. (1996) Optical measurement of liquid film thickness and wave velocity in liquid film flows. Exp. Fluids. 21 (5): 357–362.

[47] Shedd, T.A. and Newell, T.A. (1998) Automated optical liquid film thickness measurement method. Rev. Sci. Instrum. 69 (12): 4205–4213.

[48] Ribeiro, A.M., Ferreira, V. and Campos, J.B.L.M. (2006) On the comparison of new pressure drop and hold-up data for horizontal air–water flow in a square cross-section channel against existing correlations and models. International Journal of Multiphase Flow. 32: 1029–1036.

[49] Sawai, T., Kaji, M., Kasugai, T., Nakashima, H. and Mori, T. (2004) Gas–liquid interfacial structure and pressure drop characteristics of churn flow. Experimental Thermal and Fluid Science. 28: 597–606.

[50] Vlachos, N.A. (2003) Studies of Wavy Stratified and Stratified/Atomization Gas-Liquid Flow. Journal of Energy Resources Technology, Transactions of the ASME. 125: 131-136.

[51] Cole, J.S., Donnelly, G.F. and Spedding, P.L. (2004) Friction factors in two-phase horizontal pipe flow. International Communications in Heat and Mass Transfer. 31 (7): 909-917.

[52] Plaskowski, A., Beck, M.S., Thorn, R. and Dyakowski, T. (1995) Imaging Industrial Flows: Applications of Electrical Process Tomography
Bristol, UK, Philadelphia Institute of Physics Pub.

[53] Beck, M.S., Dyakowski, T. and Williams, R.A. (1998) Process Tomography - the state of the art. ransactions of the Institute of Measurement and Control. 20 (4): 163-177.

[54] Reinecke, N., Petritsch, G., Schmitz, D. and Mewes, D. (1998) Tomographic Measurement Techniques - Visualization of Multiphase Flows. Chem. Eng. Technol. 21 (1): 7-18.

[55] Shao, F. and Mong, Q. (1999) A method for measuring low capacitance for tomography. Review of Scientific Instruments. 70 (7): 3177-3179.

[56] Jeanmeure, L.F.C., Dyakowski, T., Zimmerman, W.B.J. and Clark, W. (2002) Direct flow-pattern identification using electrical capacitance tomography. Experimental Thermal and Fluid Science. 26 763–773.

[57] Cartellier, A. (1990) Optical probes for local void fraction measurements: Characterization of performance. Rev. Sci. Instrum. 61 (2): 874–886.

[58] Cartellier, A. and Achard, J.L. (1991) Local phase detection probes in fluid/fluid two-phase flows. Rev. Sci. Instrum. 62 (2): 279–303.

[59] Serdula, C.D. and Loewen, M.R. (1998) Experiments Investigating the Use of Fiber-Optic Probes for Measuring Bubble-Size Distributions. EEE Journal of Oceanic Engineering. 23 (4): 385-339.

[60] Changa, K., Lim, H. and Su, C.B. (2003) Fiber optic reflectometer for velocity and fraction ratio measurements in multiphase flows. Rev. Sci. Instrum. 74 (7): 3559-3565.

[61] Pettigrew, M.J., Zhang, C., Mureithi, N.W. and Pamfil, D. (2005) Detailed flow and force measurements in a rotated triangular tube bundle subjected to two-phase cross-flow. Journal of Fluids and Structures. 20 (4): 567-575.

[62] Hamad, F.A., Pierscionek, B.K. and Bruun, H.H. (2000) A dual optical probe for volume fraction, drop velocity and drop size measurements in liquid-liquid two-phase flow. Measurement Science & Technology. 11 (9): 1307-1318.

[63] Miller, N. and Mitchie, R.E. (1970) Measurement of local voidage in liquid/gas two-phase flow systems. J. Br. Nucl. Energy Soc. 9: 94–100.

[64] Calderbank, P.H. and Pereira (1977) The prediction of distillation plate efficiencies from froth properties J Chem. Eng. Sci. 32: 1427–1433.

[65] Bell, R., Boyce, B.E. and Collier, J.G.T. (1972) The structure of a submerged impinging gas jet J. Br. Nucl. Energy Soc. 11: 183–193.

[66] Spindler, K., Bierer, M., Lorenz, G., Erhard, A. and Hahne, E. (1988) Measurements in vertical gas–liquid two-phase flows using an optical fiber probe.

Proc. 1st World Conf. on Experimental Heat Transfer, Fluid Mechanics and Thermodynamics Dubrovnik, Yugoslavia.

[67] Abro, E., Khoryakov, V.A., Johansen, G.A. and Kocbach, L. (1999) Determination of void fraction and flow regime using a neural network trained on simulated data based on gamma-ray densitometry. Measurement Science & Technology. 10 (7): 619-630.

[68] Jiang, Y.J. and Rezkallah, K.S. (1993) An Experimental-Study of the Suitability of Using a Gamma Densitometer for Void Fraction Measurements in Gas-Liquid Flow in a Small Diameter Tube. Measurement Science & Technology. 4 (4): 496-505.

[69] Rodriguez, O.M.H. and Oliemans, R.V.A. (2006) Experimental study on oil-water flow in horizontal and slightly inclined pipes. International Journal of Multiphase Flow. 32 (3): 323-343.

[70] Heidrick, T.R. and Saltvold, J.R. (1978) Cross-section average density and mass flux measurements in two-phase flow through pipes, measurement in polyphase flow. The American society of mechanical engineers, San Francisco, CA, December 10-15. 1-9.

[71] Ahmed, W.H. (2006) Capacitance sensorsor void-fraction measurements and flow-pattern identification in air-oil two-phase flow Ieee Sensors Journal. 6 (5): 1153-1163.

[72] Pawloski, J.L., Ching, C.Y. and Shoukri, M. (2004) Measurement of void fraction and pressure drop of air-oil two-phase flow in horizontal pipes. Journal of Engineering for Gas Turbines and Power-Transactions of the Asme. 126 (1): 107-118.

[73] Elkow, K.J. and Rezkallah, K.S. (1996) Void fraction measurements in gas-liquid flows using capacitance sensors. Measurement Science & Technology. 7 (8): 1153-1163.

[74] Darnault, C.J.G., Dicarlo, D.A., Bauters, T.W.J., Steenhuis, T.S., Parlange, J.Y., Montemagno, C.D. and Baveye, P. (2002) Visualization and measurement of multiphase flow in porous media using light transmission and synchrotron X-rays, 2002: 103-110.

[75] Kehler, P. and Thome, J.R. (1978) Two-phase flow measurement by pulsed neutron activation techniques. Measurements in polyphase flows, The American society of mechanical engineers, December 10-15,San Francisco, CA.

[76] Snell, C.C., Dechene, R.L. and Nweton, R.E. (1978) Two-phase relative volume fraction measurement with a rotating filed conductance gauge. Measurements in polyphase flows, The American society of mechanical engineers, December 10-15, San Francisco, CA.

[77] Chang, J.S., Ichikawa, Y. and Irons, G.A. (1982) Flow regime characterization and liquid film thickness measurement in horizontal gas-liquid two-phase flow by an ultrasonic method. Measurements in polyphase flows, AIAA/ASME joint fluids, plasma, thermophysics and heat transfer conference, June 7-11, St. Louis, Missouri.

[78] Fossa, M. and Guglielmini, G. (2002) Pressure drop and void fraction profiles during horizontal flow through thin and thick orifices. Experimental Thermal and Fluid Science. 26: 513–523.

[79] Everson, J. (2005) Foster-Miller, Inc. See also:http://www.foster-miller.com/projectexamples/cc_icd_sensor_development/microwave_flow_sensor.htm.

[80] Koyama, S., Lee, J. and Yonemoto, R. (2004) An investigation on void fraction of vapor-liquid two-phase flow for smooth and microfin tubes with R134a at adiabatic condition. International Journal of Multiphase Flow. 30 (3): 291-310.

[81] Kim, H.Y., Koyama, S. and Matsumoto, W. (2001) Flow pattern and flow characteristics for counter-current two-phase flow in a vertical round tube with wire-coil inserts. International Journal of Multiphase Flow. 27 (12): 2063-2081.

[82] Spedding, P.L., Woods, G.S., Raghunathan, R.S. and Watterson, J.K. (1998) Vertical two-phase flow - Part II: Experimental semi-annular flow and hold-up. Chemical Engineering Research & Design. 76 (A5): 620-627.

[83] Lemonnier, H., Nakach, R., Favreau, C. and Selmerolsen, S. (1991) Sensitivity Analysis of an Impedance Void Meter to the Void Distribution in Annular-Flow - a Theoretical-Study. Nuclear Engineering and Design. 126 (1): 105-112.

[84] Bjork, E. (2005) A simple technique for refrigerant mass measurement. Applied Thermal Engineering. 25: 1115–1125.

[85] Chien, K.-H., Lin, W.-K. and Tsai, Y.-C. (1997) Effect of the side-tube configuration on the void fraction measurement. Nuclear Technology. 120 (2): 171-178.

[86] Flemmer, R.L.C. and Clark, N. (1984) A technique for synchronizing valves and determining bubble rise velocities in two-phase flow. Fluid engineering winter annual meeting, ASME, December 9-14, New Orleans, LA.

[87] Coleman, J.W. and Garimella, S. (1999) Characterization of two-phase fow patterns in small diameter round and rectangular tubes International Journal of Heat and Mass Transfer. 42 (15): 2869-2881.

[88] Al-Wazzan, A., Than, C.F., Moghavvemi, M. and Yew, C.W. (2001) Video imaging measurement of interfacial wave velocity in air-water flow through a horizontal elbow. Photonic Systems and Applications, Yakov S. Sidorin, Dingyuan Tang, Editors, Proceedings of SPIE. 4595 243-253.

[89] Augier, F., Morchain, J., Guiraud, P. and Masbernat, O. (2003) Volume fraction gradient-induced flow patterns in a two-liquid phase mixing layer. Chemical Engineering Science. 58 3985-3993.

[90] Cui, Z. and Fan, L.S. (2004) Turbulence energy distributions in bubbling gas–liquid and gas–liquid–solid &ow systems. Chemical Engineering Science. 59 1755 – 1766.

[91] Der, D.B. and Sommerfeld, M. (2002) An advanced LIF-PLV system for analysing the hydrodynamics in a laboratory bubble column at higher void fractions. Experiments in Fluids. 33 826–837.

[92] Hardalupas, Y. and Horender, S. (2003) Fluctuations of particle concentration in a turbulent two-phase shear layer International Journal of Multiphase Flow. 29 1645–1667.

[93] Hassan, Y. and Blanchat, T. (1991) Full-field bubbly flow velocity measurements by digital image pulsed laser velocimetry. Experiments in Fluids. 11: 293-301.

[94] Kashdana, J.T., Shrimptona, J.S. and Whybrew, A. (2007) A digital image analysis technique for quantitative characterisation of high-speed sprays Optics and Lasers in Engineering. 45 106–115.

[95] Kawaguchi, T., Akasaka, Y. and Maeda, M. (2002) Size measurements of droplets and bubbles by advanced interferometric laser imaging technique. Meas. Sci. Technol. 13 308–316.

[96] Kowalewski, T.A. (2002) Particle Image Velocimetry and Thermometry for Two-Phase Flow Problems. Ann. N.Y. Acad. Sci. 972: 213–222.

[97] Murai, Y., Oishi, Y., Takeda, Y. and Yamamoto, F. (2006) Turbulent shear stress profiles in a bubbly channel flow assessed by particle tracking velocimetry. Experiments in Fluids. 41: 343–352.

[98] Ottens, M., Klinkspoor, K., Hoefsloot, H.C.J. and Hamersma, P.J. (1999) Wave characteristics during cocurrent gas±liquid pipe flow. Experimental Thermal and Fluid Science. 19 140-150.

[99] Shamoun, B., Beshbeeshy, M.E. and Bonazza, R. (1999) Light extinction technique for void fraction measurements in bubbly flow. Experiments in Fluids. 26 16-26.

[100] Sunde, C., Avdic, S. and Pazsit, I. (2005) Classification of Two-Phase Flow Regimes via Image Analysis and a Neuro-Wavelet Approach. Progress in Nuclear Energy. 46 (3-4): 348-358.

[101] Tafreshi, Z.M., Kirpalani, D., Bennett, A. and McCracken, T.W. (2002) Improving the efficiency of fluid cokers by altering two-phase feed characteristics. Powder Technology. 125 234– 241.

[102] Tu, X. and Tragardh, C. (2002) Methodology development for the analysis of velocity particle image velocimetry images of turbulent, bubbly gas–liquid flows. Meas. Sci. Technol. 13 1079–1086.

[103] Taitel, Y. and Dukler, A.E. (1976) A model for predicting flow regime transitions in horizontal and near horizontal gas-liquid flow AIChE J. 22 (2): 47-55.

[104] Lambrechts, A. (2005) Heat transfer performance during in-tube condensation in horizontal smooth, micro-fin and herringbone tubes, MIng, Mechanical and Manufacturing Engineering, University of Johannesburg.

[105] Ewing, M.E., Weinandy, J.J. and Christensen, R.N. (1999) Observation of Two-phase Flow Patterns in a Horizontal Circular Channel. Heat Transfer Engineering. 20 (1): 9-13.

[106] Breber, G., Palen, J. and Taborek, J. (1980) Prediction of horizontal tubeside condensation of pure components using flow regime criteria. Journal of Heat Transfer. 102: 471-476.

[107] Baker, O. (1954) Simultaneous Flow of Oil and gas. The Oil and gas Journal. 53: 185-195.

[108] Whalley, P.B. (1987) Boiling, Condensation and Gas-Liquid Flow, Oxford, New York.

[109] Mandhane, J.M., Gregory, G.A. and Aziz, A. (1974) A flow pattern map for gas-liquid flow in horizontal pipes. Int. J. Multiphase Flow. 1: 537-553.

[110] Damianides, C. and Westwater, J.W. (1988) Two-phase flow patterns in a compact heat exchanger and in small tubes. Proceedings of Second U.K. National Conference On Heat Transfer, vol II, Glasgow, Scotland.

[111] Hesketh, R.P., Etchells, A.W. and Russell, T.W.F. (1991) Experimental observations of bubble breakage in turbulent flow. Ind. Eng. Chem. Res. 30 (5): 835–841.

[112] Hesketh, R.P., Etchells, A.W. and Russell, T.W.F. (1991) Bubble breakage in pipeline flow. Chem. Eng. Sci. 46: 1–9.

[113] Hesketh, R.P., Russell, T.W.F. and Etchells, A.W. (1987) Bubble size in horizontal pipelines. AIChE J. 33: 663–667.

[114] Walter, J.F. and Blanch, H.W. (1986) Bubble break-up in gas–liquid bioreactors: break-up in turbulent flows. Chem. Eng. J. 32: B7–B17.

[115] Simmons, M.J.H. and Azzopardi, B.J. (2001) Drop size distributions in dispersed liquid–liquid pipe flow. Int. J. Multiphase Flow. 27: 843–859.

[116] Angeli, P. (2001) Droplet size in two-phase liquid dispersed pipeline flows. Chem. Eng. Technol. 24: 431–434.

[117] Angeli, P. and Hewitt, G.F. (2000) Drop size distributions in horizontal oil–water dispersed flows. Chem. Eng. Sci. 55: 3133–3143.

[118] Kostoglou, M. and Karabelas, A.J. (1998) On the attainment of steady state in turbulent pipe flow of dilute dispersions. Chem. Eng. Sci. 53: 505–513.

[119] Parthasarathy, R., Jameson, G.J. and Ahmed, N. (1991) Bubble breakup in stirred vessels-prediction of the Sauter mean diameter. Trans. IChemE. 69 (Part A): 295–301.

[120] Karabelas, A.J. (1978) Droplet size spectra generated in turbulent pipe flow of dilute liquid/liquid dispersions. AIChE J. 24: 170–180.

[121] Kubie, J. and Gardner, G.C. (1977) Drop sizes and drop dispersion in straight horizontal tubes and in helical coils. Chem. Eng. Sci. 32: 195–202.

[122] Holmes, T.L. (1973) Fluid mechanics of horizontal bubble flow, Ph.D. Thesis, University of Delaware.

[123] Swartz, J.E. and Kessler, D.P. (1970) Single drop breakup in developing turbulent pipe flow. AIChE J. 16: 254–260.

[124] Collins, S.B. and Knudsen, J.G. (1970) Drop-size distributions produced by turbulent pipe flow of immiscible liquids. AIChE J. 16: 1072-1080.

[125] Ward, J.P. and Knudsen, J.G. (1967) Turbulent flow of unstable liquid–liquid dispersions: drop sizes and velocity distributions. AIChE J. 13: 356–365.

[126] Kolmogoroff, A.N. (1949) On the breaking of drops in turbulent flow. Dokl. Akad. Nauk SSSR. 66: 825–828.

[127] Kashdan, J.T., Shrimpton, J.S. and Whybrew, A. (2003) Two-Phase Flow Characterization by Automated Digital Image Analysis. Part 1: Fundamental Principles and Calibration ofthe Technique. Part. Part. Syst. Charact. 20 387-397.

[128] Yule, A.J., Chigier, N.A. and Cox, N.W. (1978) Measurement of Particle Sizes in Sprays by the Automated Analysis of Spark Photographs, Heyden Press.

[129] Lecuona, A., Sosa, P.A., Rodriguez, P.A. and Zequeira, R.I. (2000) Volumetric characterization of dispersed two-phase flows by digital image analysis. Meas. Sci. Technol. 11: 1152–1161.

CHAPTER 3

Literature: Two-Phase Spray[1]

3.1. Introduction

Gas-assisted liquid atomization is employed in several industrial processes such as in fluid coking where a mixture of bitumen and steam is injected into a fluidized bed of coke particles via effervescent nozzles. A class of this type of nozzle requires mixing the gas and liquid well upstream prior to feeding the mixture through the nozzles using a pipe. One of the drawbacks in the operation of effervescent nozzles is the development of instabilities or pulsations in the spray caused by the two-phase flow pattern formed inside or upstream of the nozzle. This pulsation is attributed to the two-phase fluid conditions (gas-to-liquid mass ratio (β), void fraction (α) or mixing pressure (P_m), the design of the mixing chamber, the geometry of nozzle or due to the back pressure from the high temperature reactor [1]. These pulsations result in poor atomization and in most instances, a slug of liquid is ejected out of the nozzle. This also results in a decrease in plant efficiency and a reduction in product yield, which is undesirable. To remedy this situation, it is desirable to attain a homogeneous two-phase mixture in the nozzle to obtain a stable spray with well-atomized and properly distributed liquid droplets.

Enhanced heat and mass transfer can be achieved from a spray, which is composed of dispersed droplets with larger spread rates. Moreover, as the droplet or particle sizes are reduced, the energy of the droplets is more readily transferred to the surrounding fluid [2]. This would ensure proper mixing with the surrounding fluids. Furthermore, in processes where the feed needs to be injected

[1] A version of this chapter has been published. Rahman *et al.* (2009) International Review of Mechanical Engineering. 3(1):110-125

into a cross-flowing stream, the droplets in the spray must have enough momentum to penetrate the cross-flowing fluid stream [3]. Continuous and fine spray characteristics are desirable in the effervescent atomization.

Quantitative experimental determination of spray stability can be obtained by measuring the relative amounts of fluctuation at different locations in the nozzle feeding pipe. These fluctuations can be measured using dynamic and static pressure transducers inserted in the pipe. Photonics measurements and image analysis can also help to understand the flow structure in the feeding pipe. Corresponding reliable drop size measurements within the spray can verify the dispersed and minimum spherical droplet size formation from effervescent atomization. This study will enable a better understanding of two-phase flows and sprays issuing from effervescent nozzles. Knowledge acquired from enhancing spray stability in laboratory tests can be used to optimize commercial process conditions. Even so, accurate measurement techniques of two-phase gas/liquid sprays are a ubiquitous challenge. Existing two-phase spray measurement techniques have been unsuccessful in obtaining accurate results due to dense and unstable spray development. Thus, there is an utmost need to explore the novel experimental techniques in the literature in order to obtain a better understanding of the state-of-the-art spray measurement advances of effervescent atomization.

3.2. Two-Phase Spray Theory

3.2.1. Stokes Number Effects

The Stokes number (St) can be defined as the ratio of droplet time scale (τ_d) to that of the fluid time scale (τ_c), and can be mathematically expressed as [4]:

$$St = \frac{\rho_c D_{32}^2 / 18\mu_c}{2\delta / u_x} \tag{1}$$

where $\delta = w/2$ is the jet half-width, D_{32} is the droplet Sauter mean diameter, μ_c is the viscosity of the carrier fluid and ρ_c is the density of the carrier fluid. For $St \ll 1$, the droplets are fully responsive to the fluid fluctuations. For very high

Stokes numbers (St>>1), the droplets have excess inertia and do not follow the fluctuations in the carrier phase. In the previous study [4], it was found that bigger droplets exhibit higher Stokes number profiles as the particle time scale is proportional to the square of the droplet diameter.

3.2.2. Axial Variation of Jet Half-Width

The jet half-width (δ) is defined as the radial distance at which one-half of the centerline or maximum velocity exists. One study [4] predicts the intercept of the jet half-width that is much higher than the other studies [5, 6].

3.2.3. Droplet Size-Velocity Correlation Factor

A strong positive correlation may be the result of smaller droplets having lower velocities or larger droplets traveling at higher velocities. Similarly, a strong negative correlation may result, either due to larger droplets associated with lower velocities or smaller droplets associated with higher velocities [4]. A previous study presented a plot of the size-probability function, $f(D)$ at various radial locations at a certain axial position. In this instance $f(D)$ was obtained by dividing the number of droplets in a particular size class by the total number of samples (N= 10,000). In the previous study [4] it was pointed out that large droplets exist near the spray periphery and smaller droplets exist at the center of the spray. In addition, they showed that the correlation factors were close to zero at the center of the spray, whereas a strong positive correlation exists at the periphery of the spray. However, in the present study the author observed that large droplets exist near the spray periphery and smaller droplets exist in between the center and the periphery of the spray. Near the tip of the nozzle the droplet sizes are slightly higher due to the existence of the large liquid ligaments at the center of the spray. However, further downstream in the spray (axially), this effect diminishes and primary and secondary break-up of the spray is completed.

3.2.4. Phase Doppler Particle Anemometer Measurements and Sprays

The set-up of the PDPA for this thesis and the basic principle of the PDPA are discussed in Chapter 7. The PDPA measurement quality is sometimes validated by the integration of the scalar volume flux profiles as follows [4, 7]:

$$V = \int_{i=1}^{n} \frac{N_i (\Pi / 6) D_{30,i}^3}{A_{pi} T_i} dA \tag{2}$$

where, V is the liquid volumetric flow rate at a particular jet cross section, N indicates the number of droplets measured at location i, $D_{30,i}$ volume mean diameter at location i, A is the area of space associated with the measurement, A_{pi} is the projected probe volume surface area and T_i is the run time at location i. However, implementation of the above equation to calculate volume flux profiles for pulsating sprays will lead to errors [4]. The PDPA measurement in low number density sprays necessitates a compromise between collecting a large number of samples for adequate statistics and practical data acquisition times [8]. In the present study, the author found that the volume flux measurement necessitates a compromise between the data rate and validation of the data. The probe area and volume flux measurements described by Widmann *et al.* [8] is discussed below. The volume flux (V) is obtained from the volumetric flow rate as:

$$V = \frac{volumetric\ \ flow\ rate}{probe\ area} = \frac{\Pi N_{cor} D_{30}^3}{6 T_{acq} A_p} \tag{3}$$

where, N_{cor} is the probe volume corrected number density, T_{acq} is the acquisition time, and A_p is the probe area. The probe area is determined from [9]:

$$A_p = \frac{D(d_{\max})_{\max} \omega_{slit}}{\sin\theta} \tag{4}$$

where ω_{slit} is the projected image length of the slit aperture, which limits the length of the probe volume; and θ is the scattering angle measured from the direction of propagation of the laser beams. The diameter of the probe volume, $D(d_{max})_{\max}$, corresponds to the effective diameter of the laser beam where the light

intensity is sufficient for the largest droplets to be detected. The volume mean diameter, D_{30}, is given by [10]:

$$D_{30} = \left(\frac{\sum_{i=1}^{n} c_i^{cor} d_i^3}{\sum_{i=1}^{n} c_i^{cor}} \right)^{1/3} \tag{5}$$

where d_i is the diameter of the i-th droplet size class. The probe volume corrected count, c_i^{cor} is a correction applied to account for the dependence of the probe volume on the droplet size. This correction is also applied to the measured number density to obtain N_{cor} in Equation (3). The number density, N_{cor}, is calculated as [9]:

$$N_{cor} = \frac{1}{t_{acq}} \sum_i \left(\frac{1}{v_i} \sum_j t_{trans}(i,j) \right) \tag{6}$$

where t_{trans} is the transit time of the droplets and v_i is the effective probe volume for the i-th size class. The indices i and j indicate the size class and droplet occurrence, respectively. The probe volume corrected count, c_i^{cor}, is related to the effective probe volume, v_i, through the relation as:

$$c_i^{cor} = c_i \left(\frac{v_{\max}}{v_i} \right) \left(\frac{D(d_i)_{\max}}{D(d_{\max})_{\max}} \right) \tag{7}$$

where c_i is the uncorrected count in size class i, and v_{max} is the effective probe volume for the largest size class.

3.3. Atomization

Atomization of liquids described by Crowe [11] is discussed in detail in this section. Within atomization, the bulk fluid (continuous liquid phase) is transformed into a spray system (dispersed phase: droplets). This disintegration process might be caused two ways: i) by intrinsic/potential energy, or ii) extrinsic/kinetic energy. In atomization the liquid is typically fed into the process in the form of a liquid jet that is atomized by the interaction of the liquid jet with a

high-velocity gas. A typical twin-fluid internal and external mixing atomizer is depicted in Fig. 3.1.

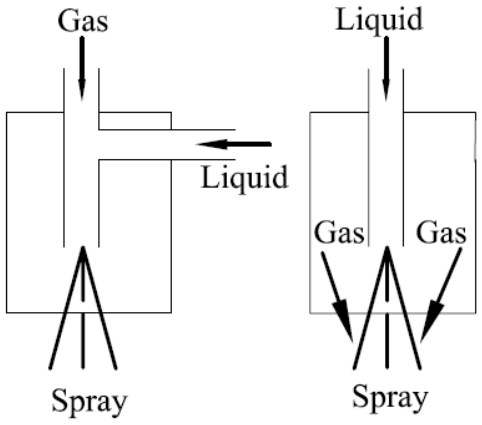

Fig. 3.1. Twin-fluid pneumatic atomizer with internal mixing (left) and external mixing (right). Adapted from [11].

The material property of the liquid that is to be atomized plays an important role in the atomization process. The significant properties of the liquid material are (in order of significance): viscosity, surface tension and density [11]. Based on the disintegration of the liquid, the atomizer can be classified as follows: a) Pressure atomizer: energy or pressure from the liquid itself is implemented, b) Pneumatic Atomizer: energy from the gas energy is implemented, c) Rotary Atomizer: mechanical energy or rotation is implemented, d) Ultrasonic Atomizer: acoustic energy is implemented, e) Electrostatic Atomizer: an electrically charged liquid is accelerated in an electric field, thereby forming an accelerating tiny liquid jet, which finally breaks down into fine droplets at the tip. Internal mixing or effervescent twin-fluid atomizer literature can be found in [12-22]. In the present case, we have studied the characteristics of a two-phase gas/liquid effervescent nozzle. The energy required for an atomization process is given by:

$$E = E_s + E_k + E_l \tag{8}$$

where, E_s is the surface energy of the liquid, i.e., the energy used to overcome the resistance or surface tension forces during disintegration of the liquid into

droplets; E_k is the kinetic energy, i.e., the energy used to accelerate the liquid and droplets in the spray; and E_l is the energy loss due to friction in the atomizer. Thus, the efficiency of atomization can be expressed as:

$$\eta = \frac{E_s}{E} \tag{9}$$

Several important characteristic numbers implemented in spray and atomization process are as follows:

Liquid Reynolds Number: $$\mathrm{Re}_l = \frac{\rho_l u_l D}{\mu_l} \tag{10}$$

Liquid Weber Number: $$We_l = \frac{\rho_l u_l^2 D}{\sigma} \tag{11}$$

Density Ratio: $$\rho_r = \frac{\rho_g}{\rho_l} \tag{12}$$

Viscosity Ratio: $$\mu_r = \frac{\mu_g}{\mu_l} \tag{13}$$

Aerodynamic/Gas Weber Number: $$We_g = \frac{\rho_g u_{rel}^2 D}{\sigma} \tag{14}$$

Ohnesorge Number/Laplace Number: $$Oh = \frac{\sqrt{We}}{\mathrm{Re}_l} = \frac{\mu_l}{\sqrt{\rho_l \sigma D_l}} = \frac{1}{\sqrt{Lp}} \tag{15}$$

Momentum Ratio: $$M = \frac{\rho_g u_g^2}{\rho_l u_l^2} \tag{16}$$

Gas-to-Liquid-Ratio: $$\beta = \frac{m_g}{m_g} \tag{17}$$

Euler Number: $$Eu_l = \frac{P_l}{\rho_l u_l^2} \tag{18}$$

3.3.1. Mean Drop Diameter

It is convenient to work with mean drop sizes instead of complete drop size distributions. The mean drop size distribution is generalized as follows [23, 24]:

$$(D_{ab})^{a+b} = \frac{\int_{D_0}^{D_m} D^a (DN/dD) dD}{\int_{D_0}^{D_m} D^b (DN/dD) dD} \tag{19}$$

The value of the sum of $a+b$ can be found in Table 3.1. Generally MMD or SMD provides a good indication of the drop size dispersion characteristics.

Table 3.1. Mean diameters and their application (adapted from [23]).

$a+b$	Symbol	Name of Mean Diameter	Expression	Application
1+0	D_{10}	Length	$\frac{\sum N_i D_i}{\sum N_i}$	Comparisons
2+0	D_{20}	Surface area	$\left(\frac{\sum N_i D_i^2}{\sum N_i}\right)^{1/2}$	Surface area controlling
3+0	D_{30}	Volume	$\left(\frac{\sum N_i D_i^3}{\sum N_i}\right)^{1/3}$	Volume controlling
2+1	D_{21}	Surface area-length	$\frac{\sum N_i D_i^2}{\sum N_i D_i}$	Absorption
3+1	D_{31}	Volume- length	$\left(\frac{\sum N_i D_i^3}{\sum N_i D_i}\right)^{1/2}$	Molecular diffusion
3+2	D_{32}	Sauter mean (SMD)	$\frac{\sum N_i D_i^3}{\sum N_i D_i^2}$	Mass transfer
4+3	D_{43}	De Brouckere or Herdan	$\frac{\sum N_i D_i^4}{\sum N_i D_i^3}$	Combustion equilibrium

Other parameters that describe the drop size dispersion are as follows [11]:

Droplet uniformity index : $\psi = \sum_i V_i (D_{0.5} - D_i) / D_{0.5}$ (20)

Where D_i is the midpoint of size class i and V_i is the volume fraction in the size class. Relative span factor: $\Delta = \frac{D_{0.9} - D_{0.1}}{D_{0.5}}$ (21)

Dispersion boundary factor: $\Delta_B = \frac{D_{0.999} - D_{0.5}}{D_{0.5}}$ (22)

There are also several representative diameters, which are defined in Table 3.2.

Table 3.2. Representative diameters that define the distribution function (adapted from [23]).

Symbol	Explanation
$D_{0.1}$	Drop diameter such that 10% of the total liquid volume is in drops of smaller diameter.
$D_{0.5}$	Drop diameter such that 50% of the total liquid volume is in drops of smaller diameter. This is the mass median diameter (MMD).
$D_{0.632}$	Drop diameter such that 63.2% of the total liquid volume is in drops of smaller diameter.
$D_{0.9}$	Drop diameter such that 90% of the total liquid volume is in drops of smaller diameter.
D_{peak}	Value of D corresponding to peak of drop size frequency distribution curve.

3.4. Spray Disintegration Process

The disintegration process of a spray can be characterized as follows, which is depicted in Fig. 3.2 i) at low aerodynamic Weber numbers, the jet mainly breaks due to Rayleigh instabilities with axisymmetric and nonaxisymmetric Rayleigh mode. ii) with increased aerodynamic Weber numbers, the surface tension effect diminishes and ligaments of the continuous phase are observed. This breakup regime is called the membrane mode. iii) with further increases of the aerodynamic Weber numbers, the ligament sizes decrease and breakup occurs in the form of fibres. A jet breaks up further downstream from the tip of a nozzle.

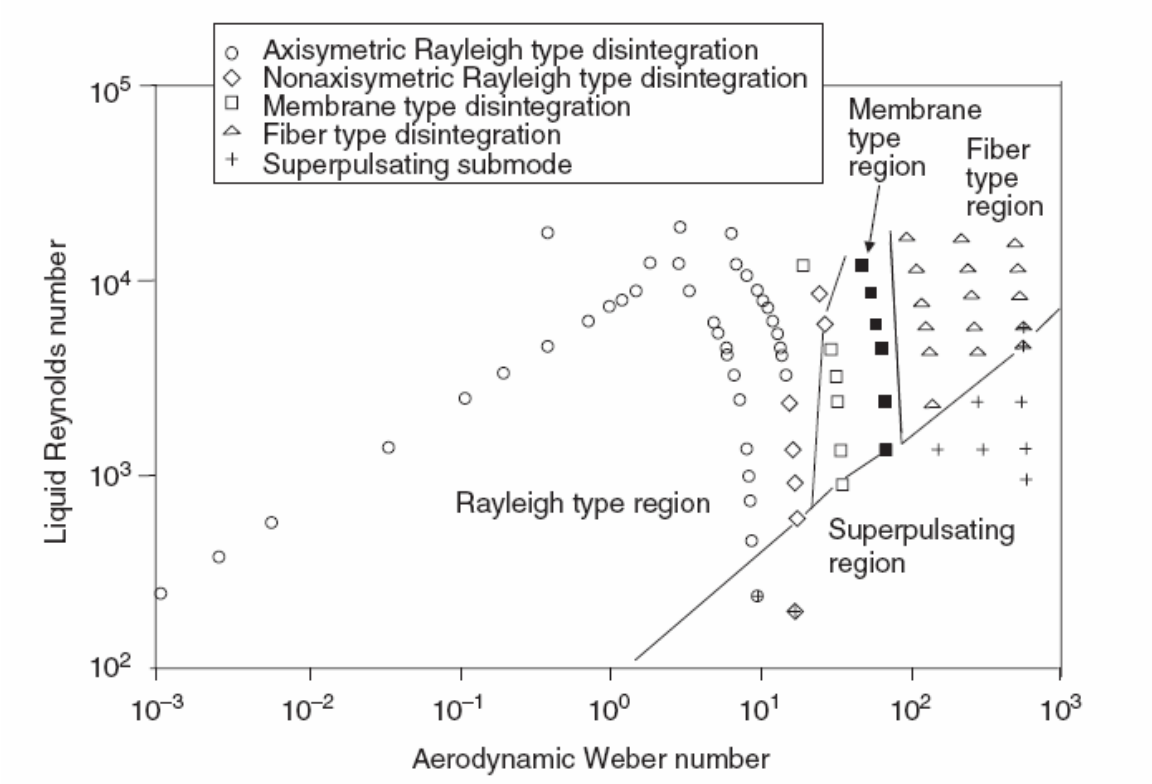

Fig. 3.2. Disintegration modes in twin-fluid atomization. (Adapted from [25]).

A jet break-up process with jet velocity is illustrated in Fig. 3.3. The laminar flow region exists between A and B sections. In this region, the jet breaks up linearly with jet velocity. An empirical expression that describes the jet break-up length in this region is as follows [26]:

$$\frac{L}{D_N} = 19.5\, We^{0.5}(1+3Oh)^{0.85} \tag{23}$$

In the transition region the jet break-up length decreases. However, in the turbulent region due to enhanced interaction between the gas and liquid phase, jet break-up length increases. An empirical expression that describes the jet break-up length in this region is as follows [26]:

$$\frac{L}{D_N} = 8.51\, We^{0.32} \tag{24}$$

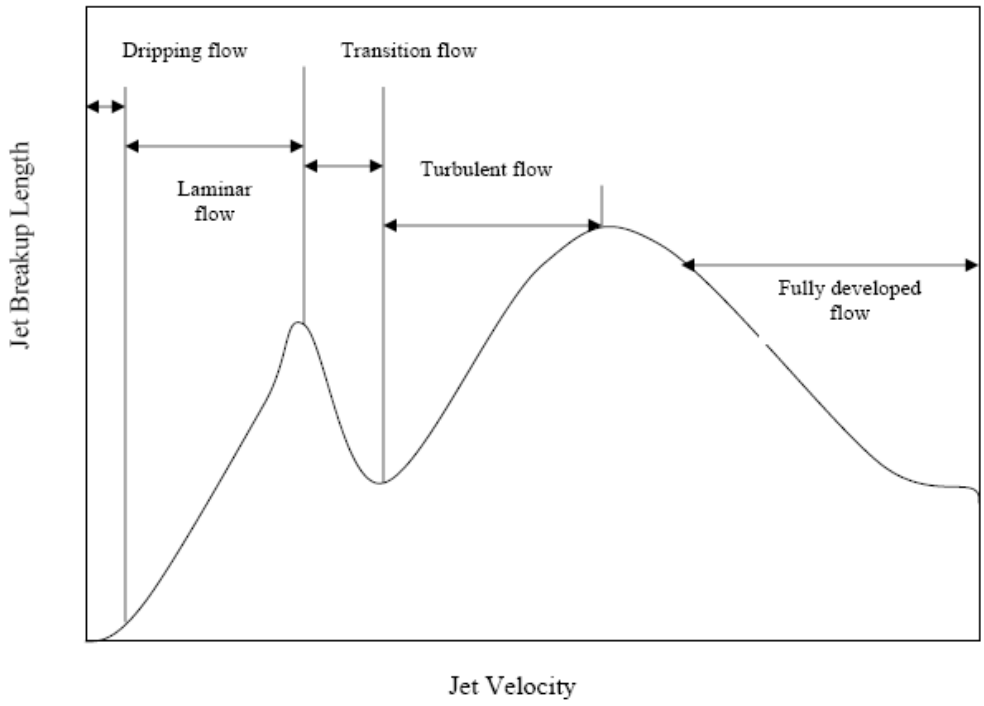

Fig. 3.3. Breakup length of a spray. (Adapted from [11]).

It is always important to know when and where a growing liquid element is separated from the excited liquid jet to form a primary droplet. The aerodynamic disintegration process for the plane liquid jet emerging from a planar slit nozzle is illustrated in Fig. 3.4. Starting from the growth of instability on the interface, the liquid elements or ligaments in the longitudinal direction plane first separate from the jet and deform into cylindrical elements further downstream. In the next step, these cylindrical ligaments disintegrate due to capillary instabilities (Rayleigh) in the fragments that form the resulting droplet structure in the initial spray due to the surface tension action [27].

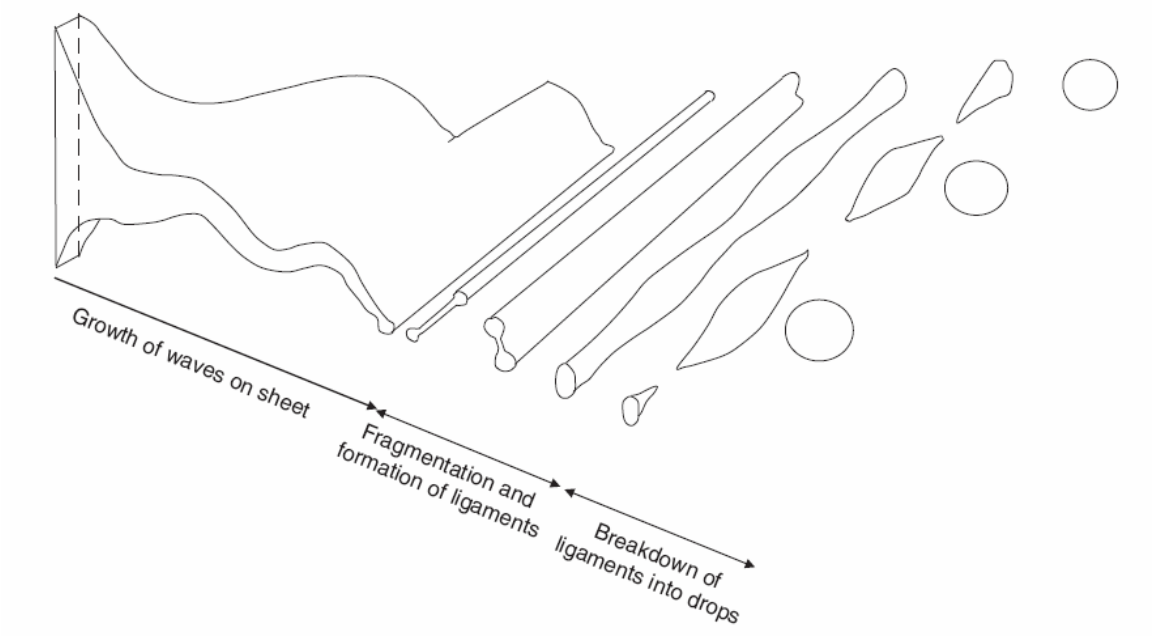

Fig. 3.4. Principle of aerodynamic disintegration of a planar liquid jet. (Adapted from [27]).

Secondary break-up in a spray occurs when larger droplets or liquid ligaments break down into smaller droplets. The breakup of a single droplet in a gas is caused by either relative velocity, turbulence or shock structure interaction acting separately [11]. If the relative velocity between the two phases is small, the droplet will be stable. If the relative velocity between the phases is larger, the droplet starts to break up. At this stage, aerodynamic forces overcome the surface tension of the liquid phase. Moreover, as the viscosity has a stabilizing effect, an increase in viscosity damps unstable perturbations [11]. If the aerodynamic forces overcome the forces due to surface tension, the droplet will deform [28]. The aerodynamic Weber number plays an important role in droplet break-up. If the aerodynamic Weber number exceeds the critical Weber number, secondary break-up occurs. Several correlations found in the literature related to critical Weber number are discussed below:

$$We_{crit} = \text{constant for } Oh < 0.1 \quad \text{or} \quad = \approx Oh^2 \text{ for } Oh > 0.1 \tag{25}$$

The critical Weber number found for low-viscosity liquids ranges from 6 to 13, but usually is assumed as We_{crit} =12 [29]. The critical Weber number found for low-viscosity liquids is found as [30, 31]:

$$We_{crit} = 12\,(1 + 1.077 Oh^{a}) \tag{26}$$

The above equation is applicable for the ranges of $5 < We_g < 200$. The exponential factor a has been given in the range 1.6 to 1.64. For highly viscous liquids, the break-up behavior is different from that of low-viscosity liquids. Also, if the droplet size becomes smaller, the effect of viscosity increases [11]. In general there are two main types of break-up mechanisms in sprays: the bag break-up for low Weber numbers (200<We_{crit}<350) and the shear breakup for high Weber numbers (We_{crit}>350), as illustrated in Fig. 3.5. While the bag break-up is associated with the Kelvin–Helmholtz instability (parallel shear flow), the shear breakup, particularly for very high Weber numbers, is associated with the Rayleigh–Taylor instability (cross-flow) [32].

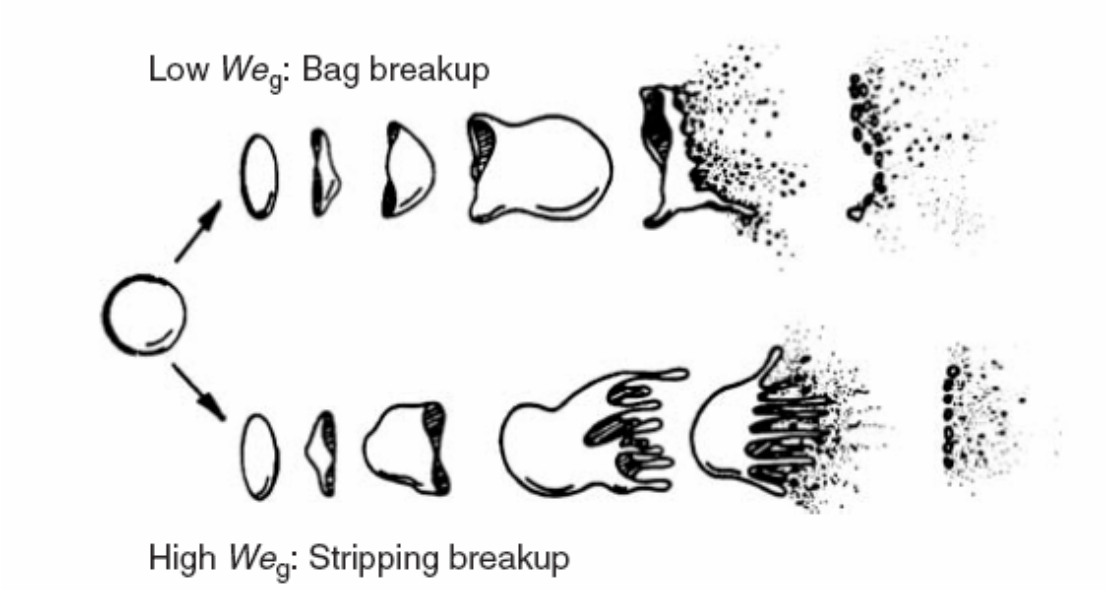

Fig. 3.5. Secondary fragmentation of a liquid drop. (Adapted from [33]).

3.5. Advanced Experimental Techniques for Spray Systems

Ariyapadi *et al.* [4] investigated the spray characteristics of a turbulent gas-liquid jet with Re_{water} =24,000. The nozzle configuration of their tests is indicated in Fig. 3.6. They used air and water as the test fluids. The spray profile was measured using a Phase-Doppler-Particle-Analyzer (PDPA). In their study they observed that the centerline mean droplet velocities (15~20 m/s) increased in the initial region of the jet; attained a maximum and then decreased at larger distances from the nozzle exit. They also indicated that most of the entrainment occurred at the tip of the nozzle and the jet expansion rate decreased significantly at distances where the spray velocity profiles became self-similar.

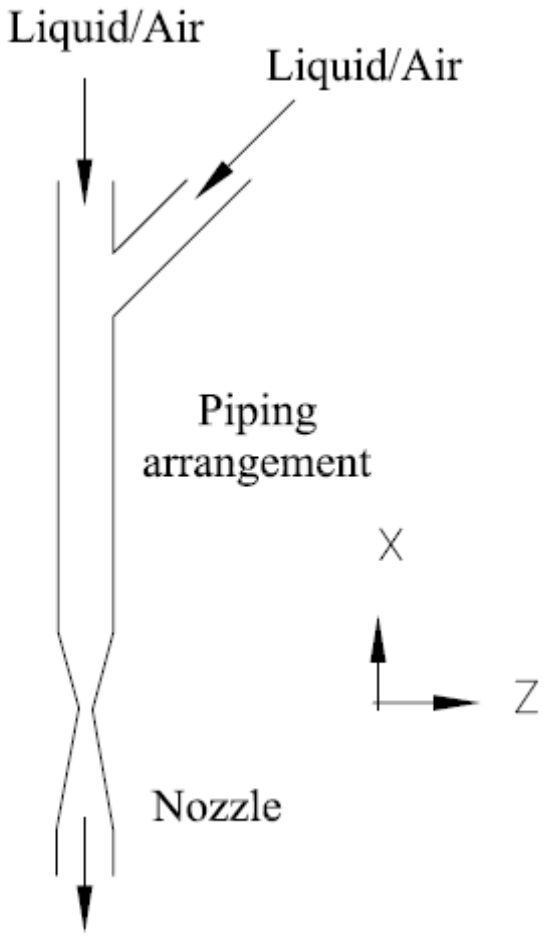

Fig. 3.6. Mixer configurations (adapted from [4]).

In this study, the photomultiplier tube voltage was 373V and the sample size was 10,000. In the current study I have increased the sample size (20,000) and used a higher voltage (1,050). This would eventually assist to increase the data rate and the validation of the large number of data. In their study they did not indicate the data rate, spherical validation and overall validation of the data. In addition, they did not mention the vertical velocity profiles or mass flux in the vertical and horizontal directions. Moreover, most of their axial velocity data is not symmetric about the centerline, which is very important to meet the proper validation of the measurement. They also obtained data in the horizontal plane. In the horizontal plane the PDPA receiver cannot observe the far section of the spray as clearly as in the closer part of the spray. This will eventually provide erroneous results. In the current study all the data was obtained in the vertical direction. This arrangement removes the asymmetric effects of the PDPA measurement. They used five different bilateral mixer configurations as presented in Table 3.3.

Table 3.3. Mixer configurations detail (adapted from [4]).

Configuration	θ	**Liquid**	**Air**
A	90°	↓	←
B	90°	←	↓
C	45°	↓	↙
D	45°	↙	↓
E	20°	↓	↙

As mentioned in Table 3.3, different types of mixer configurations were implemented in their study. One of the results on droplet size indicates that the mixer configuration does not have any remarkable effects on the spray characteristics. In the present study we implemented a configuration similar to 'B' type as shown in Table 3.3. The airflow line is aligned with the feeding conduit plane and water comes from a downward direction at a 90° angle. In the previous study, the feeding conduit arrangement ahead of the nozzle was fabricated using stainless steel, hence visualization of the two-phase flow structure was not possible. Qiu *et al.* [34] proposed a calibration method in order to correct the particle size distribution measured by the PDPA. The measurement volume of the PDPA system is shown in Fig. 3.7.

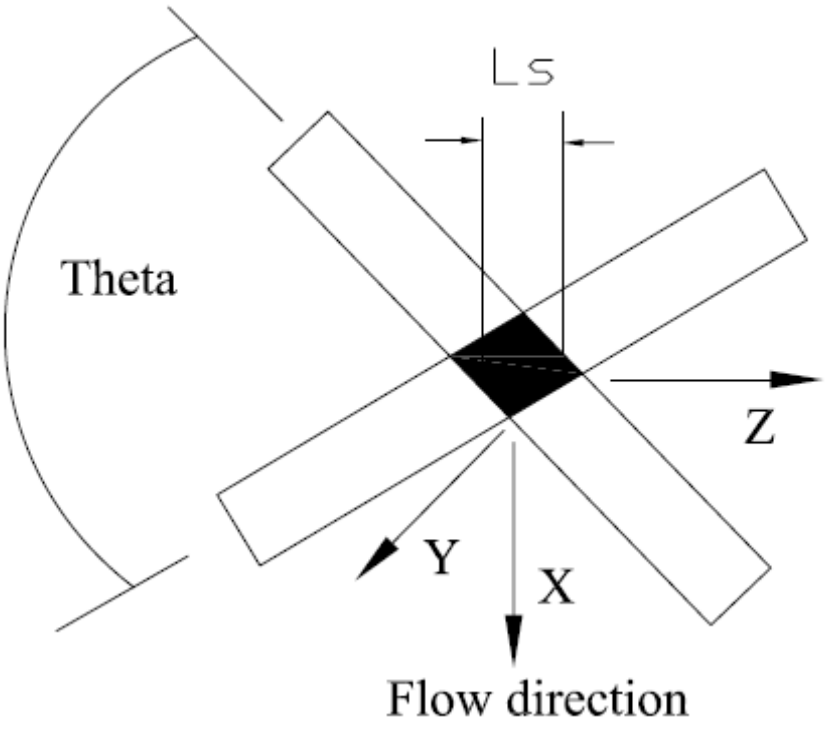

Fig. 3.7. Geometry of PDPA measurement volume (adapted from [34]).

Qui *et al.* [34] measured several cross-stream profiles of the droplet mass flux in the *x*-direction for water spray issuing from a pressure atomizer. They found that differences of the integration of the scalar volume flux profile and the global liquid mass flow rate (0.404 g/s) were -5.4%, -3.9% and 2.7%, respectively, for the planes considered in the spray at z =15, 25; and 50 mm downstream of the nozzle exit. Uncertainties involved in the first two cross-sections were mainly due to the low data rate caused by the higher concentration of droplets. The number of rejected signals may be reduced by decreasing the diameter of the measurement volume [34, 35].

Dullenkopf *et al.* [36] studied the performance of the different PDPA instruments and comparative flux measurements in two-phase sprays using a patternator. The patternator is a device which is used to measure average mass flux and penetration rate of the spray. Liquid spray is collected in channels aligned perpendicular to the spray nozzle. Dullenkopf *et al.* [36] indicated that in dense sprays, mass flux determination by the phase-Doppler technique is still critical. However, the dual-mode PDPA systems showed a significant improvement compared with the other instruments under investigation. Generally two different types of patternator were employed for a spray flux measurement: a) systems in which the total fluid in the spray is collected; and b) systems using isolated probes or an array of probes in which only a fraction of the fluid in the spray is captured. Dullenkopf *et al.* [36] implemented in their study the latter group. As an atomizer they used a pressure swirl atomizer and an airblast atomizer. They showed that for the pressure swirl atomizer the best reproducibility of the patternation in the center of the core was given by the DualPDA; significant errors only occurred in the boundary areas of the spray, possibly owing to a higher statistical variance. On the other hand, the airblast atomizer procured a large deviation between the patternation device and DualPDA for all cases. It appeared that the high data rate was an obstacle in obtaining correct mass flux measurements and velocity measurements in the case of the airblast atomizer [36]. Particle concentration or

mass flux measurements by phase-Doppler anemometry are based on counting the number of particles crossing the probe volume [37].

Ariyapadi *et al.* [38] studied the pulsation characteristics of a spray generated with a feed nozzle commonly used in the petrochemical industry. They acquired data using the PDPA. However, they investigated the two-phase vertical sprays generated using air and water. They effectively characterized pulsation in sprays using the intermittency factor, γ, coupled with the droplet size-velocity distribution. In their case, liquid mass flow rates ranged from 7×10^{-5} m^3/s to 11×10^{-5} m^3/s and the Reynolds number was 24,000 (at the nozzle tip). Their nozzle dimension similar to the present study is depicted in Fig. 3.8.

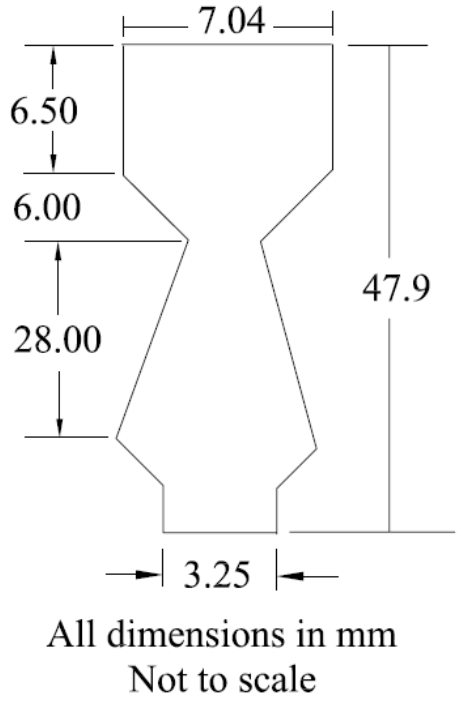

Fig. 3.8. Nozzle dimensions used by Ariyapadi *et al.* [38].

Ariyapadi *et al.* [38] used two cases to compare the pulsation in the two-phase two-component flows. Fig. 3.9 presents plots of the droplet interarrival time (Δt) versus the total measurement time (T) for cases 1 and 2. The time interval between two successive particles entering the measuring volume is defined as the

interarrival time. Case 1 represents the no pulsation case, however Case 2 represents artificially induced pulsation in the nozzle. From Fig. 3.9a, it is evident that the Δt values are small and uniform when there is no pulsation (Case 1). However, in Fig. 3.9b for Case 2, the Δt values are large (no-spray condition) and peak when there is pulsation. The peaks in the signal indicate the first droplet passing through the measuring volume after the no-spray condition. The number of peaks occurring in 1s represents the frequency of the pulsation [38].

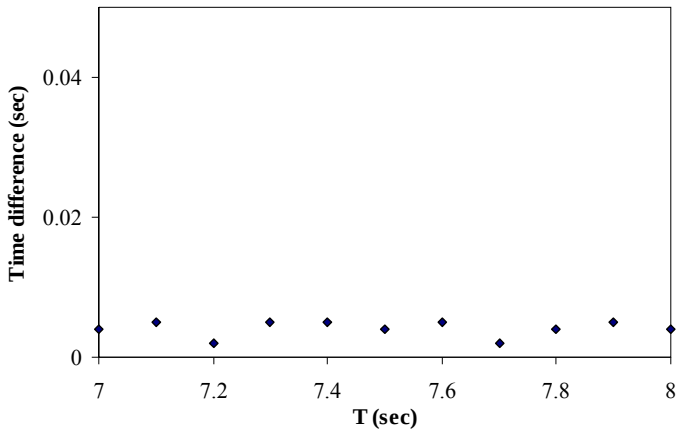

(a)

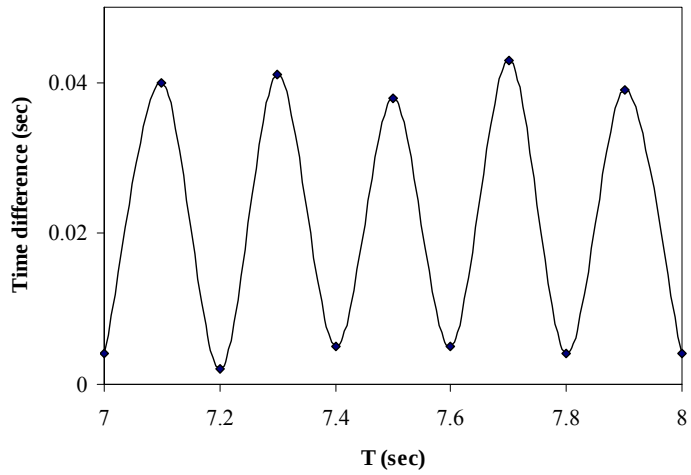

(b)

Fig. 3.9. Inter-arrival time versus total measurement time for (a) no-pulsation case, (b) pulsation case [38].

The two-phase, two-component spray pulsation can be characterized as follows:

$$\gamma = \frac{T_{at}}{T} \tag{27}$$

where, T_{at} represents the summation of all of the inter-arrival times during the atomization phase and $T = \sum \Delta t$ is the total measurement time for total number samples (N). A lower γ value indicates better atomization and thus lower jet pulsation [39]. When the spray is not pulsating, a continuous stream of droplets passes through the measuring volume, and consequently, the inter-arrival times are very small and fairly uniform. However, if a big liquid chunk passes through the probe volume of the PDPA, the measurements are not made, as the liquid chunk is highly non-spherical and much larger than the measuring range of the instrument. The next measurement is made only when the next set of smaller droplets pass through the probe volume. This results in a phase wherein the inter-arrival time is large.

A recently developed digital image analysis technique is potentially capable of sizing particles of arbitrary shape and size, and with a wide dynamic range [40]. A study conducted by Kashdan *et al.* [40] indicated that the depth-of-field varied with object diameter approximately linearly in the measured range of 18 to 145 μm. The method utilized a broadband light source to illuminate a section of the flow field and two solid-state cameras to image the spatial distribution of the illuminated particles. Individual particle image intensities were related to particle size by comparison with Mie scattering calculations [41]. Instantaneous size and spatial distribution of small spherical droplets and bubbles in two-phase flows were measured by the Interferometric laser imaging for droplet sizing (ILIDS) [42]. Simultaneous measurement of droplet size and three-components velocity fields issuing from the swirl nozzle for fuel spray were measured by the focused image of glare points, which was captured by a stereoscopic arrangement; and droplet size and the three-components velocity fields were evaluated from the doublet image [43]. A technique for characterizing the stability of two-phase sprays was investigated by high-speed visualization, and tested for a variety of feed nozzles and test fluids in both open-air and in a gas–solid fluidized bed [44]. In a recent study [45], laser Doppler velocimeterry (LDV) was implemented to

examine the effects of bubbles on the turbulence levels of a water jet. In this study, mean bubble diameters ranged from 0.6 to 2 mm and the void fractions were up to about 20%. The liquid Reynolds numbers were approximately 5,000 to 10,000. The measurements extended from an axial distance of 4-12 cm. It was observed that bubbles did not significantly affect the average velocity profiles in the jet. However, bubbles increased the turbulence intensities in the core of the jet near the jet exit.

The PDAP was used [46] to characterize a scaled-down version of an industrial feed nozzle in the presence of a cross flow. Aerated liquid nitrogen was injected through the nozzle to generate the spray. The study indicated that the spray momentum flux determined the extent of the jet bending. The droplets were accelerated significantly in the initial jet region as a result of flashing. However, further downstream of the nozzle, the vaporization of the droplets was considered to be negligible. The size-velocity correlation changed significantly for the case where the spray was shifted due to the cross flow.

Laser Doppler Velocimetry (LDV), Particle Image Velocimetry (PIV) and Laser-induced Fluorescence (LIF), Electrical Aerosol Analyzer (EAA), Light Absorption and Light Scattering methods can be found in a study done by Crowe [47] . In addition, mass transfer between liquid and gas [48], various spray models [49], and a range of exit orifice aspect ratios were characterized [50] by 2D Phase-Doppler Anemometry. Spray cone angles were studied in high ambient density environments for diesel fuel injection [51]. Flow pattern maps and nominal commercial operating conditions for the feed system of an air and water industrial nozzle were investigated by a Dantec PDPA laser interferometer [1]. Particle dispersion and particle velocities were measured with laser sheets and a position sensitive photomultiplier tube to track particles characteristics [52]. Monodispersed hexadecane droplets were injected onto the centerline of a turbulent air jet with Reynolds numbers in the range of 10,000-32,400 [52]. The

spray cone emerging during an extended metal atomization process (called spray forming) was investigated in order to quantify the influence of highly concentrated multiphase flows on the PDPA measurements [53]. Copan *et al.* [54] implemented liquid nitrogen that went vaporization upon injection into the processing vessel and air as the carrier gas. Measurements were conducted using the PDAP. The results indicated that the droplet size distributions were sensitive to changes in the aeration rate, and nozzle geometry.

3.6. Conclusions

Advanced measurement techniques for two-phase gas/liquid spray systems have been reviewed in this chapter. Most of the measurements of two-phase gas/liquid spray characteristics were conducted by the PDPA and a few of the droplet size measurements were conducted by image analysis. The PDPA has been used for spray characteristic measurements issuing from a wide variety of nozzles. However, the application of the PDPA is still a challenge in highly concentrated multiphase sprays. High speed videos and shadowgraphs of the nano-second freezing images and subsequent reliable image analysis techniques should be explored in the future to evaluate the two-phase gas/liquid effervescent atomization characteristics.

Effervescent atomization depends on many factors, such as i) liquid types: Newtonian/non-Newtonian fluid, ii) liquid physical properties: viscosity, surface tension and density, iii) operating parameters: gas/liquid ratio, injection pressure, void fraction, iv) atomizer internal geometry, v) gas properties: gas molecular weight, bubble size, flow regimes, vi) ambient density, vii) temporal and spatial coordinates. Several parameters are important to characterize the spray after proper atomization; such as i) liquid mass flux, ii) drop size distribution, iii) drop velocity distribution, iv) spray cone angle, v) penetration, vi) spray momentum rate and vii) entrained gas flow rate.

3.7. References

[1] Tafreshi, Z.M., Kirpalani, D., Bennett, A. and McCracken, T.W. (2002) Improving the efficiency of fluid cokers by altering two-phase feed characteristics. Powder Technology. 125 234– 241.

[2] MacGregor, S.A. (1991) Air Entrainment in Spray Jets. Int. J. Heat and Fluid Flow. 12: 279–283.

[3] Ariyapadi, S., Balachandar, R. and Berruti, F. (2000) Effect of Cross-Flow on the Spray Characteristics of an Industrial Feed Nozzle. AIChE Spring Annual meeting, Atlanta, GA.

[4] Ariyapadi, S., Balachandar, R. and Berruti, F. (October 2003) Spray Characteristics of Two-phase Feed Nozzles. The Canadian Journal of Chemical Engineering. 81: 923-939.

[5] Balachandar, R., Mulpuru, S.R. and Ungurian, M.H. (1998) A Note on Particle Size Measurements in Two-Phase Flows. Journal of Fluids Engineering, Trans. ASME. 120: 390–397.

[6] Hestroni, G. and Sokolov, M. (1971) Distribution of Mass, Velocity and Intensity of Turbulence in a Two-phase Turbulent Jet. ASME Journal of Applied Mechanics. 38: 315–327.

[7] McDonell, V.G. and Samuelsen, G.S. (1996) Intra- and interlaboratory experiments to assess performance of phase Doppler interferometry, 1996: 57.

[8] Widmann, J.F., Presser, C. and Leigh, S.D. (2001) Improving phase Doppler volume flux measurements in low data rate applications. Meas. Sci. Technol. 12 1180–1190.

[9] Zhu, J.Y., Rudoff, R.C., Bachalo, E.J. and Bachalo, W.D. (1993) Number density and mass flux measurements using the phase Doppler particle analyser in reacting and non-reacting swirling flows, paper AIAA-93-0361. AIAA 31st Aerospace Sciences Meeting Exhibit, Reno, NV.

[10] Taylor, G.I. (1932) The viscosity of a fluid containing small drops of another fluid. Proceedings of the Royal Society of London Series. 138 (834): 41-48.

[11] Crowe, C.T. (2006) Multiphase flow handbook Boca Raton, FL CRC: Taylor & Francis.

[12] Buckner, H.N. and Sojka, P.E. (1991) Effervescent atomization of high-viscosity fluids: Part I, Newtonian liquids. Atomization and Sprays. 1: 239-252.

[13] Chen, S.K. and Lefebvre, A.H. (1994) Discharge coefficients for plain-orifice effervescent atomizers. Atomizations and Sprays. 4: 275–290.

[14] Chin, J.S. and Lefebvre, A.H. (1993) Flow patterns in internal-mixing, twin-fluid atomizers. Atomizations and Sprays. 3: 463–475.

[15] Kim, J.Y. and Lee, S.Y. (2001) Dependence of spraying performance on the internal flow pattern in effervescent atomizers. Atomizations and Sprays. 11: 735–756.

[16] Lund, M.T., Sojka, P.E., Lefebvre, A.H. and Gosselin, P.G. (1993) Effervescent atomization at low mass flow rates. Part 1: the influence of surface tension. Atomization and Sprays. 3: 77-89.

[17] Luong, J.T.K. and Sojka, P.E. (1999) Unsteadiness in effervescent sprays. Atomization Spray. 9: 87–109.

[18] Oshinowo, T. and Charles, M.E. (1974) Vertical two-phase flow, Part 1: flow pattern correlations. Can. J. Chem. Eng. 52: 25–35.

[19] Richter, H.J. (1983) Separated two-phase flow model, application to critical two-phase flow. Int. J. Multiphase Flow. 9: 511–530.

[20] Whitlow, J.D. and Lefebvre, A.H. (1993) Effervescent atomizer operation and spray characteristics. Atomizations and Sprays. 3: 137–155.

[21] Nasr, G.G., Yule, A.J. and Bendig, L. (2002) Industrial sprays and atomization: design, analysis and applications, Springer-Verlag London Limited.

[22] Lörcher, M., Schmidt, F. and Mewes, D. (2003) Flow field and phase distribution inside effervescent atomizers. Proceedings of the 9th International Conference on Liquid Atomization and Spray System, ICLASS 2003, Sorrento, Italy.

[23] Lefebvre, A.H. (1989) Atomizations and Sprays, New York, Hemisphere.

[24] Mugele, R. and Evans, H.D. (1951) Drop size distributions is sprays. Ind. Eng. Chem. 43 (6): 1317-1324.

[25] Farago, Z. and Chigier, N. (1992) Morphological classification of disintegration of round liquid jets in a coaxial air stream. Atomization and Sprays. 2: 137–153.

[26] Grant, R.P. and Middleman, S. (1966) Newtonian jet stability. AIChE J. 12: 669-678.

[27] Dombrowski, N. and Johns, W.R. (1963) The aerodynamic instability and disintegration of viscous liquid sheets. Chem. Eng. Sci. 18: 203–214.

[28] Low, T.B. and List, R. (1982) Collision, coalescence and breakup of raindrops. J. Atmos. Sci. 39: 1591–1618.

[29] Hsiang, L.P. and Faeth, G.M. (1995) Drop deformation and breakup due to shock wave and steady disturbances. International Journal of Multiphase Flow. 21 (4): 545-560.

[30] Hsiang, L.P. and Faeth, G.M. (1992) Near-limit drop deformation and secondary breakup. Int. J. Multiphase Flow. 18: 635–652.

[31] Pilch, M. and Erdman, C.A. (1987) Use of breakup time data and velocity history data to predict the maximum size of stable fragments for acceleration-induced breakup of a liquid drop. International Journal of Multiphase Flow. 13: 741-757.

[32] Anderson, W.H. and Wolfe, H.E. (1965) Aerodynamic breakup of liquid drops- I. Theoretical. Proceedings of the International Shock Tube Symposium, Naval Ordinance Laboratory, White Oak, Maryland, USA.

[33] Yule, A.J. and Dunkley, J.J. (1994) Atomization of Melts, Clarendon Press, Oxford.

[34] Qiu, H.H. and Sommerfeld, M. (1992) A reliable method for determining the measurement volume size and particle mass fluxes using phase-Doppler anemometry. Experiments in Fluids. 13: 393-404.

[35] Kuo, K.K. (1995) Progress in Astronautics and Aeronautics: Recent advances in spray Combustion: Spray Atomization and Drop Burning Phenomena, vol 166, Reston, Virginia, American Institute of Aeronautics and Astronautics, Inc.

[36] Dullenkopf, K., Willmann, M., Wittig, S., Schöne, F., Stieglmeier, M., Tropea, C. and Mundo, C. (1998) Comparative mass flux measurements in sprays using a patternator and the phase-doppler technique. Particle and Particle Systems Characterization. 15: 81-89.

[37] Sommerfeld, M. and Qiu, H.H. (1995) Particle concentration measurements by phase-doppler anemometry in complex dispersed two-phase flows. Experiments in Fluids. 18 187-198.

[38] Ariyapadi, S., Balachandar, R. and Berruti, F. (2001) Characterizing Spray Pulsations Using a Phase-Doppler Particle Analyzer. Ind. Eng. Chem. Res. 40: 5282-5290.

[39] Ariyapadi, S.V. (2000) A study on droplet-laden jets, Master's thesis, Department of Chemical Engineering, University of Saskatchewan.

[40] Kashdan, J.T., Shrimpton, J.S. and Whybrew, A. (2003) Two-Phase Flow Characterization by Automated Digital Image Analysis. Part 1: Fundamental Principles and Calibration ofthe Technique. Part. Part. Syst. Charact. 20 387-397.

[41] Hofeldt, D.L. and Hanson, R.K. (1991) Instantaneous imaging of particle size and spatial distribution in two-phase flows. Applied Optics. 30 (33): 4936-4948.

[42] Kawaguchi, T., Akasaka, Y. and Maeda, M. (2002) Size measurements of droplets and bubbles by advanced interferometric laser imaging technique. Meas. Sci. Technol. 13 308–316.

[43] Zama, Y., Kawahashi, M. and Hirahara, H. (2004) Simultaneous Measurement of Droplet Size and Three-Components of Velocity in Spray. Optical Review. 11 (6): 358–364.

[44] Ariyapadi, S., Berruti, F., Briens, C., Knapper, B., Skwarok, R. and Chan, E. (2005) Stability of horizontal gas–liquid sprays in open-air and in a gas–solid fluidized bed. Powder Technology. 155 161 – 174.

[45] Kumar, S., Nikitopoulos, D.N. and Michaelides, E.E. (1989) Effect of bubbles on the turbulence near the exit of a liquid jet. Experiments in Fluids. 7: 487-494.

[46] Ariyapadi, S., Berruti, F. and Ram, B. (2003) Effect of Crossflow on the Spray Characteristics of an industrial Feed Nozzle. Chem. Eng. Comm. 190: 1: 681-1704.

[47] Crowe, C.T. (2006) Advanced Experimental Techniques, Multiphase flow handbook, Boca Raton, FL, CRC : Taylor & Francis.

[48] Kies, F.K., Benadda, B. and Otterbein, M. (2004) Experimental study on mass transfer of a co-current gas–liquid contactor performing under high gas velocities. Chemical Engineering and Processing. 43 1389–1395.

[49] Darby, R. (2000) Evaluation of Two-Phase Flow Models for Flashing Flow In Nozzles. Process Safety Progress. 19 (1): 32-39.

[50] Cleary, V., Bowena, P. and Witlox, H. (2007) Flashing liquid jets and two-phase droplet dispersion I. Experiments for derivation of droplet atomization correlations. Journal of Hazardous Materials. 142 786–796.

[51] Sovania, S.D., Choua, E., Sojkaa, P.E., Gorea, J.P., Eckerleb, W.A. and Crofts, J.D. (2001) High pressure effervescent atomization: effect of ambient pressure on spray cone angle. Fuel. 80: 427-435.

[52] Kennedy, I.M. and Moody, M.H. (1998) Particle dispersion in a turbulent round jet. Experimental Thermal and Fluid Science. 18 11-26.

[53] Ziesenis, J. and Bauckhage, K. (2002) Absorption and Scattering of Light by Highly Concentrated Two-phase Flows. Part. Part. Syst. Charact. 19 195-202.

[54] Copan, J., Balachandar, R. and Berruti, F. (2001) Droplet size-velocity characteristics of sprays generated by two-phase feed nozzles. Chemical Engineering Communications. 184: 105-124.

CHAPTER 4

Two-Phase Atomization Characterization: Droplet Size -Velocity[1]

4.1. Introduction

Enhanced heat and mass transfer can be achieved from a spray, which is composed of dispersed droplets with larger spread rates. Moreover, as the droplet sizes are reduced, the energy of the droplets is more readily transferred to the surrounding fluid [1]. This ensures proper mixing with the surrounding fluids. Furthermore, in processes where the feed needs to be injected into a cross-flowing stream, the droplets in the spray must have enough momentum to penetrate the cross-flowing fluid stream [2]. Continuous and fine spray characteristics are desirable in the effervescent nozzle. One of the applications of the effervescent nozzle is in the heavy oil process industry. In heavy oil upgrading, preheated bitumen and steam are mixed upstream of the nozzle and are subsequently injected into fluid bed coker reactors via effervescent nozzles. One of the drawbacks of the spray issuing from the effervescent nozzle is the potential pulsation within the spray and in the feeding conduit, which is highly undesirable to yield high productivity. These pulsations result in poor atomization and in most instances, a slug of liquid is ejected out of the nozzle. This pulsation is attributed to the two-phase fluids conditions (gas-to-liquid ratio, β, void fraction, α or the mixing pressure, P_m), the design of the mixing chamber of the effervescent nozzle, the geometry of the effervescent nozzle and the back pressure from the high temperature bed coker [3].

---

[1] A version of this chapter has been published. Rahman *et al.* (2008) Proceedings of the FEDSM 2008, ASME Fluids Engineering Conference, FEDSM2008- 55330, Jacksonville, Florida USA, August 10-14.

4.2. Experimental Set-Up

In this study, a laboratory scale nozzle assembly was used. The dimension was one-quarter scale of a patented full-scale design (US Patent #: 6003789) employed in a fluidized bed coker for heavy oil upgrading. A feeding conduit of 36.8 cm length and 6.35 mm ID was used prior to the nozzle. The nozzle diameter (D_n) was 3.10 mm. This nozzle assembly was mounted on a 3-D automated traversing rig. The experimental schematic diagram is presented in Fig. 4.1. Mean drop size was measured using a 2D-Phase Doppler Particle Anemometer (PDPA) from the Dantec Dynamics specifications [4]. The focal lengths of the PDPA transmitter and receiver lenses were 400 and 310 mm, respectively. During data collection, the PDPA was operated in refraction and forward-scatter mode, while the receiver was set to a scattering angle (φ) of 30° for the air-water tests.

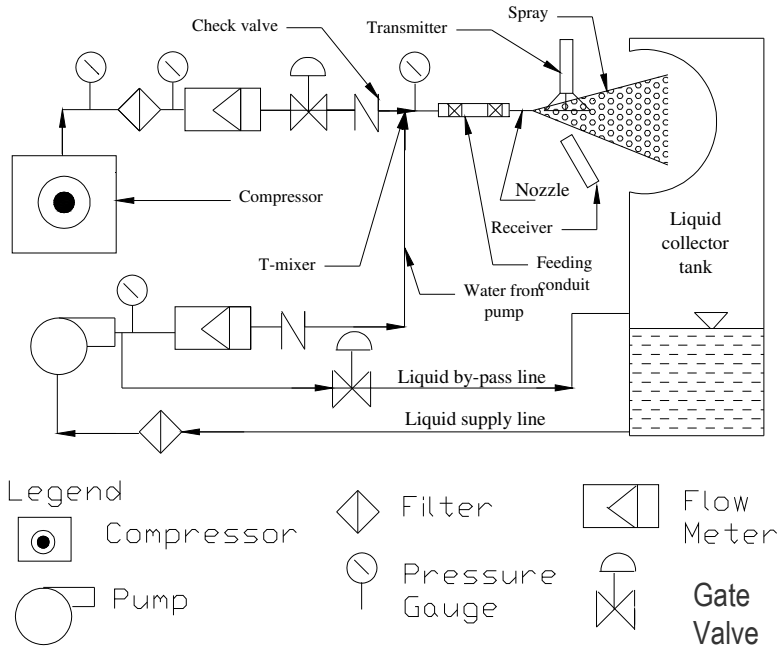

Fig. 4.1. Schematic of the experimental set-up.

Dantec [5] specified that first order refraction is the most dominant scattering mode at φ= 30° for water droplets in air. More on the PDPA set-up can be found in 7. Chapter Radial spray profiles were measured using the PDPA system on $15D_n$, $30D_n$, $60D_n$, $120D_n$ (D_n represents nozzle diameter =3.10 mm) axial distances downstream of the nozzle. The measurements were taken varying the radial positions (R) of +30 mm to –30 mm by the 3-D traversing rig. The values of D_{32}, D_{10}, and u_x were measured with changing the β and α. Schematic of the different experimental techniques is presented in Fig. 4.2. Due to the inability of measurement instruments to access the interior of the industrial reactors, the atomization behavior of the full-scale nozzle at commercial operating conditions is currently unknown. Hence small-scale laboratory tests will provide inexpensive and easily accessible methods of obtaining the two-phase gas/liquid flow and spray characteristics. Thus, in the replicated quarter-scale horizontal nozzle assembly (L of 36.8 cm and ID of 6.35 mm), I performed the following experiments using mixtures of water with air and the air-to-liquid ratio by mass (β) of 1% to 4%:

a) the α of the two-phase gas/liquid flow was measured by isolating a section in the nozzle feeding conduit, termed as the quick-closing-valve (QCV) technique.
b) the upstream flow patterns were investigated by the high-speed-video-shadowgraphy (HSVS) technique.
c) the bubble size distribution of the two-phase gas/liquid flow was estimated by the stroboscopic-back-scattered-imagery (SBSI).
d) local α_H ('$_H$' stands for homogeneous) and pressure drop of the two-phase gas/liquid flow was measured by the high response static-pressure transducers (SPT).
e) spray profiles (u_x, u_y, d_d) were measured using the Phase-Doppler-Particle-Anemometer (PDPA) on $15D_n$, $30D_n$, $60D_n$, $120D_n$ (D_n represents nozzle diameter of 3.10mm) axial distances.

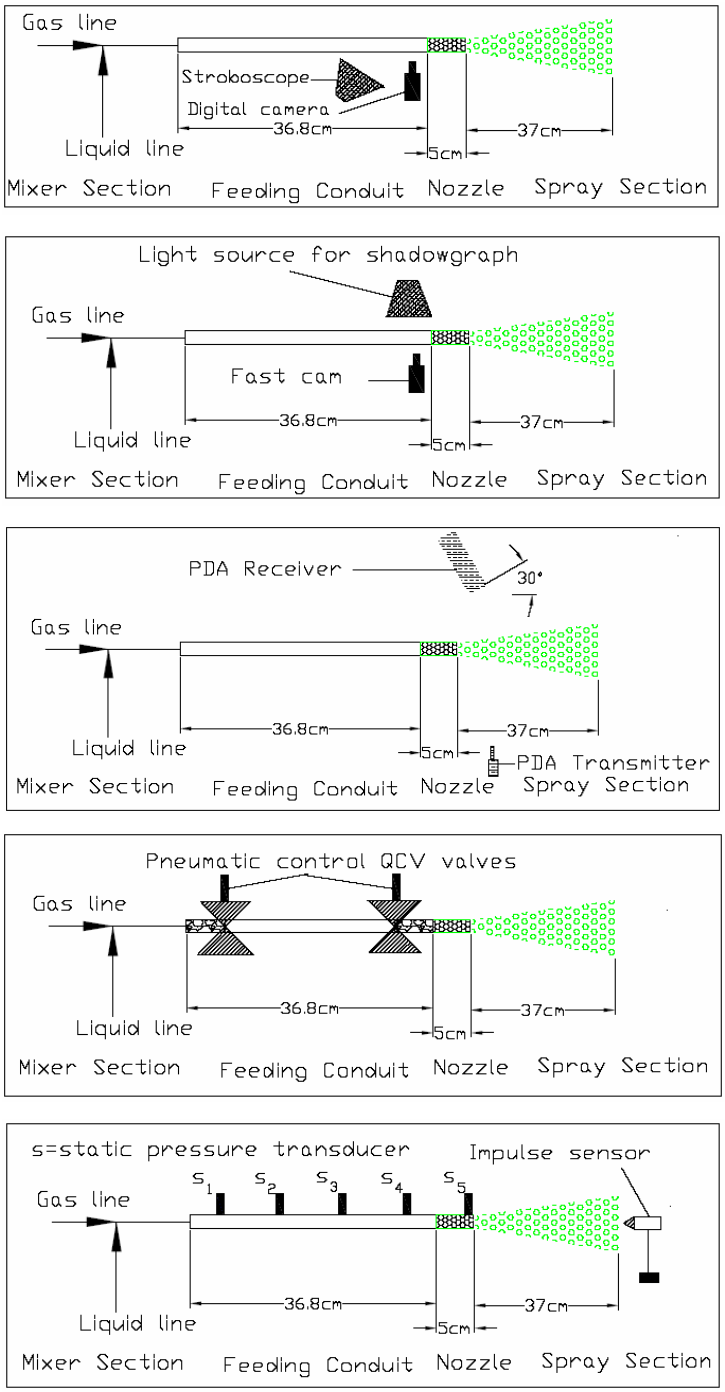

Fig. 4.2. Schematic of the different experimental technique. The *L* and *ID* of the nozzle feeding conduit is 36.8 cm and 6.35 mm. The tip of the nozzle is 3.10 mm. (a) Experimental set-up for the SBSI method, (b) Experimental set-up for the HSVS method, (c) Schematic diagram of the PDPA set-up, (d) Schematic diagram of the QCV method set-up, e) Schematic diagram of the IS and SPT set-up.

f) to better simulate the 'hot' flow commercial operation (steam as a gas phase), a 'mixed-gas' of 81.4 % Helium, and 18.6 % Nitrogen was used in the 'cold' flow nozzle assembly as the gas phase. Corresponding image analysis and PDPA measurements were also conducted.

g) the 'impact force' of the spray downstream of the nozzle was measured by an impulse sensor, which provides a better understanding of the mass flux throughout the entire spray.

Studies have been conducted in the laboratory scale nozzle assembly at the University of Alberta. In the study, the gas flow rates were varied from 4.40×10^{-4} kg/s to 4.74×10^{-2} kg/s and water flow rates were varied from 1.19×10^{-1} kg/s to 3.14×10^{-2} kg/s, under the constant pressure of 428 kPa to 683 kPa. A brief summary of each experimental technique is discussed as follows:

a) A 1531-A electronic stroboscope was used to freeze the bubble motion with back illumination in the SBII technique. A D100 high-performance single-lens-reflex (SLR) digital camera was used to capture the back illuminated images. A representative SBSI technique image is illustrated in Fig 4.3.

b) A Phroton 1280×1024 monochrome *PCI* fast cam (4000 f/s with 640×128 pixel) was used to capture the bubble motion using the HSVS method. Photron Motion Tools software was used to calculate the characteristic local bubble velocity.

c) Mean drop size was measured using a 2D-PDPA from the Dantec Dynamics specifications [77]. The focal lengths of the PDPA transmitter and receiver lenses were 400 and 310 mm, respectively. During data collection, the PDPA was operated in refraction and forward-scatter mode, and the receiver was set to a scattering angle (ϕ) of 30° for the air-water tests.

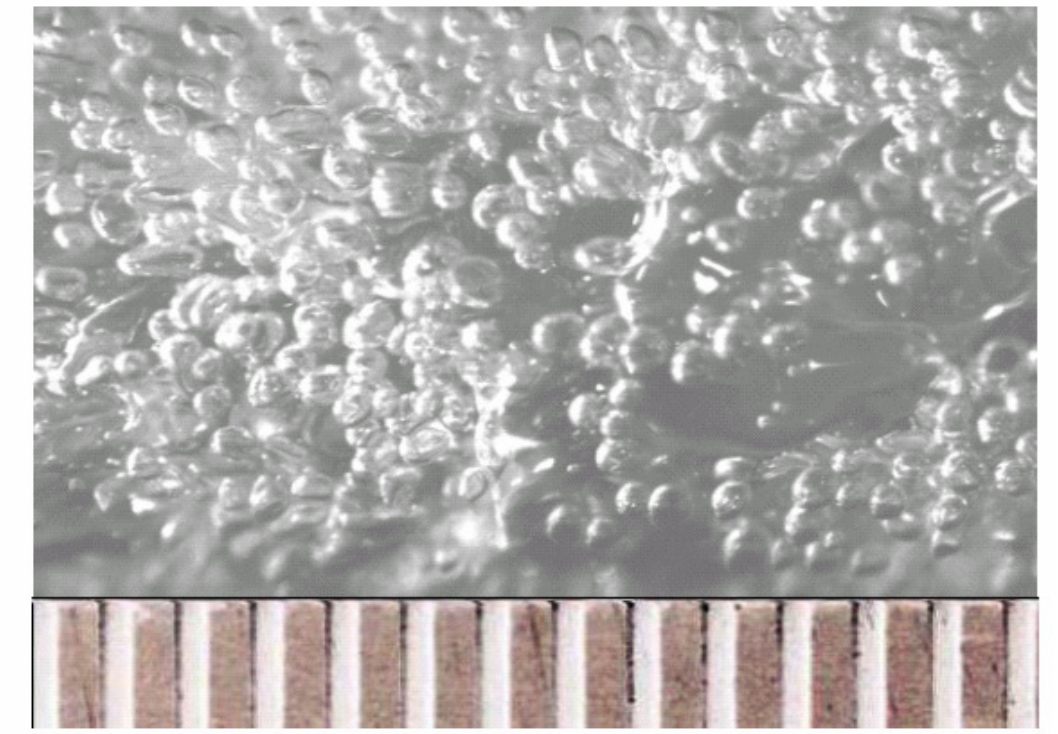

Fig. 4.3. The bubble images obtained by the SBII method for the 1% β. The subsequent vertical lines in the scale correspond to 0.5 mm.

d) In the QCV method, a fast-cam was implemented (250 f/s) to capture the asynchronization time between the pneumatic controlled valves. The ball valve was suddenly closed pneumatically to capture the water-phase in a particular section of the nozzle feeding conduit.

e) In the SPT method, four thin film OMEGA pressure transducers (PX613-100G5V) were inserted at four different locations along the nozzle feeding conduit to measure the local static pressure.

f) A high sensitivity Kistler quartz force transducer (9203 type with mounting thread of M10x1) was used to measure impact force at a carrying radial position with the 3-D traversing rig. In addition, a Kistler dual mode charge amplifier

(5010B) was implemented to convert the charge signal from a high impedance piezoelectric force sensor into a high level output voltage.

4.3. Results and Discussions

A strong positive correlation may be a result of smaller droplets having lower velocities or larger droplets traveling at higher velocities. Similarly, a strong negative correlation may result either due to larger droplets associated with lower velocities or smaller droplets associated with higher velocities [6]. In the previous studies [1, 4, 6], the total number of samples (N) were 10,000. In the present study, 20,000 samples were used. Previous studies [1, 4, 6] pointed out that large droplets exist near the spray periphery and smaller droplets exist at the center of the spray. In addition, they indicated that the correlation factors close to zero at the center of the spray, whereas a strong positive correlation exists at the periphery of the spray. However, in the present study it was observed that large droplets exist near the spray periphery and at the center, while smaller droplets exist in between the center and periphery of the spray. Due to the existence of the large liquid ligaments at the center of the spray, the droplet sizes are also larger near the tip of the nozzle. Further downstream in the spray (axially) this effect diminishes and primary and secondary break-up completes. In , axial velocity with changing axial distances across the spray (radial) is depicted for the 2% β case. In each case the radial distance, R, is –30 mm to +30 mm. Here 'r' represents the radial axis. In , it is demonstrated that axial velocity of the spray decreases with axial distances further downstream of the spray ($30D_n$, $60D_n$, and $120D_n$). However, near the tip of the spray ($15D_n$) axial velocity is lower than further downstream of the spray. In two-phase, gas/liquid spray near the tip of the nozzle there is a sudden expansion of the gas phase in the radial direction. However, the liquid phase does not follow this sudden expansion. In addition, near the tip of the nozzle the mixture pressure is not atmospheric as in a single-phase flow. It requires a certain amount of time to reach the atmospheric pressure further downstream of the spray. Near the tip of the nozzle ($15D_n$), the gas phase

momentum is not totally transferred to the liquid phase. Thus, a substantial amount of drag force reduces the axial velocity of the spray near the tip of the nozzle.

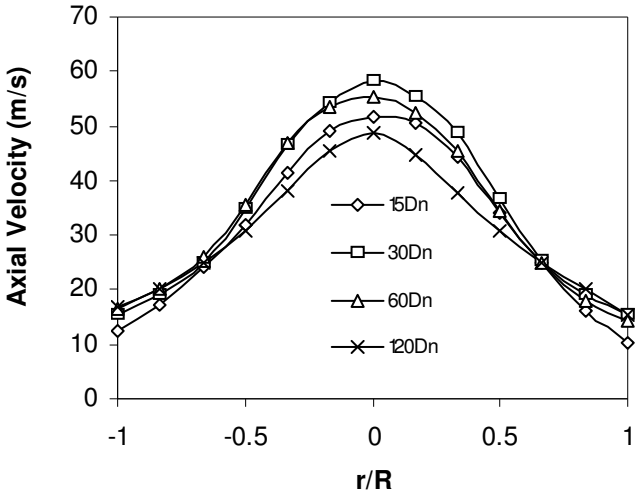

Fig. 4.4. Axial velocity variation with the radius of the spray for the changing axial distances (15D_n, 30D_n, 60D_n, 120D_n) and 2% β.

In , the β was changed from 0.30% to 9.3%. In this case the mixture pressure was kept constant at 620 kPa. The axial velocity decreased with an increase in β. It is recognized that higher β (9.3%, 5.9%, 3.2%) induces higher axial velocity at the center of the spray. However, near the center of the spray the axial velocity decreases steeply as the droplet diameter starts to decrease. This steep decrease of the axial velocity is more dominant with the higher β, as at the higher β the droplets are smaller. In , the D_{32} with changing axial distances across the spray (radial) is depicted for the 2% β case. The radial distance, R, varies from –30 mm to +30 mm. Generally the D_{32} provides a good indication of the drop size dispersion characteristics. The D_{32} can be expressed as follows:

$$D_{32} = \frac{\sum N_i D_i^3}{\sum N_i D_i^2} \tag{1}$$

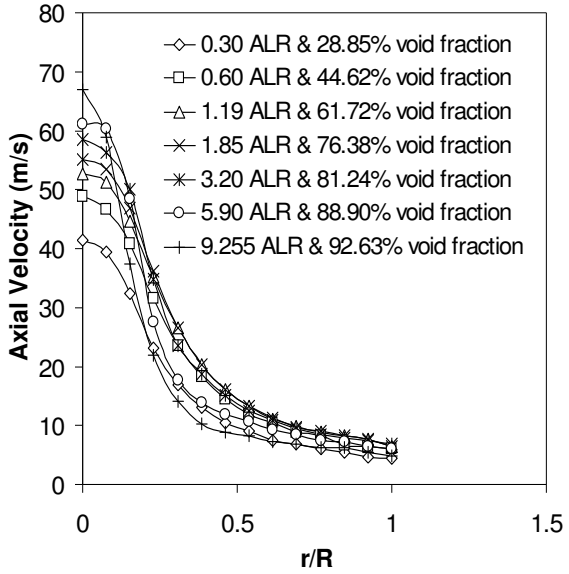

Fig. 4.5 Axial velocity variation with the radius of the spray for the changing the β. In this case mixture pressure was remained constant at 620 kPa.

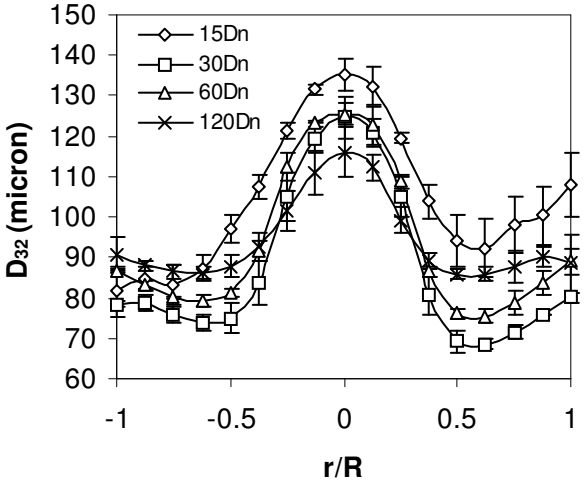

Fig. 4.6. Sauter mean diameter (D_{32}) variation with the radius of the spray for the changing axial distances ($15D_n$, $30D_n$, $60D_n$, $120D_n$) and 2% β.

A remarkable peak is observed at the center and at the periphery of the spray. As the D_{32} is based on the volume-to-surface ratio, a few larger droplets will increase the D_{32} value significantly in the spray. It is observed that at the center of the spray, the D_{32} values are 135 μm (204 μm for 1% β case), 125 μm (182 μm for 1%

β case), 124 μm (177 μm for 1% β case) and 116 (153 μm for 1% β case) at $15D_n$, $30D_n$, $60D_n$, $120D_n$, respectively. Whereas in between the center and periphery (r/R=0.7-0.8), the D_{32} values decrease to values of 92 μm (154 μm for 1% β case), 69 μm (138 μm for 1% β case), 76 μm (137 μm for 1% β case) and 86 μm (133 μm for 1% β case) at $15D_n$, $30D_n$, $60D_n$, $120D_n$, respectively. At the periphery (r/R=1, which corresponds to 30 mm from the center of the spray) again the values of the D_{32} increases to values of 108 μm (161 μm for 1% β case), 80 μm (142 μm for 1% β case), 89 μm (141 μm for 1% β case) and 88 μm (139 μm for 1% β case) at $15D_n$, $30D_n$, $60D_n$, $120D_n$, respectively. In , the β was changed from 0.30% to 9.3% and the corresponding change in the D_{32} values are depicted. In this case the mixture pressure was kept constant at 620 kPa. The D_{32} values decrease with the increases in the β. It is recognized higher D_{32} values exist at the center of the spray. This behavior is more dominant for the lower β. However, in the radial direction the D_{32} values decrease steeply. This decrease of the D_{32} values is steeper for the lower β cases. This also indicates the existence of a stronger positive correlation between the droplet diameter and axial velocity at the center of the spray and in between the spray and periphery; and a stronger negative correlation at the periphery of the spray. In addition, it is observed that at the 9.3% β and at the center of the spray there is an increase of the D_{32} value. This increase of the D_{32} occurs due to enhanced pulsation at the center of the spray with this high β. Moreover, in this case the high amount of air mass flow might cause a gas explosion at the tip of the nozzle, which induces substantial amount of drag force inhibiting proper spray breakup.

In , the mean diameter with changing axial distances across the spray (radial) is depicted for 2% β case. In each case the radial distance, R, is –30 mm to +30 mm. Mean diameter can be expressed as:

$$D_{10} = \frac{\sum N_i D_i}{\sum N_i} \tag{2}$$

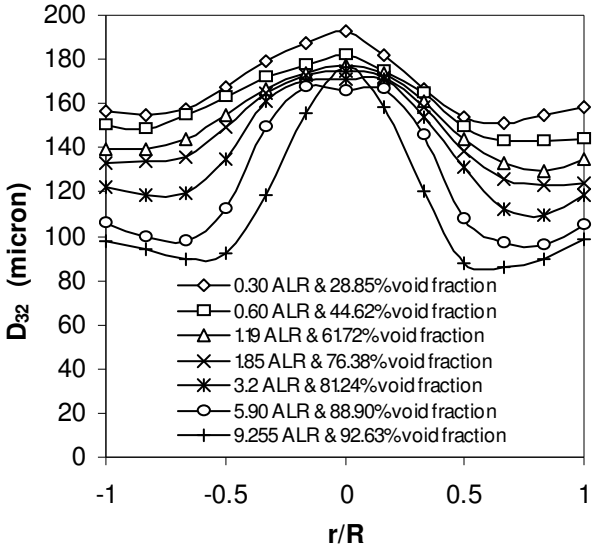

Fig. 4.7. Sauter mean diameter (D_{32}) variation with the radius of the spray for the changing β. In this case mixture pressure was remained constant at 620 kPa.

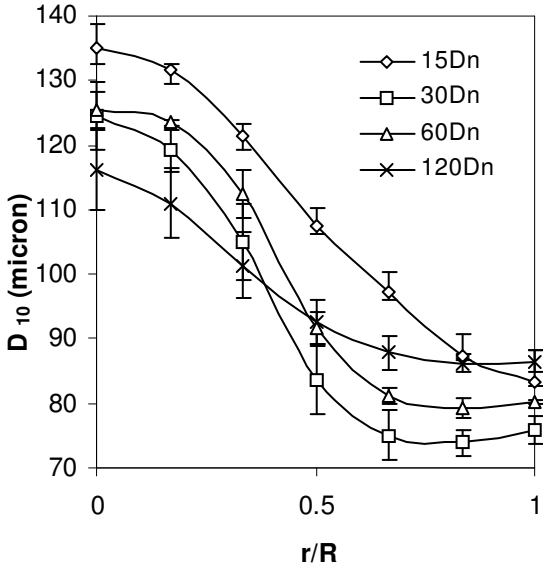

Fig. 4.8. Mean diameter (D_{10}) variation with the radius of the spray for the changing distances ($15D_n$, $30D_n$, $60D_n$, $120D_n$) and 2% β.

If the mean diameter is small, the droplets are fully responsive to the fluid fluctuations. If the mean diameter is large, the droplets have excess inertia and do not follow the fluctuations in the carrier phase. The droplet response with the

fluctuations can be better represented by the Stokes numbers, which will be shown in future data analysis. In , it is observed that at the center of the spray near the tip of the nozzle ($15D_n$) the droplet sizes are larger. However, further downstream of the nozzle ($30D_n$, and $60D_n$) the D_{10} values are smaller at the center of the spray and shortly further from the spray center, the values of the D_{10} decreases steeply. Further downstream of the spray ($120D_n$), the secondary break-up of the spray completes and the D_{10} profile is likely to attain a flattened profile illustrating that the equilibrium condition would shortly be achieved further downstream. Secondary break-up in a spray occurs when larger droplet or liquid ligaments break down into smaller droplets. The breakup of a single droplet in a gas is caused by either relative velocity or turbulence; or shock structure interaction, acting separately [7]. If the aerodynamic forces overcome the forces due to surface tension, the droplet will deform [8]. If the relative velocity between the two phases is small, the droplet will be stable. If the relative velocity between the phases is larger, the droplet starts to break-up. At this stage aerodynamic forces overcome the surface tension of the liquid phase. The aerodynamic Weber number plays an important role in droplet break-up. If the aerodynamic Weber number exceeds the critical Weber number, secondary break-up occurs. As surface tension has a stabilizing effect, an increase in viscosity damps unstable perturbations [7]. In , the β was changed from 0.30% to 9.3% and the corresponding change in the D_{10} values is depicted. In this case the mixture pressure remained constant at 620 kPa. The D_{10} values decrease with the increase in the β ratio. It is recognized that higher D_{10} values exist at the center of the spray. This behavior is dominant with the lower β cases. However, slightly further from the center of the spray in a radial direction, the D_{10} values decrease steeply. This decrease of the D_{10} values is more prominent for the higher β cases.

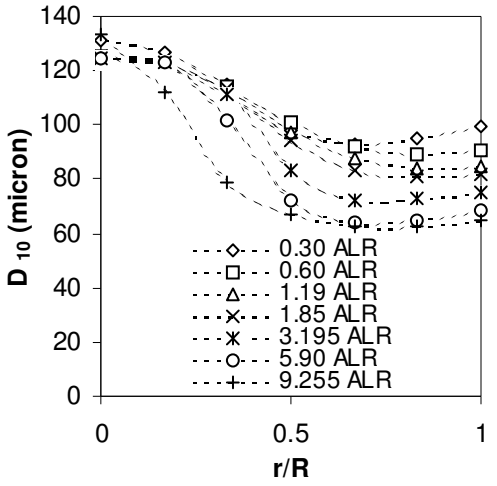

Fig. 4.9. Mean diameter (D_{10}) variation with the radius of the spray for the changing β. In this case mixture pressure remained constant at 620 kPa.

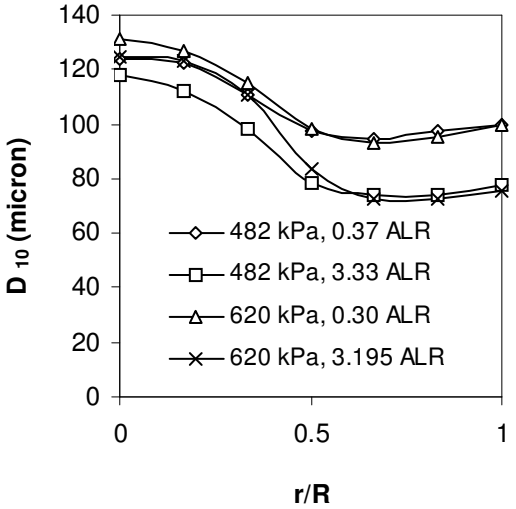

Fig. 4.10. Mean diameter (D_{10}) variation with the radius of the spray for the changing mixture pressure of 482 kPa and 620 kPa.

The effects of the mixture pressure in the D_{10} profile is depicted in . In this figure it is observed that the D_{10} values at the center of the spray are 118 μm and 124 μm at the lower mixture pressure (482 kPa, 3.3% β) and the higher mixture pressure (620 kPa, 3.2% β), respectively. However, at the periphery of the spray, this variation of the D_{10} value is not significant with the change in mixture pressure.

4.4. Conclusions

The PDPA has been used for spray characteristic measurements issuing from a wide variety of nozzles. However, the application of the PDPA is still a challenge in highly concentrated multiphase spray. In this study, it is observed that the axial velocity of spray is predominant at the center of the spray. Further downstream of the spray this axial velocity reduces. At this point secondary break-up of the spray completes. This completion of the break-up induces more dispersed and tiny droplets further downstream of the spray. The mean droplet and Sauter mean diameter is an important parameter to characterize a spray. This study indicates that there exists a strong positive correlation between the droplet diameter and axial velocity at the center of the spray. A strong positive correlation also exists between the center and periphery of the spray (r/R=0-0.5). A strong negative correlation exists at the periphery of the spray (r/R=1).

4.5. References

[1] MacGregor, S.A. (1991) Air Entrainment in Spray Jets. Int. J. Heat and Fluid Flow 12, 279–283.

[2] Ariyapadi, S., Balachandar, R., Berruti, F. (2000) Effect of Cross-Flow on the Spray Characteristics of an Industrial Feed Nozzle, paper 75b Proc. AIChE Spring Annual meeting, Atlanta, GA.

[3] Tafreshi, Z.M., Kirpalani, D., Bennett, A., McCracken, T.W. (2002) Improving the efficiency of fluid cokers by altering two-phase feed characteristics. Powder Technology 125, 234– 241.

[4] Ejim, C.E., Fleck, B.A., Amirfazli, A. (2005). A Scaling Study of the Atomization of a Two-Phase Industrial Nozzle: Part 1 - Effect of Surface Tension and Viscosity on Mean Drop Size Profiles. Proceedings of the 20th ILASS - Europe Meeting, Sept. 5-7, Orléans, France.

[5] Dantec Dynamics, A.S. (2003). BSA Flow Software, Version 2.1: Installation and User's guide, Skovlunde.

[6] Ariyapadi, S., Balachandar, R., Berruti, F., (2003) Spray Characteristics of Two-phase Feed Nozzles. The Canadian Journal of Chemical Engineering 81, 923-939.

[7] Crowe, C.T. (2006) Multiphase flow handbook CRC: Taylor & Francis, Boca Raton, FL.

[8] Low, T.B., List, R. (1982) Collision, coalescence and breakup of raindrops. J. Atmos. Sci. 39, 1591–1618.

CHAPTER 5

Two-Phase Atomization Characterization: Stokes Number & Aerodynamic Weber Number[1, 2]

5.1. Introduction

In fluid coking, the gas (steam) and liquid (bitumen) mix well upstream of the feed nozzles where the mixture is atomized to form a spray. One of the drawbacks found with the fluid coking nozzles is the development of instabilities in the spray caused by the two-phase gas/liquid flow patterns formed inside or upstream of the nozzle at the higher β [1, 2]. A stable spray is demonstrated by a good dispersion of the liquid phase. It is desirable to produce a stable spray with minimum Sauter Mean Diameter (D_{32}) and well-dispersed liquid droplets. A desired bitumen drop size in contact with a given coke particle is one with the same nominal diameter as the coke particle. This ensures that the coke is adequately and sufficiently coated with a thin layer of bitumen [3]. On the other hand, an unstable spray is characterized by intermittency or pulsation in its flow regime with the random formation of fine and coarse droplets in the spray. These pulsations are attributed to the two-phase gas/liquid fluid conditions, such as gas to liquid mass ratio (β), void fraction (α), the mixing pressure (P_m), the design of the mixing chamber and the geometry of nozzle [4]. Previous studies [5, 6] showed that as the β is increased, for a constant operating pressure at a certain transition point (e.g. β >1.0% in the large-scale nozzle), the spray becomes unstable. A homogeneous mixture of the gas-liquid entering the nozzle would maximize the effect of the decompression of the gas phase, resulting in a stable spray. On the other hand, a heterogeneous flow entering into the nozzle causes an unstable spray formation

[1] A version of this chapter has been published. Rahman *et al.* (2009) (2009) IOP Journal of Physics – Conference Series. 147: 1-15

[2] A version of this chapter has been published. Rahman *et al.* (2010) ILASS Europe- 2010, Brno, Czech Republic, 6-8th September.

[7].

Enhanced heat and mass transfer can be achieved from a spray, which is composed of dispersed droplets with larger spread rates. Moreover, as the droplet sizes are reduced, the energy of the droplets is more readily transferred to the surrounding fluid [8]. This would ensure proper mixing with the surrounding fluids. Furthermore, in processes where the feed needs to be injected into a cross-flowing stream, the droplets in the spray must have enough momentum to penetrate the cross-flowing fluid stream [9]. Continuous and fine spray characteristics are desirable in the feeding nozzle. This feed nozzle is used in the heavy oil process industry. Preheated bitumen and steam is mixed upstream of the nozzle and subsequently injected into fluid bed coker reactors via feed nozzles. One of the drawbacks of this spray characteristic is the pulsation within the spray and in the feeding conduit, which is highly undesirable to yield high productivity. These pulsations result in poor atomization and in most instances, a slug of liquid is ejected out of the nozzle.

It is convenient to work with mean drop sizes instead of complete drop size distributions in the two-phase gas/liquid atomization characterization. The mean drop size distribution is generalized as follows [10, 11]:

$$(D_{ab})^{a-b} = \frac{\int_{D_0}^{D_m} D^a (DN/dD) dD}{\int_{D_0}^{D_m} D^b (DN/dD) dD} \qquad (1)$$

The values of a and b can be found in [10]). Generally D_{32} provides a good indication of the drop size dispersion characteristics and is used for mass transfer application. The D_{10} diameter is used for comparison purposes, the D_{20} diameter is used for surface area controlling applications, the D_{30} diameter is used for volume controlling applications and the D_{43} diameter is used for combustion equilibrium application. In the droplet motion, the *Stokes number (St)* is a very important

parameter. The *St* is defined as the ratio of the particle momentum response time over a flow system time, defined as: $St = \tau_p / \tau_c = \rho_p d_p^2 u_c / 18\mu_c L$. Two types of situations can be observed for particles (bubbles/droplets) suspended in fluid, namely: a) if the *St*<<1, the particles will have ample time to respond to changes in flow velocity, b) if *St*>>1, then the particle will have essentially no time to respond to the fluid velocity changes and the particle velocity will be little affected by fluid velocity change [12].

A spray breaks up further downstream from the tip of a nozzle. A typical two-phase gas/liquid atomization process involves a) primary atomization (*PA*), b) secondary atomization process (SA). The dominant forces involved in the atomization process are: (i) hydrodynamic or inertial forces attributed to undulations/perturbations, (ii) aerodynamic forces attributed to drag/shearing effects, (iii) viscous forces attributed to opposing a change in liquid geometry, and (iv) surface tension forces attributed to a minimum surface energy [13]. The first two forces are disruptive in nature while the second two forces are cohesive in nature. The interaction of internal forces such as: a) turbulence, b) inertial effects, c) momentum transfer between transverse layers of a jet are mainly responsible for the PA [14]. At this stage the disruptive forces exceed the consolidating forces, resulting in oscillations on the liquid surface and subsequently disintegration of the bulk liquid into drops [15, 16]. The SA in a spray occurs when larger droplets or liquid ligaments break down into smaller droplets. The break-up of a single droplet in a gas is caused by either greater relative velocity, or turbulence [12]. The SA occurs due to two force ratios acting on the drop [17]. Firstly, if the aerodynamic forces overcome the forces due to the surface tension, the droplet will further deform [18]. The ratio of these two forces can be represented by the *Weber number*, which can be defined as: i) aerodynamic/gas *Weber number*: $We_g = \rho_g u_{rel}^2 d_d / \sigma$ or ii) liquid *Weber number*: $We_l = \rho_l u_l^2 d_d / \sigma$. Secondly, the *Ohnesorge number or Laplace number*, denoted by: $Oh = \sqrt{We_l} / \mathrm{Re}_l$

$= \mu_l / \sqrt{\rho_l d_d \sigma} = 1/\sqrt{Lp}$, which is the ratio of liquid viscous force to surface tension force on the drop, also plays an important role in the SA. Here Re_l is the liquid *Reynolds number* defined: $\mathrm{Re}_l = \rho_l u_l d_d / \mu_l$. Mathematically, if the We_g exceeds the We_{crit}, the SA occurs. For low-viscosity liquids, We_{crit} = 6 to 13 for $Oh < 0.1$, $We_{crit} \approx Oh^2$ for $Oh > 0.1$ [19]. In the two-phase gas/liquid spray characteristics measurement, the PDPA system and digital image analysis techniques have been used as advanced experimental techniques. The PDPA measurement techniques to measure the two-phase gas/liquid spray can be found in the literature [20-23]. Recently developed digital image analysis techniques are also potentially capable of sizing particles of arbitrary shape and size and with a wide dynamic range [1, 24, 25].

Measurement techniques of the two-phase gas/liquid flows/sprays are a challenge. Due to highly non-uniform volumetric flow distributions and intermittency in the flow, it is extremely difficult to predict accurate droplet sizes (d_d) and flow pattern distributions in this type of flow. This uncertainty of the d_d prediction is exaggerated if the nozzle feeding length is short, as in the present study (36.8 cm); since the two-phase gas/liquid flow cannot be fully developed within this short pipe length. The nozzles currently used in this study do not belong specifically to any of the nozzle classes for the two-phase gas/liquid flows existing as twin-fluid nozzles. Moreover, in recent years several studies [10, 13, 26-28] conducted atomization studies in the feed nozzles. However, these studies were based on the equilibrium flow condition, in vertical nozzle configurations and in a larger length scale set-up. In contrast to the above studies, the current study deals with the non-equilibrium flow condition (in which the nozzle feeding conduit is very short), in a horizontal nozzle configuration and in a smaller length scale set-up.

The objectives of this study are: i) to predict correlations between the spray disintegration process and the nozzle feeding conduit flow characteristics, ii) to

understand the fundamentals of the two-phase gas/liquid flow patterns, and spray characteristics. The proposed study will contribute to the fundamental knowledge of the two-phase gas/liquid flows and make concrete headway in the design of an industrial nozzle used in a large-scale high impact operation.

5.2. Experimental Set-Up

In this study, a laboratory scale nozzle assembly was implemented. The dimension was at one-quarter scale of a patented full-scale design (US Patent #: 6003789) employed in a fluidized bed coker for heavy oil upgrading. A feeding conduit of 36.8 cm in length and 6.35 mm ID was used upstream of the nozzle. The nozzle diameter (D_n) was 3.10 mm. Gas (air) was supplied from a compressor and liquid was supplied from a reciprocating pump. These two fluids mixed together at a T-mixer prior to the feeding conduit. This nozzle assembly was mounted on a 3-D automated traversing rig. The experimental schematic diagram is presented in Fig. 5.1.

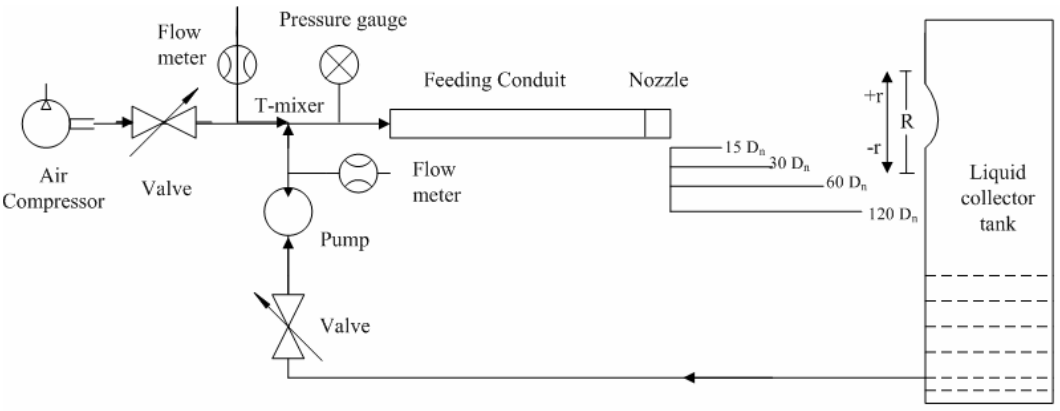

Fig. 5.1. Schematic of the experimental set-up (adapted from [29]).

Mean drop size was measured using a 2D-PDPA from the Dantec Dynamics specifications [30]. The focal lengths of the PDPA transmitter and receiver lenses were 400 mm and 310 mm, respectively. During data collection, the PDPA was operated in refraction and forward-scatter mode, and the receiver was set to a

scattering angle (ϕ) of 30° for the air-water tests. Dantec [31] specified that first order refraction was the most dominant scattering mode at ϕ = 30° for water droplets in air (about 10^2 orders of magnitude higher compared to the backward scattering mode). This technique can simultaneously measure velocity and particle size of known refractive index. This method is termed as "2D-PDPA" as this technique can measure velocity of two orthogonal axes. The optical setting of the 2D-PDPA is presented in

. The green Nd-YAG and red He-Ne laser power are 200 mW and 20 mW, respectively. Their wavelengths are 532 and 632.8 nm, respectively. Each laser split in two laser beams using the unit's Bragg cell. The resulting four beams (two pairs for each laser) are set at a distance of 90^o apart from each other and converge at the focal length of the transmitter lens to form a control volume.

Table 5.1. Optical settings of the PDPA unit used in the study

Parameter	**Unit**	**Values**
Scattering angle	(-)	30°
Beam spacing	mm	38.0
Beam expansion ratio	(-)	1.0
Receiver focal length	mm	310
Beam diameter	mm	1.35
Transmitter focal length	(mm	400
Receiver slit width or aperture	mm	0.1
He-Ne laser wavelength	nm	632.8
Nd-YAG laser wavelength	nm	532

Droplet size was measured by detecting the incident droplets on the receiver detectors. The size of a droplet is directly proportional to the phase shift of scattered light in the control volume. The velocity of droplets can also be found by detecting the incident droplets on the receiver detectors. However, in this case the droplets passing through the control volume transmit Doppler frequencies or

signals that are directly proportional to their velocity. These Doppler frequencies are detected by the receiver. Radial spray profiles were measured using the PDPA on the $30D_n$, $60D_n$, and $120D_n$ axial distances downstream of the nozzle orifice. Measurements were taken varying the radial positions (r) by the 3-D traversing rig. The values of D_{32}, D_{10}, and u_x were measured with the changing β, r, and x positions. The measurement uncertainty and sample size information is provided in Chapter 7.

5.3. Results and Discussions

The D_{32} provides a good indication of the drop size dispersion characteristics in the two-phase gas/liquid spray. From Fig. 5.2 it is evident that D_{32} values are greater at the center of the two-phase gas/liquid spray due to higher non-spherical droplet density persisting around this zone. However, further away from the center of the spray, the D_{32} values significantly decrease, as around this zone droplets are more disperse. At the periphery of the spray, the D_{32} values are flattened out and in some cases increase a bit, as around these region droplets does not encounter any aerodynamic shear force.

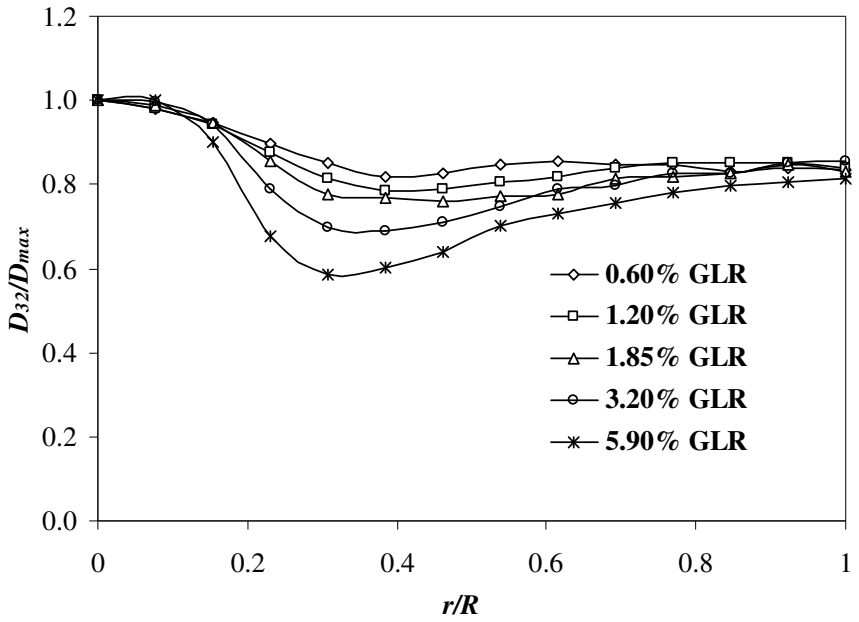

Fig. 5.2. Effects of the β on the D_{32} profiles with changing r at a fixed axial distance of *60* D_n and 620 kPa mixing pressure. The uncertainty in the PDPA measurement is reported in Chapter 8.

In Fig. 5.3, D_{10}, D_{20}, D_{30}, D_{32} and D_{43} profiles with changing r at a fixed axial distance of *60* D_n and 620 kPa mixing pressure (P_m) is depicted. All the profiles indicate that the droplet sizes are greater at the center of the spray. However, further away from the center of the spray, the droplet size decreases significantly and finally flatten out at the periphery of the spray. The PDPA provides the two-component droplet velocity (u_x, u_y) and droplet diameter (d_d). However, it cannot provide the continuous phase gas (air) velocity data in the two-phase gas/liquid sprays. Experimentally it is difficult to obtain the continuous phase gas velocity data in the two-phase gas/liquid atomization process.

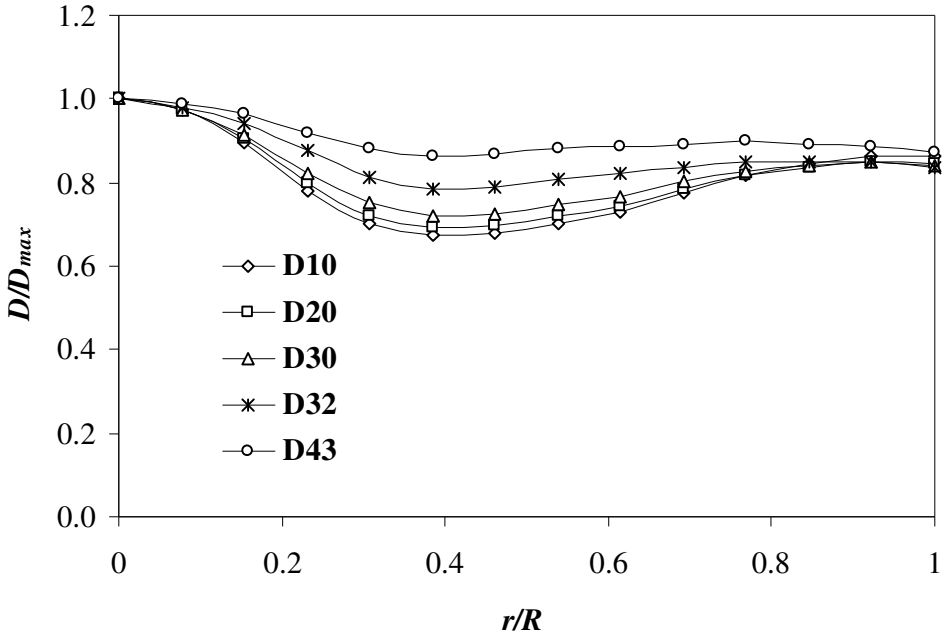

Fig. 5.3. Profiles of D_{10}, D_{20}, D_{30}, D_{32}, D_{43} with changing r at a fixed axial distance of *60* D_n and 620 kPa mixing pressure.

However, a study [32] provided a correlation for how to obtain the continuous phase gas velocity by solving a particle motion equation and knowing the droplet velocity from the PDPA. This correlation is defined: $U_d/U_g \cong 1/(1+St)$. Here, *St* was the *Stokes number*. If the *St* Number tends to be zero, there would be no slip between the two phases of fluid. In this study, the U_g value was obtained from the *St* number and by knowing the U_d and D_{10} values from the PDPA data.

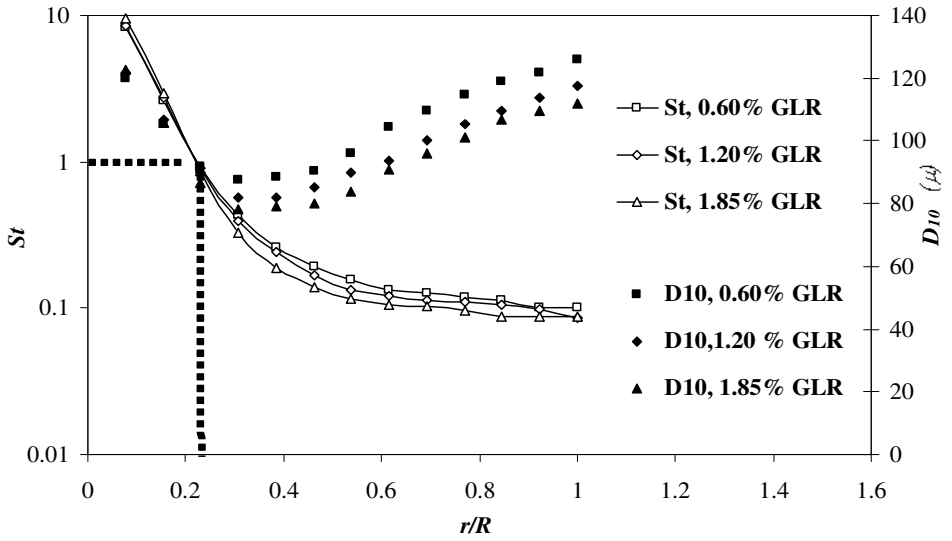

Fig. 5.4. Effects of the β on the *St* and D_{10} profiles with changing *r* at a fixed axial distance of $60D_n$ and 620 kPa mixing pressure.

In the atomization process, the *St* number is a very important parameter. The *St* number is defined as the ratio of the droplet momentum response time over a flow system response time, defined as: $St = \tau_p/\tau_c = \rho_l D^2_{10} U_l/18\mu_l r$. In Fig. 5.4, the droplet *St* number and D_{10} profiles with changing *r* and β at a fixed axial distance of $60\ D_n$ are depicted. The P_m was maintained at a constant pressure of 620 kPa and the flow rates of gas/liquid were varied to obtain different β of 0.60%, 1.20% and 1.85% at the constant pressure of 620 kPa. Here, *R* is the radius of the spray which is 65 mm. First, it is observed that if the '*r*' increases, the *St* number decreases remarkably due to the smaller droplet response time at the periphery of

the spray. If the $St<<1$, the droplets will have ample time to respond to changes in continuous phase flow velocity. However, if $St>>1$, then the droplets will have essentially no time to respond to the continuous phase fluid velocity changes and the droplet velocity will be affected very little by the fluid velocity change [12]. In the current study similar observations for droplets suspended in the atmospheric air were noticed. The *St* number reached a value of one at *r/R* of 0.25. Thus, at the center of the spray the droplet response time is much higher than that of the continuous air phase. At the center of the spray, a remarkable amount of slip exists between the liquid and gaseous phases. However, at the spray outer region, the droplet response time followed the continuous phase response time. In addition to the above fact, it is also observed that the *St* Number profiles do not differ significantly in the radial direction for the β values of 0.60%, 1.20%, and 1.85% at the constant pressure of 620 kPa until the point where the *St* Number is equal to 1. However, after the point where the *St* Number is equal to 1, the higher β exhibits the lower *St* Numbers in the radial direction due to the reduction of the jet half width.

Droplet response with the *St* number can be further demonstrated by the D_{10} profile data set. In Fig. 5.4, it is initially observed that if the β values are increased, the D_{10} values are decreased. Secondly, until the $St = 1$ at the radial distance of $r/R = 0.25$, the D_{10} values are decreased as the droplets continue to break-up up to this point. However, as soon as the *St* reaches 1, droplet break-up began to cease; thus the droplets started to coalesce forming bigger droplets (higher D_{10} values) with increasing radial distances.

The two-phase gas/liquid atomization behavior can be fully understood by the aerodynamic *Weber* number (We_g) and droplet *Reynolds* number (Re_d). The We_g is the measure of the relative importance of the fluids' inertia compared to its surface tension, which can be defined as $We_g = \rho_l (U_l - U_g)^2 \, r/\sigma$. Whereas the Re_d is the measure of the relative importance of the droplet's inertia compared to its

viscosity, which is defined as $Re_d = \rho_l U_l r/\mu$. A spray breaks up further downstream from the tip of a nozzle. A mechanism for the two-phase gas/liquid atomization is the '*bubble energy*' explosion [5, 27]. It was postulated that jet break-up occurs when the bubbles within the bulk liquid possess enough energy to overcome the surface tension forces that hold the liquid jet together. When the bubbles have enough energy, the droplets further atomize through bubble explosions.

In Fig. 5.5, the droplet break-up mechanism was investigated by the We_g, Re_d and U_g profiles with changing r and β at a fixed axial distance of $60D_n$. Here, R was the radius of the spray which was 65 mm. The P_m was maintained at a constant pressure of 620 kPa and the flow rates of gas and liquid were varied to obtain the β of 1.20%, 1.85% and 3.20% at that constant pressure. An interesting observation is that the U_g has higher values between the center and periphery of the spray in the radial direction (r). Due to this peak of the U_g value, the droplets break-up further downstream radially and axially, which is termed as the SA. In the literature, several correlations were hypothesized to predict the SA in terms of the We_g. The interaction of internal forces such as turbulence, inertial effects and momentum transfer between transverse layers of a jet, are mainly responsible for the PA [14]. At this stage the disruptive forces exceeded the consolidating forces which resulted in oscillations on the liquid surface and subsequently disintegrated the bulk liquid into drops [15, 16]. The SA in a spray occurs when larger droplets or liquid ligaments break down into smaller droplets. The break-up of a single droplet in a gas is caused by either greater relative velocity, or turbulence [12]. In Fig. 5.5, the greater relative velocity exists at this peak point of U_g profile. The SA occurs due to two force ratios acting on the drop [17]. If at first the aerodynamic forces overcome the forces due to the surface tension, the droplet will further deform [18]. The two dimensionless numbers can represent the ratio of these two forces. The We_g plays a vital role in the first stage of the SA process. Secondly, the *Ohnesorge number*, denoted by Oh ($\mu_l/\sqrt{\rho_l d_d \sigma}$), which is the ratio of liquid

viscous force to surface tension force on the drop, also plays an important role in the SA process. It was postulated that if the We_g exceeds the We_{crit} ('*crit*' denotes for critical), the SA occurs. For low-viscosity liquids, We_{crit} = 6 to 13 for Oh<0.1, $We_{crit} \approx Oh^2$ for Oh>0.1 [33]. To find out the We_{crit}, in Fig. 5.5 a perpendicular line was drawn from the peak value of the U_g profile that intersects the We_g number profile at a point. The value of the We_g number at this point can be termed as the We_{crit} which is approximately 500. In Fig. 5.5, it is also observed that the We_g and Re_d decreased remarkably with the radial distances up to the We_{crit} limit. However, after a few radial distances from the We_{crit} limit; the We_g and Re_d decrease slightly with the variation of the β values.

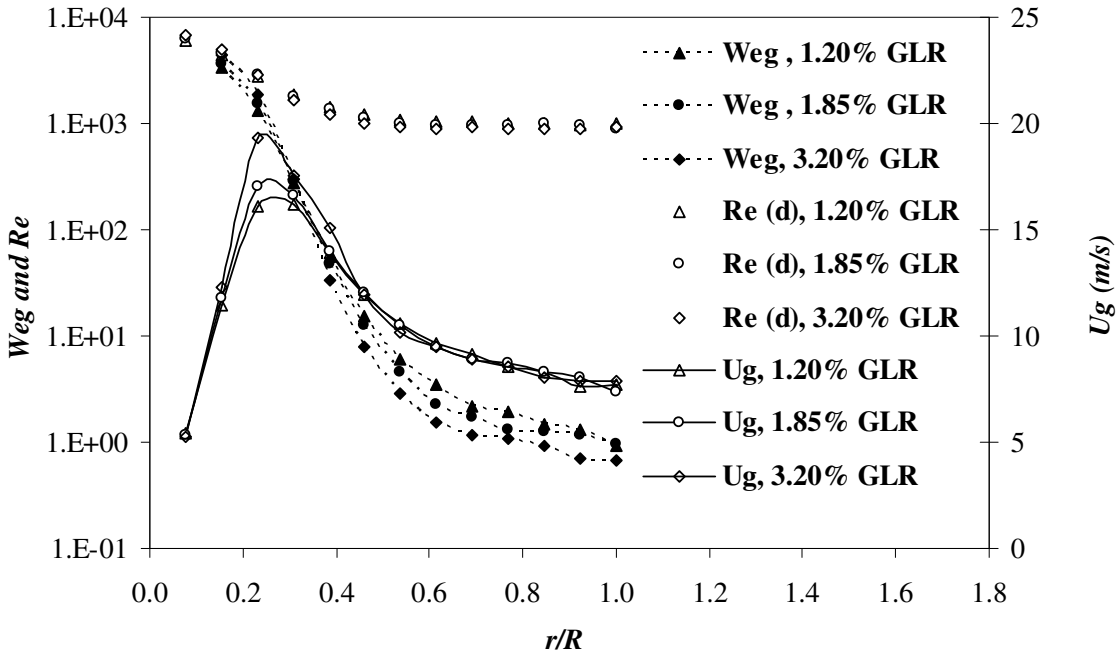

Fig. 5.5. Effects of the β on the We_g, Re_d and U_g profiles with changing r at a fixed axial distance of *60* D_n and 620 kPa mixing pressure.

In Fig. 5.5, it also observed that the Re_d varied from 700 to 7,000 due to the variation of the *r/R* values. If the Re_d<<1, the two-phase gas/liquid flow can be termed as *Stokes* flow. In the *Stokes* flow regime, viscous droplets remain spherical. The wake formed behind the droplets became stronger as the Re_d

increased and the inertia of the flow around the droplets overcame the viscosity effects on the surface of the droplets [12]. It is also observed that the Re_d value decreased with the radial distances. However, the U_g still has enough momentum, which can induce a slip between the two phases. Thus, although the R_d value decreases with the r, the higher relative velocity between the phases is still responsible for the SA process.

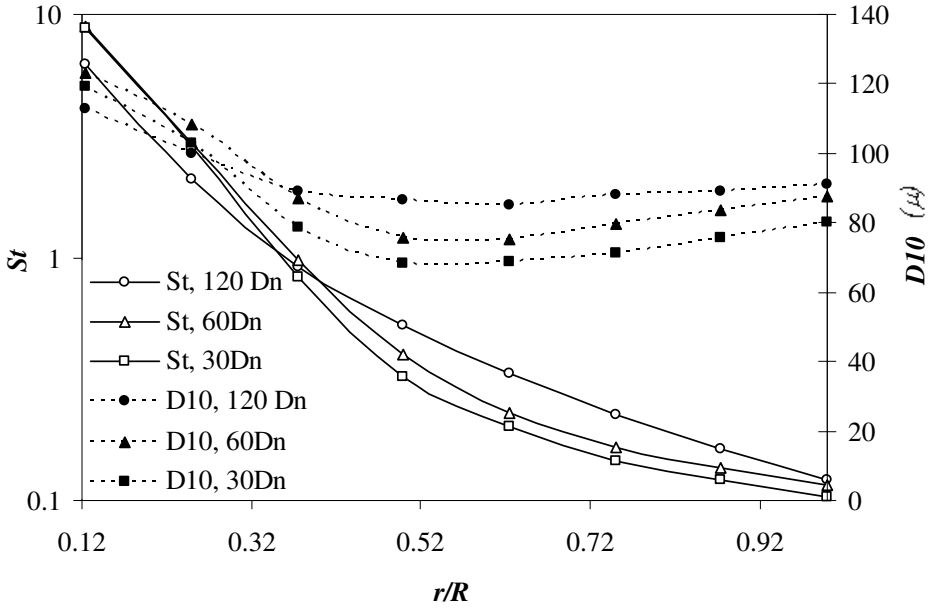

Fig. 5.6. Effects of the axial distances on the droplet *St* and D_{10} profiles with changing radial distances (r) at 2% β.

In Fig. 5.6, the droplet *St* and D_{10} profiles with changing axial distances (x of $30D_n$, $60D_n$, $120D_n$) and radial distances (r) are depicted. Here, R is the radius of the spray which was 40 mm with the β of 2% at a P_m of 520 kPa. It was initially observed that if the 'r' and 'x' increase, the *St* number decreases remarkably due to smaller droplet response time compared to that of the continuous phase gaseous medium. Secondly, the *St* number reaches the value of 1 at *r/R* of 0.40 for axial distances of $30D_n$, $60D_n$, $120\ D_n$, respectively. Droplet break-up characteristics

with the *St* number can also be verified with the D_{10} data. It was observed that at $120D_n$ downstream of the nozzle orifice, the droplets are more disperse compare to other two cases. Thus, near the center (r=0) of the spray at $120D_n$ downstream from the nozzle orifice, the D_{10} values are lower than at $30D_n$ and $60D_n$ downstream D_{10} values at the similar radial position (r =0). In the later cases, the droplets were not fully atomized, which can be further explained with the We_g and Re_d profiles. However, as soon as the *St* Number reaches 1, further away from the center, the D_{10} values are higher at $120D_n$ downstream from the nozzle orifice than at $30D_n$ and $60D_n$ downstream values at the similar radial position. This is due to the coalescence of droplets around this zone.

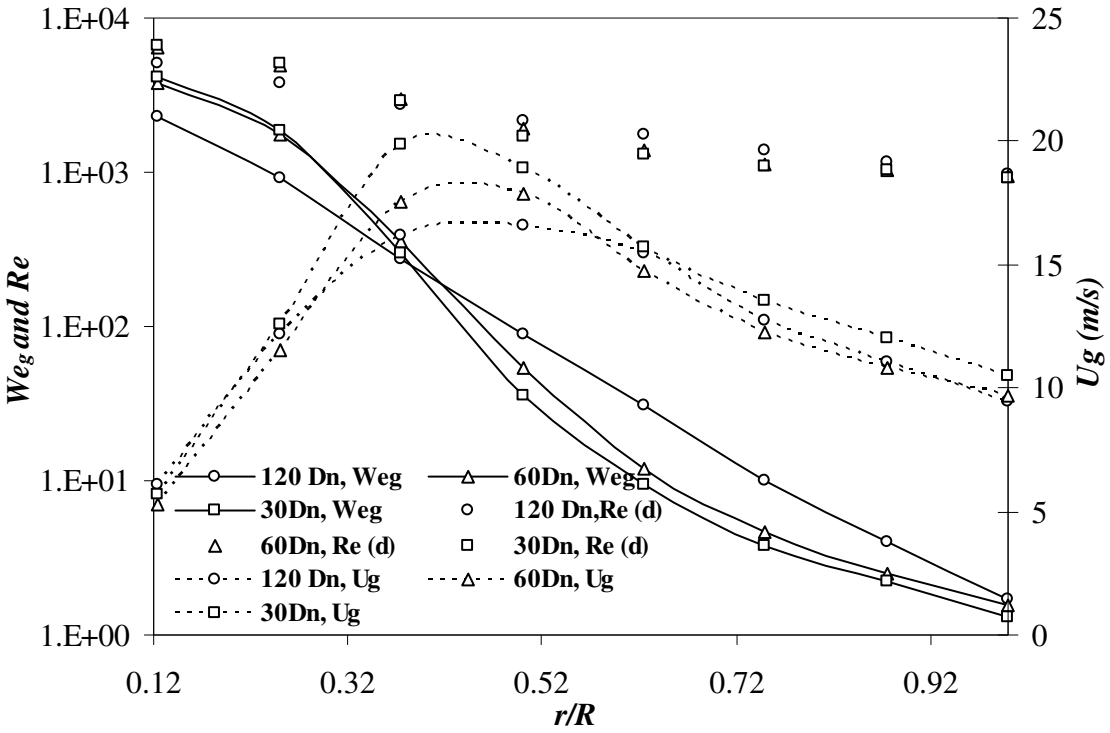

Fig. 5.7. Effects of the axial distances on the We_g, Re_d and U_g profiles with changing radial distances (r) at 2% β.

In Fig. 5.7, the droplet break-up mechanism was examined by the We_g, Re_d and U_g profiles with changing axial distances ($30D_n$, $60D_n$, $120D_n$) and radial distances (r). Here, R is the radius of the spray which was 40 mm. The β for this condition

was maintained at 2% with a P_m of 520 kPa. An interesting observation in Fig. 5.7 is that the U_g had higher values between the center and periphery of the spray in the radial direction. Until the highest U_g value, the droplets had a tendency to break-up further. Thus, in Fig. 5.7, again the We_{crit} value was obtained by drawing a perpendicular line from the U_g profile that intersects the We_g profile at a certain point. The value obtained at this point is termed the We_{crit}. In Fig. 5.7, it also observed that the We_g and Re_d decreased remarkably with axial distances and radial distances. If the We_g exceeds the We_{crit}, droplets will have the tendency to break-up further due to higher momentum transfer between the phases. Thus, it was observed that further downstream of the spray ($120D_n$), the We_{crit} value was less compared to the upstream condition ($30D_n$). However, the reverse case was observed for the U_g values. At $120D_n$ downstream from the orifice of the nozzle, the U_g had greater values compared to $30D_n$ downstream of the spray, indicating the bubble explosion imparted higher momentum than the gas phase further downstream.

In Fig. 5.7, it is also observed that the Re_d varied from 800 to 6,500 in the radial direction. Downstream of the spray ($120D_n$), the momentum of the droplet decreased remarkably compared to the upstream condition ($30D_n$). However, for similar positions the gas phase still had enough momentum as it had just been exploded at the nozzle orifice. This also provides the basis for why the U_g exhibits higher values at $120D_n$ compared to $30Dn$ and $60D_n$ downstream from the nozzle orifice. However, it seems that the Re_d values are lower further downstream as the droplets lose momentum. Thus, the Re_d values are not fully capable of explaining the droplet atomization behavior further downstream of the spray.

The available standard dimensionless numbers are effective tools to describe the break-up mechanism of two-phase gas/liquid atomization. From Fig. 5.8, it is evident that the Froude number and the Galileo number are the important numbers that demonstrate the dominant forces acting on the atomization. Thus, the gravity

force, inertia force, and the drag force are the dominant forces in the droplet formation from a nozzle which has a hybrid design of an effervescence nozzle and twin fluid nozzle. Gravity forces tries try to stabilize the system, thus inhibiting further break-up of droplets. On the contrary, the inertia force and drag force disrupt the system, thus enhance enhancing further break-up of droplets. When there is equilibrium between these forces, the droplet break up completes. Moreover, from this study is it evident that the gas phase velocity has an important role on the break up mechanism and while the mixing pressure has less effect on the atomization.

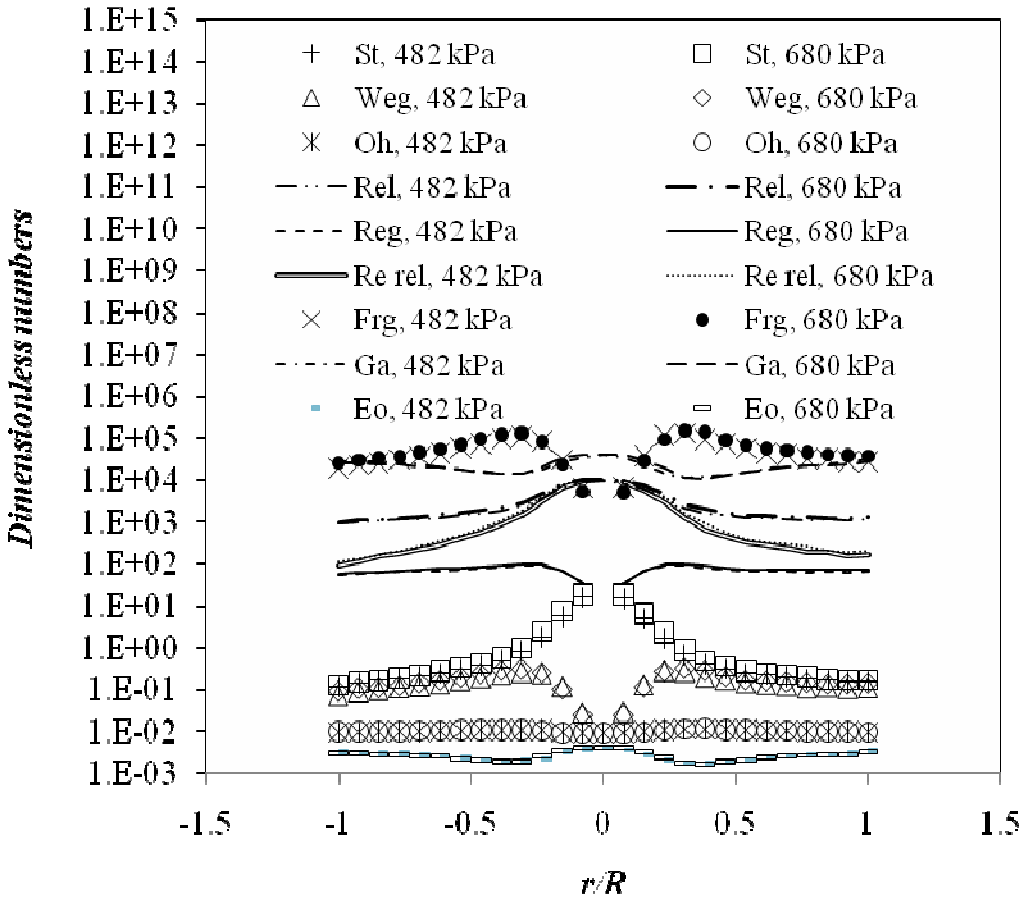

Fig. 5.8. Effects various dimensionless numbers of the spray beak up mechanism at 3% gas to liquid mass ratio and different mixing pressure.

5.4. Conclusions

The fundamental knowledge of the two-phase gas/liquid flow and atomization process in nozzles is important for many industrial and chemical reactions. The outcome of this research will help in the optimization of commercial process conditions and provide a comprehensive means of improving the design conditions of the two-phase gas/liquid flow and atomization process. Specifically, this study will assist to optimize the operating range of the existing steam/bitumen fluid cooking nozzles used in the heavy oil upgrading process. Knowledge obtained will contribute to the development of a new series of nozzles that the heavy oil industry is currently bringing to market.

Effervescent atomization from the nozzle likely depends on flow patterns, void fractions and bubble size distribution in the upstream nozzle fluid conduit. Thus, it is essential to have a good understanding and a reasonable estimation of the bubble size, flow regime, void fraction, pressure drop and subsequent droplet size distribution in turbulent two-phase gas/liquid flow. The *St* number is useful to evaluate the U_g values using a particle motion equation. Eventually, the U_g value is required to obtain the We_g and Re_d values, which are very useful dimensionless numbers used to predict the two-phase gas/liquid spray atomization and especially the droplet SA commencement. In this study, two types of conditions were studied. The value of β was first varied from 0.60%, 1.20% and 1.85% at the constant pressure of 620 kPa at a fixed axial downstream of $60D_n$. It was observed that the *St* number reached the value of 1 at the *r/R* of 0.25 distance. Thus, at the center of the spray the droplets' response time was much higher than that of a continuous phase gaseous medium. However, at the outer region of the spray, the droplet response time followed the continuous phase response time. As soon as the *St* reached 1, break-up stopped, thus the droplets started to coalesce forming bigger droplets (higher D_{10} values) with increasing radial distances. It was also observed that the We_g and Re_d decreased remarkably with the radial distances (r) before the We_{crit} limit. However, the We_g and Re_d decreased slowly with the

variation of the β values after the We_{crit} limit.

In the second set of studies, the droplet atomization behavior was examined with changing axial distances (x of $30D_n$, $60D_n$, $120D_n$) and radial distances (r). In this case the β was 2% at a P_m of 520 kPa. It was observed that if the 'r' and 'x' was increased, the St number decreased remarkably due to smaller droplet response times compared to the continuous phase response time. The St number reached the value of 1 at the r/R of 0.40 for axial distances of $30D_n$, $60D_n$, $120\ D_n$, respectively. Thus, near the center (r = 0) of the spray at $120D_n$ downstream, the D_{10} values were lower than that of $30D_n$ and $60D_n$ at the similar radial positions (r = 0) due to greater droplets break-up in further downstream.

5.5. References

[1] Ariyapadi, S., Berruti, F., Briens, C., Knapper, B., Skwarok, R. and Chan, E. (2005) Stability of horizontal gas–liquid sprays in open-air and in a gas–solid fluidized bed. Powder Technology 155 161 – 174.

[2] Maldonado, S. (2006) Improving the Stability of Gas-Liquid Sprays by Modifying the Two-Phase Flow Entering The Nozzle, MASc. , MASc. Thesis, University of Alberta.

[3] Ejim, C.E. (2008) Effect of Liquid Viscosity, Surface Tension and Nozzle Size on Atomization in Two-Phase Nozzles, PhD Thesis, Mechanical Engineering, University of Alberta, .

[4] Tafreshi, Z.M., Kirpalani, D., Bennett, A. and McCracken, T.W. (2002) Improving the efficiency of fluid cokers by altering two-phase feed characteristics. Powder Technology. 125 234– 241.

[5] Roesler, T.C. and Lefebvre, A.H. (1989) Studies on aerated-liquid atomization. International Journal of Turbo Jet Engines. 6: 221-230.

[6] Whitlow, J.D. and Lefebvre, A.H. (1993) Effervescent atomizer operation and spray characteristics. Atomizations and Sprays. 3: 137–155.

[7] Barker, C.L., Cody, G.D., Joseph, C.A. and Sela, U. (1991) Acoustic Monitoring of Two-Phase Feed Nozzles. US Patent 5 004 152.

[8] MacGregor, S.A. (1991) Air Entrainment in Spray Jets. Int. J. Heat and Fluid Flow. 12: 279–283.

[9] Ariyapadi, S., Balachandar, R. and Berruti, F. (2000) Effect of Cross-Flow on the Spray Characteristics of an Industrial Feed Nozzle. AIChE Spring Annual meeting, Atlanta, GA.

[10] Lefebvre, A.H. (1989) Atomizations and Sprays, New York, Hemisphere.

[11] Mugele, R. and Evans, H.D. (1951) Drop size distributions is sprays. Ind. Eng. Chem. 43 (6): 1317-1324.

[12] Crowe, C.T. (2006) Multiphase flow handbook Boca Raton, FL CRC: Taylor & Francis.

[13] Nasr, G.G., Yule, A.J. and Bendig, L. (2002) Industrial sprays and atomization: design, analysis and applications, Springer-Verlag London Limited.

[14] McCarthy, M.J. and Molloy, N.A. (1974) Review of stability of liquid jets and influence of nozzle design. Chemical Engineering Journal. 7: 1-20.

[15] Liu, S. and Li, D. (1999) Drop coalescence in turbulent dispersions. Chem. Eng. Sci. 54: 5667–5675.

[16] Shavit, U. and Chigier, N. (1996) Development and evaluation of a new turbulence generator for atomization research. Experiments in Fluids. 20 (4): 291-301.

[17] Pilch, M. and Erdman, C.A. (1987) Use of breakup time data and velocity history data to predict the maximum size of stable fragments for acceleration-induced breakup of a liquid drop. International Journal of Multiphase Flow. 13: 741-757.

[18] Low, T.B. and List, R. (1982) Collision, coalescence and breakup of raindrops. J. Atmos. Sci. 39: 1591–1618.

[19] Hsiang, L.P. and Faeth, G.M. (1995) Drop deformation and breakup due to shock wave and steady disturbances. International Journal of Multiphase Flow. 21 (4): 545-560.

[20] Ariyapadi, S., Balachandar, R. and Berruti, F. (2001) Characterizing Spray Pulsations Using a Phase-Doppler Particle Analyzer. Ind. Eng. Chem. Res. 40: 5282-5290.

[21] Ariyapadi, S., Berruti, F. and Ram, B. (2003) Effect of Crossflow on the Spray Characteristics of an industrial Feed Nozzle. Chem. Eng. Comm. 190: 1: 681-1704.

[22] Copan, J., Balachandar, R. and Berruti, F. (2001) Droplet size-velocity characteristics of sprays generated by two-phase feed nozzles. Chemical Engineering Communications. 184: 105-124.

[23] Ziesenis, J. and Bauckhage, K. (2002) Absorption and Scattering of Light by Highly Concentrated Two-phase Flows. Part. Part. Syst. Charact. 19 195-202.

[24] Zama, Y., Kawahashi, M. and Hirahara, H. (2004) Simultaneous Measurement of Droplet Size and Three-Components of Velocity in Spray. Optical Review. 11 (6): 358–364.

[25] Kashdan, J.T., Shrimpton, J.S. and Whybrew, A. (2003) Two-Phase Flow Characterization by Automated Digital Image Analysis. Part 1: Fundamental Principles and Calibration ofthe Technique. Part. Part. Syst. Charact. 20 387-397.

[26] Hsiang, L.P. and Faeth, G.M. (1992) Near-limit drop deformation and secondary breakup. Int. J. Multiphase Flow. 18: 635–652.

[27] Lefebvre, A.H., Wang, X.F. and Martin, C.A. (1988) Spray characteristics of aerated-liquid pressure atomizers. AIAA Journal of Propulsion and Power. 4 (6): 293-298.

[28] Roesler, T.C.e.a. (1989) Studies on aerated-liquid atomization. International Journal of Turbo Jet Engines. 6: 221-230.

[29] Rahman, M.A., Heidrick, T. and Fleck, B.A. (2008) Characterizing the Two-Phase, Air/Liquid Spray Profile Using a Phase-Doppler-Particle-Analyzer. proceedings of the 14TH International Symposium on Applications of Laser Techniques to Fluid Mechanics, 7-10 July, Lisbon, Portugal.

[30] Ejim, C.E., Fleck, B.A. and Amirfazli, A. (2005) A Scaling Study of the Atomization of a Two-Phase Industrial Nozzle: Part 1 - Effect of Surface Tension and Viscosity on Mean Drop Size Profiles. Proceedings of the 20th ILASS - Europe Meeting Sept. 5-7, Orléans, France.

[31] Dantec Dynamics A/S (2003). BSA Flow Software, Version 2.1: Installation and User's guide, Skovlunde

[32] Crowe, C.T. (2006) Multiphase flow handbook, Boca Raton, FL CRC: Taylor & Francis.

[33] Faeth, G.M. (1990) Structure and atomization properties of dense turbulent sprays. 23rd Symposium on Combustion, The Combustion Institute, Pittsburgh.

CHAPTER 6

Multiphase Atomization Characterization: Coupled Impulse Probe and PDPA Technique[1]

6.1. Introduction

Gas assisted atomization is a popular technique in industrial applications. Two-phase gas/liquid atomization characterization is a challenging task [1-4]. It is very common to have pulsations in the gas assisted atomization. My experimental observations indicate that the available experimental techniques, such as the Phase Doppler Particle Anemometer (PDPA), are not able to characterize the multiphase spray accurately. The PDPA technique can only reliably measure the droplet velocity. However, the PDPA cannot measure the mass flux very accurately due to the high rejection rate of non-spherical data. Thus, using the velocity data from the PDPA and force data from the impulse probe can assist to calculate the momentum flux very reliably. A study [5] in fuel spray indicated that spray momentum flux information is very critical to characterize a spray, as spray momentum determines the spray penetration, spray cone, air entrainment and mixing potential in the reactor (jet bed interaction). In the experiment, they used an impingement force measurement technique and validated the results obtained by the macroscopic spray visualization method. Several other studies are found in the literature that used the spray momentum flux to understand the spray characteristics [6, 7]. A simulation of a water jet which was validated by the experimental data indicated that the peak of a impulsive impact force in the pulsating spray was found to be 3.5 – 4 times greater than that of the continuous water jet [8]. There are few other studies that used the impact probe to measure

1 A version of this chapter has been published. Rahman *et al.* (2010) Proceedings of the 22nd Annual ILASS – Americas Conference on Liquid Atomization and Spray Systems, ILASS-AMERICAS, Cincinnati, Ohio, May 16-19.

the spray momentum in a multiphase spray. In one study, a piezoelectric dynamometer was used to measure high-speed water jet characteristics [9]. In the current study, two-phase spray momentum was measured using a coupled PDPA and an impulse probe technique. This novel method assists in understanding the fundamental behavior of multiphase spray in industrial applications.

6.2. Theory

Consider a steady flow impinging on a perpendicular flat plate as shown in Fig. 6.1.

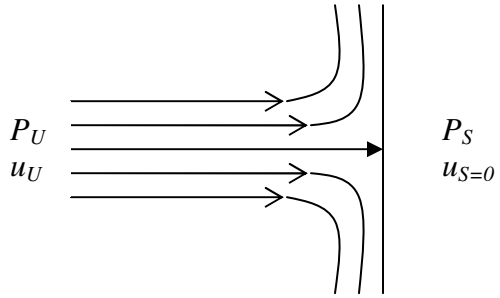

Fig. 6.1. Stagnation point flow

The streamline in Fig. 6.1. divides into two segments. The stream line goes above the dividing line and flows over the plate and a second stream line goes under the dividing line and flows under the plate. Since the flow of the dividing stream line cannot pass through the plate, the fluid must come to rest at a point. Thus, fluid along this line slows down without deflection at the plate and it stagnates. The Bernoulli's equation along the stagnation streamline gives:

$$P_u + \frac{1}{2}\rho\, u_u^2 = P_S + \frac{1}{2}\rho\, u_S^2 \qquad (1)$$

here, the subscript '*u*' indicates the upstream condition and subscript 'S' indicates the stagnation condition. Since at the stagnation condition the stagnation velocity is zero, Equation (1) can be written as follows:

$$P_u + \frac{1}{2}\rho\, u_u^2 = P_S \qquad (2)$$

In other words we can write: static pressure + dynamic pressure = stagnation pressure or total pressure. The stagnation pressure is the highest pressure in the flow where the fluid motion comes to a rest. The effects of the gas phase pressure are negligible as the density of air is far less than the density of water. Sometimes the piezoelectric sensors only measure the dynamic pressure of the fluid motion, which reflects the momentum flux of droplets impacting on the tip of the sensor. In any axial location perpendicular to the spray, the liquid mass flux is conservative. Thus, the liquid mass flux exiting the nozzle orifice should be equal to the integral mass flux at any cross section in the spray. One can write:

$$M_S = \int_{r=-R}^{r=+R} M_x \, dr \qquad (3)$$

where, '*x*' indicates the axial location and '*i*' indicates local mass flux. As the mean dynamic force can be measured inside the spray and any section perpendicular to the spray axis, the mean droplet velocity can be calculated for each point on this section. As this force is referred to the effect of droplets, the total water mass flow rate can be obtained if the mean velocity is integrated in this section. To measure the droplet velocity, the Phase Doppler Particle Analyzer was used.

6.3. Experimental Set-up

In this study, a one-quarter of a patented full-scale nozzle, US Patent of 6003789 [10], was used as shown in Fig. 6.2. The full scale nozzle is used in a fluidized bed coker for heavy oil upgrading. In the laboratory experiment, a feeding conduit of 36.8 cm length and 6.35 mm ID was used prior to the nozzle. The nozzle diameter (D_n) was 3.10 mm. This nozzle assembly was mounted on a 3-D automated traversing rig. The experiments were performed using mixtures of water (0.04 *l/s* to 0.11 *l/s*) with air or mixed gas (0.16 *l/s* to 0.48 *l/s*), which gave air to liquid mass ratios (β) of 1 to 4%. The experimental schematic diagram is presented in Fig. 6.2. Mean drop size was measured using a 2-D Phase Doppler Particle Anemometer (PDPA) from the Dantec Dynamics specifications [11]. The working principal of the Phase Doppler Particle Analyzer can be found in the

literature [12-16]. The force generated from droplets in any axial cross section of the spray was measured by a piezoelectric force sensor, Kistler 9203, and a charge amplifier, Kistler 5010B. This force sensor is high sensitive and capable of resolving the smallest changes in contact force. A charge amplifier was used to convert the transmitted charge from high impedance piezoelectric force into a high level output voltage and provide excitation power . This high level voltage output can be read online using an oscilloscope. In the current experiment, a digitizing oscilloscope Tektronnix TDS 410A with record length of 15000 points per minute was used to read the output voltage.

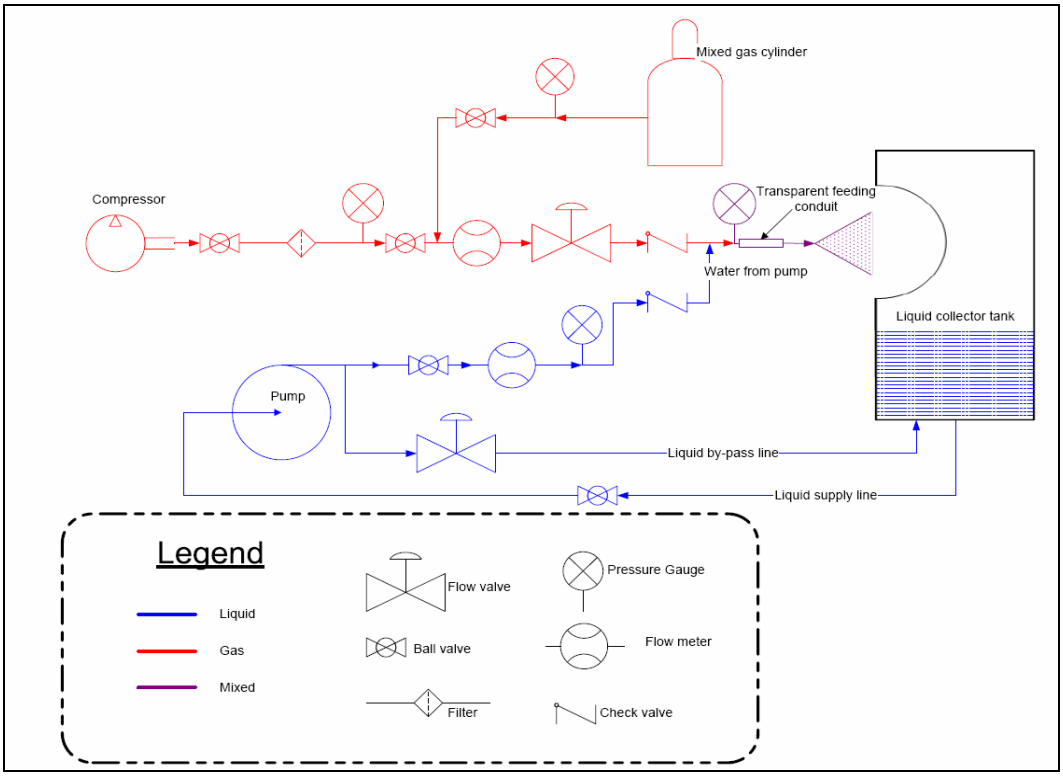

Fig. 6.2. Experimental set-up.

A quartz force sensor as shown in Fig. 6.3(a) measured dynamic and quasistatic forces. The device can measure the force in the range of a few Newton up to 400 kN. The quartz force sensor is mounted tightly in a welded steel housing. Quartz yields an electric charge proportional to the mechanical load. Fig. 6.3(b) shows

the schematic of the charge amplifier used to convert the transmitted charge into a high level output voltage.

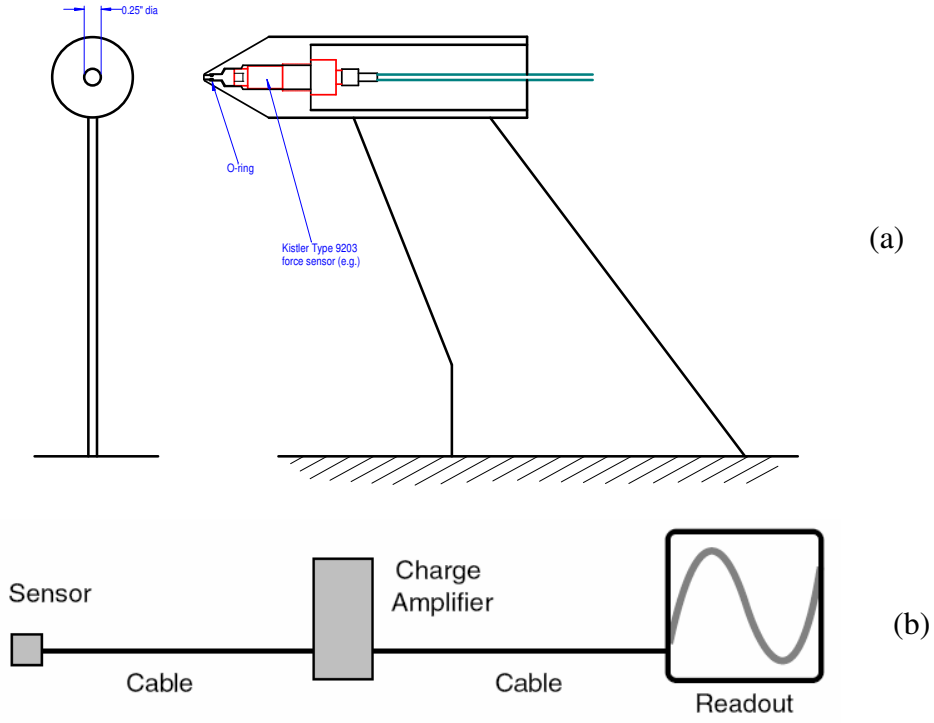

Fig. 6.3. Quartz force sensor (a) and the charge amplifier output.

6.4. Results and Discussions

In Fig. 6.4, a well and poorly atomized spray is depicted. Due to greater pulsations in Fig. 6.4 (a), the droplets are non uniform. However, due to fewer pulsations in Fig. 6.4 (b), the droplets are nicely dispersed. In Fig.6.5, droplet force data obtained by the impulse sensor is depicted. The brevity of the force data is the uniformity in both radial directions. Data obtained from the Phase Doppler Particle Anemometer is not symmetrical in both the radial directions due to the decreased visibility for the receiver if one traverses from one direction to another direction. In Fig. 6.6, the effects of the air to liquid mass ratio on the droplet force are presented. Fig. 6.6, (a), (b), (c) and (d) correspond to the $15D_n$, $30D_n$, $60D_n$, and $120D_n$, nozzle downstream form the tip of the nozzle. Here, D_n

corresponds to the nozzle diameter of 3.10 mm. In all the cases of the downstream nozzle, the force profiles are similar. Most importantly it is notable that if the air to liquid mass ratio increases, the force produced from the droplets also increases. At a higher air to liquid mass ratio, the momentum is transferred to the liquid phase and provides greater force in the droplets.

(a) coarse atomization

(a) fine atomization

Fig. 6.4. Spray images.

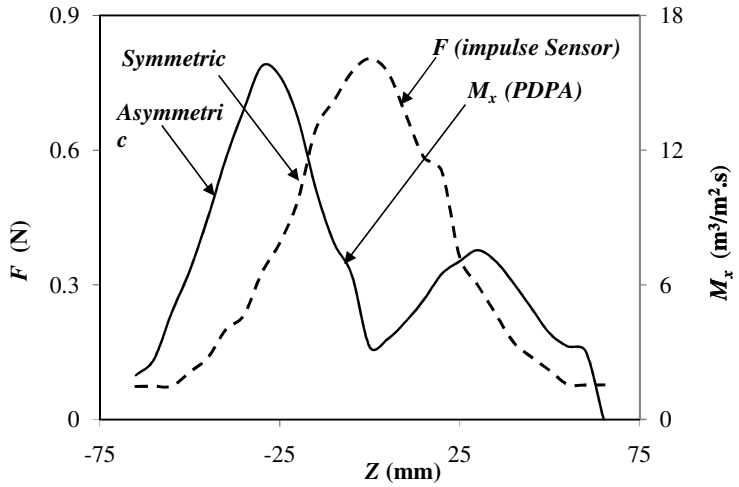

Fig. 6.5. Symmetry obtained in the impulse sensor measurement. Data obtained for 2% air to liquid mass ratio, $30D_n$ nozzle downstream and 482 kPa mixing pressure.

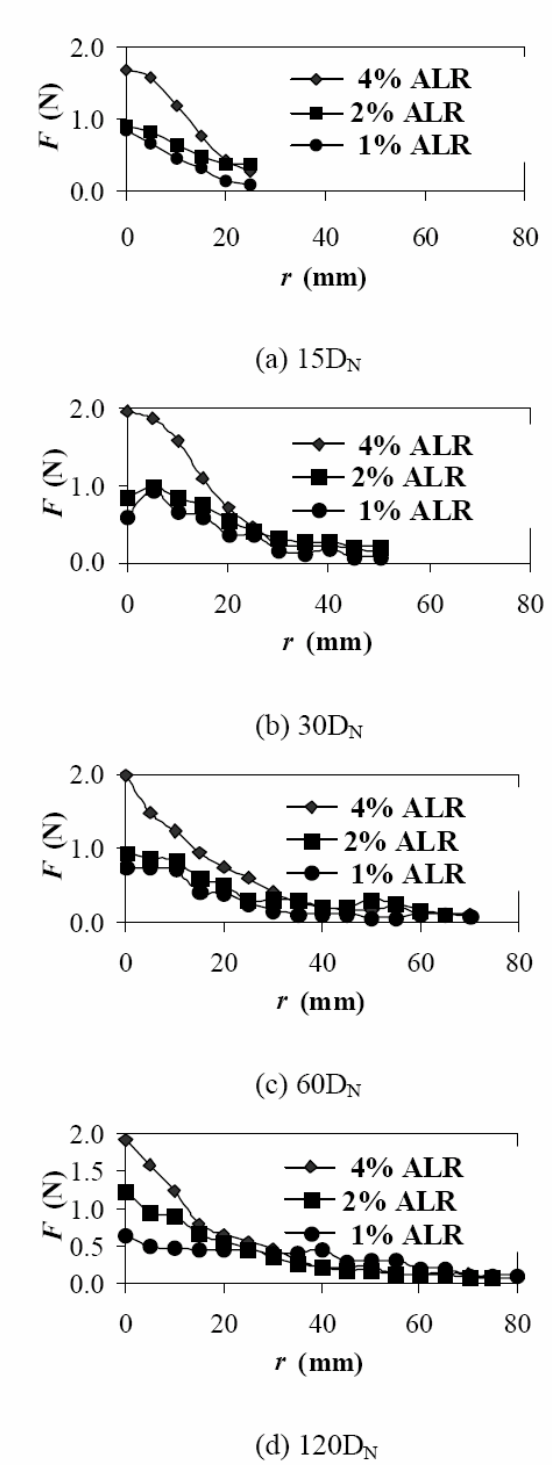

Fig. 6.6. Force (*F*) produced from a spray with changing air to liquid mass ratio and radial distances (*r*).

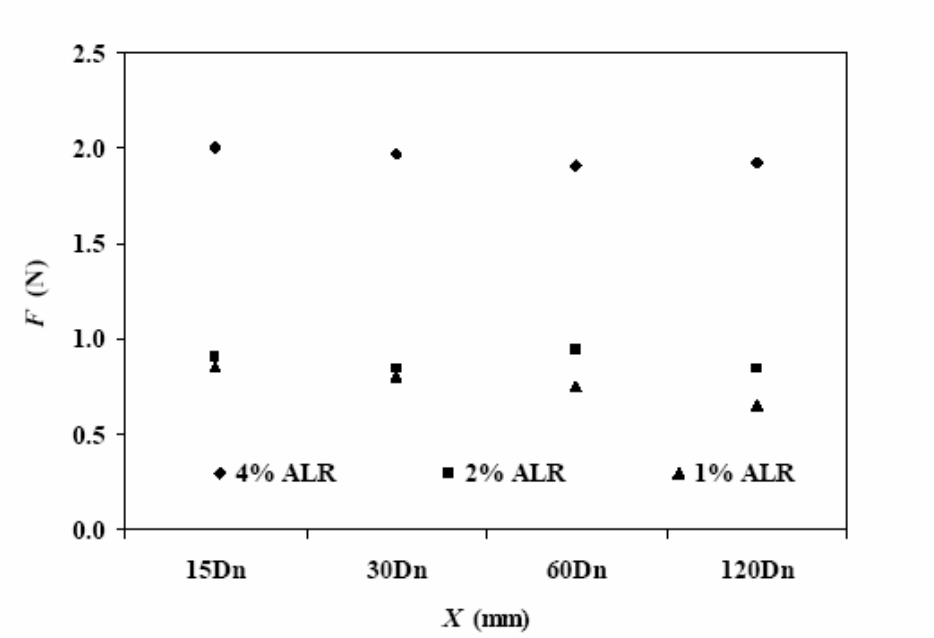

Fig. 6.7. Force (F) produced from a spray with changing axial position (x) and air to liquid mass ratio.

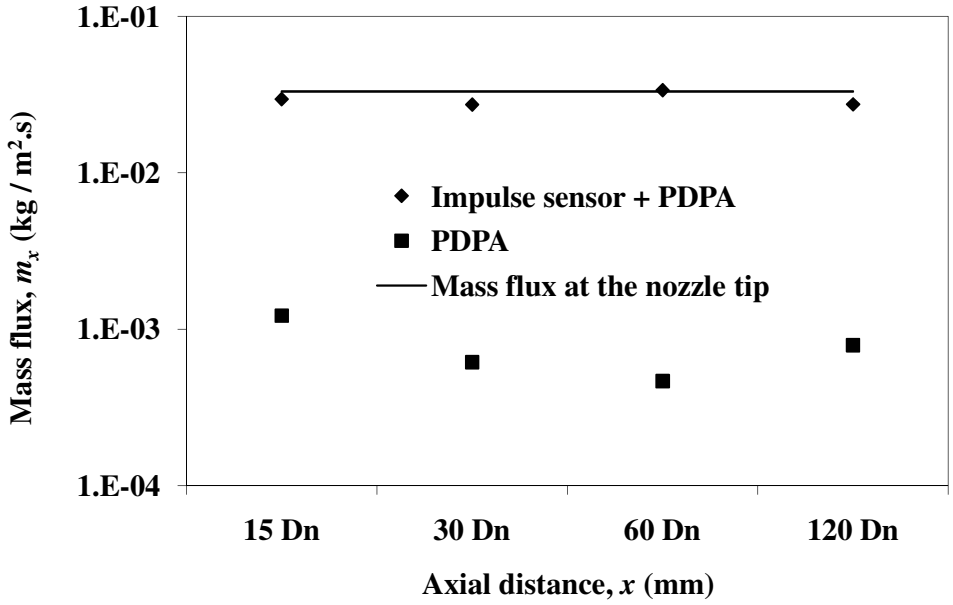

Fig. 6.8. Mass flux variation with axial distance from the tip of the nozzle. Here, D_n indicates diameter of the of the nozzle tip of 3.10 mm.

Similar observations can be observed in Fig. 6.7, where the effects of the air to liquid mass ratio and the progress of the droplet force in different downstream nozzles are presented. As shown in the previous figure, the droplet force increases linearly if the air to liquid mass ratio increases. Moreover, the droplet force decreases gradually if the droplet travels downstream of the spray. If the droplet travels downstream of the spray, the droplets looses its momentum, providing less force further downstream.

Fig. 6.8 is the most interesting figure obtained from the impulse probe. Fig 6.8 validates the mass conservation for the liquid volume. In Fig 6.8, the theoretical values were obtained from the liquid input condition, which was known in our experiment. Two experimental data sets were plotted varying the axial distances. (from 15Dn to 120Dn). From Fig 6.8 it is evident that the impulse probe mass flux data conserves the input liquid content. However, due to poor data rates and spherical validation, the Phase Doppler Particle Analyzer underestimates the input liquid content, thus failing to conserve the liquid volume in the system.

6.5. Conclusions

The mass flux measurement in a two-phase gas liquid spray is a challenging task as the traditional laser diagnostics cannot reliably measure all the droplet shapes (such as non-spherical droplets). However, the Phase Doppler Particle Anemometer can measure the droplet velocity data very reliably. Thus, combining the Phase Doppler Particle Anemometer technique with the impulse probe technique can measure the mass flux of a multiphase pulsating spray very accurately.

6.6. References

[1] Ejim, C.E., Rahman, M.A., Amirfazli, A. and Fleck, B.A. (2010) Effects of Liquid Viscosity and Surface Tension on Atomization in Two-Phase, Gas/Liquid Fluid Coker Nozzles. Fuel. 89: 1972-1882.

[2] Rahman, M.A., Heidrick, T. and Fleck, B.A. (2009) A Critical Review of Two-Phase Gas/Liquid Industrial Spray Systems. International Review of Mechanical Engineering. International Review of Mechanical Engineering. 3 (1): 110-125.

[3] Rahman, M.A., Heidrick, T. and Fleck, B.A. (2009) Characterizing the Two-Phase, Air/Liquid Spray Profile Using a Phase-Doppler-Particle-Analyzer. IOP Journal of Physics – conference series. 147: 1-15.

[4] Ejim, C.E., Rahman, M.A., Amirfazli, A. and Fleck, B.A. (2010) Scaling Analysis of Nozzle Size on Atomization in Two-Phase, Gas-Liquid Nozzles. Multiphase Science and Technology. 22 (2): 133-155.

[5] Payri, R., Ruiz, S., Salvador, F.J. and Gimeno, J. (2007) On the Dependence of Spray Momentum Flux in Spray Penetration: Momentum Flux Packets Penetration Model. Journal of Mechanical Science and Technology. 21: 1100-1111.

[6] Payri, R., Garcia, J.M., Salvador, F.J. and Gimeno, J. (2005) Using Spray Momentum Flux Measurements to Understand the Influence of Diesel Nozzle Geometry on Spray Characteristics. Fuel. 84: 551–561.

[7] Payri, R., Tormos, B., Salvador, F.J. and Araneo, L. (2008) Spray Droplet Velocity Characterization for Convergent Nozzles with three Different Diameters. Fuel. 87: 3176–3182.

[8] Anantharamaiah, N., Tafreshi, H.V. and Pourdeyhimi, B. (2006) A Study on Hydroentangling Waterjets and their Impact Forces. Experiments in Fluids. 41: 103–113.

[9] Momber, A.W. (2001) Energy Transfer during the Mixing of Air and Solid Particles into a High-Speed Waterjet: an Impact-Force Study. Experimental Thermal and Fluid Science. 25: 31-41.

[10] Base, T.E., Chan, E.W., Kennett, R.D. and Emberley, D.A. (1999) Nozzle for Atomizing Liquid in Two-phase Flow. US Patent 6003789.

[11] Dantec Dynamics A/S (2003). BSA Flow Software, Version 2.1: Installation and User's guide, Skovlunde.

[12] Albrecht, H.E., Borys, M., Damaschke, N. and Tropea, C. (2003) Laser Doppler and Phase Doppler Measurement Techniques, Germany, Springer.

[13] Damaschke, N., Gouesbet, G., Gréhan, G., Mignon, H. and Tropéa, C. (1998) Response of Phase Doppler Anemometer Systems to Nonspherical Droplets. Applied Optics. 37 (10): 1752-1761.

[14] Dodge, L.G., Rhodes, D.J. and Reitz, R.D. (1987) Drop-size Measurement Techniques for Sprays: Comparison of Malvern Laser-Diffraction and Aerometrics Phase/Doppler. Applied Optics. 26 (11): 2144-2154.

[15] Gréhan, G., Gouesbet, G., Naqwi, A. and Durst, F. (1993) Particle Trajectory effects in Phase Doppler Systems. Part. Part. Syst. Charact. 10: 332-338.

[16] Gréhan, G., Gouesbet, G., Naqwi, A. and F., D. (1994) Trajectory Ambiguities in Phase Doppler Systems: study of a near forward and a near backward geometry. Part. Syst. Charact. 11: 133-144.

CHAPTER 7

Two-Phase Atomization Scaling: Fluid Properties & Geometric Size[1,2]

7.1. Introduction

The primary objective of this chapter was to compare the Sauter Mean Diameter (D_{32} or $D_{qp}^{q-p} = \int_{D_{\min}}^{D_{\max}} D^q \frac{dn}{dD} dD \Big/ \int_{D_{\min}}^{D_{\max}} D^p \frac{dn}{dD} dD$) of the effervescent atomization for different viscosities (μ_L), surface tensions (γ) and throat diameters (D). Compressed air was used as the gas phase; the liquid phases were water, canola oil and a glycerine-water solution. The μ_L was varied from 1 mPa-s to 67 mPa-s, and γ was varied from 25 mN/m to 61 mN/m. The liquid flow rates were varied from 0.095 L/s to 0.105 L/s, and the gas to liquid mas ratio ($\beta = m_g/m_l$) was fixed at 2%, similar to the ratio used in commercial fluid coker nozzles. Fluid mixing pressures in the test were between 400 kPa to 700 kPa. The D_{32} within the spray was measured using a Dantec 2-D fibre mode Phase-Doppler-Particle-Anemometer (PDPA). Measurements were performed at axial distances of 100 and 202 mm from the nozzle orifice and within a spray radius of 40 mm. The results showed that the 67 fold increase in μ_L results in 46 μm increase in $D_{32,}$ which roughly extrapolates to a power law relationship exponent of 0.11 (based on two points). In contrast, the 2.4 fold increase in γ indicates roughly a 42 μm increase in D_{32}, giving an exponent of -0.24. For both parameters the exponent is small, indicating weak dependence. The γ effects appear stronger, but the modest increase barely exceeds the margin of error. Experimental results also show that if the D is increased from D = 3.1 mm to D = 4.1 mm (1.3 times), the D does not

[1] A version of this chapter has been published. Rahman *et al.* (2010) FUEL. 89: 1972-1882.

[2] A version of this chapter has been published. Rahman *et al.* (2010) Multiphase Science and Technology. 22(2): 133-155.

show a change on D_{32} and equates to the power of 0.1 (glycerine solution sprays at μ_L = 67 mPa-s) to 0.9 (water sprays at μ_L = 1 mPa-s).

7.2. Two-Phase Atomization Scaling Based on Fluid Properties

7.2.1. Literature

Liu [1] indicated three measurement techniques to characterize the two-phase spray such as a mechanical method e.g. spray patternator, an electrical method, e.g. impulse sensor, and a photonics method, e.g. Phase Doppler Particle Anemometer. Elkotb [2] used a special sampling apparatus mounted 60 mm downstream from the injector orifice for measuring the droplet size. In the study, the droplet size distribution and mean droplet diameter were found experimentally and the proposed model for the multifuel spray was verified. The model and experimental data were in good agreement. In a later study, Elkotb [3] used the slide sampling method and a photographic system to measure the droplet size. In their study it was found that the atomizing air pressure provided smaller droplet size distribution. In contrast, the increase in liquid/fuel pressure provided larger droplet size distribution. Rizkalla *et al.* [4] used a light scattering technique to find the droplet size of airblast atomization. The proposed correlation suggested that the droplet size increased if the liquid surface tension and density increased. On the contrary, the droplet size decreased if air velocity, air density and air to liquid ratio increased. Lefebvre [5] conducted a literature review on the airblast atomization. In the study it was found that the droplet size increased if the liquid surface tension, viscosity and liquid to air ratio increased. The density appeared to have little effect on the droplet size.

In twin-fluid atomizers, liquid atomization depends on the liquid properties, atomizer dimension and ambient gas properties, atomizing gas density, gas-to-liquid mass ratio and turbulence in the mixture. Relative velocity between the atomizing gas and liquid at the nozzle exit also affected droplet formation [6]. In effervescent atomizers, the atomizing gas injection pressure, gas-to-liquid mass

ratio, ambient gas density, design of atomizer internal geometry, liquid viscosity and surface tension affected the liquid atomization [7]. The main forces responsible for liquid atomization are: hydrodynamic (or inertial), aerodynamic, viscous and surface tension forces [8]. Atomization studies by Pilch and Erdman [9] have shown that the susceptibility of a drop to undergo secondary atomization depends on the ratios of aerodynamic drag force and surface tension force acting on a drop. The ratio of liquid internal viscous force to surface tension force on the drop also effects the atomization. Studies by Hsiang and Faeth [10] and a documented atomization review by Rissio [11] have shown that for low viscous drops, the onset of secondary atomization occurs at a minimum Weber Number (*We*) ~ 12. Brodkey [12] has provided a useful empirical correlation for the critical *Weber number* as a function of the *Ohnesorge number*. Atomization studies by Lefebvre *et al.* [13], and Roesler and Lefebvre [14] have shown that jet break up occurs when the bubbles within the bulk liquid possess enough energy to overcome the surface tension forces that hold the liquid jet together.

In more recent years, Buckner *et al.* [15] investigated the effervescent atomization quality for a high viscosity fluid (0.5 to 1 Pa.s) at low air to liquid ratios (up to 15%) by shadowgraphy. It was found that the mean droplet size was a strong function of air to liquid ratio. However, the mean droplet is nearly independent from the liquid viscosity and liquid supply pressure. Lund *et al.* [16] used high speed photography (500 ns duration) to obtain the droplet size in effervescent atomization at a very low air to liquid ratio (<0.002) and at modest pressure (<377 kPa). It was found that liquid viscosity did not have any effect on the drop size for the range of viscosities investigated (20 to 80 mPa.s). However, increased liquid surface tension decreased the droplet diameter for the range of surface tensions investigated (30 to 67 mN/m). Santangelo *et al.* [17] investigated the effervescent atomization using focused image holography techniques and observed the droplet diameter was independent from the liquid viscosity. However, the droplet diameter slightly decreased if the liquid surface tension and density increased.

Kirpalani *et al.* [18] indicated that the D_{32} depends on flow characteristics within the nozzle, such as flow regime (intermittent flow/slug flow, bubbly flow, annular flow) and gas-to-liquid-ratio ($\beta=m_g/m_l$). Current experimental studies show that intermittent flow/slug flow results in coarse droplets while bubbly flow contributed well atomized droplets [19, 20]. The effect of annular flow on the droplet size is still unknown and under investigation. The effervescent atomization was studied by Tafreshi *et al.* [21] using laser interferometry and dynamic pressure measurements. When the air-to-liquid ratio was increased from 0.75% to 1.5%, the flow regime inside the horizontal nozzle transformed from intermittent to bubbly flow. This transformation resulted in a decrease of 550 to 360 µm droplet diameter and 17% greater coverage of the spray. Copan *et al.* [22] showed that the β influences the magnitude of the D_{32}. In the study the droplet measurements were conducted using a Phase Doppler Particle Analyzer. Similar observations were made by Ariyapadi *et al.* [23]. In that study the Phase Doppler Particle Analyzer was also used to measure droplet size and velocity. In the two-phase gas/liquid effervescent atomization, if the gas phase mass flow rate and pressure are increased, the value of D_{32} decreases. The above studies [21-23] on effervescent atomization were conducted using one type of liquid phase in every case and thus did not demonstrate the effects of μ_L and γ on atomization. Lefebvre [6] investigated the effects of viscosity and surface tension on the D_{32}. However, the investigation was conducted for a particular nozzle design, such as the airblast nozzle.

In the current study, a hybrid design of a classical twin-fluid and effervescent nozzle was used [24]. The nozzle is designed to allow for unclogging of the tip which is prone to coke buildup, by a ramrod forcefully inserted from the feed inlet, thus having the advantage of no internal flow obstructions and a clear passageway through the centerline. The effects of viscosity and surface tension were still unknown for this novel industrial nozzle. For the last two decades the Maximum Entropy Formalism has been proposed to understand drop-diameter

distribution. A review paper [25] summarizes the pros and cons of the different models proposed in the literature to model spray drop-size distribution. The Generalized Gamma function reported by Lecompte *et al*. [26] indicated that the proposed function was capable of representing drop-size distributions for twin fluid sprays.

7.2.2. Effects of Viscosity on the Two-Phase Gas/Liquid Atomization

The literature review of the effects of μ_L on the Two-Phase Gas/Liquid atomization is presented in Table 7.1. A power law is chosen as the simplest monotonic fit of data where only positive values are possible (diameter vs. fluid property) and with this simple extrapolated fit, the importance of the fluid property as a predictor for droplet size is implied by the magnitude of the power law exponent.

Table 7.1. Effects of Viscosity on the Two-Phase Gas/Liquid Atomization

Literature	**μ_L ratio**	**Extrapolated Power Law**
Buckner *et al.* [15]	≈ 2.4	$D_{32} = 202\,\mu_L^{0.07}$
Lund *et al.* [16]	≈ 4.0	$D_{32} = 235\,\mu_L^{0.08}$
Santangelo *et al.* [17]	≈ 7.5	$D_{32} = 80\,\mu_L^{0.30}$

A possible explanation of μ_L effects on the D_{32} can be related to the bubble size dependence on the μ_L. Larger bubbles (higher μ_L) in the conduit and nozzle exit core impart bigger droplet sizes. However, smaller bubbles (lower μ_L) in the conduit and nozzle exit core possess greater surface area and transfer greater surface energy to the liquid phase, proving smaller droplets.

7.2.3. Effects of Surface Tension on the Two-Phase Gas/Liquid Atomization

Literature review of the effects of γ on the Two-Phase Gas/Liquid atomization is presented in Table 7.2.

Table 7.2. Effects of Surface Tension on the Two-Phase Gas/Liquid Atomization

Literature	**γratio**	**Power Laws**
Lund *et al.* [16]	≈ 2.2	$D_{32} = 568\,\gamma^{-0.20}$
Santangelo *et al.* [17]	≈ 2.6	$D_{32} = 568\,\mu_L^{-0.20}$
El-Shanawany *et al.*[27]	≈ 2.0	$D_{32} = 212\,\mu_L^{0.20}$

7.2.4. Experimental Procedure

The measured exit orifice diameter (D) is 3.1×10^{-3} m, whereas the corresponding tube (or conduit) length (L_t) and internal diameter (D_t) is 368×10^{-3} and 5.2×10^{-3}m, respectively. The nozzle is geometrically one-quarter scale of a patented full-scale design (US Patent # 6003789) employed in a fluid coker for bitumen/heavy oil upgrading. The β in the experiments was 1% and 2%. The mixing pressure of air and water at the mixing zone ranged from approximately 400 kPa to 700 kPa. To measure the droplet size (D_d) and velocity (U_d) within the spray, a 57x50 2D-Fiber Phase Doppler Particle Anemometer (PDPA) was used. The working principal of the Phase Doppler Particle Analyzer can be found in the literature [28-32]. The Phase Doppler Particle Analyzer is good for use in applications where a very high precision of droplet velocity and droplet size are required [30]. Using the PDPA technique, the velocity and corresponding momentum of each drop is found. Obtaining the velocity information is crucial in a two-phase gas/liquid atomization process. Using the PDPA technique, the velocity of the individual droplet can measure quite accurately. Velocity data is very useful if one knows the mass of each droplet. The PDPA technique is a very commonly used, popular technique in the spray research community. This is a very advanced

laser diagnostic technique and a great number of advanced spray laboratories around the world have been using this technique successfully. With the optical settings, the PDPA system was able to measure the droplet size in the range of 1-300 μm. In this study, the maximum droplet size was under 200 μm. Thus, we were able to measure the larger droplets of the size distributions. The PDPA was operated in the Fiberflow mode. The axial (x) and radial (r) components of the velocity were measured with the PDPA. Another important parameter is the fringe spacing of the PDPA system. The fringe spacing was 5.606 μm for the beam system U1 and 6.669 μm for the beam system U2. The laser powers for the Nd-YAG and He-Ne were 200 mW and 20 mW, respectively. For data collection, the PDPA was operated in forward-scatter and refraction mode; and the receiver was set to a scattering (or off-axis) angle (ϕ) of 30° for the air-water tests. To enable measurement of D_d and U_d at different sections of the spray, the nozzle assembly was mounted on a traverse mechanism. Data using the PDPA unit were obtained by traversing the nozzle in 3-D to enable positioning of the PDPA probe volume at different locations in the spray.

In the PDPA theory, one of the vital assumptions is that the particles have to be spherical. In Fibre mode PDPA, three detectors (U1, U2 and U3) are used as shown in Fig. 7.1. (a). Based on the size of the particle, a mask is chosen. The phase difference corresponding to each detector pair (Φ_{13} and Φ_{12}) provides information about the curvature over a certain arc of the particle surface. In the PDPA system the curvature of a particle was measured at two different locations with the above mentioned pairs. If the two curvatures were similar ($\Phi_{13} - \Phi_{12} = D$) the particle was deemed to be spherical. If the two curvatures differed ($\Phi_{13} - \Phi_{12} = \Delta D$) the particle measurement was rejected as not spherical. The working principal of the sphericity check of a particle/droplet is depicted in Fig. 7.1. (b). In my experiment, if the ΔD exceeded a certain limit (10% of size range) the particle/droplet was rejected by the PDPA set-up.

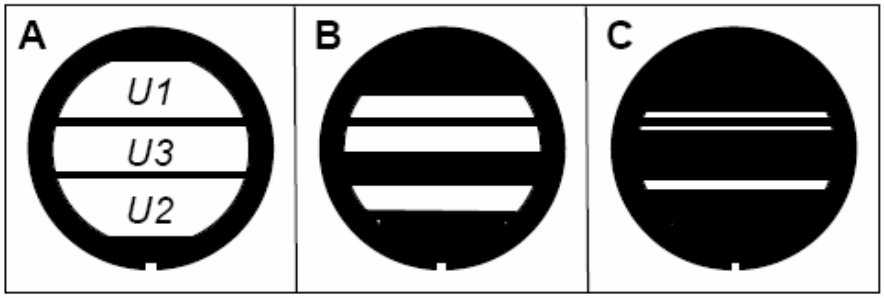

(a)

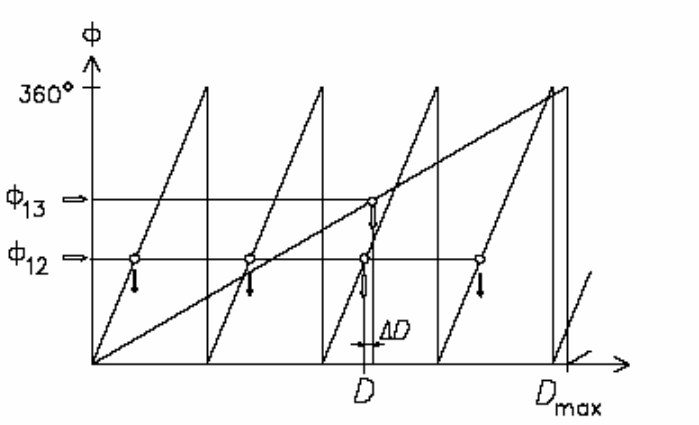

(b)

Fig. 7.1. (a) Three different masks used in the PDPA system depending on the size of the particle. (b) Different slopes of the diameter-phase relation obtained in a Fibre mode PDPA system with two pairs of photo-detectors at different separations. Difference, ΔD, in the diameter value corresponding to the two-phase differences Φ_{12} and Φ_{13} [28].

A typical phase plot for a Fiber PDPA set-up is shown in Fig. 7.2.. The displayed phases were the measured values. The continuous diagonal line (at the center) represents the theoretical relationship between the two-phase differences for perfectly spherical particles. To account for a finite accuracy of the system, a 10% deviation from the ideal line was tolerated. Therefore, a tolerance band, indicated by the two dashed lines, was defined by a 10% value. A schematic representing measurement location in the spray is depicted in Fig. 7.3.

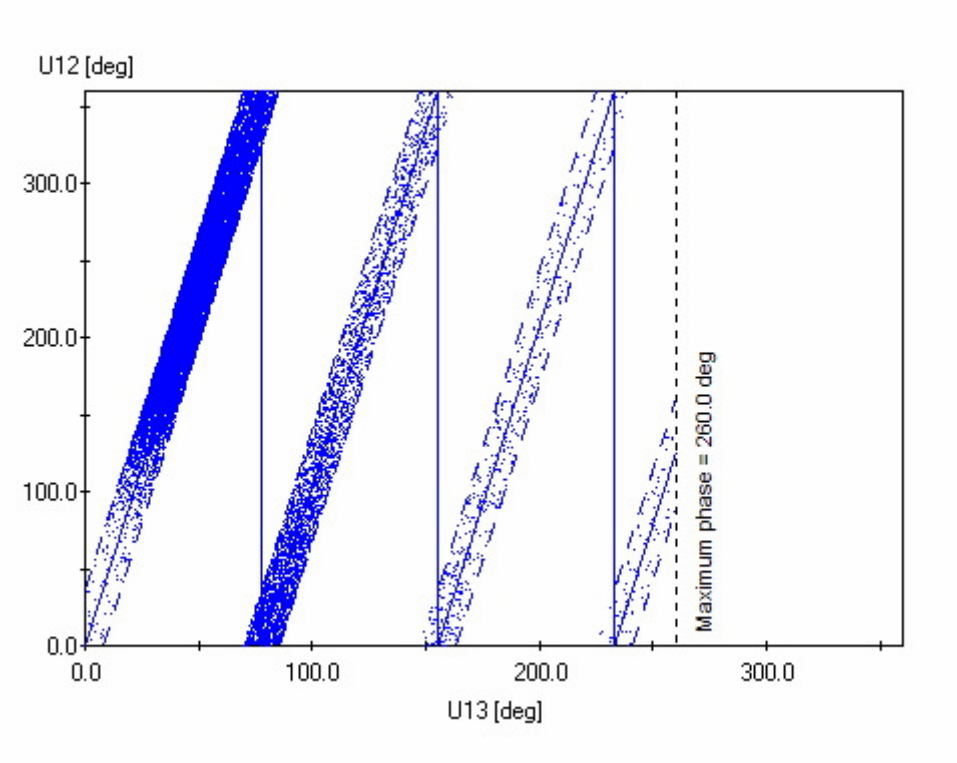

Fig. 7.2. A typical fiber PDPA phase plot.

7.2.5. The PDPA Experimental Challenges

To ensure the measurement reproducibility at each point, three test runs were conducted. From these three runs standard deviation and a 95% confidence interval estimate were estimated. Due to the pulsation in these types of two-phase gas/liquid dense sprays, in some instances the 95% confidence interval estimate may be high; however, the overall accuracy of measurement is very realistic (e.g. 95% confidence interval was ± 0.5 m/s for the velocity measurement and ± 1 μm for the droplet measurement). The probe volume correction is one of the proposed methods to correct the liquid volume measurements. Debate continues in the PDPA user community about the 'probe volume correction' method as to whether or not we should take into account this factor. Moreover, taking into consideration the 'probe volume correction' (using the data processing software) does not significantly improve the liquid volume measurement accuracy. As our validation

rate is about 80% across the spray and at each point we took a sample of 12,000 droplets; the liquid volume calculation is a reasonable estimate/indicator of liquid volume flux. However, due to the dense and pulsating spray, obviously some uncertainty exists in the mass flux measurements.

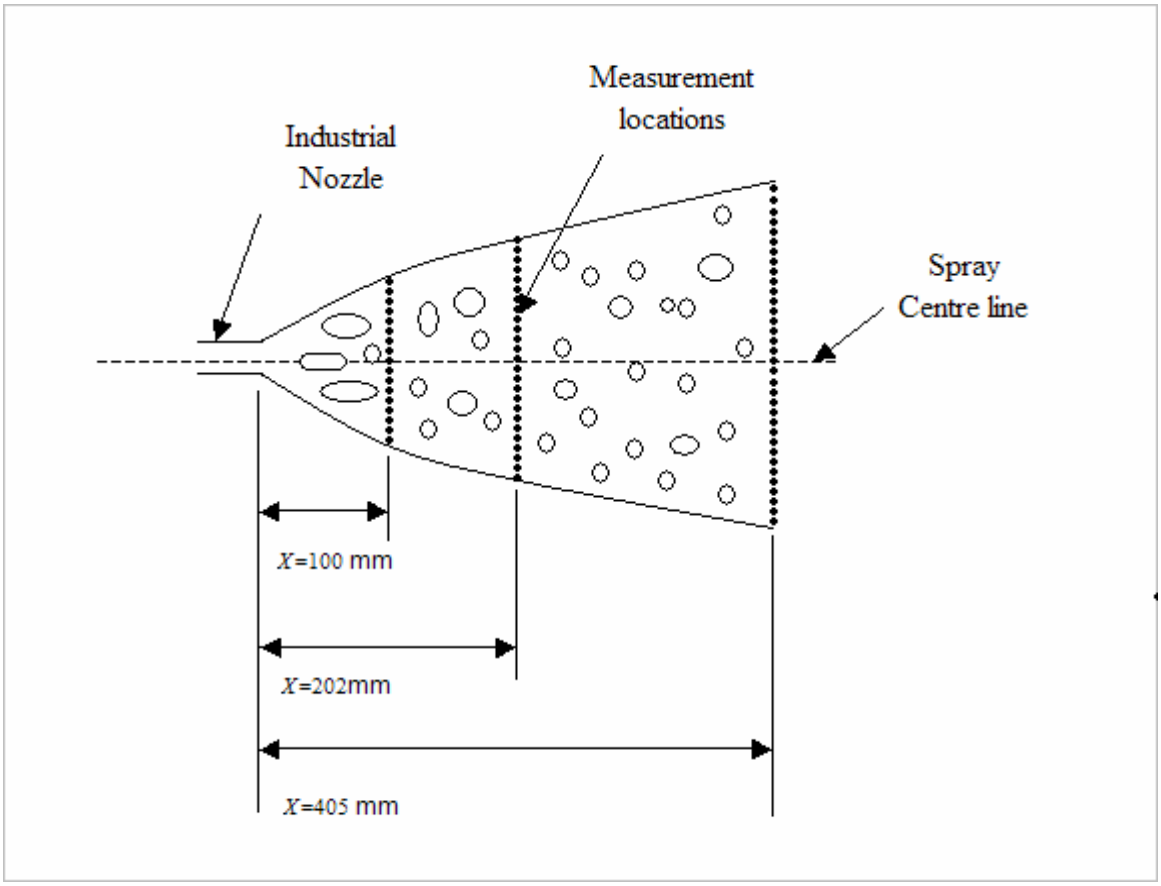

Fig. 7.3. The measurement locations in the spray are represented by the solid black circles. A pair of solid circles is separated by a 5 mm. Thus, in x = 100 mm, the value of R (furthest point in the spray envelope where the velocity is zero) is +40 mm and -40 mm. In x = 202 mm, the value of R is +60 mm and -60 mm. In x = 405 mm, the value of R is +80 mm and -80 mm.

It was observed that in lower air-to-liquid ratio (by mass) situations, the spray breakup length increases. High-speed video images confirm that if the gas to liquid ratio by mass decreases, spray break-up completes at about 180-200 mm

axial distances. One of the validation criterions in my measurements was to reject the non-spherical droplets. Using these non-spherical validation criteria, I was able to count the spherical droplets.

7.2.6. Results and Discussions

The experimental results for a two-phase gas/liquid spray radius of 40 mm and at axial distances of 100 and 202 mm from the nozzle orifice indicate that the 67 fold increase in μ_L results in 46 μm increases in D_{32} and equates to a power law relationship exponent of 0.11 (based on two points). Whereas, the 2.4 fold increase in γ indicates roughly a 42 μm increase in D_{32}, giving an exponent of -0.24. The γ effects appear stronger, but the modest increase barely exceeds the margin of error. Since a power law relationship exponent for both μ_L and γ parameters are small, it can be concluded that there is a weak dependence of D_{32} on these parameters. At 300°C (coker operating temperature) the μ_L and γ of bitumen were 2 mPa.s and 14 mN/m, respectively [33]. In contrast, at 20°C (lab temperature) the μ_L and γ of water were 1 mPa.s and 70 mN/m, respectively [34]. These results therefore establish the similarity of the lab scale experiments (conducted with air/water phase at 20°C), with the commercial scale operations (conducted with steam/bitumen at 300°C) as no appreciable change was observed on D_{32} values for the range of μ_L and γ investigated in this study.

The PDPA measurement is quite accurate and precise. 12,000 droplets/three minutes were taken during measurements. Out of 12,000 drops, 20% of the droplets were rejected due to the validation criteria. The 95% confidence interval was ± 0.5 m/s for the velocity measurement and ± 1 μm for the droplet measurement for each measurement. This indicates a very precise measurement. To check the repeatability, experiments were conducted three times for each condition. The mean axial velocity for each diameter class of droplets is depicted in Fig. 7.4. From Fig. 7.4, it is difficult to understand the cross correlation between the droplet velocity and diameter at different axial and radial locations of

the spray, in the spray. Thus, the cross correlation is required to understand or predict the behavior of larger and smaller droplets.

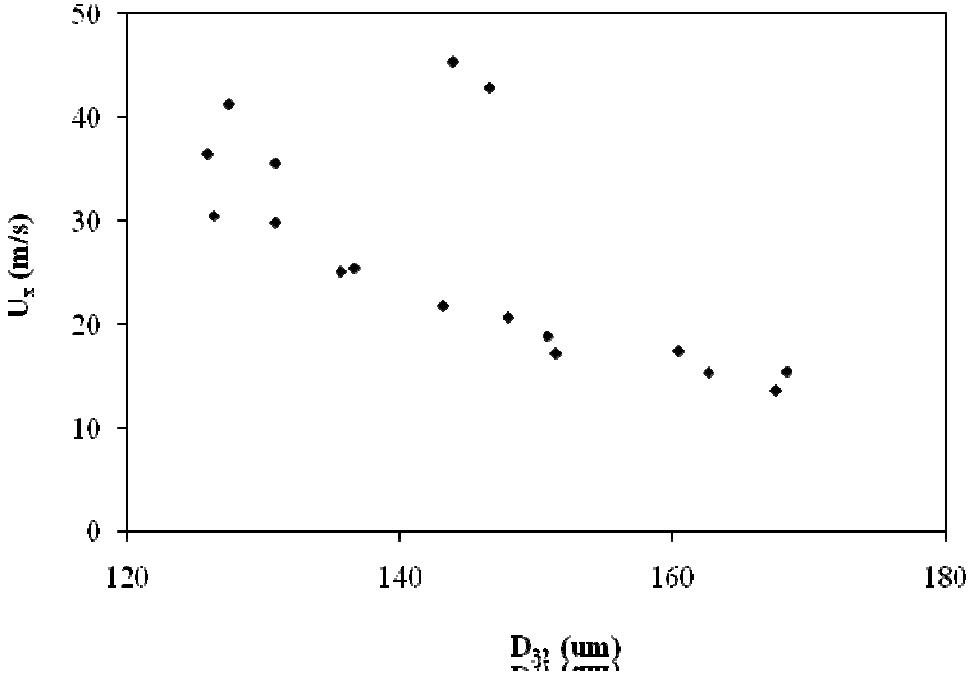

Fig. 7.4. An example of a profile of mean axial velocity for each diameter class of droplets.

Apart from the fundamental interest of this relationship, the immediate value of this work is in validating atomization similarity between air/water and hot steam/bitumen systems. For this specific application, in fact the steam/bitumen system at 300°C (typical feed temperature for this application) has similar viscosity; but significant differences are apparent in surface tension compared to the air/water system. The findings suggest acceptable similarity if the value surface tension is 14 mN/m and 70 mN/m at 300^{o}C and room temperature, respectively [33, 34]. Thus, the surface tension ratio is 5 and the power law exponent of -0.24 implies a diameter ratio of 0.69, which is not significant. This validates air/water testing, greatly increasing the value of this modeling technique and making design testing for heavy oil atomizers significantly easier.

7.3. Size Scaling

Lefebvre *et al.* [13] and Roesler *et al.* [14] identified that D_{32} increases by only 11 to 12% with increases in D i.e. varies ~ $D^{0.1 \text{ to } 0.2}$. For brevity, the two small-scale nozzles will be denoted SS-1.0 (D = 3.1 mm) and SS-1.3 (D = 4.1 mm). The D of SS-1.3 is 1.3 times larger compared to the SS-1.0 nozzle. On the other hand, the SS-1.0 nozzle is a one quarter of the full scale commercial nozzle.

The presence of the larger drops from the SS-1.3 nozzle may seem to be attributed to the delay in atomization due to lower aerodynamic and hydrodynamic forces in the two-phase gas/liquid atomization. Lower momentum produced from the SS-1.3 nozzle attributed to fewer shearing effects between the liquid and air phases. However, the 1.3 fold increase in nozzle size results in 7 μm increase in D_{32} at x = 100 and equates to a power law relationship exponent of 0.14 (based on two points). This small exponent indicates a weak dependence of D_{32} on D. Moreover, a 1.3 fold increase in nozzle size results in 13 μm increase in D_{32} at x = 202 and equates to a power law relationship exponent of 0.25 (based on two points). This small exponent again indicates a weak dependence of D_{32} on D. The exponents 0.14 (at x = 100 mm) and 0.25 (at x = 202 mm) are in agreement with the findings of Lefebvre *et al.* [13] and Roesler *et al.* [14] , which was about 0.1-0.2. In this study, different spray breakup lengths due to different operating conditions were visualized by high-speed video images. These images show that if the gas to liquid ratio (by mass) decreases, spray breakup completes at about 180-200 mm axial distances from the tip of the nozzle (at lower air to liquid ratio by mass condition). However, if the gas to liquid ratio (by mass) is increased, the complete spray breakup length decreases significantly. Eroglu *et al.* [35], measured breakup lengths of round liquid jets with annular coaxial air streams. It was observed that the breakup length increases with the Weber number and decreases with the liquid jet Reynolds number according to the relation:

$$\frac{L}{D_N} = 0.5 We^{-0.4} \, \mathrm{Re}_L^{0.6} \qquad (1)$$

A calculation using different operating conditions applied to this study confirms that the maximum spray breakup length is 189 mm, which is consistent with our visual observation (180-200 mm). If the droplets travel from 100 mm to 202 mm, the change in D_{32} was -3 μm and +3 μm for the SS-1.0 and SS-1.3 nozzles, respectively. This shows a non remarkable change in the $D_{32(gb)}$ values further downstream of the nozzle.

7.4. Conclusions

Since the surface tension ratio between the lab and industrial setting is 5, a first estimate based on a power law extrapolation would indicate 30% smaller drops in the industrial system. It would be prudent to further investigate a greater ratio of surface tensions to build a stronger case, though finding manageable fluids for the lab that offer this ratio is challenging. Certainly future work should consider the possibility of surface tension ratios closer to 5, to build greater confidence in this scaling law. Clearly the ratio of viscosities in the presented experiments is sufficient to rule out viscosity scaling problems for similitude. A power law correlation was proposed based on the experimental data [36] as follows:

$$\frac{D_{32(gb)}}{D_N} = 1641\left[(\beta)^{-0.55}(\rho_r)^{1.20}(Re_L)^{-0.15}(Fr_L)^{-0.48}(We_L)^{-0.06}\right] \qquad (2)$$

The correlation indicates that the $D_{32(gb)}$ depends to some extent on the D_N and ρ_r. However, experimental results shows that there is no remarkable change in $D_{32(gb)}$ due to the 1.3 fold increase in D. To test the accuracy of the above correlation, a $D_{32(gb)}$ obtained from the correlation was compared with an actual $D_{32(gb)}$ obtained from measured data. The results are presented in Fig. 7.5. From Fig. 7.5 it is evident that the proposed correlation in Equation (2) is able to predict the $D_{32(gb)}$ to some extent. To check the general validity of the proposed correlation in Equation 2, the following available correlations were tested to obtain a D_{32} data set:

[37] $D_{32} = C\left(\frac{\rho_L^{0.25}\mu_L^{0.06}\sigma^{0.375}}{\rho_G^{0.375}}\right)\left(\frac{m_L}{m_L U_{LS} + m_G U_{GS}}\right)$, Where C= 1×10^{-3} (3)

[38] $D_{32} = \frac{U_{LS}^{0.08} D_N^{0.16} \mu_L^{0.34}}{\rho_G^{0.30} U_m^{1.33}}$ (4)

[Classical Mechanism] $D_{32} = \frac{1.5 D_N}{\left[1+\frac{CWe_L}{(1+1/\beta)}\right]}$ where C=0.3 (5)

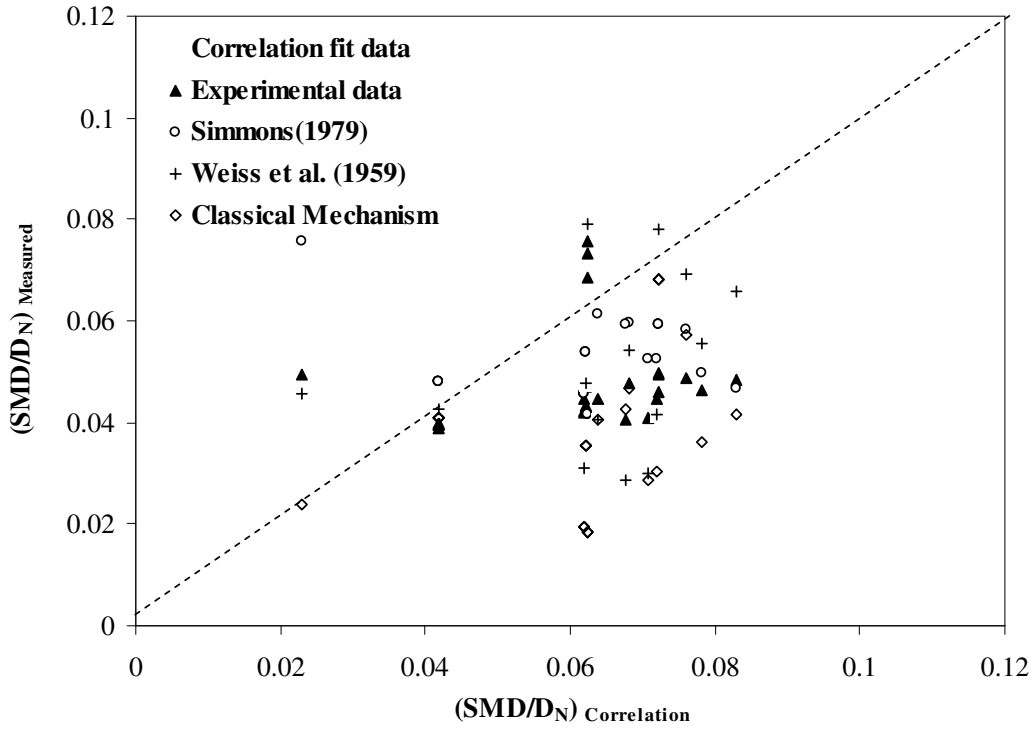

Fig. 7.5. Comparison of D_{32} using different correlations.

The open squares denoted 'correlation-fit data' are the data set obtained from the proposed correlation in Equation (2). The D_{32} corresponding to the closed triangles were obtained from the experiment. The D_{32} corresponding to the circles, pluses and diamonds were obtained from the available correlations in the literature. From Fig. 7.5 it is evident that the estimated D_{32} obtained from different correlations are spread over the dotted equality line. Thus, the proposed

correlation in Equation (2) assures the general validity, which may be interesting for wider applications. However, further investigations should be performed to provide additional data to strengthen the validity of the correlation obtained. The proposed correlation cannot predict the large scale two-phase spray droplet size. It is noted that data of this chapter was taken from Ejim [36]. In this chapter further analysis was conducted to obtain better confidence in establishing the scaling laws.

7.5. References

[1] Liu, H. (1999) Science and Engineering of droplets - Fundamentals and Applications, William Andrew Inc. Noyes Publications.

[2] Elkotb, M.M. (1982) Fuel atomization for spray modeling. Progress in Energy and Combustion Science 8(1): 61-91.

[3] Elkotb, M.M., Mahdy, M.A. and Montaser, M.E. (1982) Investigation of external-mixing airblast atomizers. Proceedings of the 2nd International Conference on Liquid Atomization and Sprays, Madison, Wisconsin, U.S.A.

[4] Rizkalla, A.A. and Lefebvre, A.H. (1975) The influence of air and liquid properties on airblast atomization. Transactions of ASME Journal of Fluids Engineering. 97 (3): 316-320.

[5] Lefebvre, A.H. (1980) Airblast atomization. Progress in Energy and Combustion Science. 6: 233-261.

[6] Lefebvre, A.H. (1989) Atomization and Sprays, New York, Hemisphere Publishing Corporation.

[7] Sovani, S.D.S., P.E. and Lefebvre, A. H. (2001) Effervescent atomization. Progress in Energy and Combustion Science. 27: 483-521.

[8] Nasr, G.G., Yule, A.J. and Bendig, L. (2002) Industrial sprays and atomization: design, analysis and applications, Springer-Verlag London Limited.

[9] Pilch, M. and Erdman, C.A. (1987) Use of breakup time data and velocity history data to predict the maximum size of stable fragments for acceleration-induced breakup of a liquid drop. International Journal of Multiphase Flow. 13: 741-757.

[10] Hsiang, L.P. and Faeth, G.M. (1995) Drop deformation and breakup due to shock wave and steady disturbances. International Journal of Multiphase Flow. 21 (4): 545-560.

[11] Rissio, F. (2000) The mechanisms of deformation and breakup of drops and bubbles. Multiphase Science and Technology. 12: 1-50.

[12] Brodkey, R.S. (1967) The phenomena of fluid motions, Reading, Massachusetts, Addison-Wesley Publication Company.

[13] Lefebvre, A.H., Wang, X.F. and Martin, C.A. (1988) Spray characteristics of aerated-liquid pressure atomizers. AIAA Journal of Propulsion and Power. 4 (6): 293-298.

[14] Roesler, T.C. and Lefebvre, A.H. (1989) Studies on aerated-liquid atomization. International Journal of Turbo Jet Engines. 6: 221-230.

[15] Buckner, H.N. and Sojka, P.E. (1991) Effervescent atomization of high-viscosity fluids: Part I, Newtonian liquids. Atomization and Sprays. 1: 239-252.

[16] Lund, M.T., Sojka, P.E., Lefebvre, A.H. and Gosselin, P.G. (1993) Effervescent atomization at low mass flow rates. Part 1: the influence of surface tension. Atomization and Sprays. 3: 77-89.

[17] Santangelo, P.J. and Sojka, P.E. (1995) A holographic investigation of the near nozzle structure of an effervescent atomizer produced spray. Atomization and Sprays. 5: 137-155.

[18] Kirpalani, D.M. and McCracken, T.W. (2002) Performance diagnostics for nozzles fed with multiphase flow. ILASS-Europe 2002, Zaragoza.

[19] Rahman, M.A., Gomez, J., McMillan, J., Heidrick, T. and Fleck, B.A. (2008) Correlations of the Droplet Size-Velocity of the Two-Phase, Air/Liquid Spray Using a Particle-Dynamic-Analyzer, August 10-14. Proceedings of the FEDSM 2008, ASME Fluids Engineering Conference, Jacksonville, Florida USA.

[20] Rahman, M.A., Heidrick, T. and Fleck, B.A. (2009) A Critical Review of Two-Phase Gas/Liquid Industrial Spray Systems. International Review of Mechanical Engineering. International Review of Mechanical Engineering. 3 (1): 110-125.

[21] Tafreshi, Z.M., Kirpalani, D., Bennett, A. and McCracken, T.W. (2002) Improving the efficiency of fluid cokers by altering two-phase feed characteristics. Powder Technology. 125 234– 241.

[22] Copan, J., Balachandar, R. and Berruti, F. (2001) Droplet size-velocity characteristics of sprays generated by two-phase feed nozzles. Chemical Engineering Communications. 184: 105-124.

[23] Ariyapadi, S., Balachandar, R. and Berruti, F. (2003) Spray characteristics of two-phase feed nozzles. Canadian Journal of Chemical Engineering. 81: 923-939.

[24] Base, T.E., Chan, E.W., Kennett, R.D. and Emberley, D.A. (1999) Nozzle for Atomizing Liquid in Two-phase Flow. US Patent 6003789.

[25] Dumouchel, C. (2009) The Maximum Entropy Formalism and the Prediction of Liquid Spray Drop-Size Distribution. Entropy. 11 (4): 713-747.

[26] Lecompte, M. and Dumouchel, C. (2008) On the Capability of the Generalized Gamma Function to Represent Spray Drop-Size Distribution. Particle & Particle Systems Characterization. 25 (2): 154 – 167.

[27] El-Shanawany, M.S.M.R. and Lefebvre, A.H. (1980) Airblast atomization: The effect of linear scale on mean drop size. Journal of Energy. 4 (4): 184-189.

[28] Albrecht, H.E., Borys, M., Damaschke, N. and Tropea, C. (2003) Laser Doppler and Phase Doppler Measurement Techniques, Germany, Springer.

[29] Damaschke, N., Gouesbet, G., Gréhan, G., Mignon, H. and Tropéa, C. (1998) Response of Phase Doppler Anemometer Systems to Nonspherical Droplets. Applied Optics. 37 (10): 1752-1761.

[30] Dodge, L.G., Rhodes, D.J. and Reitz, R.D. (1987) Drop-size Measurement Techniques for Sprays: Comparison of Malvern Laser-Diffraction and Aerometrics Phase/Doppler. Applied Optics. 26 (11): 2144-2154.

[31] Gréhan, G., Gouesbet, G., Naqwi, A. and F., D. (1993) Particle Trajectory effects in Phase Doppler Systems. Part. Part. Syst. Charact. 10: 332-338.

[32] Gréhan, G., Gouesbet, G., Naqwi, A. and F., D. (1994) Trajectory Ambiguities in Phase Doppler Systems: study of a near forward and a near backward geometry. Part. Syst. Charact. 11: 133-144.

[33] Crickmore, B. (1998) Density, Viscosity and Interfacial Tension of Bitumen Derived Samples as a Function of Temperature Part I. Syncrude Report,. 27 (2): 25-31.

[34] White, F.M. (1999) Fluid Mechanics, U.S.A, McGraw-Hill Series.

[35] Eroglu, H. and Chigier, N. (1991) Wave characteristics of Liquid Jets from Airblast Coaxial Atomizers. Atomization and Sprays. 1 (4): 349-366.

[36] Ejim, C.E. (2008) Effect of Liquid Viscosity, Surface Tension and Nozzle Size on Atomization in Two-Phase Nozzles, PhD Thesis, Mechanical Engineering, University of Alberta, .

[37] Simmons, H.C. (1979) The Prediction of Sauter Mean Diameter for Gas Turbine Fuel. Nozzles of Different Types. ASME paper 79-WA/GT-5.

[38] Weiss, M.A. and Warsham, C.H. (1959) Atomization in high velocity Air-Streams. J. Am. Rocket Soc. 29 (4): 252-259.

CHAPTER 8

Two-Phase Atomization Scaling: Gas Properties[1, 2]

8.1. Introduction

In the oil sands industry, bitumen recovered from the oil sands, is upgraded to sweet light crude oil by fluid coking, hydroprocessing, hydrotreating and reblending. During the fluid coking process, a multiphase flow of steam and bitumen droplets interact with coke particles in a fluidized bed reactor in order to crack the hydrocarbons into lighter fractions. The size of atomized bitumen droplets formed plays a critical role in the efficiency of the process; thus it is essential to understand properly the phenomena involved in their formation [1]. The development of nozzles is generally performed on air-water systems. My plan was to begin with the study of small-scale sprays using air and water to compare to real industrial operations on the full scale air-water or steam-bitumen system, to determine size scaling relationships as indicated in Fig. 8.1. During coker feed nozzle development, cold flow spray tests of the pilot nozzles should closely mimic the actual atomization and its subsequent jet-bed interaction behaviors of the commercial nozzle. In the laboratory, the one-quarter scale nozzle should ideally match as many jet-bed interaction parameters as possible. These parameters include liquid droplet size distribution, momentum flux of the spray, gas/liquid mass ratio and solid's entrainment behaviors, among others. Excessively large bitumen droplets in conjunction with inadequate mixing momentum would severely deteriorate jet-bed interaction effectiveness, as the resultant thick bitumen film on the contacted coke solids or "wet" bitumen/coke

[1] A version of this chapter has been submitted. Rahman *et al.* (2010) International Journal of Multiphase Flow, 25 pp.

[2] A version of this chapter has been published. Rahman *et al.* (2010) Proceedings of the 13th International Symposium on Flow Visualization, Nice Acropolis Center, French Riviera, July 1st to 4th.

agglomerates would severely limit mass and heat transfer. This is attributable to poor liquid product yield and operability in the fluid cokers [1].

The majority of the cold flow spray nozzle tests have been performed using air as the atomization gas [2-9]. Very few attempts were previously undertaken to investigate the effects of gas phase molecular weight on the two-phase atomization [10, 11]. In the current study, in order to simulate the atomization performance of the commercial coker feed nozzles at actual *hot* operating conditions (350°C) under *cold* flow conditions, the liquid phase, bitumen, is simulated with water [12]; and the small amount of steam (~1-4 wt %) is simulated with a mixed helium/nitrogen gas instead of air. This mixture of 82 wt% Helium and 18 wt% Nitrogen was used because it compares the density of the atomization steam that is used in the commercial system. Since helium is expensive, small-scale laboratory tests provided an inexpensive and easily accessible alternative to study the realistic spray atomization behaviors of fluid coker nozzles *in situ*. The similitude in the atomization parameters between the commercial operation and lab scale operation by matching the air to liquid mass ratio, void fraction, liquid Froude number, mixture Euler number and density ratio as indicted in Table 1.

Once the scaling of the gas phase density is established, the large volume of experimental data using air and water as the process fluids in the lab scale experiments help to find the effects of upstream flow patterns and bubble diameter (d_b) on the droplet size (d_d) distribution in the downstream spray [13]. However, due to the highly non-uniform volumetric flow distribution and intermittency in the two-phase flow, it is extremely difficult to accurately predict the bubble size and flow pattern distribution in this type of flow [14]. Thus, a fairly reliable experimental method and statistical tools are required to determine the uncertainty level in the bubble size estimation. There are very few experimental studies that have been conducted to study bubbly flows in strictly

horizontal pipes [8, 15-24]. Also, little information is available regarding studies oriented towards the determination of bubble size in two-phase flows [6, 8, 24-32]. In a recent study, images of particles produced by shadowgraph and back-illumination using an infrared diode laser were investigated with a digital image analysis technique [33]. This technique was potentially capable of sizing particles of arbitrary shape and size and with a wide dynamic range. Another study [34] implemented a digital-based image analysis system for the determination of size and the distribution of particles suspended in any clear fluid flow. However, the above study was for relatively large particles (some mm in diameter). Defocusing digital particle image velocimetry (DDPIV) was used to obtain scalar and vector information within large length scales [35]. The DDPIV method is the natural extension of planar particle image velocimetry (PIV) techniques to the third spatial dimension. Implementing the DDPIV technique made it possible to calculate the number density, the size distribution, the associated local void fraction and the velocity of bubbles in two-phase flows. Further studies on advanced photonics measurements can be found in the literature [2, 36-50]. There are also several studies [51-63] found in the literature related to the transport of two-phase, gas/liquid flows through pipelines. The literature referenced above demonstrates that usually in turbulent two-phase two-component flows, bubble break-up and coalescence takes place continuously and these processes determine the bubble size distribution. Bubbles smaller than d_{min} in diameter will have a high tendency to coalesce, whereas those with diameters larger than d_{max} will have a high tendency to break up [8]. Thus, in two-phase flow it is extremely critical to determine the length scale of the largest diameter and smallest diameter bubbles. These smallest and largest diameter bubbles actually determine the coalescence and break up of bubbles. Bubble coalescence and break up also plays a critical role in determining the two-phase flow regime transition. To predict the d_{max} and d_{min} in two-phase flow, several correlations were proposed [64-66]. A detailed description of various flow regimes can also be obtained in the literature [67]. Most previous studies were conducted in vertical flows, with different working

fluids and with higher or lower gas/liquid input content. Several studies dealing with two-phase flow maps are also found [9, 67-78]. Taitel and Dukler [67, 77] attempted to predict the flow regimes for concurrent gas-liquid flow in pipes using a momentum balance. The Breber Map [74] is divided into square regions, which is easier to implement in some cases. The Baker map [68, 74] works well for water/air and oil/gas mixtures in tubes with smaller diameters no bigger than 50 mm [78]. However, these flow maps cannot accurately predict all the two-phase flow classes and transitions between the flow regimes, as available flow maps are applicable only for particular fluids, local temperatures and pressure conditions.

In petrochemical process industries, most of the light crude oil upgrading processes are associated with two-phase, gas/liquid (steam/bitumen) flows in feed nozzles. Atomization and droplet formation from the nozzle likely depends on flow patterns and bubble size in the feeding conduit. Thus, it is imperative to have a good understanding and reasonable estimates of the bubble size and flow regime distribution in turbulent two-phase, gas/liquid flows. This knowledge assists in the design and operation of a system that can achieve high product yield (such as bitumen) recoveries. Moreover, it is important to understand the effects changing gas phase density (mixed gas and air) in two-phase flows on bubble size and flow patterns and its subsequent effects on the atomization characteristics. Since gas assisted atomization is becoming increasingly important in many industrial applications such as physical, chemical and petroleum processes, it is critical to understand the fundamental physics behind the upstream two-phase flow transport phenomena and its subsequent effects on the downstream atomization behavior.

8.2. Scaling Criteria

For scaling considerations in the development of future feed nozzle prototypes, the challenge is to minimize the dissimilitudes between the real, i.e. *hot*, operation of the nozzle and *cold* flow spray tests. In commercial or *hot* pilot plant operation of the nozzles, steam is used to atomize bitumen at 350^{o}C. In *cold* flow spray

tests, air is usually used to atomize water at ambient temperatures, ~20^{o}C. Simulation of *hot* operating conditions with *cold* flow tests has always been a challenge. My past efforts were mostly designed to match the volumetric flow ratio between the gas and the liquid in an attempt to match the gas void fraction in the nozzle. By doing so, the gas flow rate and density were inevitably compromised, as they could not match the commercial *hot* conditions. The typical steam to bitumen mass ratio (β) for the commercial nozzle operation is ~1 %, which results in a nozzle pressure of approximately 1651 kPa (225 psig). By matching the volumetric void fraction of the gas (α) in the nozzle conduit, *cold* flow tests on a scale similar to commercial nozzles were conducted with an air to water mass ratio (β) of ~2 %. If the system were operated at 1% β using air and water, the nozzle operating pressure would be approximately 1350 kPa. When the system is operated at 2% β using air and water, the nozzle operating pressure is 1,651 kPa (225 psig), which matches the commercial case.

To obtain the desired flow conditions in the one quarter scale nozzle in the laboratory, the similitude technique adopted in the literature [79-81] was followed assuming the isothermal gas/liquid flow without mass transfer. Characteristic diameter (D_A) was used as the characteristic length in the dimensionless analysis. The nozzle throat diameter (D_N) is the critical diameter that governs the liquid flow rate. In a large scale nozzle, pressure at the nozzle throat and mixing zone was found to be 551 kPa and 1,651 kPa, respectively; at a liquid flow rate of 2.95×10^{-03} m^3/s and gas to liquid mass ratio of 1%. On the other hand, in a small scale nozzle, pressure at the nozzle throat and mixing zone was found 167 kPa and 551 kPa at a liquid flow rate of 9.43×10^{-05} m^3/s and a gas to liquid mass ratio of 1%. Thus, pressure ratios between the large and small scale nozzles at the nozzle throat and mixing zone were 3.2 and 3.1, respectively. These two ratios indicate the incorporation of either D or D_N in the dimensionless analysis results in a similar outcome. For a nozzle spraying into ambient surroundings of given

temperature and pressure, and assuming an ideal gas law, the dimensional analysis yields:

$$\frac{D_{32}}{D_A} = f\left(\frac{L}{D_A},\ \frac{m_G}{m_L}, \frac{\rho_G}{\rho_L}, \frac{\mu_G}{\mu_L},\ \frac{\rho_g u_{gs}^2}{\rho_L u_{Ls}^2}, \frac{Q_g}{Q_g + Q_L}, Re_m,\ Fr_m,\ We_m,\ Eu_m\right) \quad (1)$$

In Equation (1), for nozzle D_A corresponds to D_N and for nozzle conduit D_A corresponds to D. Since the Morton Number, $Mo \sim We^3/(Fr*Re^4)$, the Equation (1) can be finally re-written as:

$$\frac{D_{32}}{D_A} = f\left(\frac{L}{D_A},\ \beta, \rho_r, \frac{\mu_G}{\mu_L},\ S, \alpha, Mo_m,\ Eu_m\right) \quad (2)$$

The first term *L/D* indicates the conservation of geometric similarity, which was achieved by the similar nozzle design. The second term comes from the gas to liquid mass ratio. The third and fourth terms are density ratio and viscosity ratio, respectively. The last four terms are the superficial momentum ratio (S), superficial void fraction (α), mixture Morton number (Mo), and mixture Euler Number (Eu_m), respectively. Previous dimensional analysis indicates that restrictions on some of the quantities may be relaxed depending on knowledge of the dominant forces in the system [82]. Another study also concluded that matching all the terms in the dimensional analysis may not be practically feasible [81]. Since $\mu_G << \mu_L$, the viscosity ratio can be ignored. In a two-phase horizontal flow, the *Froude number* is an important number as it predicts the initiation of disturbance by the Bernoulli force versus the stabilizing gravity force [83, 84]. The density ratio term is another important parameter, as a previous study showed that the two-phase gas/liquid atomization quality is intensively dependent on the gas phase density and pressure [7, 12, 85, 86]. The mixture *Euler Number* is another important parameter because it helps to determine the mixing pressure for different scale atomization. Moreover, the momentum ratio and void faction are important dimensionless numbers as these numbers determine the slip and flow pattern, respectively in two phase flow and atomization. A previous study proposed a power law correlation [4]:

$$\frac{D_{32(gb)}}{D_N} = 1641\ \left[(\beta)^{-0.55}(\rho_r)^{1.20}(Re_L)^{-0.15}(Fr_L)^{-0.48}(We_L)^{-0.06}\right] \quad (3)$$

In addition to the above mentioned correlation, several studies [51, 87, 88] reported other correlations for droplet sizing in an effervescent nozzle, such as:

$$D_{32} = C\left(\frac{\rho_L^{0.25}\mu_L^{0.06}\sigma^{0.375}}{\rho_G^{0.375}}\right)\left(\frac{m_L}{m_L U_{LS} + m_G U_{GS}}\right), \text{ Where } C = 1\times10^{-3}$$

[Simmons ([51])] (4)

$$D_{32} = \frac{U_{LS}^{0.08} D_N^{0.16} \mu_L^{0.34}}{\rho_G^{0.30} U_m^{1.33}}$$ [Weiss et al. ([89])] (5)

Equation obtained by the 'Classical Mechanism' is not indicated here as proper reference for this mechanism cannot found elsewhere. Typical flow conditions and steam-bitumen properties of the commercial coker nozzle are as follows: liquid volume flow rate, Q_L (USGPM): 47 (3 *l*/s), gas to liquid mass ratio, β (%):1.0, steam-bitumen mixing pressure, P_m (kPa): 1651 (225 psig), feed temperature (°C): 350°C, characteristic gas constant of steam, R_{gas} (J/kgK): 461.4, steam density, ρ_G (kg/m^3): 6.0, bitumen density, ρ_L (kg/m^3): 897, steam absolute viscosity, μ_G ($1x10^{-5}$kg/m.s): 2.227. The laboratory scale nozzle is geometrically one quarter of the full scale commercial nozzle. In the lab scale nozzle, air and water were used as the gas and liquid phase, respectively. To match the superficial liquid *Froude Number* to that of the full scale nozzle, the corresponding liquid flow rate in the lab scale nozzle (Q_L) needs to be 0.095 *l*/s (1.5 USGMP). Based on the mixture's *Euler Number* and *Froude Number* dynamic similarity, the P_m (lab-scale) was found to be 531 kPa (62 psig). In addition to the *Froude number* (*Fr*) and gas to liquid mass ratio (β) similarity, the density ratio between the two scales has to be matched. For equal density ratios in both scales, the mixing pressure at the inlet to the lab scale nozzle should correspond to 531 kPa (62 psig). The superficial liquid *Reynolds Numbers* (*Re*) are 2.9×10^4 and 2.0×10^4 for the full scale and lab scale nozzle, respectively. Scaling comparisons from commercial to pilot and lab scale nozzles based on the gas to liquid mass ratio, Froude number, Euler number and density ratio matching is presented in Table 8.1. To overcome the dissimilitude, previous attempts [12] endeavoured to scale the liquid viscosity and surface tension in the *cold* flow tests

with that of bitumen viscosity and surface tension in the *hot* flow tests. It was also necessary to scale the density of the gas phase. Thus, it was decided to use a mixed helium/nitrogen gas to replace air in the *cold* flow lab scale spray tests. Disadvantages to the mixed gas are the expense associated with the premixed compressed gas from cylinders and the logistics and technical difficulties of conducting the tests quickly to minimize gas consumption. For scale-up considerations, the following parameters were taken into consideration in the *cold* flow tests to yield similitude with the *hot* commercial operation of the nozzles. It must be noted that mixed gas tests will entrain ambient air after exiting the nozzle - secondary atomization occurs.

8.2.1. Gas-Liquid Mass Ratios

The gas to liquid mass ratio (β) is an important atomization parameter in gas-liquid flows; hence it was kept constant in the dimensional analysis, such as β of 1%, when comparing two different scales of nozzles in the analysis. The weakness of matching gas to liquid mass ratio with the commercial *hot* operation with the air/water *cold* flow experiments is the difference in pressure drops at the same liquid flow rate. At 531 kPa and 15°C in the lab scale environment, the density of air is 6.5 kg/m^3. At commercial nozzle operating conditions of 350°C and 1,651 kPa (225 psig), steam has a density of 5.74 kg/m^3 (0.358 lb/ft^3). All things considered, if air were to be used to simulate steam, the temperature of the air would have to be raised to 728°C at the comparable pressure of 1,651 kPa (225 psig) and a density of 5.74 kg/m^3 (0.358 lb/ft^3). This would not be practical, as the temperature would exceed the boiling point temperature of 203°C at the same pressure and this also negates the convenience and objectives of *cold* flow simulations. Mixing helium with nitrogen yields a mixture molecular weight of 8.4 with a gas density equal to 1.84 kg/m^3.

8.2.2. Volumetric Gas/Liquid Ratios

A second scaling parameter to be considered for *cold* flow simulation is the volumetric flow rate ratio between liquid and gas in the two-phase atomization

nozzle. By matching the pressure by dimensional analysis in the laboratory scale nozzle operating pressure (531 kPa) to that of the commercial nozzle (1651 kPa), one can expect the void fractions within the nozzle conduit can also be matched; assuming firstly the gas and liquid densities were matched between the lab scale nozzle and commercial scale operations and secondly no-slip condition exists. With the mixed gas/water system, the momentum of the jet should compare closely between the commercial *hot* steam/bitumen and the *cold* flow mixed gas/water system, yielding reasonable similitude.

8.2.3. Atomization Gas Molecular Weight

As discussed in the previous sections, the current, novel experimental technique is used to scale the commercial atomization steam (gas) molecular weight with a mixture of a light gas (helium, He) with a heavier gas (nitrogen, N_2) for the lab scale tests. The commercial feed nozzle operates at ~1651 kPa (225 psig) and ~350^{o}C. By apportioning helium and nitrogen in a gaseous mixture, a nozzle operating at the pressure of 531 kPa and at a room temperature of 15°C, yields a gas density of 1.84 kg/m^3 and molecular weight of 8.46. At 1,651 kPa or 225 psig, 350^{o}C and characteristic gas constant of 461 J/kg.K, ρ_G was found to be 5.74 kg/m^3 (0.358 lb/ft^3) and molecular weight of 18. However, at 531 kPa, 15^{o}C and air gas constant of 287 J/kg.K, ρ_G was found to be 6.5 kg/m^3 and molecular weight of 29. The equivalent temperature in the lab scale nozzle to work in the operating pressure of steam (1,651 kPa or 225 psig and at a room temperature of 15^{o}C) was found to be 729 ^{o}C. The volumetric (molar) composition of the mixed gas (He/N_2) to yield the equivalent molar mass was determined as follows:

$$MF_{Helium}(4\frac{kg}{mol}) + MF_{Nitrogen}(28\frac{kg}{mol}) = 8.46\frac{kg}{mol} \quad (6)$$

$$MF_{Helium}(4\frac{kg}{mol}) + (1 - MF_{Helium})(28\frac{kg}{mol}) = 8.46\frac{kg}{mol} \quad (7)$$

$$MF_{Helium} = 0.814 \quad (8)$$

$$MF_{Nitrogen} = 0.186 \quad (9)$$

With a composition of 81.4 vol % helium and 18.6 vol % nitrogen; and a molecular weight of 8.4, the mixed gas was used to scale gas phase molecular weight.

8.3. Two-Phase Flow Theory

Bubble coalescence and break-up are continuous processes in the transport phenomena of two–phase flows in a nozzle conduit. If the liquid flow rate increases, the associated liquid turbulent dissipation increases. This increase is attributed to the break up mechanism due to severe turbulent splitting. As a result of the predominant splitting action, the relatively large bubbles in the slug flows will divide into smaller almost spherical bubbles. With a decrease in the volume of the bubble, the interfacial tension dominates maintaining a spherical bubble shape. Under such extreme conditions, dispersed bubbles or homogeneous flow patterns exist, even at high void fractions. Thus, highly turbulent dissipation and breaking is the key mechanism responsible for flow pattern transition in turbulent two-phase flows. Brodkey [90] has demonstrated that the critical 'non-coalescent' spherical bubble size would have a diameter of:

$$d_{cr\ Brodkey} = \left[\frac{0.4\ \gamma}{\Delta\rho\ g}\right]^{1/2} \tag{10}$$

Equation (10) is a classical equation that describes how the transition from the intermittent flow to the homogeneous flow maintains the critical Brodkey bubbles in the two-phase flow regime. Interestingly, the critical bubble diameter that maintains the spherical bubble can only be described by the cohesive surface tension force, the stabilizing stratifying force and finally the density difference between the two fluids. The expression does not depend on the geometry or length scale of the conduit, viscosity of the fluids, nor the operating pressure of the nozzle. The diameter of Brodkey bubbles for changing surface tensions and densities for different fluids is presented in Table 8.2. The values of Brodkey bubbles found in Table 8.2 ranges from 0.6 μm to 1.4 μm indicating the gravity term is a tempting and convenient dimensional number for scaling that is never varied; nevertheless, the density difference or surface tension scaling works. It is

strongly believed that apart from the nozzle geometry, the mean length scale of bubbles in the upstream flow greatly influences the mean length scale of droplets in the spray. Thus, it is critical to understand the physics behind the bubble size distribution in two-phase flows, as well as having an awareness of a reliable statistical tool for finding the mean length scale of bubbles in two-phase flows. A study [76] was conducted with air and water in a large circulating rig with a 0.105 m diameter test section. The bubble diameter, d_b was expressed as [76]:

$$d_b = \sqrt[3]{d_1^2\, d_2} \tag{11}$$

where d_1 and d_2 are the major and minor axis lengths of the ellipsoid, respectively. The number average bubble diameter, $(d_b)_{ave}$ can be subsequently calculated as follows [76]:

$$(d_b)_{ave} = \sum_{i=1}^{N_b} d_b / N_b \tag{12}$$

Where, N_b is the number of bubbles. In addition to the mean bubble diameter, the prediction of an accurate maximum and minimum bubble diameter is critical as the density of maximum and minimum bubbles determine the coalescence and break-up of bubbles in two-phase flows. In the literature several statistical correlations have been proposed to estimate the maximum bubble size in two-phase, two-component flows. The maximum bubble size [72] was expressed as follows:

$$d_{\max} = \frac{4\,\gamma^{0.5}}{g^{0.5}\,(\rho_L - \rho_G)^{0.5}} \tag{13}$$

The maximum diameter of bubble in the pipe can also be written by a statistical correlation as [32]:

$$d_{\max} = 1.38\,(We_c)^{0.6}\left[\frac{\gamma^{0.6}}{\rho_c^{0.5}\mu_c^{0.1}}\right]\left(\frac{\rho_c^{0.2}}{\rho_d^{0.2}}\right)\left(\frac{D_c^{0.5}}{[u_L^S]^{1.1}}\right) \tag{14}$$

Subscripts, c and d correspond to the continuous (i.e. water) and the dispersed phases (i.e. air), respectively. Several studies [32, 58, 59] determined We_c=1.1 (c stands for critical) and others [54] confirmed that for an air-water low void

fraction system, We_c=1.05; and for the oil-water emulsion, it was proposed [59] that We_c=1.18. Another statistical correlation estimating the maximum particle diameter in the pipe was also proposed by Holmes [59] for oil-water emulsion using Equation (15). Hinze [91, 92] using Kolmogorov's model described the turbulent dissipation in a three dimensional spectrum versus energy containing eddies. The model demonstrated that a maximum stable diameter of the bubble would result in a balance between the surface tension force maintaining the integrity of a bubble and the turbulent shear force maintaining the splitting of the bubbles [64]:

$$d_{\max} = K\left(\frac{\gamma}{\rho_d}\right)^{3/5}\left(\frac{1}{\varepsilon}\right)^{2/5} \tag{15}$$

In Equation (15), K is a dimensionless constant value, which can be found from the experiments. Here, γ is the surface tension (N/m) that provides the cohesive force and ε is the turbulent energy dissipation (m^2/s^3 or watt/kg) that provides the splitting force. Only eddies with length scales smaller than $d_{cr\ Brodkey}$ cause a turbulent splitting action; larger eddies corresponding to $d_{cr\ Brodkey}$ only contribute to the transportation of bubbles. The rate of energy dissipation per unit mass for turbulent pipe flow can be obtained as follows, if the flow is truly homogeneous:

$$\varepsilon = \left(\frac{dp}{dx}\right)_{fr}\left(\frac{u_m}{\rho_m}\right) \tag{16}$$

The frictional pressure gradient (dp/dz) in the nozzle conduit can be used to describe the turbulent dissipation, ε, as follows:

$$\left(\frac{dp}{dx}\right)_{fr} = f_{Darcy}\left(\frac{\rho_m\, u_m^2}{2\, D_c}\right) \tag{17}$$

where, f_{Darcy} is the Darcy friction factor. In reality, it is difficult to keep a dispersed homogeneous flow in a horizontal pipe flow due to the inherent characteristics of two-phase gas/liquid flow. Thus, the homogeneous flow model in calculating the two-phase energy dissipation does not work very well in most practical cases. However, the homogeneous flow model is a superior tool to understand the preliminary behavior of the two-phase flow due to its simplicity to

calculate. Thus, the critical energy dissipation is estimated differently in the literature [64] and is written as follows:

$$\varepsilon = A_4 \frac{\gamma^{1.45} \mu_c^{2.91}}{\rho_c^3 C_{L-V}^{1.36}} \tag{18}$$

where, $A_4 = (A_1 / 3.19)^{1/0.11}$ and according to Hinze [93] $A_1 = 0.725$. In the literature several analytical formulations have also been proposed to estimate the minimum bubble size in two-phase, gas/liquid flow. As the two colliding bubbles approach each other, a liquid film is trapped between them. For coalescence to occur this liquid film must drain out and rupture. The minimum bubble diameter with a tangentially immobile interface can be expressed by a statistical correlation as follows [9]:

$$d_{\min} = 2.4 \left(\frac{\gamma^2 \, h^2}{\mu_c \, \rho_c \, \varepsilon} \right)^{1/4} \tag{19}$$

where, h is the film thickness at rupture between the two bubbles, which was 1 μm [9]. The minimum diameter of a particle, which is stable against coalescence in a turbulent dispersion with a tangentially immobile interface, was also expressed by another statistical correlation as [64]:

$$d_{\min} = \left(\frac{\gamma^{1.38} C_{L-V}^{0.46}}{0.0272 \mu_c \rho_c^{0.84} \varepsilon^{0.89}} \right)^{1/3.11} \tag{20}$$

Here, γ is the surface tension of water (N/m), ε is the turbulent kinetic energy dissipation rate (m^2/s^3) and ρ and μ are the density (kg/m^3) and dynamic viscosity (Pa.s), respectively. $C_{L\text{-}V}$ is the London Van der Waals constant (10^{-28} J.m). Since there is a bubble break up and coalescence action predominant in two-phase flows based on the maximum and minimum diameter of bubble, the flow transition occurs contentiously in two-phase flows. Different flow transitions may also occur due to the pressure gradient in the axial direction of the flow. Attaining slug flows is very common in two-phase flows. Thus, it is critical to know the physics behind the slug formation and slug frequency in two-phase flows. From the data collected in a 3.81 cm ID conduit of an air-water system, a correlation was proposed [94] to calculate the slug frequency per second:

$$f_s = B\left[\frac{u_L^S}{g\ D_c}\left(\frac{19.75}{u_m}+u_m\right)\right]^{1.2} \tag{21}$$

Another study conducted in air and water reconfirmed the proposed correlation as indicated in Equation (21) and rearranged the correlation indicating the importance of the *Froude number* ($[(u_L^S+u_G^S)^2]/D_c\ g$) in determining the slug frequency as follows [95]:

$$f_s = B\left[\frac{u_L^S}{u_L^S+u_G^S}\left(\frac{2.20}{D_c}+\frac{(u_L^S+u_G^S)^2}{g\ D_c}\right)\right]^{1.2} \tag{22}$$

The coefficient B is experimentally fitted with a value of 0.0226. In our current study, experimental data is compared with the proposed correlations indicated in Equation (21) and Equation (22).

8.4. Experimental Set-up

In this study, a one-quarter scale of a patented full-scale nozzle, US Patent 6003789 [96], was used. The full scale nozzle is used in a fluidized bed coker for heavy oil upgrading. In the laboratory experiment, a feeding conduit of 36.8 cm in length and 6.35 mm ID was located upstream of the nozzle. The nozzle diameter (D_n) was 3.10 mm. This nozzle assembly was mounted on a 3-D automated traversing rig. The experiments were performed using mixtures of water (0.04 *l/s* to 0.11 *l/s*) with air or mixed gas (0.16 *l/s* to 0.48 *l/s*), which gave air to liquid mass ratios (β) of 1 to 4%. The experimental schematic diagram is presented in Fig. 8.2.

8.4.1. Measurement of the Droplet Size in the Spray

The mean drop size was measured using a 2-D Phase Doppler Particle Anemometer (PDPA) using Dantec Dynamics specifications [97]. The working principal of the Phase Doppler Particle Analyzer can be found in the literature [98-102]. A round, transparent plexiglass pipe was used to visualize the two-phase gas/liquid flow regimes and bubble size distribution inside the nozzle conduit.

8.4.2. Measurement of the Bubble Size in the Conduit

A 1531-A STROBOTAC electronic stroboscope was used to freeze the bubble motion with back illumination. This device can measure up to 250,000 rpm speed with $\pm 1\%$ accuracy within 0.8 μs flash duration. A D100 high-performance single-lens-reflex (SLR) digital camera was used to capture the back scattered illuminated images. The Micro-Nikkor 55 mm/f: 3.5 micro reverse lens was used with a reversing ring for macrophotography. This highly rated lens can reach a maximum magnification ratio of 1:2 (*0.5X*) with its internal helical focus mechanism. To obtain even higher magnification, a Bellow unit (Nikon PB-4) was used. With this combination, the magnification ratio reached up to 2X-5X. MATLAB 7.1 code was utilized to filter the highly dense bubble population. The filtering procedure is depicted in Fig. 8.3. By utilizing this code, the area average bubble mean diameter, maximum diameter, minimum diameter, major axis length, minimum axis length, eccentricity and centroid of each bubble were extracted. The average eccentricity was found to be 0.66. Photron Motion Tools software was used to track an individual local bubble and subsequently calculate the characteristics of bubble velocity. By selecting the point of interest within the recorded image sequence, it was possible to track down the bubble motions within the sequence as shown in Fig.8.4.

8.4.3. Measurement of Voidage in the Conduit

Pneumatically controlled ball valves were used to suddenly close a section (33.4 cm in length) in the feeding conduit. It took 200 ms to close the valves. There was an average 8 ms asynchronization time between the two valves during closing. The ball valves were closed rapidly to capture the water phase in a particular section (33.4 cm in length) of the feeding conduit (36 cm in length). From the known volume of the segmented section between the two valves and trapped water volume in the same segment, air volume and thus void fraction can be calculated experimentally.

8.4.4. Measurement of Slug Frequency

A Phroton 1280×1024 monochrome PCI fast cam was implemented to capture the bubble and slug motion using the shadowgraph method. An ARRISUN 12 HMI 1200W lamp-head was used as the light source on the opposite side of the fast cam. Also a built-in blackbody slit was used to concentrate the light in the 6.35 mm (ID) conduit section. For the power source a flicker-free ARRI 575/1200 kW electronic ballast was implemented. Recording rates ranged from a full pixel resolution of 500 frames per second, to a low pixel resolution of 16,000 frames per second. In this study, 4,000 frames per second with 640×128 pixel resolution and 2,000 frames per second with 1,280×256 pixel resolution were used for the air-water and mixed gas-water experiments, respectively. Using the Photron Motion Tools Software, the motion of each slug was captured slowly frame by frame. The number of slugs in a fixed number of frames per second was counted and the slug frequency was calculated.

8.5. Results and Discussions

Our experimental observations indicate that two-phase gas/liquid spray pulsation and atomization quality depends remarkably on the two-phase fluid conditions (β, α, P_m), the design of the two-phase fluid mixing arrangements and the geometry of nozzle and flow regimes in the conduit of the nozzle. Recent studies in effervescent atomizers by Buckner *et al.* [103], Lund *et al.* [104], Santangelo *et al.* [105], Copan *et al.* [106], Ejim *et al.* [12] and Rahman *et al.* [7] indicate that mean droplet size was a strong function of air to liquid mass ratio (β) and a weak function of surface tension (γ) and viscosity (μ_L).

The nozzle used in our experiment is the hybrid design of a classical twin-fluid and effervescent nozzle. A study conducted by Tafreshi *et al.* [49] and Hulet *et al.* [107] using a feed nozzle for fluid cokers, indicated the flow patterns (such as slug flow, bubbly flow and annular flow) and gas to liquid mass ratio affects the droplet size. An illustration of a good and poorly atomized spray as a consequence

of good and poor two-phase upstream flow found in our experiments is depicted in Fig. 8.5. The first image indicates a well atomized spray due to the effects of the upstream dispersed bubbly flow condition. In this case, the two-phase flow contains large spherical bubbles attributing to a stable flow pattern. In the second image, the stability of the flow in the nozzle conduit perturbs, attributing to a coarse atomization. In the final image, the flow stability diminishes, which results in liquid ligament and pulsation formation in the spray. Thus, upstream flow patterns directly affect the downstream spray condition, such as atomization quality. For a certain flow rate, fluid properties and conduit length, the transition from one pattern to another can be described as a function of the superficial gas and liquid velocities:

$$u_L^S = f \left| u_G^S \right|_{local\,T\,\&\,P} \tag{23}$$

8.5.1. Flow Pattern in the Feeding Conduit

Taitel *et al.* [77] proposed a typical flow pattern map for gas/liquid horizontal pipe flow as shown in Fig. 8.6. However, Fig. 8.6 is applicable to certain pipe geometry, flow rate and fluid property conditions. Fig. 8.6 is a classical image used in two-phase gas/liquid horizontal flow to explain the transition conditions from one flow pattern to another. Dukler *et al.* [108] observed and analyzed the physics behind the evolution and distortion of a smooth, stratified gas/liquid interface in a horizontal flow. Our experimental observations indicate that the two-phase pipe flow is a highly chaotic turbulent flow denoting no possibilities of the existence of a stratified flow pattern. Thus, the flow pattern could be either dispersed bubble flow, intermittent/slug flow or annular flow pattern. A model is proposed in the literature that explains the liquid turbulent energy requirement to maintain the dispersed bubble population in the flow regime [77, 109]. Thus, the transition from the intermittent to the dispersed bubble pattern is achieved when turbulent energy is dissipated by radial velocity. My experimental observations indicate that the two-phase pipe flow is a highly chaotic, turbulent flow denoting no possibilities of the existence of a stratified flow pattern. Thus, the flow pattern

could be either dispersed bubble flow, intermittent/slug flow or annular flow pattern. A model is proposed in the literature that explains the liquid turbulent energy required to maintain the dispersed bubble population in the flow regime [77, 109]. Thus, the transition from the intermittent to the dispersed bubble pattern is achieved when turbulent energy dissipated by radial velocity fluctuations is greater than the surface free energy of stable, micro-bubble populations involving the gas volume. In the dimensionless form:

$$\frac{u_L^S}{u_G^S} \geq 12.65\left(\frac{X_L}{Eo^{1/2}}\right) \tag{24}$$

where, *Eo* is the modified *Eotvos number*:

$$Eo = \frac{g\,(\rho_L - \rho_G)\,D_h^2}{\sigma} \tag{25}$$

and the dimensionless variable X_L is defined as:

$$X_L = \frac{g\,(\rho_L - \rho_G)}{\frac{4A_L}{D_h}\left(\frac{D_h u_L^S}{\nu_L}\right)\left(\frac{\rho_L\left[u_L^S\right]^2}{2}\right)} \tag{26}$$ and where: $$D_h = \frac{4A}{S} \tag{27}$$

From experimental observations and Table 8.3, it is evident that in both cases of mixed gas and air as the gas phase medium at 483 kPa mixing pressure (P_m) and air to liquid mass ratio (β) in the range of 1-7%, the flow regime is not dispersed bubbly (DB) flow. Our experimental observations indicate that at higher liquid flow rates, the liquid and gas phases do not mix properly and liquid ligaments are formed after atomization through the nozzle. As the liquid flow rates decrease and gas flow rates increase, the rate of slug formation possessing greater momentum increases. However, at this stage the length of the slug is relatively small; producing enlarged annular gas pockets in the nozzle conduit. The increase in β assists in the transition of the flow pattern into annular flow. The formation of an intermittent (I) flow pattern following the tendency of an annular flow pattern formation in all the cases of mixed gas-water two-phase flow experiments shown in Table 8.3 indicates the benefit of lighter density gas phase fluids in atomization.

The above mentioned mechanism of flow pattern formation in the small scale laboratory nozzle can be reconfirmed from Fig. 8.7, where the evolution of the different flow patterns in the two-phase gas/liquid flow is illustrated with time. Although Fig. 8.7 is a typical illustration of a flow pattern in the lab scale nozzle assembly for the mixed gas and water atomization experiment, similar flow patterns were observed for the air and water experiments in the lab scale nozzle as evidenced by the high speed video shadowgraphy. For brevity, only the mixed gas and water two-phase flow images are illustrated in Fig. 8.7. The white zone in the conduit denotes the air phase. The black zone in the conduit denotes the liquid phase containing numerous bubbles. The intensity of the back color in the conduit is increased if the bubble population is increased. The light scattered from the bubbles will not be obviously noticeable due to the obstruction from other bubbles. Thus, the zone where the bubble population is greater appears as a black object in the image. When the gas phase mostly occupies the nozzle conduit as an annular flow structure, the liquid phase accelerates with the gas phase velocity. Thus, a high speed liquid slug containing a large number of bubbles advances very quickly, providing the momentum to the fluids ahead of the slug. Due to the chaotic nature of slug flow, the slug is followed by a good mixture of small bubbles in the liquid phase. Immediately after this situation, again an annular gas pocket is formed and a similar flow pattern formation mechanism is repeated consecutively.

In the current study, slugs of liquid with a large number of small bubbles were formed following the tendency of annular flow pattern formation with increasing gas flow rates observed in the lab scale nozzle conduit. Thus, to obtain both smaller bubble size and lesser pulsation, the flow regime should be operated either in dispersed bubble flow regime or annular flow regime. Experimental observations indicate the frequency of slug formation increased slightly with β, as the liquid phase is accelerated with greater gas flow rates as shown in Fig. 8.8. The slug frequency was 33 Hz, 37 Hz and 43 Hz for 1%, 2% and 4% β,

respectively; for the air-water two-phase flow experiments. For similar conditions, the slug frequency was 35 Hz, 37 Hz and 40 Hz for 1%, 2% and 4% β, respectively, for the mixed gas-water two-phase flow experiments. From Fig. 8.8 it is evident that slug frequency increases slightly with air to liquid mass ratios with an exponent of 0.2, indicating a weak function of β to the slug frequency (f_S). Moreover, the available correlations for the slug frequency prediction indicated in Equation (21) and Equation (22) are properly matched with the experimental data of air-water and mixed gas-water two-phase flow experiments. Another notable finding from Fig. 8.8 is that the lighter mixed gas, simulating the steam in the commercial case, does not remarkably change the flow structure in the two-phase lab scale flows where air is used as the gas phase.

To identify the correct flow regime in the current study, the flow regime prediction was also conducted based on different flow maps found in the literature. From our experimental flow properties and conditions it was observed that the flow regimes in the current study mostly match with the flow regime obtained from the Baker flow map [74]. When the current experimental conditions were plugged in the Taitel and Dukler flow pattern map, it indicated slug flow patterns for both air-water and mixed gas-water experiments. A comparison of different flow maps in an effort to find appropriate flow regimes using the current experimental conditions is presented in Table 8.4. For brevity, only the air-water two-phase flow case is presented as mixed gas-water two-phase flows indicate similar results. Although the different flow maps found in the literature are only applicable for certain local flow conditions and length scales, the standard flow maps were used in this study to obtain a general sense of the transition of flow patterns with changing β.

8.5.2. Bubble Size in the Feeding Conduit

The image filtering process indicated in Fig. 8.3 was used to find the mean bubble diameter in the feeding conduit both in air-water and mixed gas-water experiments. The effects of mixed gas-water and air-water fluid properties on the

mean bubble size were noticeably evident, as shown in Fig. 8.9. In Fig. 8.9 the square indicates the mixed gas-water experiments and the filled circle indicates the air-water experiments. At a constant pressure of 483 kPa, if the β is increased from 1-4%, the bubble diameter (d_b) in the feeding conduit decreases progressively. The decrease of d_b with an increase in β was observed in both air-water and mixed gas-water experiments indicating no remarkable effects of mixed gas on the bubble size distribution. At 3% β and 483 kPa P_m, the d_b was found to be 271 µm and 270 µm for air-water and mixed gas-water experiments, respectively. Similarly, at 4% β and 483 kPa P_m, the d_b was found to be 270 µm and 250 µm for air-water and mixed gas-water experiments, respectively. In Fig. 8.9, the solid line indicates the best-fit line for the mixed gas-water experiments and the dotted line indicates the best-fit line for the air-water experiments. Both best-fit lines indicate that the exponent of β is -0.16 and -0.19 in air-water and mixed gas-water experiments, respectively demonstrating a weak dependence of gas phase molecular weight on the d_b. However, due to the lower weight associated with the mixed gas experiments, slightly smaller bubbles were found in the mixed gas-water experiments due to greater shear force associated with mixed gas experiments. However, this small decrease in the values of d_b is negligible and sometimes within the margin of experimental uncertainty.

Although at a particular mixing pressure (P_m) there is no significant effect on the gas phase density, the mixing pressure (P_m) is an important parameter in determining the length scale of bubbles in two-phase gas/liquid flows. Mixing pressure provides enhanced inertia to the two-phase gas/liquid flows and thus the turbulent splitting action increases against the stabilizing gravity force. The effects of mixing pressure (P_m) on the bubble size (d_b) are depicted in Fig. 8.10. As shown in Fig. 8.10, the mean bubble size (d_b) is 400 µm, 340 µm, 300 µm and 290 µm at 428 kPa, 517 kPa, 614 kPa and 683 kPa, respectively. Thus, bubble size (d_b) decreases remarkably due to the increase in mixing pressure (P_m) in the nozzle conduit (D_c).

From Table 8.5 it was observed that the bubble shape is not fully spherical due to greater eccentricity values. Data obtained in Table 8.5 is for the air-water atomization condition. Similar results were obtained for the mixed gas-water case; however, for brevity only an air-water case is presented in this study. Another important observation obtained in Table 8.5 is that the bubble sizes (d_b) obtained from both stroboscopic back scattered imagery (SBSI) and high speed video shadowgraphy (HSVS) are almost identical. As can be seen, the d_b and e values are very similar using both techniques. Thus, both the SBSC and HSVS technique verify the repeatability and validity of the data. It is now critical to determine the mean, maximum and minimum bubble size range in the experiments to find the tendency of bubble break-up or coalesence in the feeding conduit. In this effort the the average of 26,772 bubbles obtained experimentally for different operating condtions (such as 1-4% β, 428 - 683 kPa P_m) in lab scale experiments for both air-water and mixed gas-water experiments are depicted in Fig. 8.11. To obtain an idea, the experimental maximum and minimum bubble diameter values are also illustrated in Fig. 8.11. From Fig. 8.11 it is evident that the mean size range of 26,772 bubbles is within the range of the maximum and minimum bubble size. In Equation (10) it was found that the Brodkey bubbles, which are non-coalescent bubbles, are in the range of 0.5 to 1.5 μm. Thus, from the Brodkey line illustrated in Fig. 8.11, it is obvious that the average and the minimum bubble population do not exist in the non-coalesecent regime. On the contrary, the maximum bubble diameter value is well below the theoretical maximum bubble diameter data points indicated in Fig. 8.11. The maximum bubble diameter data points were obtained using Equation (13) to Equation (15). Thus, the average and the maxium bubble population is well below the theoretical coalescent bubble points, indicating coalescent regime exists in the nozzle conduit. Morevoer, the pressure drop in the small length conduit (L= 36.5 cm) is negligible which does not result in any significant changes of the compressible bubble behavior. A comparision of the bubble size obtained in this study and in the literature is presented in Table

8.6. A greater number of the bubble population was analyzed in this study in contrast to the previous studies.

The characteristic local bubble velocity with changing β is depicted in Fig. 8.12. This bubble velocity was obtained from the high-speed video shadowgraph. Another variable that was studied was the average void fraction in the conduit, which was measured by isolating a section in the feeding conduit of a horizontal nozzle assembly, termed as the quick-closing-valve (QCV) technique. From the data obtained from the QCV technique, the actual velocity of water and air in the feeding conduit were calculated. Once the actual velocity of water and air is obtained, the slip between the phases can easily be obtained. From Fig. 8.12, it is evident that the local bubble velocity follows a similar trend of the average air velocity in the feeding conduit of the nozzle. As the β increases, the local and average air velocity increases linearly, as greater momentum is induced into both of the phases. Moreover, if the β increases, the slip between the air and water phases increases linearly. Thus, the homogeneous two-phase flow model at higher β cannot be implemented reliably.

8.5.3. Droplet Size in the Spray

In Fig. 8.13 the effects of gas phase molecular weight on the droplet Sauter mean diameter (D_{32}) is depicted. The Sauter mean diamter (D_{32}) is the characterestic length scale for a fluid jet [4]. At first glance it is observed in Fig. 8.13 that the Sauter mean diamter (D_{32}) decreases gradually with the radial distances at $60D_n$ and $120D_n$ downstream and at a constant mixing pressure (P_m) of 483 kPa. Experimental results indicate that at $120D_n$ downstream of the nozzle tip and at the centre of the spray, the D_{32} values of are 143.5 µm and 142.8 µm for the mixed gas-water and air-water atomization conditions, respectively. Similarly, at $120D_n$ downstream of the nozzle tip and at the r = 20 mm radial distance from the centre (r =0), the D_{32} values of are 121.3 µm and 121.7 µm for the mixed gas-water and air-water atomization conditions, respectively. Similar resutls can be found at the $60D_n$ nozzle downstream. Thus, changing the gas phase density does

not significantly affect the droplet length scale. This outcome basically validates the lab scale experiments where air is used as the gas phase at room temparature and pressure conditions, and demonstrates that the results are similar to the commercial scale conditions where steam is used at elevated temperature and pressure conditions.

In Fig. 8.14, the effects of the molecular weight of the mixed gas and air on the droplet velocity in the radial direction are depicted. As can be seen in Fig. 8.14, the droplet velocity decreases gradually with the radial distance due to loss of momentum. The droplet velocity at $60D_n$ downstream is greater compared to the $120D_n$ downstream. At $60D_n$ the droplet sustains greater droplet momentum compared to the $120D_n$ downstream. However, at r =20 mm radial distances, the velocity profiles cross each other due to the conical shape of the spray. Experimental results indicate that at $120D_n$ downstream of the nozzle tip and at the centre of the spray (r = 0), the droplet velocity values of are 40 m/s and 33 m/s for the mixed gas-water and air-water atomization conditions, respectively. Similarly, at $120D_n$ downstream of the nozzle tip and at r = 20 mm radial distance, the D_{32} values of are 23 m/s and 18 m/s for the mixed gas-water and air-water atomization conditions, respectively. Similar results can be found at $60D_n$ downstream. Since the mixed gas has a lower molecular weight compared to the air phase, the mixed gas provides greater shear force on the liquid phase, producing slightly smaller droplets. From these experimental observations it is evident that the lighter gas density and molecular weight as observed in the steam phase of the commericial operating conditions do not have any remakable effects on the the droplet size (D_{32}) in the spray. Thus, two-phase atomization experiments conducted with air (at 20°C) instead of steam (at 300°C) validate the simulitude conditions.

8.5.4. Bubble and Droplet Size Correlation

The mean, maximum and minimum bubble diameters with changing β are depicted in Fig. 8.15. Good consistency is observed between the SBSI and HSVS.

Results show that for 1% β, the mean bubble diameter (d_{mean}) is 395 μm and 418 μm, which were obtained from SBSI and SHVS methods, respectively. For 2% β, the mean bubble diameter (d_{mean}) is 342 μm and 335 μm, which were obtained from the SBSI and SHVS methods, respectively. For 4% β, the mean bubble diameter (d_{mean}) is 306 μm and 290 μm, which were obtained from the SBSI and SHVS methods, respectively. Moreover, bubble mean diameter obtained from a proposed correlation suggested by Sotiriadis *et al.* [76] can predict the experimental data. The drawback of the Sotiriadis *et al.* [76] method is the calculation of the mean bubble diameter by averaging the major and minor axis lengths assuming a perfect ellipsoid. In the current study, the mean bubble diameter in the SBSI and SHVS methods were calculated by area averaging, which is more accurate than the Sotiriadis *et al.* method [76]. Also, the experimental data used to obtain the proposed correlation is applicable for large diameter (in the *cm* range) pipes. However, my lab scale nozzle is a very small, one-quarter of commercial scale (2.54 cm or 1 inch) nozzle. Thus, some modifications in the power of fluid properties such as density, viscosity, surface tension and turbulent splitting energy in the proposed correlations available in the literature (Equation 13-15 and Equation 19-20) are essential to predict accurate bubble sizes in small scale two-phase pipe flows. Accordingly, to match the experimental data in Fig. 8.15, the modified correlations are proposed as follows:

$$d_{\max} = \frac{4\,\gamma^{0.01}}{g^{0.8}\,(\rho_L - \rho_G)} \tag{28}$$

Where γ, g and (ρ_L-ρ_G) are the surface tension (N/m), gravitational acceleration (m/s^2) and density difference (kg/m^3), respectively. Similarly, Equation (14) and Equation (15) are re-written as follows:

$$d_{\max} = 1.38\,(We_c)^{0.6}\left[\frac{\gamma^{0.6}}{\rho_c^{0.5}\mu_c^{0.46}}\right]\left(\frac{\rho_c^{-0.7}}{\rho_d^{-1.2}}\right)\left(\frac{D_c^{0.5}}{[u_L^S]^{1.1}}\right) \tag{29}$$

$$d_{\max} = \left(\frac{\gamma^{0.01}}{\rho_d}\right)\left(\frac{1}{\varepsilon}\right)^{1/5.5} \tag{30}$$

where, γ is the surface tension (N/m) that provides the cohesive force and ε is the turbulent energy dissipation (m^2/s^3 or watt/kg) that provides the splitting force. Likewise, the proposed minimum bubble diameter correlations indicated in Equation (19) and Equation (20) were modified to match the experimental data in Fig. 8.15 as follows:

$$d_{\min} = 2.4\left(\frac{\gamma^{0.01}\, h^2}{\mu_c\ \rho_c\ \varepsilon^{0.35}}\right)^{0.25} \tag{31}$$

where, h is the film thickness at rupture between the two bubbles, which was 1 μm [9].

$$d_{\min} = \left(\frac{\gamma^{0.01} C_{L-V}^{0.46}}{0.0272\mu_c \rho_c^{0.84} \varepsilon^{0.30}}\right)^{1/3.11} \tag{32}$$

Here, γ is the surface tension of water (N/m), ε is the turbulent kinetic energy dissipation rate (m^2/s^3) and ρ and μ are the density (kg/m^3) and dynamic viscosity (Pa.s), respectively. $C_{L\text{-}V}$ is the London Van der Waals constant (10^{-28} J.m). The modified equations can predict the mean, maximum and minimum bubble size very accurately as depicted in Fig. 8.15. Data obtained from the PDPA measurement shows that at the center ($r = 0$) and $120D_n$ (D_n stands for the nozzle diameter of 3.10 mm) downstream of the spray, the mean droplet diameter decreases slightly with changing β. In this study, taking into consideration the mechanics of horizontal two-phase gas/liquid flows in the nozzle conduit, a correlation is proposed to predict the bubble size based on the small scale and large scale bubble data sets as follows:

$$\frac{(D_{32})_{gb}}{D} = 163\,\beta^{-0.13}\rho_r^{0.1}\, Mo_m^{0.01}\, S^{-0.1}\, \alpha^{-0.63}\, Eu_m^{0.04} \tag{33}$$

The above correlation fit data and experimental data are depicted in Fig. 8.16(a). There is a good agreement between the correlation fit data and experimental data. Interestingly, taking into consideration only the β, ρ_r, S and α parameters in Equation (33) can predict the experimental data quite accurately as depicted in Fig. 8.16(b).

$$\frac{(D_{32})_{gb}}{D} = 139\ \beta^{-0.13} \rho_r^{0.1}\ S^{-0.1}\ \alpha^{-0.63} \tag{34}$$

Thus, this simple equation is a breakthrough for calculating the bubble size in the feeding conduit of effervescent nozzles. In Fig. 8. 17 (a) average bubble diameter based on 26,700 bubbles was calculated for the air to liquid ratio of 1%, 2%, 3% and 4%. The pressure was varied from 480 kPa to 690 kPa. Similarly, the droplet Sauter mean diameter was calculated based on 20,000 droplets (80% validation rate) for the similar air to liquid ratio ranges. A power law correlation of 5.21 coefficient and 0.58 exponent of D_b can fit the experimental data with the correlation coefficient (R^2) of 0.83. To obtain a simple power law correlation for predicting the droplet size as a function of bubble size a compromise was made in regression analysis obtaining lower value of correlation coefficient. In Fig. 8.17 (b) the proposed correlation was validated with the theoretical droplet and bubble size correlations. The bubble diameter was calculated using the available correlation in the literature [64] based on the β of 1-4%. Corresponding droplet size for the range of β was calculated using the available correlation in the literature [4, 51, 88]. It was observed that the proposed correlation can predict the theoretical correlations available in the literature and experimental data available in this study for the range of β was investigated. The proposed power law correlation [4] in Equation (3) obtained from the small scale nozzle cannot predict the large scale droplet diameter precisely. Thus, in the current study a new correlation is established based on the small scale and large scale droplet data sets as follows:

$$\frac{(D_{32})_{gb}}{D_N} = 106\ \beta^{-0.13} \rho_r^{0.1}\ Mo_m^{0.01}\ S^{-0.1}\ \alpha^{-0.63}\ Eu_m^{0.04} \tag{35}$$

The above correlation fit data and experimental data are depicted in Fig. 8.18 (a). There is a good agreement between the correlation fit data and the experimental data. However, taking into consideration only the β, ρ_r, S and α parameters in the Equation (35) can predict the experimental data quite accurately as depicted in Fig. 8.18 (b).

$$\frac{(D_{32})_{gb}}{D_N} = 101\,\beta^{-0.13}\rho_r^{0.1}\,S^{-0.1}\,\alpha^{-0.63} \tag{36}$$

Thus, this simple equation is a breakthrough for calculating the droplet size in effervescent atomization.

8.6. Conclusions

This novel research is a breakthrough in establishing a baseline of conditions between the lab scale experiments (conducted with air/water at 20°C) and the commercial scale operation (conducted with steam/bitumen at 350°C). In this effort, a mixed gas of 81.4 % helium, and 18.6% nitrogen (on a volumetric basis) was used to scale the density of steam of 5.74 kg/m^3. Experimental results indicate that the mixed gas does not provide a significant change in the bubble (< ±10% difference) and droplet (< ±1.5% difference) length scale when compared to results obtained with air as the atomization gas. This outcome validates the lab scale experiments using air as the gas phase. In addition to identifying the similitude condition, this study was a first attempt to obtain a correlation between the downstream spray characteristics and the upstream two-phase flow patterns. This study also attempted for the first time to obtain the bubble size and different flow regimes in the small scale two-phase conduit flows where the wall effects play a critical role. Current experimental studies also show that if the liquid flow rates decrease, there is a tendency to attain the intermittent flow/slug flow, which provides coarse droplets and liquid ligament in the spray. Moreover, this study shows that at a constant mixing pressure, if the air flow rates increase at certain points there is a tendency of the flow to attain an annular type flow regime, which is beneficial to obtain dispersed bubble and droplet populations. Finally, a correlation is proposed to predict the droplet diameter based on the known bubble size in the effervescent nozzle used in this study.

Experimental observations indicate that the frequency of slug formation increased slightly with β as the liquid phase was accelerated with greater gas flow rates. The

slug frequency was increased with the increment of β, for both the air-water and mixed gas-water two-phase flow experiments. At a constant pressure of 483 kPa, if the β is increased from 1-4%, the bubble diameter (d_b) in the feeding conduit is progressively decreased. The best-fit lines indicate that the exponent of β is -0.16 and -0.19 in air-water and mixed gas-water experiments, respectively; demonstrating a weak dependence of molecular weight on the d_b. If the P_m varied from 428 kPa to 690 kPa and the β varied from 1-4%, the bubble diameter (d_b) was decreased. From these experiments it is also evident that the bubble shape is not fully spherical due to greater eccentricity values. Experimental results indicate that at different nozzles downstream of the spray, the D_{32} values do not change remarkably for both the mixed gas-water and air-water atomization conditions. Since the mixed gas has less weight compared to the air phase, the mixed gas provided greater shear force on the liquid phase, producing slightly smaller droplets. The experimental results in this study validate the lab scale experiments where air is used, as the gas phase at room temparature and pressure conditions of the commercial scale conditions are similar to conditions in which steam is used at elevevated temperature and pressure conditions.This study indicates that if the bubble size in the upstream of the nozzle decreases, the droplet size in the spray also decreases gradually.

8.7. References

[1] Gray, M., Tuyet, T., McCaffrey, W., Berruti, F., Soundararajam, S., Chan, E., Huq, I. and Thorne, C. (2001) Coupling of Mass Transfer and Reaction in Coking of Thin Films of Athabasca Vacuum Residue. Ind. Eng. Chem. Res. 40: 3317 – 3324.

[2] Al-Wazzan, A., Than, C.F., Moghavvemi, M. and Yew, C.W. (2001) Video imaging measurement of interfacial wave velocity in air-water flow through a horizontal elbow. Photonic Systems and Applications, Yakov S. Sidorin, Dingyuan Tang, Editors, Proceedings of SPIE. 4595 243-253.

[3] Barrau, E., Riviere, N., Poupot, C.H. and Cartellier, A. (1999) Single and double optical probes in air–water two-phase flows: real time signal processing and sensor performance. Int. J. Multiphase Flow. 25 229–256.

[4] Ejim, C.E. (2008) Effect of Liquid Viscosity, Surface Tension and Nozzle Size on Atomization in Two-Phase Nozzles, PhD Thesis, Mechanical Engineering, University of Alberta, .

[5] Elkow, K.J. and Rezkallah, K.S. (1996) Void fraction measurements in gas-liquid flows using capacitance sensors. Measurement Science & Technology. 7 (8): 1153-1163.

[6] Hesketh, R.P., Etchells, A.W., and Russell, T.W.F. (1987) Bubble size in horizontal pipelines. AIChE Journal. 33: 663-667.

[7] Rahman, M.A., Heidrick, T. and Fleck, B.A. (2009) Characterizing the Two-Phase, Air/Liquid Spray Profile Using a Phase-Doppler-Particle-Analyzer. IOP Journal of Physics – conference series. 147: 1-15.

[8] Razzaque, M.M., Afacan, A., L., S., K., N., Masliyah, J.H. and Sanders, R.S. (2003) Bubble size in coalescent dominant regime of turbulent air-water flow through horizontal pipes. International Journal of Multiphase Flow. 29: 1451-1471.

[9] Thomas, R.M. (1981) Bubble coalescence in turbulent flows. Int. J. Multiphase Flow. 7: 709–717.

[10] Lund, M.T.J., C. Q.; Sojka, P. E.; Gore, J. P and Pachangula, M. V. (1998) The Influence of Atomizing Gas Molecular Weight on Low Mass Flowrate Effervescent Atomizer Performance. Journal of Fluids Engineering. 120: 750-754.

[11] Rashkovan, A. and Sher, E. (2006) Flow Pattern Observations of Gasoline Dissolved CO2 inside an injector. Atomization and Sprays. 16: 615-626.

[12] Ejim, C.E., Rahman, M.A., Amirfazli, A. and Fleck, B.A. (2010) Effects of Liquid Viscosity and Surface Tension on Atomization in Two-Phase, Gas/Liquid Fluid Coker Nozzles. Fuel. 89: 1972-1882.

[13] Kim, J.Y. and Lee, S.Y. (2001) Dependence of Spraying Performance on the Internal Flow Pattern in Effervescent Atomizers. Atomization and Sprays. 11: 735-756.

[14] Huang, X., Wang, X. and Liao, G. (2008) Visualization of Two Phase Flow inside an Effervescent Atomizer. Journal of Visualization. 11 (4): 299-308.

[15] K. Ekambara, R.S.S., K. Nandakumar, J.H. Masliyah (2008) CFD simulation of bubbly two-phase flow in horizontal pipes. Chemical Engineering Journal. 144: 277-288.

[16] Iskandrani, A. and Kojasoy, G. (2001) Local void fraction and velocity field description in horizontal bubbly flow. Nuclear Engineering and Design. 204: 117-128.

[17] Holmes, T.L. and Russell, T.W.F. (1975) Horizontal bubble flow. International Journal of Multiphase Flows. 2: 51-66.

[18] Kashinskii, O.N. and Kaipova, E.V. (2008) Hydrodynamic Structure of a Two-Phase Flow in a Horizontal Channel. Heat Transfer Research. 38 (5): 461-471.

[19] Christensen, M.E.E.J.J.W.R.N. (1999) Observations of Two-Phase Flow Patterns in a Horizontal Circular Channel. Heat Transfer Enginnering. 20 (1): 9-14.

[20] Kocamustafaogullari, G., Huang, W.D. and Razi, J. (1994) Measurement and Modelling of Average Void Fraction, Bubble and Interfacial Area. Nucl. Eng. Design. 148: 437–453.

[21] Franca, F.L.J., R.T. (1992) The Use of Drift-Flux Techniques for the Analysis of Horizontal two-Phase Flows. International Journal of Multiphase Flows. 18 (6): 787-801.

[22] Gradeck, M. and Lebouché, M. (2000) Two-phase gas-liquid flow in horizontal corrugated channels. International Journal of Multiphase Flows. 26: 435-443.

[23] R.P. Hesketh, T.W.F.R., A.W. Etchells (1987) Bubble size in horizontal pipelines. AIChE Journal. 33: 663-667.

[24] M. Mahbubu Razzaque, A.A., Shijie Liu, K. Nandakumar, Jacob H. Masliyah, R. Sean Sanders (2003) Bubble size in coalescent dominant regime of turbulent air-water flow through horizontal pipes. International Journal of Multiphase Flow. 29: 1451-1471.

[25] Hesketh, R.P., Etchells, A.W., and Russell, T.W.F. (1991) Experimental observations of bubble breakage in turbulent flow. Industrial Engineering Chemical Research. 30: 835-841.

[26] Hesketh, R.P., Etchells, A.W., and Russell, T.W.F. (1991) Bubble breakage in pipeline flow. Chemical Engineering Science. 46: 1-9.

[27] Walter, J.F., Blanch, H.W. (1986) Bubble break-up in gas-liquid bioreactors: Break-up in turbulent flows. Chemical Engineering Journal. 32: B7-B17.

[28] Winterton, R.H.S. and Munaweera, J.S. (2001) Bubble size in two-phase gas-liquid bubbly flow in ducts. Chemical Engineering and Processing. 40: 437-447.

[29] Bratukhin, Y.K., Kostarev, K.G., Viviani A. and Zuev A.L. (2005) Experimental study of Marangoni Bubble migration in normal gravity. Experiments in Fluids. 38: 594-605.

[30] M.A. Rahman, T.H., B.A. Fleck, R. Skwarok, J. McMillan (2008) Horizontal Two Phase Flow Regimes and Bubble Size Distribution Prediction using High Speed Image Analysis, Nice, France, 2008.

[31] Bratukhin, Y.K., Kostarev, K.G., Viviani, A. and Zuev, A.L. (2005) Experimental study of Marangoni bubble migration in normal gravity. Experiments in Fluids. 38 (5): 594-605.

[32] Hesketh, R.P., Russell, T.W.F. and Etchells, A.W. (1987) Bubble size in horizontal pipelines. AIChE J. 33: 663–667.

[33] Kashdan, J.T., Shrimpton, J.S. and Whybrew, A. (2003) Two-Phase Flow Characterization by Automated Digital Image Analysis. Part 1: Fundamental Principles and Calibration ofthe Technique. Part. Part. Syst. Charact. 20 387-397.

[34] Lecuona, A., Sosa, P.A., Rodriguez, P.A. and Zequeira, R.I. (2000) Volumetric characterization of dispersed two-phase flows by digital image analysis. Meas. Sci. Technol. 11: 1152–1161.

[35] Pereira, F. and Gharib, M. (2002) Defocusing digital particle image velocimetry and the three-dimensional characterization of two-phase flows. Meas. Sci. Technol. 13 683–694.

[36] Augier, F., Morchain, J., Guiraud, P. and Masbernat, O. (2003) Volume fraction gradient-induced flow patterns in a two-liquid phase mixing layer. Chemical Engineering Science. 58 3985-3993.

[37] Cui, Z. and Fan, L.S. (2004) Turbulence energy distributions in bubbling gas–liquid and gas–liquid–solid &ow systems. Chemical Engineering Science. 59 1755 – 1766.

[38] Der, D.B. and Sommerfeld, M. (2002) An advanced LIF-PLV system for analysing the hydrodynamics in a laboratory bubble column at higher void fractions. Experiments in Fluids. 33 826–837.

[39] Hardalupas, Y. and Horender, S. (2003) Fluctuations of particle concentration in a turbulent two-phase shear layer International Journal of Multiphase Flow. 29 1645–1667.

[40] Hassan, Y. and Blanchat, T. (1991) Full-field bubbly flow velocity measurements by digital image pulsed laser velocimetry. Experiments in Fluids. 11: 293-301.

[41] Kashdana, J.T., Shrimptona, J.S. and Whybrew, A. (2007) A digital image analysis technique for quantitative characterisation of high-speed sprays Optics and Lasers in Engineering. 45 106–115.

[42] Kawaguchi, T., Akasaka, Y. and Maeda, M. (2002) Size measurements of droplets and bubbles by advanced interferometric laser imaging technique. Meas. Sci. Technol. 13 308–316.

[43] Kowalewski, T.A. (2002) Particle Image Velocimetry and Thermometry for Two-Phase Flow Problems. Ann. N.Y. Acad. Sci. 972: 213–222.

[44] Murai, Y., Oishi, Y., Takeda, Y. and Yamamoto, F. (2006) Turbulent shear stress profiles in a bubbly channel flow assessed by particle tracking velocimetry. Experiments in Fluids. 41: 343–352.

[45] Ottens, M., Klinkspoor, K., Hoefsloot, H.C.J. and Hamersma, P.J. (1999) Wave characteristics during cocurrent gas±liquid pipe flow. Experimental Thermal and Fluid Science. 19 140-150.

[46] Shamoun, B., Beshbeeshy, M.E. and Bonazza, R. (1999) Light extinction technique for void fraction measurements in bubbly flow. Experiments in Fluids. 26 16-26.

[47] Shedd, T.A. and Newell, T.A. (2004) Characteristics of the liquid film and pressure drop in horizontal, annular, two-phase flow through round, square and triangular tubes. Journal of Fluids Engineering-Transactions of the Asme. 126 (5): 807-817.

[48] Sunde, C., Avdic, S. and Pazsit, I. (2005) Classification of Two-Phase Flow Regimes via Image Analysis and a Neuro-Wavelet Approach. Progress in Nuclear Energy. 46 (3-4): 348-358.

[49] Tafreshi, Z.M., Kirpalani, D., Bennett, A. and McCracken, T.W. (2002) Improving the efficiency of fluid cokers by altering two-phase feed characteristics. Powder Technology. 125 234– 241.

[50] Tu, X. and Tragardh, C. (2002) Methodology development for the analysis of velocity particle image velocimetry images of turbulent, bubbly gas–liquid flows. Meas. Sci. Technol. 13 1079–1086.

[51] Simmons, M.J.H. and Azzopardi, B.J. (2001) Drop size distributions in dispersed liquid–liquid pipe flow. Int. J. Multiphase Flow. 27: 843–859.

[52] Angeli, P. (2001) Droplet size in two-phase liquid dispersed pipeline flows. Chem. Eng. Technol. 24: 431–434.

[53] Angeli, P. and Hewitt, G.F. (2000) Drop size distributions in horizontal oil–water dispersed flows. Chem. Eng. Sci. 55: 3133–3143.

[54] Andreussi, P., Paglianti, A. and Silva, F.S. (1999) Dispersed bubble flow in horizontal pipes. Chemical Engineering Science. 54 (8): 1101-1107.

[55] Kostoglou, M. and Karabelas, A.J. (1998) On the attainment of steady state in turbulent pipe flow of dilute dispersions. Chem. Eng. Sci. 53: 505–513.

[56] Parthasarathy, R., Jameson, G.J. and Ahmed, N. (1991) Bubble breakup in stirred vessels-prediction of the Sauter mean diameter. Trans. IChemE. 69 (Part A): 295–301.

[57] Karabelas, A.J. (1978) Droplet size spectra generated in turbulent pipe flow of dilute liquid/liquid dispersions. AIChE J. 24: 170–180.

[58] Kubie, J. and Gardner, G.C. (1977) Drop sizes and drop dispersion in straight horizontal tubes and in helical coils. Chem. Eng. Sci. 32: 195–202.

[59] Holmes, T.L. (1973) Fluid mechanics of horizontal bubble flow, Ph.D. Thesis, University of Delaware.

[60] Swartz, J.E. and Kessler, D.P. (1970) Single drop breakup in developing turbulent pipe flow. AIChE J. 16: 254–260.

[61] Collins, S.B. and Knudsen, J.G. (1970) Drop-size distributions produced by turbulent pipe flow of immiscible liquids. AIChE J. 16: 1072-1080.

[62] Ward, J.P. and Knudsen, J.G. (1967) Turbulent flow of unstable liquid–liquid dispersions: drop sizes and velocity distributions. AIChE J. 13: 356–365.

[63] Kolmogoroff, A.N. (1949) On the breaking of drops in turbulent flow. Dokl. Akad. Nauk SSSR. 66: 825–828.

[64] Liu, S. and Li, D. (1999) Drop coalescence in turbulent dispersions. Chem. Eng. Sci. 54: 5667–5675.

[65] Razzaque, M.M., Afacan, A., Liu, S., Nandakumar, K., Masliyah, J.H. and Sanders, R.S. (2003) Bubble size in coalescence dominant regime of turbulent air–water flow through horizontal pipes. International Journal of Multiphase Flow. 29 1451–1471.

[66] Shinnar, R. (1961) On the behaviour of liquid dispersions in mixing vessels. J. Fluid Mech. 10: 259–275.

[67] Coleman, J.W. and Garimella, S. (1999) Characterization of two-phase flow patterns in small diameter round and rectangular tubes International Journal of Heat and Mass Transfer. 42 (15): 2869-2881.

[68] Baker, O. (1954) Simultaneous flow of oil and gas. The Oil and Gas Journal. 53: 185-195.

[69] Breber, G., Palen, J. and Taborek, J. (1980) Prediction of horizontal tubeside condensation of pure components using flow regime criteria. Journal of Heat Transfer. 102: 471-476.

[70] Damianides, C. and Westwater, J.W. (1988) Two phase flow patterns in a compact heat exchanger and in small tubes. Proceedings of Second U.K. National Conference On Heat Transfer, vol II, Glasgow, Scotland.

[71] Ewing, M.E., Weinandy, J.J. and Christensen, R.N. (1999) Observation of Two-phase Flow Patterns in a Horizontal Circular Channel. Heat Transfer Engineering. 20 (1): 9-13.

[72] Hibiki, T., Goda, H., Kim, S., Ishii, M. and Uhle, J. (2004) Structure of vertical downward bubbly flow. International Journal of Heat and Mass Transfer. 47 1847–1862.

[73] Jeffreys, H. (1925) On the formation of water waves by wind. Proc. Royal Soc. A107: 189-206.

[74] Lambrechts, A. (2005) Heat transfer performance during in-tube condensation in horizontal smooth, micro-fin and herringbone tubes, MIng, Mechanical and Manufacturing Engineering, University of Johannesburg.

[75] Mandhane, J.M., Gregory, G.A. and Aziz, A. (1974) A flow pattern map for gas-liquid flow in horizontal pipes. Int. J. Multiphase Flow. 1: 537-553.

[76] Sotiriadis, A.A., Thorpe, R.B. and Smith, J.M. (2005) Bubble size and mass transfer characteristics of sparged downwards two-phase flow. Chemical Engineering Science. 60: 5917 – 5929.

[77] Taitel, Y. and Dukler, A.E. (1976) A model for predicting flow regime transitions in horizontal and near horizontal gas-liquid flow AIChE J. 22 (2): 47-55.

[78] Whalley, P.B. (1987) Boiling, Condensation and Gas-Liquid Flow, Oxford, New York.

[79] Chesters, A.K. (1975) The applicability of dynamic-similarity criteria to isothermal liquid-gas two-phase flows without mass transfer. International Journal of Multiphase Flow. 2: 191-212.

[80] Hurlbert, K.M., Witte, L.C., Best, F.R. and Kurwitz, C. (2004) Scaling two-phase flows to Mars and Moon gravity conditions. International Journal of Multiphase Flow. 30: 351-368.

[81] Geraets, J.J.M. (1988) Centrifugal scaling of isothermal gas-liquid flow in horizontal tubes. International Journal of Multiphase Flow. 14 (3): 287-303.

[82] Douglas, J.F., Gasiorek, J.M. and Swaffield, J.A. (1995) Fluid Mechanics, Singapore, Longman Scientific and Technical.

[83] Rahman, M.A., Heidrick, T. and Fleck, B.A. (2009) A Critical Review of Two-Phase Gas/Liquid Industrial Spray Systems. International Review of Mechanical Engineering. International Review of Mechanical Engineering. 3 (1): 110-125.

[84] Rahman, M.A., Heidrick, T. and Fleck, B.A. (2009) A Critical Review of Advanced Experimental Techniques to Measure Two-Phase Gas/Liquid Flow. The Open Fuels & Energy Science Journal. 2: 54-70

[85] Rahman, M.A., Gomez, J., McMillan, J., Heidrick, T. and Fleck, B.A. (2008) Correlations of the Droplet Size-Velocity of the Two-Phase, Air/Liquid Spray Using a Particle-Dynamic-Analyzer, August 10-14. Proceedings of the FEDSM 2008, ASME Fluids Engineering Conference, Jacksonville, Florida USA.

[86] Ejim, C.E., Rahman, M.A., Amirfazli, A. and Fleck, B.A. (2010) Scaling Analysis of Nozzle Size on Atomization in Two-Phase, Gas-Liquid Nozzles. Multiphase Science and Technology. 22 (2): 133-155.

[87] Ejim, C.E., Rahman, M.A., Amirfazli, A. and Fleck, B.A. (In Press, 2010) Scaling Analysis of Nozzle Size on Atomization in Two-Phase, Gas-Liquid Nozzles. Multiphase Science and Technology. 31 pp.

[88] Weisman, J., Duncan, D., Gibson, J. and Crawford, T. (1979) Effects of fluid properties and pipe diameter on two-phase flow patterns in horizontal lines. Int. J. Multiphase Flow. 5: 437-462.

[89] Weiss, M.A. and Warsham, C.H. (1959) Atomization in High Velocity Air-Streams. J. Am. Rocket Soc. 29 (4): 252-259.

[90] Brodkey, R.S. (1967, re-printed Dover Publication Inc., NY, 2005) The Phenomena of Fluid Motions, Addison-Wesley Publishing Company.

[91] Hinze, J.O. (1975) Turbulence, New York, McGraw-Hill.

[92] Hinze, J.O. (1955) Fundamentals of the hydrodynamic mechanism of splitting in dispersion processes. AIChE Journal. 1 (3): 289-295.

[93] Hinze, J.O. (1955) Fundamentals of the hydrodynamic mechanism of splitting in dispersion processes. AIChE J. 1: 289-295.

[94] Gregory, G.A. and Scott, D.S. (1969) Correlation of Liquid Slug Velocity and Frequency in Horizontal,. Cocurrent Gas Liquid Flow. AIChE J. 15 (6): 933-935.

[95] Greskovich, E.J. and Shrier, A.L. (1972) Slug Frequency in Horizontal Gas-Liquid Slug Flow. Ind. Eng. Chem. Process Des. Dev. 11 (2): 317-318.

[96] Base, T.E., Chan, E.W., Kennett, R.D. and Emberley, D.A. (1999) Nozzle for Atomizing Liquid in Two Phase Flow. US Patent 6003789.

[97] Dantec Dynamics A/S (2003). BSA Flow Software, Version 2.1: Installation and User's guide, Skovlunde

[98] Albrecht, H.E., Borys, M., Damaschke, N. and Tropea, C. (2003) Laser Doppler and Phase Doppler Measurement Techniques, Germany, Springer.

[99] Damaschke, N., Gouesbet, G., Gréhan, G., Mignon, H. and Tropéa, C. (1998) Response of Phase Doppler Anemometer Systems to Nonspherical Droplets. Applied Optics. 37 (10): 1752-1761.

[100] Dodge, L.G., Rhodes, D.J. and Reitz, R.D. (1987) Drop-size Measurement Techniques for Sprays: Comparison of Malvern Laser-Diffraction and Aerometrics Phase/Doppler. Applied Optics. 26 (11): 2144-2154.

[101] Gréhan, G., Gouesbet, G., Naqwi, A. and Durst, F. (1993) Particle Trajectory effects in Phase Doppler Systems. Part. Part. Syst. Charact. 10: 332-338.

[102] Gréhan, G., Gouesbet, G., Naqwi, A. and F., D. (1994) Trajectory Ambiguities in Phase Doppler Systems: study of a near forward and a near backward geometry. Part. Syst. Charact. 11: 133-144.

[103] Buckner, H.N. and Sojka, P.E. (1991) Effervescent atomization of high-viscosity fluids: Part I, Newtonian liquids. Atomization and Sprays. 1: 239-252.

[104] Lund, M.T., Sojka, P.E., Lefebvre, A.H. and Gosselin, P.G. (1993) Effervescent atomization at low mass flow rates. Part 1: the influence of surface tension. Atomization and Sprays. 3: 77-89.

[105] Santangelo, P.J. and Sojka, P.E. (1995) A holographic investigation of the near nozzle structure of an effervescent atomizer produced spray. Atomization and Sprays. 5: 137-155.

[106] Copan, J., Balachandar, R. and Berruti, F. (2001) Droplet size-velocity characteristics of sprays generated by two-phase feed nozzles. Chemical Engineering Communications. 184: 105-124.

[107] Hulet, C., Briens, C., Berruti, F., Chan, E. and Ariyapadi, S. (2003) Entrainment and Stability of a Gas-Liquid Jet in a Fluidized Bed. International Journal of Chemical Reactor Engineering. 1: A60.

[108] Dukler, Dukler, A.E. and Hubbard, M.G. (1975) A Model for Gas–Liquid Slug Flow in Horizontal and near Horizontal Tubes. Industrial & Engineering Chemistry Fundamentals 14: 337–347.

[109] Chen, X.T., Cai, X.D. and Brill, J.P. (1997) A general model for transition to dispersed bubble flow. Chemical Engineering Science. 52 (23): 4373-4380.

[110] Winterton, R.H.S.a.M., J.S. (2001) Bubble size in two-phase gas-liquid bubbly flow in ducts. Chemical Engineering and Processing. 40: 437-447.

8.8. Tables

Table 8.1. Comparison of scaling from commercial to pilot and lab scale nozzle based on the gas to liquid mass ratio, Froude number, Euler number and density ratio matching.

Conditions	Commercial scale (bitumen/steam)	Pilot scale (water/air)	Lab scale (water/air)
Gas to liquid mass ratio (%)	1	1	1
Liquid Froude Number, Fr_L (-)	105	105	109
Liquid volume flow rate, Q_L (USGPM)	47	47	1.5
Liquid volume flow rate, Q_L (m^3/s)	2.95×10^{-03}	2.95×10^{-03}	9.43×10^{-05}
Liquid mass flow rate, m_L (kg/s)	2.56	2.95	0.094
Liquid density, ρ_L (kg/m^3)	868	1000	1000
Gas density, ρ_G (kg/m^3)	5.74	13.30	6.51
Gas mass flow rate, m_G (kg/s)	2.56×10^{-02}	2.95×10^{-02}	9.43×10^{-04}
Gas volume flow rate, Q_G (m^3/s)	4.47×10^{-03}	2.22×10^{-03}	1.45×10^{-04}
Void fraction, α (%)	60	43	61
Mixture density, ρ_m (kg/m^3)	348.97	576.47	398.29
Liquid superficial velocity, U_{SL} (m/s)	6.37	6.37	3.25
Gas superficial velocity, U_{SG} (m/s)	9.63	4.79	5.00
Mixture velocity, U_m (m/s)	16.00	11.17	8.25
Mixture Euler number, Eu (-)	18.49	18.49	18.49
Slip factor, S (-)	-	1.06	1.06
Mixing pressure, P_m (kPa)	1651	1408	531
Mixing pressure, P_m (psig)	225	190	62
Density ratio, ρ_r (-)	0.01	0.01	0.01

Table 8.2. Prediction of length scale of Brodkey bubbles for different fluids

Gas Phase	**Liquid Phase**	γ **(N/m)**	ρ_G **(kg/m^3)**	ρ_L **(kg/m^3)**	$d_{cr\ brodkey}$ **(µm)**
Air	Water	7.00×10^{-2}	7.20	998	1.44
Air	Canola oil	2.50×10^{-2}	7.20	905	0.57
Air	Glycerine-water mixture (82%-18%)	6.10×10^{-2}	7.20	1200	1.04
Mixed gas	Water	7.00×10^{-2}	5.74	998	1.44
Mixed gas	Canola oil	2.50×10^{-2}	5.74	905	0.57
Mixed gas	Glycerine-water mixture (82%-18%)	6.10×10^{-2}	5.74	1200	1.04
Steam	Bitumen	2.50×10^{-2}	5.74	897	0.57

Table 8.3. Prediction of dispersed bubble (DB) and intermittent (I) flow regimes.

P_m (kPa)	β (%)	$\frac{u_L^S}{u_G^S}$	X_L	Eo	$12.65\left(\frac{X_L}{Eo^{1/2}}\right)$	$\frac{U_L^S}{U_G^S} \geq 12.65\left(\frac{X_L}{Eo^{1/2}}\right)$	Flow Pattern
Mixed gas-water two-phase atomization conditions							
483	1	0.23	5.60	0.20	1.08	$\frac{U_L^S}{U_G^S} < 12.65\left(\frac{X_L}{Eo^{1/2}}\right)$	I
483	2	0.16	5.60	0.22	1.15	$\frac{U_L^S}{U_G^S} < 12.65\left(\frac{X_L}{Eo^{1/2}}\right)$	I
483	3	0.09	5.60	0.54	2.86	$\frac{U_L^S}{U_G^S} < 12.65\left(\frac{X_L}{Eo^{1/2}}\right)$	I
483	6	0.04	5.60	0.98	5.24	$\frac{U_L^S}{U_G^S} < 12.65\left(\frac{X_L}{Eo^{1/2}}\right)$	I
Air-water two-phase atomization conditions							
483	1	0.63	5.60	0.15	0.58	$\frac{U_L^S}{U_G^S} < 12.65\left(\frac{X_L}{Eo^{1/2}}\right)$	DB
483	2	0.43	5.60	0.12	0.65	$\frac{U_L^S}{U_G^S} < 12.65\left(\frac{X_L}{Eo^{1/2}}\right)$	I
483	3	0.29	5.60	0.18	0.94	$\frac{U_L^S}{U_G^S} < 12.65\left(\frac{X_L}{Eo^{1/2}}\right)$	I
483	4	0.22	5.60	0.22	1.15	$\frac{U_L^S}{U_G^S} < 12.65\left(\frac{X_L}{Eo^{1/2}}\right)$	I
483	7	0.12	5.60	0.47	2.53	$\frac{U_L^S}{U_G^S} < 12.65\left(\frac{X_L}{Eo^{1/2}}\right)$	I

Table 8.4. Prediction of different flow regimes in the air-water two-phase flows.

β (%)	1	2	4
Taitel and Dukler flow maps [67, 77]	slug flow	slug & annular flow transition	slug & annular flow transition
Breber Map [74]	bubbly flow	bubbly and slug flow transition	slug flow & annular flow transition
Baker Map [74]	bubbly & slug flow transition	slug & annular flow transition	slug & annular flow transition
Experimental results at 483 kPa	bubbly and slug flow transition	slug & annular flow transition	slug & annular flow transition

Table 8.5. The average bubble size and eccentricity in the SBSC and HSVS techniques.

B %	***d*** $_{b,\ mean}$ **(SBSC) µm**	***e*** **(SBSC)**	$d_{b,\ mean}$ **(HSVS) µm**	***e*** **(HSVS)**
1	395	0.68	418	0.50
2	342	0.65	335	0.65
4	307	0.65	290	0.65

Table 8.6. Bubble size obtained in the literature and experiments. A part of the table was adopted from the literature [110].

Author(s)	D_C **(mm)**	d_{mean} **(mm)**	d_{b32} **(mm)**	***L/D***	***α***	U_{LS} **(m/s)**	**Data**
Holmes [59]	25.4	0.88 – 1.53		157	0.13 – 1.65	3 – 6	4
Holmes [59]	50.8	2.38, 2.67		79	0.69, 0.49		2
Hesketh [6]	25.4	0.94 – 1.67		157	0.13 – 1.65	3 – 6	4
Hesketh [6]	50.8		2.88, 3.13	79	0.69, 0.49		2
Kocamustafaogullari [20]	50.3		2.35 – 4.37		3.73 – 21.5	3.74 – 6.59	21
Razzaque [8]	25.4		1.53	12	0.003	2.9	1761
Razzaque [8]	25.4		1.66	1004	0.003	2.9	1356
Razzaque [8]	25.4		2.94	12	0.003	2.1	811
Razzaque [8]	25.4		2.90	1004	0.003	2.1	752
Experiment	6.35	0.46		57.50	0.50 – 0.90	1.5 – 4.00	26772

8.9. Figures

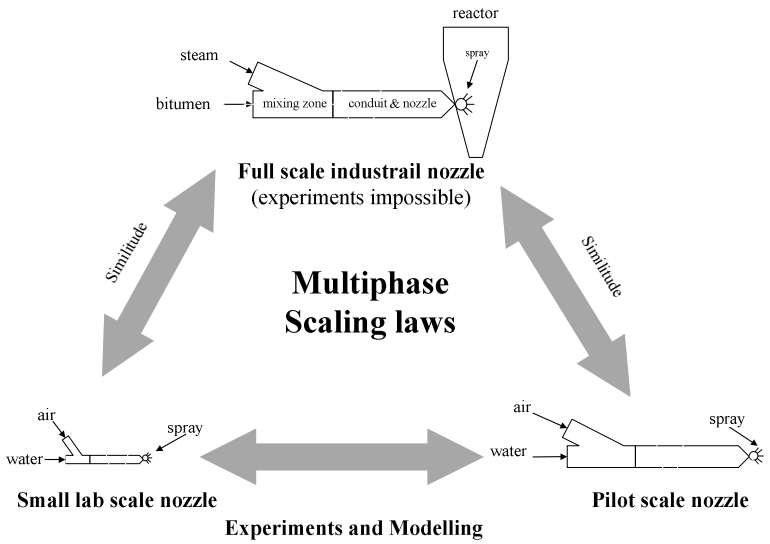

Fig. 8.1. Application of multiphase atomization scaling law on small scale air-water systems to predict the steam-bitumen system used in full scale industrial scale nozzles or air-water systems used in full scale pilot operation (not to scale).

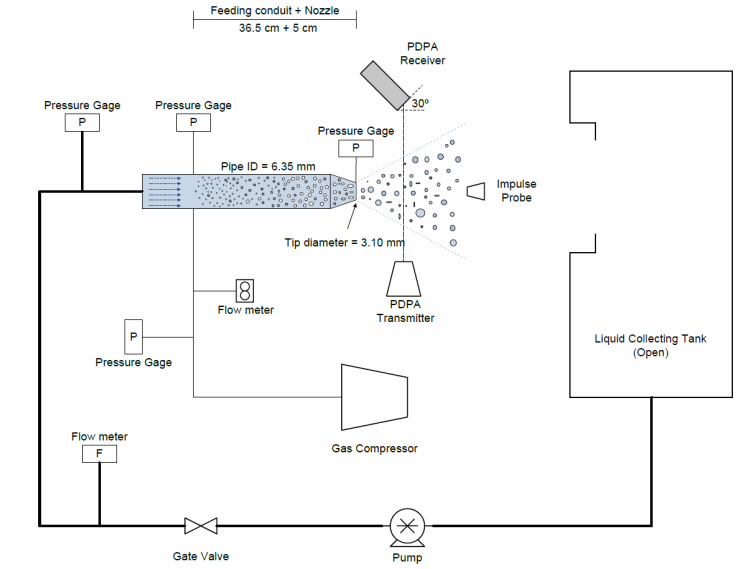

Fig. 8.2. Schematic of the experimental set-up (not to scale). The length (L) and internal diameter of the feeding conduit (D_c) is 36.8 cm and 6.35 mm. Tip of the nozzle is 3.10 mm (D_n).

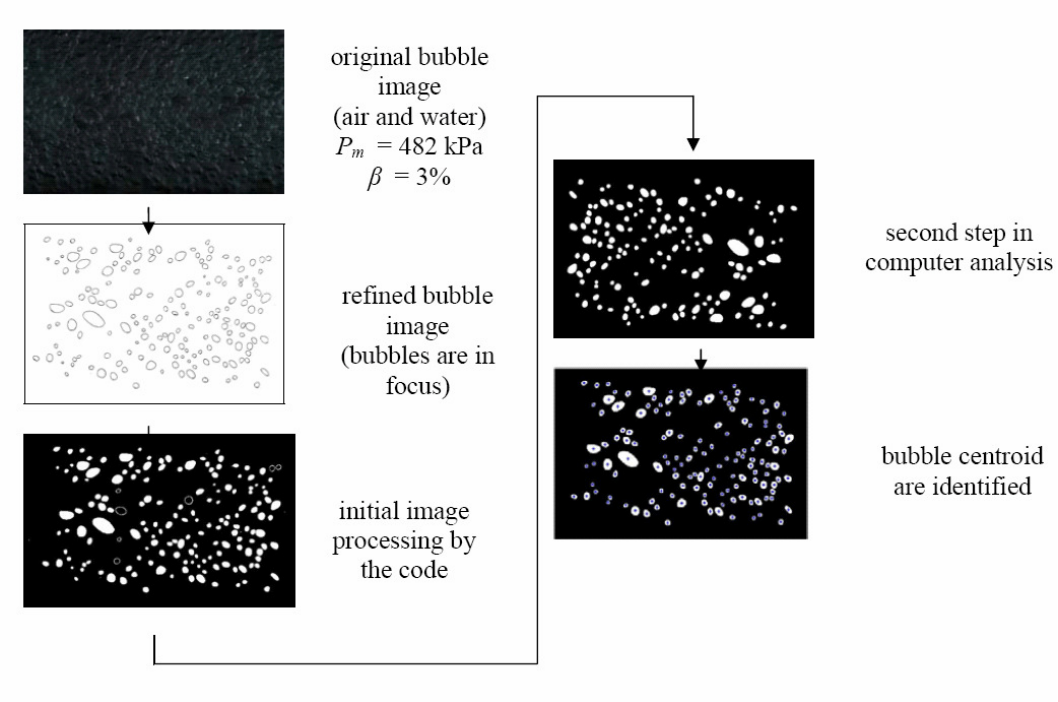

Fig. 8.3. Stroboscopic back scattered image (SBSI) filtering process (not to scale).

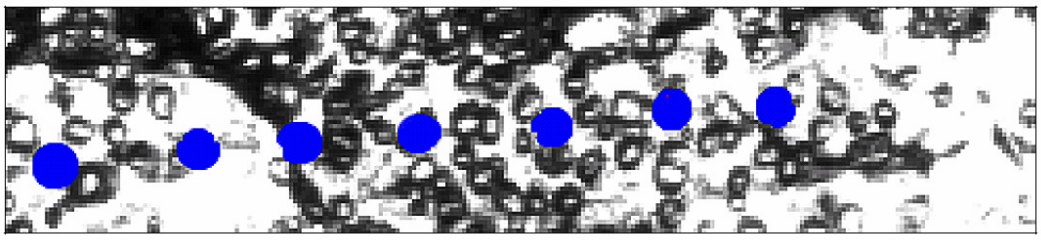

Fig. 8.4. Local characteristics bubble velocity measurement from the high-speed video shadowgraph.

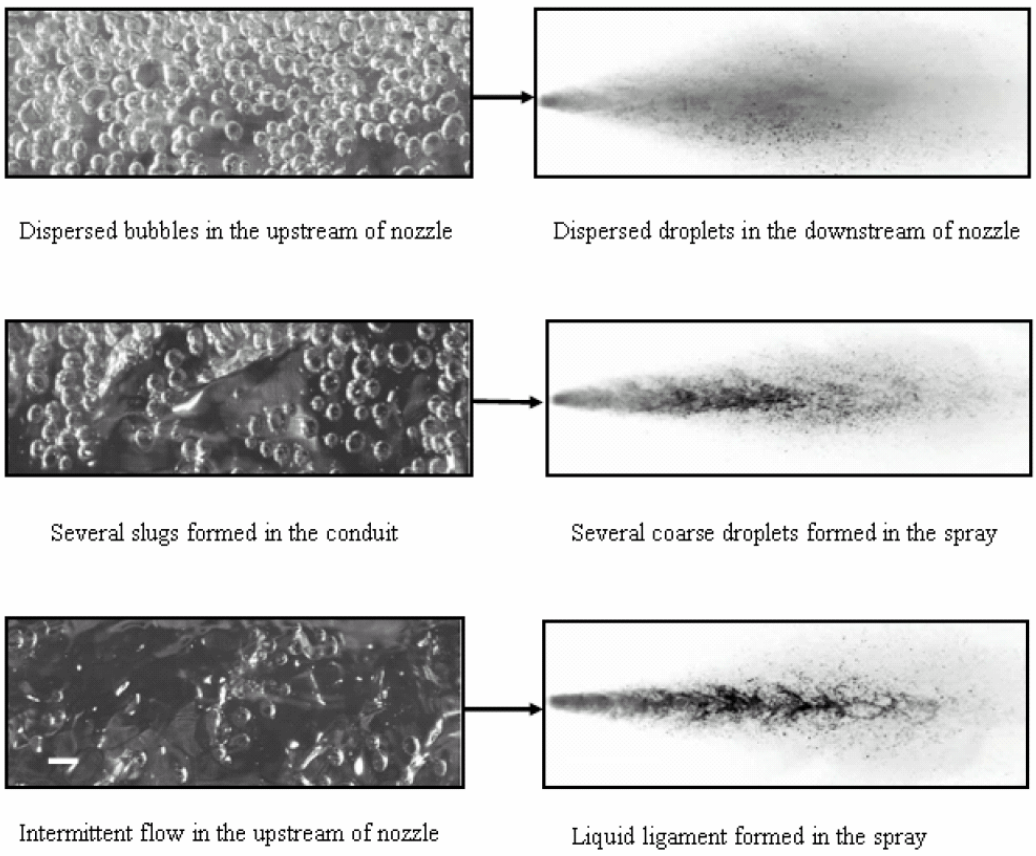

Fig. 8.5. Illustration of the well-atomized and poorly-atomized spray as consequences of the upstream bubble size distribution and flow patterns observed in the quarter scale nozzle and obtained by the high speed video shadowgraphy.

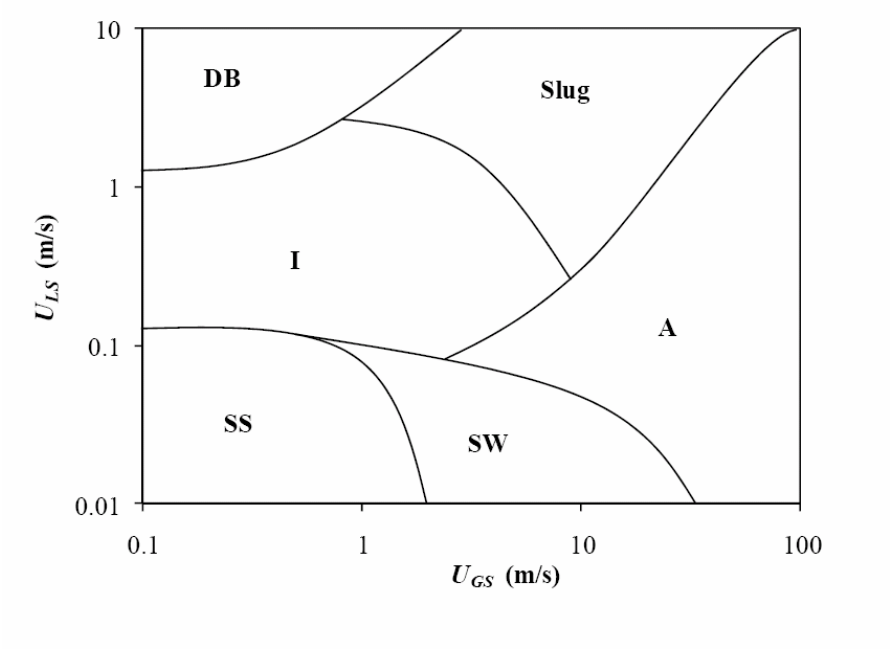

Fig. 8.6. A typical flow pattern map for specific fluid properties, geometry, local pressure and local temperature condition (adapted from [77]).

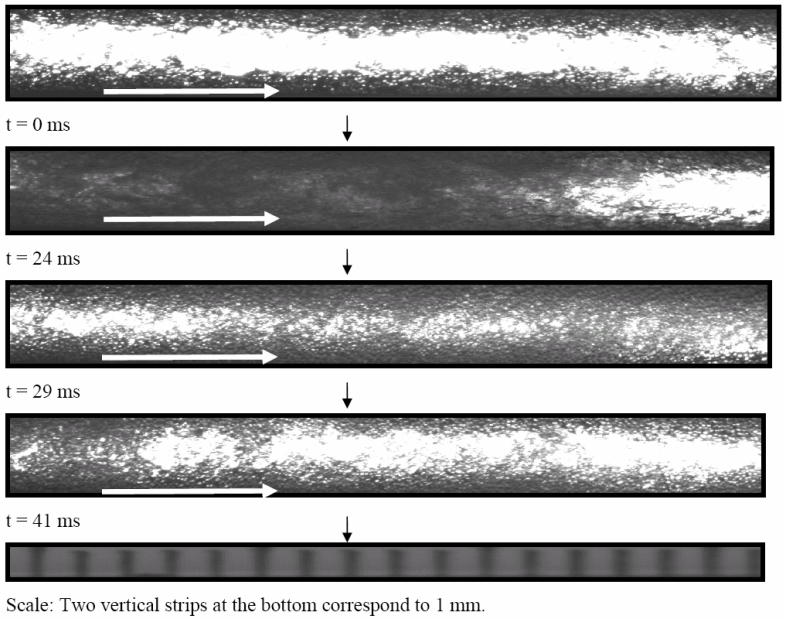

Fig. 8.7. Description of flow regimes and patterns in the mixed gas and water case at 483 kPa mixing pressure and 2% gas to liquid mass ratio. White arrow indicates the flow direction.

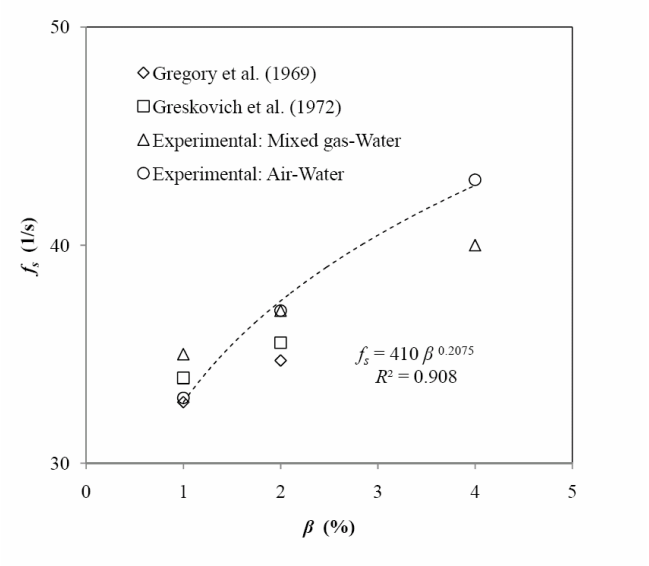

Fig. 8.8. The frequency of slug formation with changing air to liquid mass ratios.

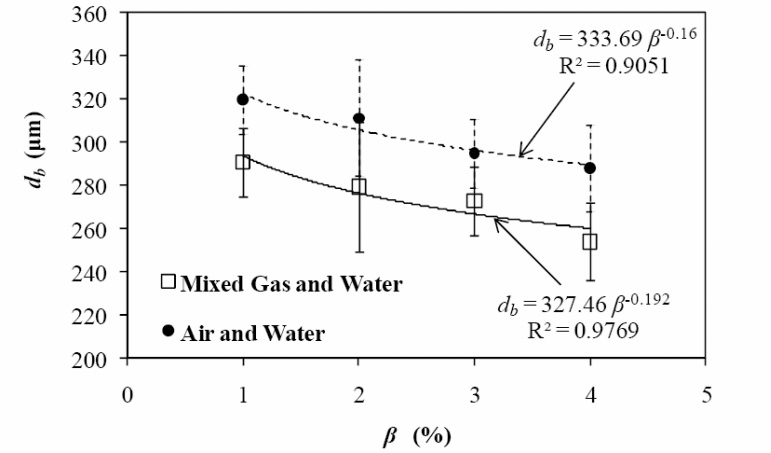

Fig. 8.9. The mean bubble diameter profile with changing air to liquid mass ratio (β). The solid line indicates the best-fit line when mixed gas (81.4 % helium and 18.6 % nitrogen on a volume basis) is used as the gas phase and water as the liquid phase. The dotted line indicates the best-fit line when air is used as the gas phase and water as the liquid phase. A total of 21,930 bubbles were counted to obtain the mean bubble diameter. In all the cases the pressure was maintained at 483 kPa.

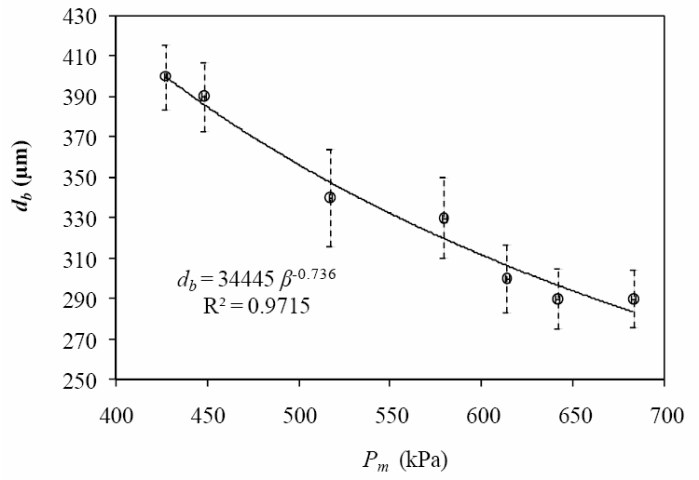

Fig. 8.10. The mean bubble diameter (db) profile with changing mixing pressure (Pm). The mixing pressures were varied from 428 to 683 kPa. In this case air was used as the gas phase and water as the liquid phase. Air to liquid mass ratio (β) was varied from 1 to 4%.

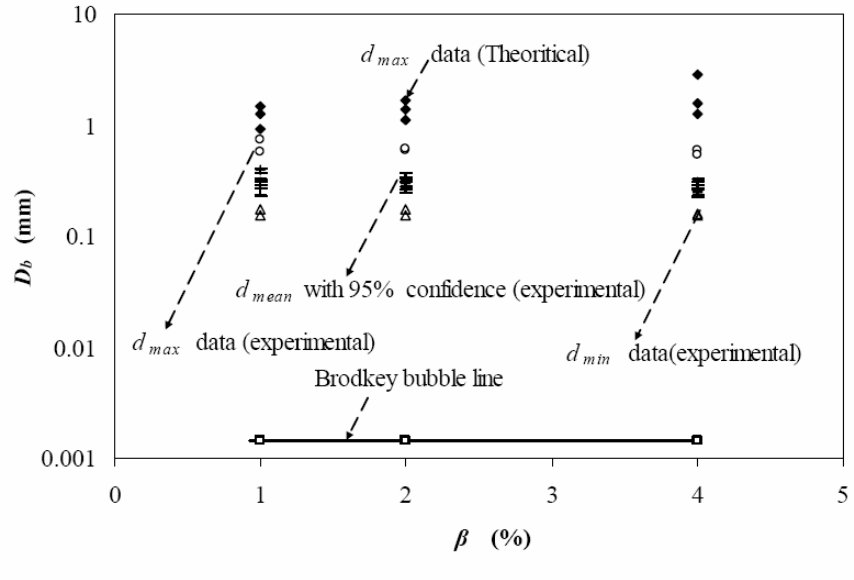

Fig. 8.11. Experimental and theoretical bubble size distributions counting 26,772 bubbles in both the air-water and mixed gas-water two-phase flow experiments.

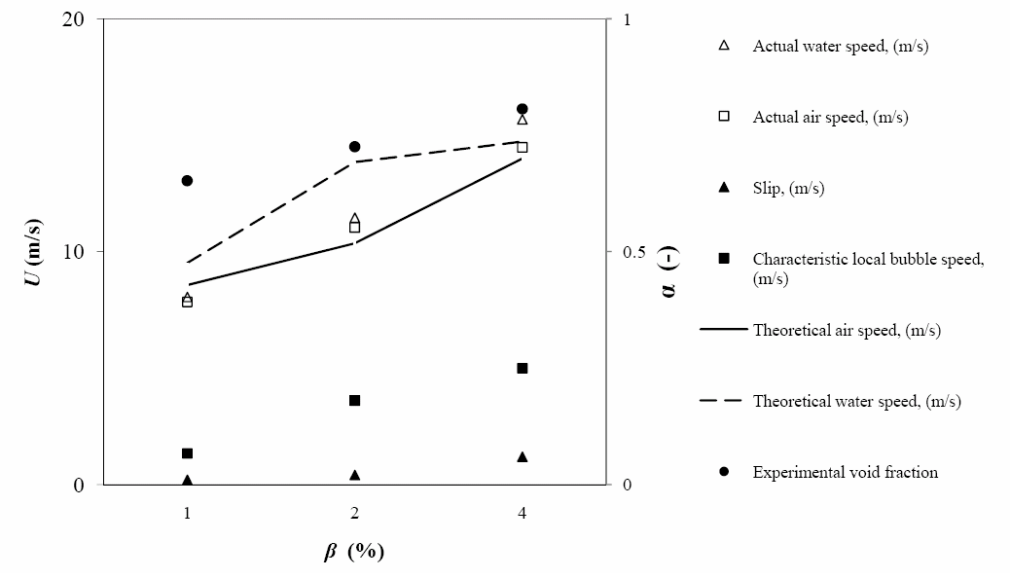

Fig. 8.12. Local characteristic bubble velocity estimation from the high-speed video shadowgraph (HSVC) air-water atomization condition.

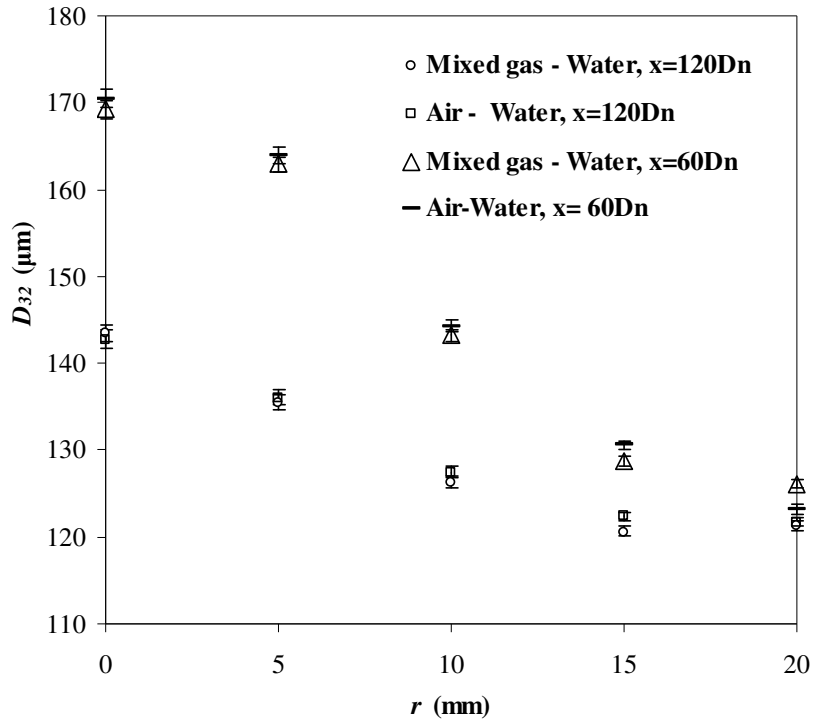

Fig. 8.13. Droplet size for changing gas phases at P_m of 428 kPa and 2% air to liquid mass ratio (β).

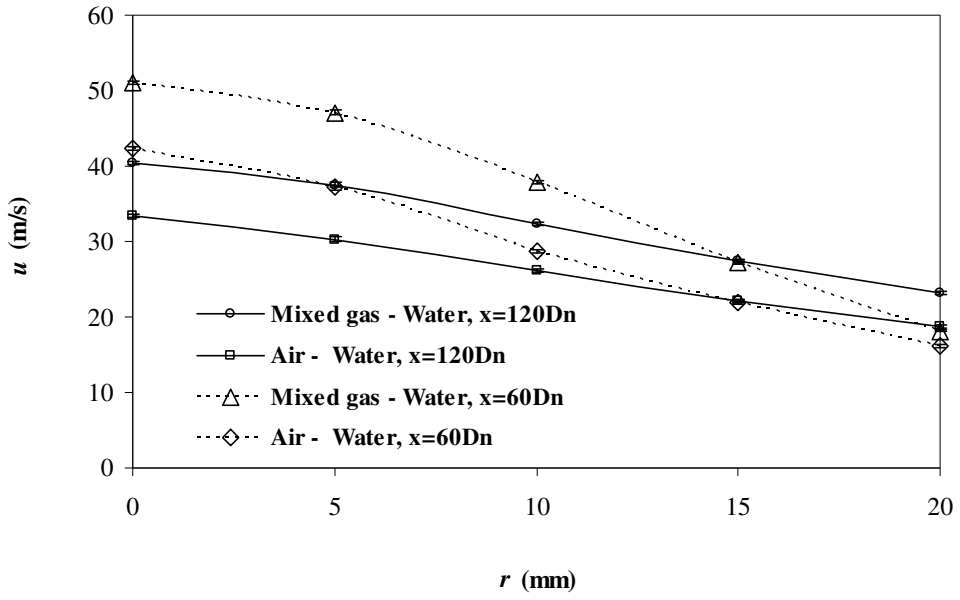

Fig. 8.14. Droplet velocity for changing gas phases at P_m of 428 kPa and 2% air to liquid mass ratio (β).

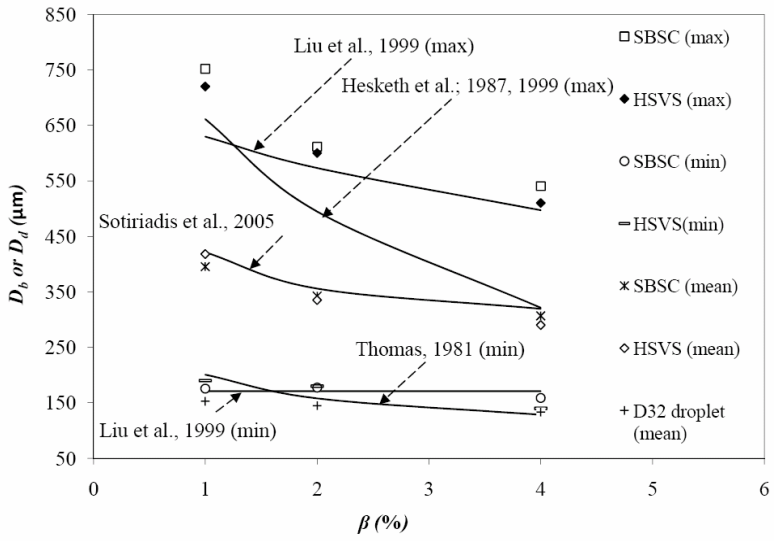

Fig. 8.15. Estimation of the mean (d_{mean}), minimum (d_{min}) and maximum (d_{max}) diameter of bubbles in the conduit from the high-speed image analysis from the air-water experiments. The mean diameter of the droplets (D_{32}) in the spray was also calculated from the PDPA measurements. SBSI indicates Stroboscopic Back Scattered Imagery, HSVS indicates High Speed Video Shadowgraphy, PDPA indicates Phase Doppler Particle Anemometer.

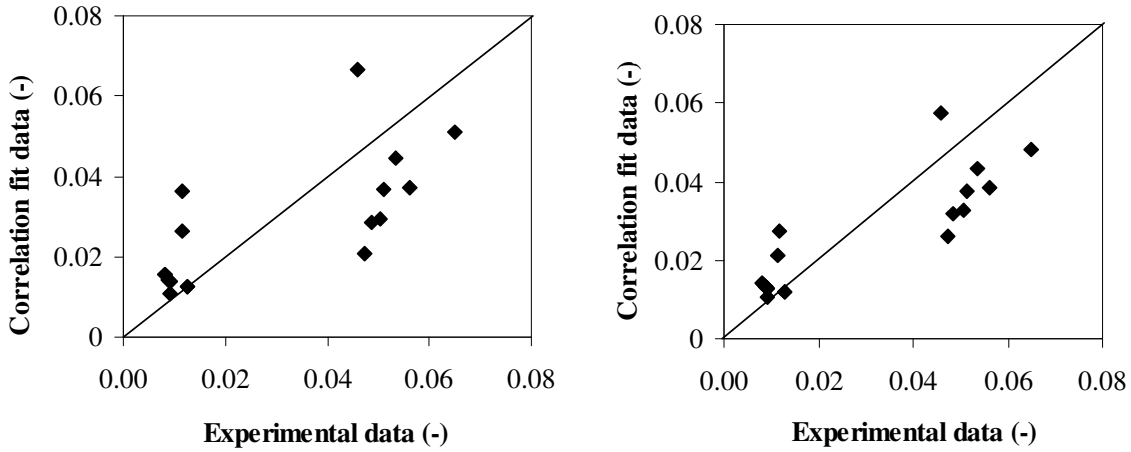

(a) (b)

Fig. 8.16 (a) A relationship between the correlation fit bubble diameter data and experimental bubble diameter data based on Equation (33), (b) A relationship between the correlation fit bubble diameter data and experimental bubble diameter data based on Equation (34).

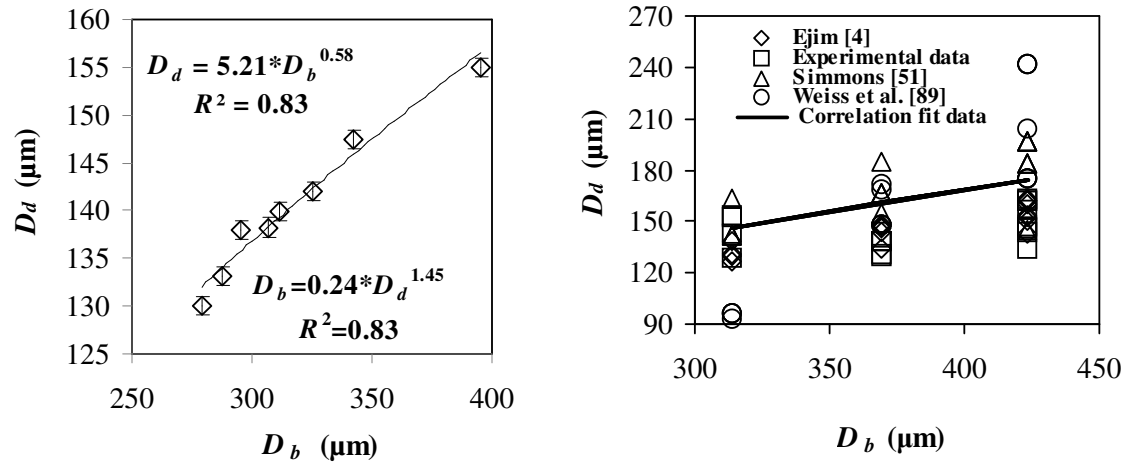

(a) (b)

Fig. 8.17 (a) A correlation between the droplet and bubble diameter based on the numbered average of statistically significant bubble and droplet size data, (b)

validation of the proposed correlation with the available correlations in the literature.

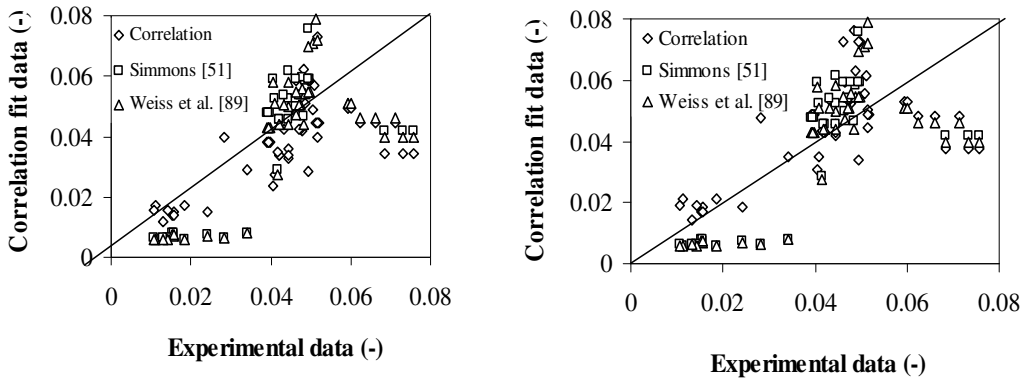

Fig. 8.18 (a) A relationship between the correlation fit droplet diameter data and experimental droplet diameter data based on Equation (35), (b) A relationship between the correlation fit droplet diameter data and experimental droplet diameter data based on Equation (36).

CHAPTER 9

Summary of Thesis - General Discussion and Conclusions

9.1. Significance

Canadian fossil fuel reserves are of critical economic and strategic importance to Canada's future. Because the oil sands operate with high capital and energy overheads, small increases in the efficiency are of great value in direct cost savings. Improving the efficiency of the refining process is aligned with federal strategic priorities; not only it is profitable, but it will reduce the overall ecological impact of using these hydrocarbon reserves. The country will undoubtedly move to using fewer fossil fuels in the future; however in the short to medium term as oil prices rise, global reserves will diminish and the conversion to non-fossil fuels will be limited by other factors. The oil sands will surely remain, even when most other global hydrocarbon reserves are depleted. It is likely that such a valuable resource will not be used as a fuel, but as a chemical building block when other sources are gone. When this day comes, Canada must be capable of low-energy intensive extraction and use of this soon-to-be rare resource. Current, poorly designed nozzles used in the low-energy intensive extraction or upgrading of oil sands cannot meet the targeted demand for the economic or environmental benefit for Canada. Understanding the performance of two phase nozzles will aid in the optimization of the two phase nozzle flow conditions and will serve as a major tool in nozzle design and development for future generation nozzles for many industrial applications.

9.2. Objectives

The objective of this project was to develop a novel understanding of the mechanics of two phase gas-liquid flows and sprays injected through industrial

effervescent nozzles. This was done using detailed experimental investigations and scaling for two-phase flows and sprays. This study helps to quantify near-field liquid and gas phase statistics that are challenging and impossible to measure in the reactors [19].

9.3. Background

The development of nozzles is generally performed on air-water systems. My plan was to begin with the study of small-scale sprays (air and water) to compare to full scale industrial conditions at pilot operation (air-water) or commercial operation (steam-bitumen), to determine size scaling relationships. A major challenge in understanding two-phase flow and effervescent atomization is the inability to take measurements, and therefore to judge the performance and behavior of the nozzle and its accompanying fluid delivery system. The relationship between the air-water experiments and real industrial operations has never been fully explained. Knowledge of this would make the development of future nozzles much less dependent on trial and error. This study was an attempt to establish fundamental scaling relationships for the prediction of two-phase spray behavior that can be applied directly to full scale industrial nozzles that would be of very significant value to industries and to the scientific community in general.

9.4. Research Results

Atomization from effervescent nozzles likely depends on flow patterns, void fractions, mixing pressure, air to liquid ratio and bubble size distribution in the upstream of the nozzle. Thus, it is essential to have a good understanding and a reasonable estimation of the bubble size, flow regime, void fraction, pressure drop and subsequent droplet size and mass flux distribution in turbulent the two-phase gas/liquid flows and sprays. Effective d_b, d_d, α, and flow regime prediction in the two-phase gas/liquid horizontal flows or sprays is crucial in many industrial applications. Thus, fairly reliable experimental methods and statistical tools are

required to find out the uncertainty level in the d_b, d_d, and, α estimation. The application of the PDPA is still a challenge in highly concentrated multiphase sprays. Thus, the coupled PDPA and impulse probe technique can measure reliable mass flux in the dense two-phase spray. Experimental results show that at 0.30% and 3.20% β, and 29% and 81% α_e ('*e*' stands for entrance) both at a constant pressure of 620 kPa, the horizontal velocities at the center of the spray and at $60D_n$ downstream were 41.36 m/s and 58.48 m/s, respectively. In similar conditions, the Sauter-mean-diameter (D_{32}) is 193μm and 171μm, respectively. Thus, the results indicate that at the higher β and α at the center of the spray, the penetration is higher and droplets are more dispersed with enhanced pulsation. The success of the α measurements in the two-phase gas/liquid flow largely depends on the respective flow regime, slip between the phases and measurement accuracy. Experimental results indicate that the average α over the closing length (33.23 cm) of the nozzle feeding conduit was 76% (α_H=75%) for 2% β ('*H*' stands for homogeneous). The average α measurement by the QCV apparatus agrees well with the α_H in the range of 1.5-10% β. However, the α_H under-predicts the experimental α in the rage of 0-1.5% β and over-predicts in the rage of 10-15% β. One of the reasons for this fact is that the α_H assumes the no-slip condition exists between the phases. In this study, it is also observed that if the β increases from 1% to 4%, the slug frequency in the nozzle feeding conduit increases from 0.4 kHz to 0.53 kHz. The flow regimes in this study mostly exhibit periodic bubbly and slug flow. The area averaged mean d_b calculated from the SBSI method provides a better estimation of bubble size distribution in the two-phase gas/liquid flow. This study also shows that the bubble mean diameter decreases with the β. The bubble size decreases from 398 μm for 1% β (428 kPa) to 300 μm for 2% β (517 kPa). This study also shows that the droplet mean diameter decreases with the β. The high response static-pressure transducers (SPT) inserted in several locations of the nozzle feeding conduit showed that for

1% β, the α_H is almost similar (60%) along the nozzle feeding conduit except at the tip of the nozzle, which is about 77%.

For scaling considerations in the development of future feed nozzle prototypes, the challenge is to minimize the dissimilitudes between the real, i.e. *hot*, operation of the nozzle and the laboratory, i.e. *cold* flow spray tests. In commercial or *hot* pilot plant operation of the nozzles, steam is used to atomize bitumen at 350^{o}C. In *cold* flow spray tests, air is usually used to atomize water at ambient temperatures, ~20^{o}C. To overcome this dissimilitude, I attempted to match the liquid viscosity, surface tension and gas density in the *cold* flow tests with those of *hot* flow tests [1019]. Experiments conducted in a nozzle sized to one quarter of the commercial scale using the Dantec 2-D fibre mode Phase-Doppler-Particle-Anemometer, PDPA [2023], impulse sensor [24], pressure sensor [25] and high speed visualization [26] show no appreciable variation of droplet Sauter Mean Diameter (D_{32}) for the two ranges of surface tension, liquid viscosity, liquid density, gas density, nozzle throat diameter and nozzle length [10, 11, 13, 26]. However, operating conditions (air-to-liquid ratio, mixing pressure) and upstream flow affect the D_{32} values significantly [10, 11, 13, 26, 27]. To measure the D_{32} within the spray, the PDPA is widely used [2022]. However, the Phase Doppler Particle Anemometer (PDPA) cannot provide accurate mass flux measurements in a highly turbulent multiphase spray due to the presence of non-spherical and multiple droplets in the probe volume [23]. A combined measurement of momentum data from the impulse probe and velocity data from the PDPA provides a reasonable estimate of mass flux data in the two phase spray envelope [24]. In this study, three correlations were proposed to compare the droplet size (in the spray) with the bubble size (in the upstream two-phase flow), to estimate the droplet size in the effervescent atomization and to estimate the bubble size in the upstream two-phase flow of the nozzle. To obtain the desired flow conditions in the one quarter scale nozzle in the laboratory, the similitude technique adopted in the literature [2831] was followed.

9.5. Recommendations

1) The proposed correlations for the effervescent atomization need to be tested for other scale operations to check for wider applicability.

2) The invented novel mass flux measurement technique for the two phase dense spray also needs to be tested for a range of operating conditions to check its wider applicability.

3) Clearly the ratio of viscosities of air-water and steam-oil is sufficient to rule out viscosity scaling problems for similitude. Since the surface tension ratio between lab (water) and industrial setting (hot bitumen) is 5, a power law extrapolation would indicate 30% smaller drops in the industrial system. Certainly it is prudent in the future to investigate further a larger ratio of surface tensions to build greater confidence in this scaling law, though finding manageable fluids that offer this ratio is challenging.

4) For similar reasons, it is also critical to investigate a variety of nozzle lengths, diameters, geometries and operating conditions.

5) Disadvantages to the gas phase similitude are the expense associated with the premixed compressed gas from cylinders, as well as the logistics and technical difficulties of conducting the tests quickly to minimize gas consumption. In addition, due to the inaccessibility of the interior of the industrial reactor, it is not possible to determine the influence of all critical operating conditions in real time and space in the full scale nozzles [32]. The implementation of Computational Multi-Fluid Dynamics (CMFD) will enable me to investigate the effects of these parameters whilst reducing the amount of field and lab research, the cost of the experiments and any ambiguity in understanding the fundamentals of two-phase flow (such as highly non symmetric volume distribution in the pipe cross-section) [3339] or atomization behavior (such as droplets break-up and collision processes in a turbulent flow field) [32, 4043]. Often existing theoretical solutions do not agree with the available experimental results. Numerical solutions using the CMFD codes enable the solution of complex flow-fields like this [15, 7, 4451]. However, to date most efforts have been devoted to one-dimensional flows [6,

52]. Three-dimensional computational solutions and expressions for two-phase flows and sprays would provide a better insight into the basic phenomena associated with the multiphase atomization.

The results obtained so far lead to more general mapping of the conditions and possible geometries, promising transformative change in nozzle design and performance. A key tool for achieving that next level of performance is numerical simulation. A two-pronged approach to numerical modeling of this complex three-component phenomenon is suggested: (a) whole field modelling using Large Eddy Simulations (LES), covering the upstream, nozzle and downstream flows and (b) detailed modelling of the bubble-liquid-air interface at the single bubble level as it leaves the nozzle. The first approach will necessitate sub-grid model development, but will result in dense mapping of flow conditions and scale–up to the full-size spray system. The second approach will help to answer fundamental questions about the role of air expansion in the initial breakup stages, ones that are critical to the overall atomization process. This is particularly important since the overall atomization process is heavily truncated in industrial situations, whereby the liquid filaments meet the fluidized bed particles before they ever enter in the later stages of the filament breakup. Simulation can also be used to obtain the optimum design, geometrical configuration and operating conditions required to guarantee a stable spray and well atomized droplets. Subsequently, previous experimental results can be applied and new experiments can be conducted (if necessary) to verify the CMFD results.

9.6. Implications

To the best of my knowledge, there has been no scaling, nor any CMFD study simulating the effects of fluid properties and nozzle size on the effervescent atomization. This study is the first for two-phase nozzles that examined the spray profile using a novel experimental technique to establish a concept of a representative (or global) drop size characteristic of a spray based on area and

liquid volume flux. This is in contrast to the use of centerline drop size to characterize sprays, which is common in the literature [4143, 5355]. Since the critical experimental data is already in hand, this novel research is a breakthrough in establishing a baseline of conditions between the lab scale experiments and the commercial scale operations.

9.7. Conclusions

The overall goal of this study was to establish a fundamental means of understanding the performance of full-scale (or commercial) industrial two-phase nozzles. The proposed scaling laws and numerical program will provide an inexpensive and easily accessible alternative to studying the two-phase flow and atomization behaviors *in situ*. This will aid in optimizing the two-phase nozzle flow conditions and will serve as a major tool in nozzle design and development for future generation nozzles for many industrial applications. This study is expected to result in industrial and economic benefits for Canada.

9.8. References

[1] Burns, A., Eickenbusch, H., Guilbert, P. and Yin, D., (2001) Application of Coupled Solver Technology to CFD Modelling of Multiphase Flows with CFX, Chemie Ingenieur Technik, 73(6), pp. 638-648.

[2] Ekambara, K., Nandakumar, K. and Joshi, J.B., (2008) CFD Simulation of Bubble Column Reactor using Population Balance, Industrial & Engineering Chemistry Research, 21, pp. 8505-8516.

[3] Ekambara, K., Sanders, R.S., Nandakumar, K. and Masliyah, J.H., (2008) CFD simulation of bubbly two-phase flow in horizontal pipes, Chemical Engineering Journal, 144, pp. 277-288.

[4] Ekambara, K.R., Sean Sanders, Nandakumar, K. and Masliyah, J.H., (2009) Hydrodynamic Simulation of Horizontal Slurry Pipeline Flow Using ANSYS-CFX, Industrial & Engineering Chemistry Research, 48 (17), pp. 8159–8171.

[5] Frank, T., (2009) Recent Advances in ANSYS CFD Multiphase Flow Model Development, Validation And Application, Seventh International Conference on CFD in the Minerals and Process Industries,9-11 December, CSIRO, Melbourne, Australia.

[6] Mor, M. and Gany, A., (2004) Analysis of two-phase homogeneous bubbly flows including friction and mass addition, Journal of Fluids Engineering-Transactions of the Asme, 126(1), pp. 102-109.

[7] Poo, N. and Ashgriz, N., (1988) Numerical Simulation of Breakup of a Liquid Jet, 41st Annual Meeting of the Division of Fluid Dynamics of American Physical Society, Nov. 20-22, Buffalo, New York.

[8] Rahman, M.A., Heidrick, T. and Fleck, B.A., (2009) A Critical Review of Two-Phase Gas/Liquid Industrial Spray Systems. International Review of Mechanical Engineering, International Review of Mechanical Engineering, 3(1), pp. 110-125.

[9] Rahman, M.A., Heidrick, T. and Fleck, B.A., (2009) A Critical Review of Advanced Experimental Techniques to Measure Two-Phase Gas/Liquid Flow, The Open Fuels & Energy Science Journal, 2, pp. 54-70

[10] Ejim, C.E., Rahman, M.A., Amirfazli, A. and Fleck, B.A., (2010) Scaling Analysis of Nozzle Size on Atomization in Two-Phase, Gas-Liquid Nozzles, Multiphase Science and Technology, 22(2), pp. 133-155.

[11] Ejim, C.E., Rahman, M.A., Amirfazli, A. and Fleck, B.A., (2010) Effects of Liquid Viscosity and Surface Tension on Atomization in Two-Phase, Gas/Liquid Fluid Coker Nozzles, FUEL, 89, pp. 1972-1882.

[12] Rahman, M.A., Heidrick, T. and Fleck, B.A., (2008) Prediction the Two-Phase Flow Patterns Implementing the Froude Number Correlation, Proceedings of the FEDSM2008, ASME Fluids Engineering Conference, FEDSM2008-55331, August 10-14, Jacksonville, Florida USA.

[13] Rahman, M.A., Heidrick, T. and Fleck, B.A., (2009) Characterizing the Two-Phase, Air/Liquid Spray Profile Using a Phase-Doppler-Particle-Analyzer, IOP Journal of Physics – conference series, 147, pp. 1-15.

[14] Lund, M.T., Sojka, P.E., Lefebvre, A.H. and Gosselin, P.G., (1993) Effervescent atomization at low mass flow rates. Part 1: the influence of surface tension, Atomization and Sprays, 3, pp. 77-89.

[15] Buckner, H.N. and Sojka, P.E., (1991) Effervescent atomization of high-viscosity fluids: Part I, Newtonian liquids, Atomization and Sprays, 1, pp. 239-252.

[16] Lefebvre, A.H., (1980) Airblast atomization, Progress in Energy and Combustion Science, 6, pp. 233-261.

[17] Lefebvre, A.H., Wang, X.F. and Martin, C.A., (1988) Spray characteristics of aerated-liquid pressure atomizers, AIAA Journal of Propulsion and Power, 4(6), pp. 293-298.

[18] Lund, M.T.J., C. Q.; Sojka, P. E.; Gore, J. P and Pachangula, M. V., (1998) The Influence of Atomizing Gas Molecular Weight on Low Mass Flowrate Effervescent Atomizer Performance, Journal of Fluids Engineering, 120, pp. 750-754.

[19] Sovani, S.D.S., P.E. and Lefebvre, A. H., (2001) Effervescent atomization, Progress in Energy and Combustion Science, 27, pp. 483-521.

[20] Damaschke, N., Gouesbet, G., Gréhan, G., Mignon, H. and Tropéa, C., (1998) Response of Phase Doppler Anemometer Systems to Nonspherical Droplets, Applied Optics, 37(10), pp. 1752-1761.

[21] Gréhan, G., Gouesbet, G., Naqwi, A. and Durst, F., (1993) Particle Trajectory effects in Phase Doppler Systems, Part. Part. Syst. Charact., 10, pp. 332-338.

[22] Gréhan, G., Gouesbet, G., Naqwi, A. and F., D., (1994) Trajectory Ambiguities in Phase Doppler Systems: study of a near forward and a near backward geometry, Part. Syst. Charact., 11, pp. 133-144.

[23] Roisman, I. and Tropea, C., (2001) Flux Measurements in Sprays Using Phase Doppler Techniques, 11(6), pp. 192-226.

[24] Rahman, M.A., Heidrick, T. and Fleck, B.A., (2010) Mass Flux Measurement of Two Phase Dense Spray Using a Coupled Impulse Probe and PDPA Technique, 22nd Annual ILASS - Americas Conference on Liquid Atomization and Spray Systems, ILASS-AMERICAS, May 16-19, Cincinnati, Ohio.

[25] Rahman, M.A., Gomez, J., McMillan, J., Heidrick, T. and Fleck, B.A., (2008) Estimation of Average Void Fraction for Gas-Liquid, Two-Phase Flow in an Industrial Nozzle Assembly Using a Quick-Closing-Valve, Proceedings of the FEDSM2008, ASME Fluids Engineering Conference, FEDSM2008- 55334, August 10-14, Jacksonville, Florida, USA.

[26] Rahman, M.A., McMillan, J., Heidrick, T. and Fleck, B.A., (2008) Horizontal Two-phase Flow Regimes and Bubble Size Distribution Prediction Using High Speed Image Analysis, Proceedings of the 13th International Symposium on Flow visualization, July 1st to 4th, Nice Acropolis Center, French Riviera.

[27] Kim, J.Y. and Lee, S.Y., (2001) Dependence of Spraying Performance on the Internal Flow Pattern in Effervescent Atomizers, Atomization and Sprays, 11, pp. 735-756.

[28] Chesters, A.K., (1975) The applicability of dynamic-similarity criteria to isothermal liquid-gas two-phase flows without mass transfer, International Journal of Multiphase Flow, 2, pp. 191-212.

[29] Hurlbert, K.M., Witte, L.C., Best, F.R. and Kurwitz, C., (2004) Scaling two-phase flows to Mars and Moon gravity conditions, International Journal of Multiphase Flow, 30, pp. 351-368.

[30] Geraets, J.J.M., (1988) Centrifugal scaling of isothermal gas-liquid flow in horizontal tubes, International Journal of Multiphase Flow, 14(3), pp. 287-303.

[31] Heskestad, G., (2002) Scaling the interaction of water sprays and flames, Fire Safety Journal, 37, pp. 535-548.

[32] Copan, J., Balachandar, R. and Berruti, F., (2001) Droplet size-velocity characteristics of sprays generated by two-phase feed nozzles, Chemical Engineering Communications, 184, pp. 105-124.

[33] Coleman, J.W. and Garimella, S., (1999) Characterization of two-phase fow patterns in small diameter round and rectangular tubes International Journal of Heat and Mass Transfer, 42(15), pp. 2869-2881.

[34] Delhaye, J.M., (1981) Two-phase flow patterns: Thermohydraulics of Two-Phase Systems for Industrial Design and Nuclear Engineering. New York, NY: McGraw-Hill.

[35] Dong, F., Liu, X., Deng, X., Lijun, X. and Xu, L.-a., (2001) Identification of two-phase flow regimes in horizontal, inclined and vertical pipes, Meas. Sci. Technol., 12, pp. 1069–1075.

[36] Ewing, M.E., Weinandy, J.J. and Christensen, R.N., (1999) Observation of Two-phase Flow Patterns in a Horizontal Circular Channel, Heat Transfer Engineering, 20(1), pp. 9-13.

[37] Hesketh, R.P., Etchells, A.W., and Russell, T.W.F., (1987) Bubble size in horizontal pipelines, AIChE Journal, 33, pp. 663-667.

[38] Hesketh, R.P., Etchells, A.W., and Russell, T.W.F., (1991) Experimental observations of bubble breakage in turbulent flow, Industrial Engineering Chemical Research, 30, pp. 835-841.

[39] Razzaque, M.M., Afacan, A., L., S., K., N., Masliyah, J.H. and Sanders, R.S., (2003) Bubble size in coalescent dominant regime of turbulent air-water flow through horizontal pipes, International Journal of Multiphase Flow, 29, pp. 1451-1471.

[40] Gray, M., Tuyet, T., McCaffrey, W., Berruti, F., Soundararajam, S., Chan, E., Huq, I. and Thorne, C., (2001) Coupling of Mass Transfer and Reaction in Coking of Thin Films of Athabasca Vacuum Residue, Ind. Eng. Chem. Res., 40, pp. 3317 – 3324.

[41] Hulet, C., Briens, C., Berruti, F., Chan, E. and Ariyapadi, S., (2003) Entrainment and Stability of a Gas-Liquid Jet in a Fluidized Bed, International Journal of Chemical Reactor Engineering, 1, pp. A60.

[42] Kirpalani, D.M. and McCracken, T.W., (2002) Performance diagnostics for nozzles fed with multiphase flow, ILASS-Europe 2002, Zaragoza.

[43] Tafreshi, Z.M., Kirpalani, D., Bennett, A. and McCracken, T.W., (2002) Improving the efficiency of fluid cokers by altering two-phase feed characteristics, Powder Technology, 125 pp. 234– 241.

[44] Aluf, O., (2005) Experimental Validation of a Simple Model for Gas–Liquid Slug Flow in Horizontal Pipes, Chemical Engineering Science, 60 pp. 1371 – 1381.

[45] Claudia, C. and Peter, M., (2004) A Finite Element Method for an Averaged Multiphase Flow Model, International Journal of Computational Fluid Dynamics, 18 (2), pp. 11–123.

[46] Deen, N.G., Solberg, T. and Hjertager, H., (2001) Large eddy simulation of the Gas–Liquid flow in a square cross-sectioned bubble column Chemical Engineering Science, 56(21-22), pp. 6341-6349.

[47] Krishna, R., Urseanu, M.I., Van Baten, J.M. and Ellenberger, J., (1999) Infuence of Scale on the Hydrodynamics of Bubble Columns Operating In The Churn-Turbulent Regime: Experiments Vs. Eulerian Simulations, Chemical Engineering Science 54 pp. 4903-4911.

[48] Luca, M. and Fabio, I., (2009) Multiphase Euler–Lagrange CFD simulation applied to Wet Flue Gas Desulphurisation technology International Journal of Multiphase Flow, 35(2), pp. 185-194.

[49] Patankar, N.A. and Joseph, D.D., (2001) Modeling and numerical simulation of particulate flows by the Eulerian-Lagrangian approach, International Journal of Multiphase Flow, 27(10), pp. 1659-1684.

[50] Sirignano, W.A., (2005) Volume averaging for the analysis of turbulent spray flows, International Journal of Multiphase Flow, 31 pp. 675–705.

[51] Soo, S., (1990) Multiphase Fluid Dynamics. Beijing, P.R.C. and Gower Technical, Brookfield, MA: Science Press.

[52] Elkotb, M.M., (1982) Fuel atomization for spray modeling, Progress in Energy and Combustion Science 8(1), pp. 61-91.

[53] Knapper, B.A., (2000) Experimental studies on the hydrodynamics of fluid bed cokers, University of Saskatchewan, Masters Thesis in Chemical Engineering.

[54] Santangelo, P.J. and Sojka, P.E., (1995) A holographic investigation of the near nozzle structure of an effervescent atomizer produced spray, Atomization and Sprays, 5, pp. 137-155.

[55] Yamane, Y., Yokota, H. and Kamimoto, T., (1994) Atomization and air-entrainment characteristics of unsteady dense sprays, Japan Society of Mechanical Engineering, 37(3), pp. 604-610.

APPENDICES

APPENDIX A1 – Void Fraction Measurements by the Quick-Closing Valve Technique[1]

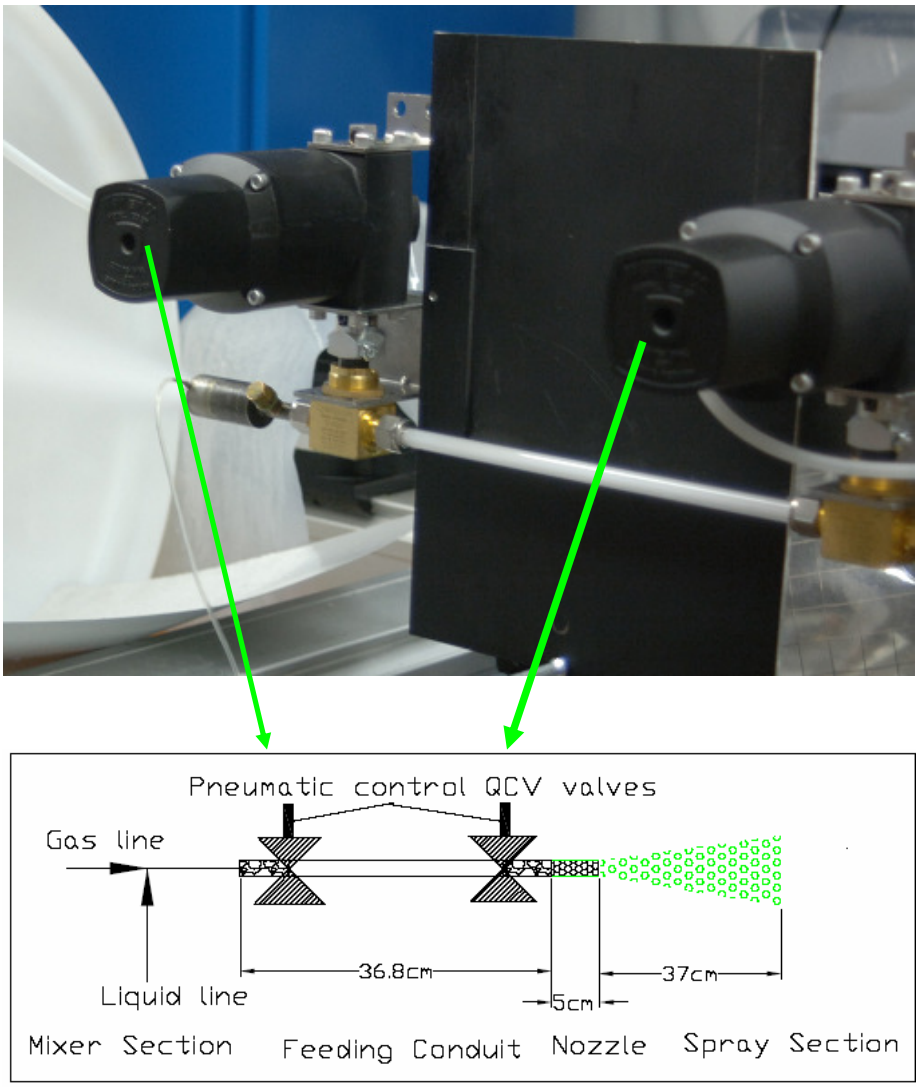

Fig. 1. Schematic of the experimental set-up. The length of the feeding conduit between the two pneumatic valves is 334.32 mm.

[1] A version of this chapter has been published. Rahman *et al.* (2008) Proceedings of the FEDSM2008, ASME Fluids Engineering Conference, FEDSM2008- 55334, Jacksonville, Florida USA, August 10-14.

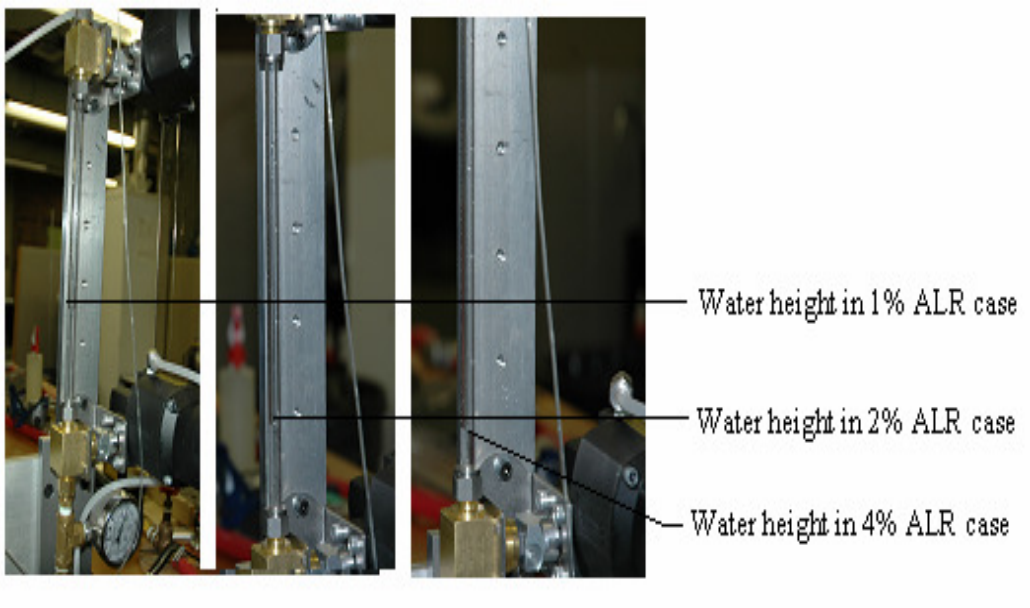

Fig. 2. Photograph of the water height in the vertical position of the conduit with changing ALRs by mass.

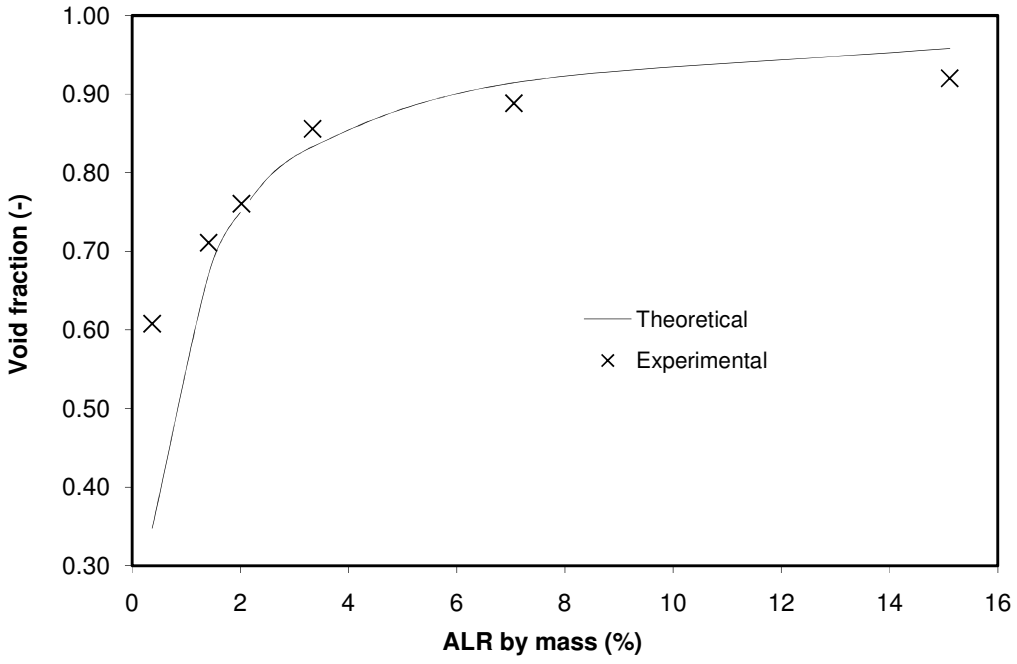

Fig. 3. Average void fraction with changing ALRs by mass at 482 kPa constant pressure.

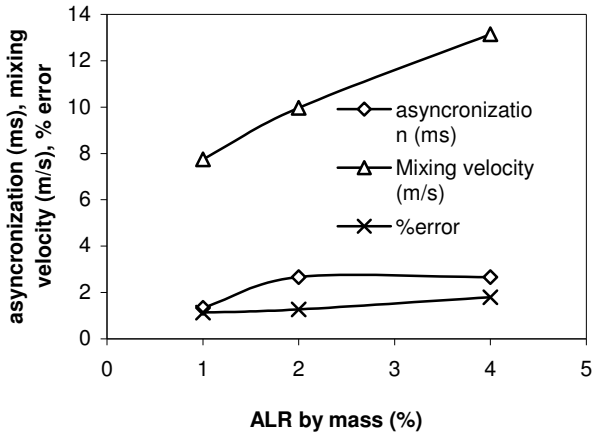

Fig. 4 Average void fraction with changing ALRs by mass at 430 kPa (1% ALR), 624 kPa (2% ALR), and 896 kPa (4% ALR) local pressure.

APPENDIX A2 –Pressure Measurements by High Speed Pressure Transducer[2]

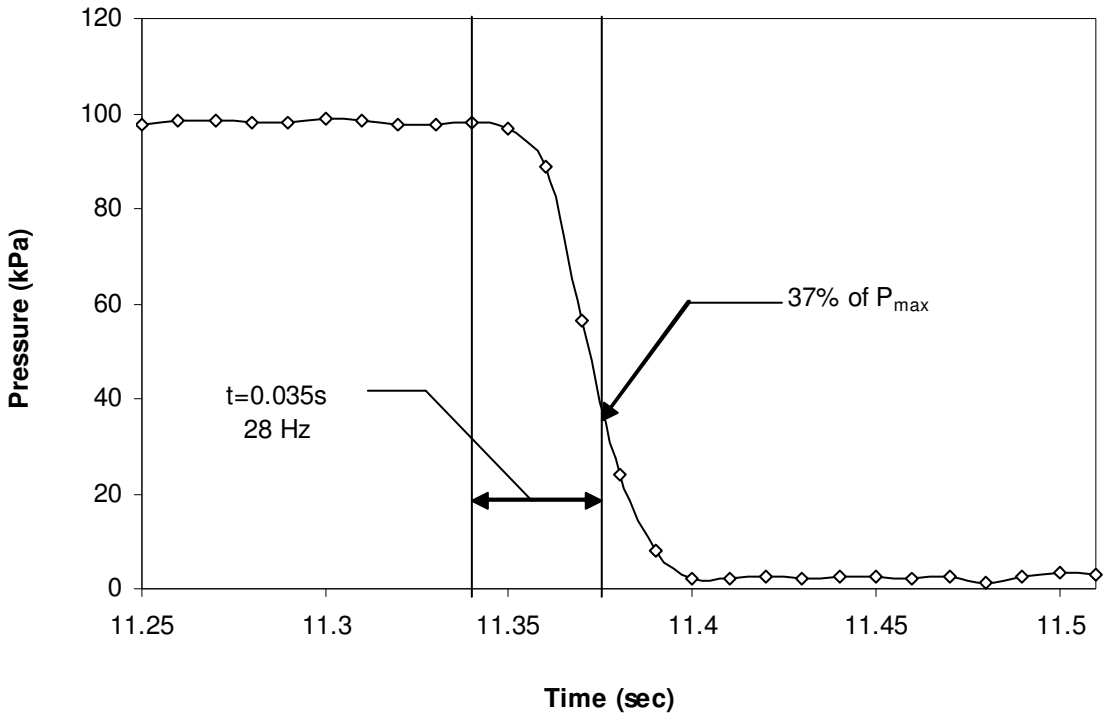

Fig. 1. At 0.10 kHz frequency.

[2] A version of this chapter has been published. Rahman *et al.* (2008) Second Annual Mechanical Engineering Graduate Research Symposium, University of Alberta, Canada, March 6.

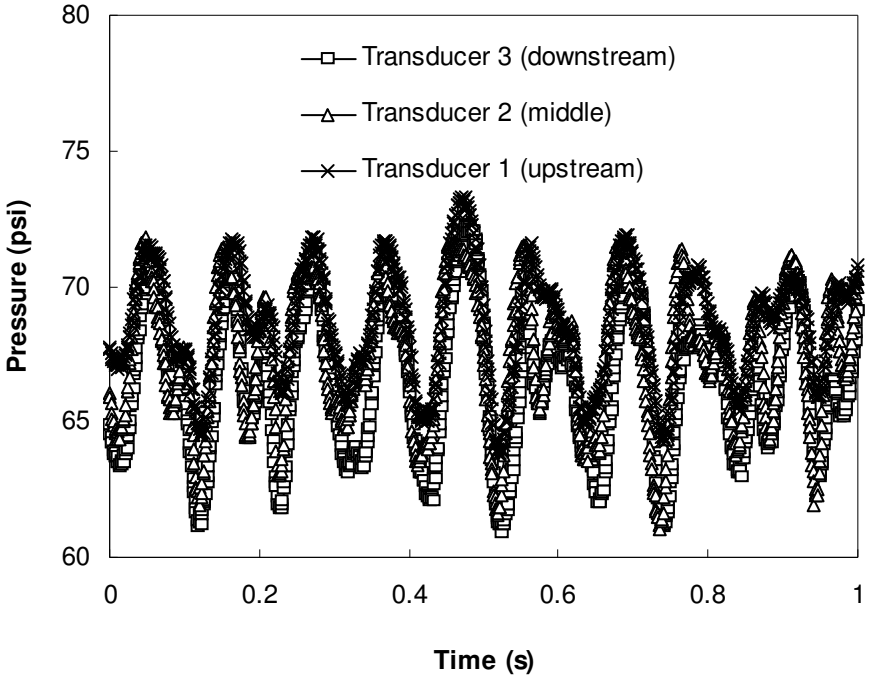

Fig. 2. 1% ALR 1 kHz frequency. Average pressure at nozzle is 29.95 psi, transducer 3 is 66.58 psi, transducer 2 is 68.22 psi, and transducer 1 is 68.85 psi. Standard deviations are 0.16, 2.75, 2.75 and 3.31 respectively. 95% uncertainties are 0.001, 0.02, 0.02 and 0.03 respectively.

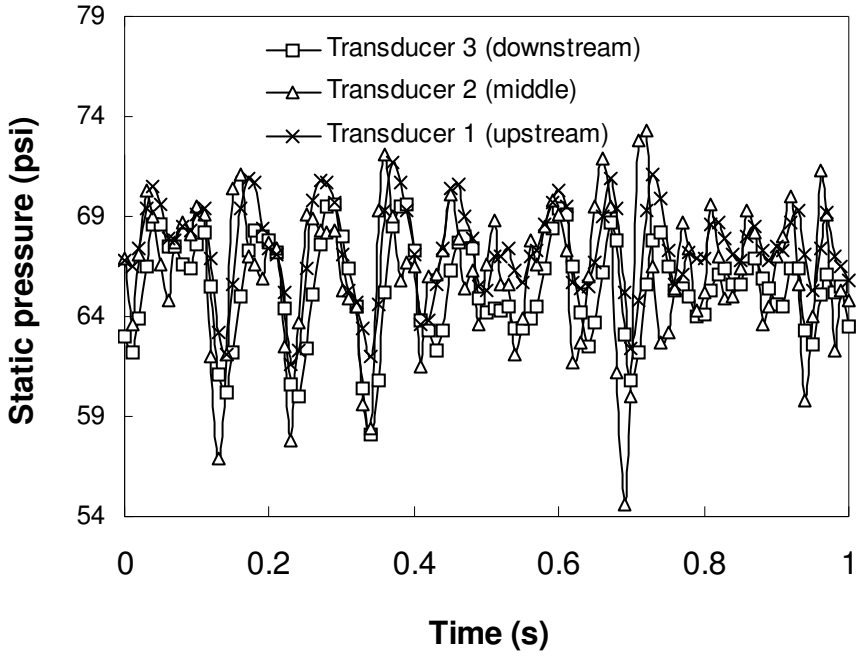

Fig. 3. 1% ALR 0.1 kHz frequency. Average pressure at nozzle is 29.25 psi, transducer 3 is 65.06 psi, transducer 2 is 65.89 psi, and transducer 1 is 67.15 psi. Standard deviations are 0.12, 2.46, 2.46 and 4.04 respectively. 95% uncertainties are 0.001, 0.06, 0.06 and 0.10 respectively.

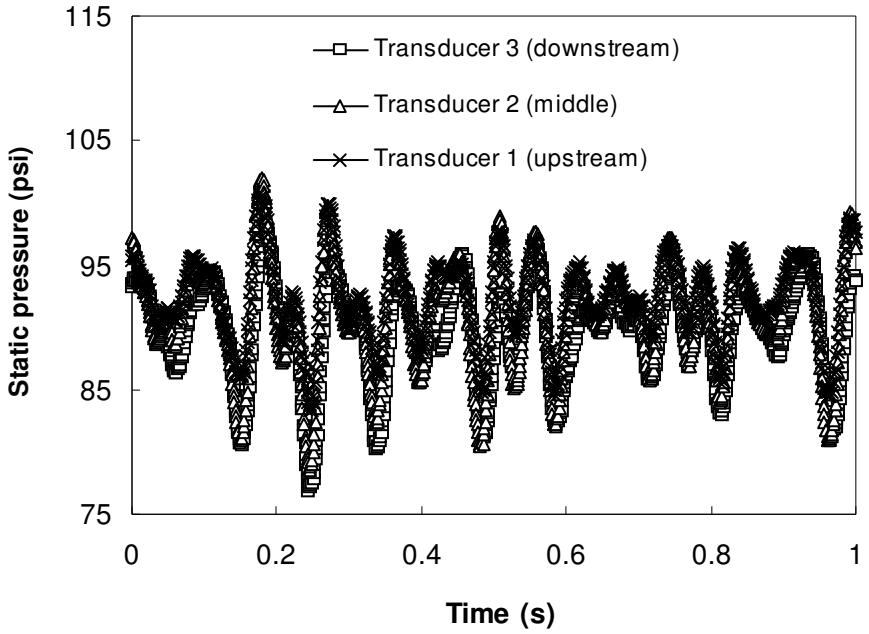

Fig. 4. 2% ALR 1 kHz frequency. Average pressure at nozzle is 46.05 psi, transducer 3 is 89.16 psi, transducer 2 is 90.41 psi, and transducer 1 is 91.79 psi. Standard deviations are 1.20, 3.81, 3.81 and 4.31 respectively. 95% uncertainties are 0.01, 0.03, 0.03 and 0.04 respectively.

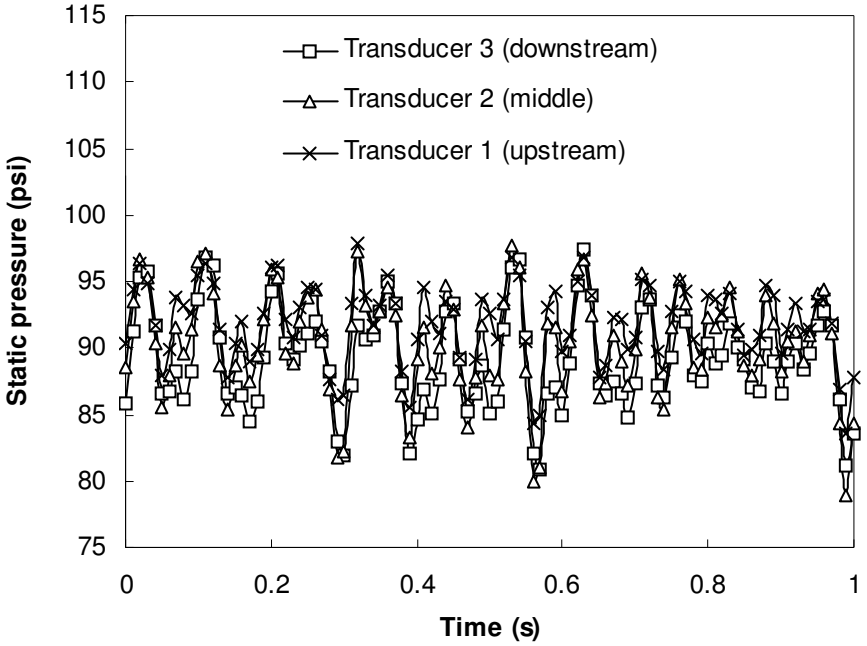

Fig. 5. 2% ALR 0.1 kHz frequency. Average pressure at nozzle: 47.43 psi, transducer 3 is 89.29 psi, transducer 2 is 90.52 psi, and transducer 1 is 91.88 psi. Standard deviations are 0.11, 3.82, 3.82 and 4.38 respectively. 95% uncertainties are 0.003, 0.1, 0.1 and 0.11 respectively.

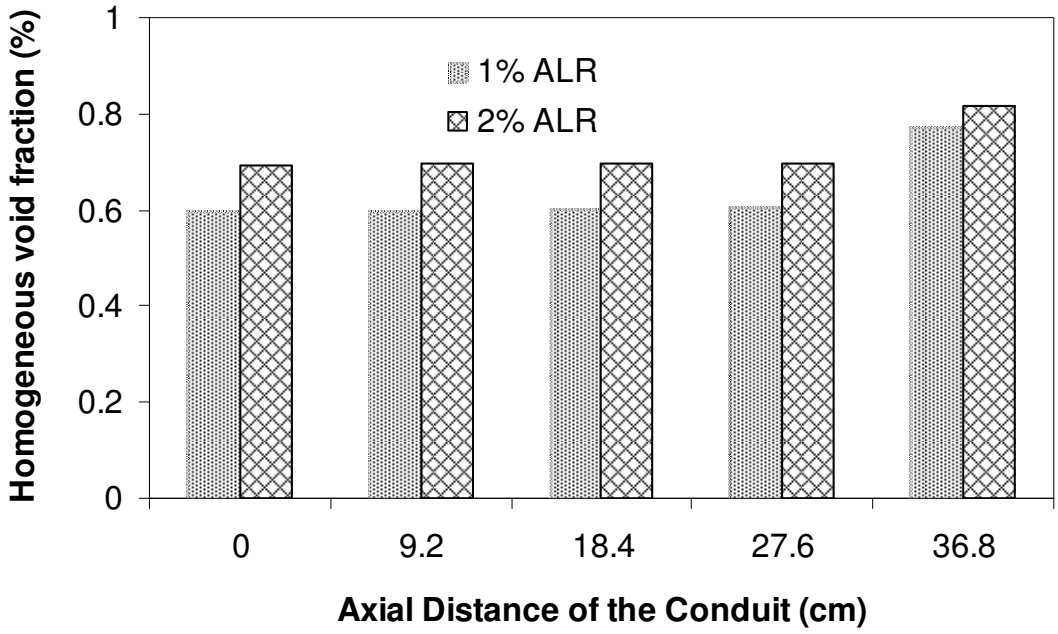

Fig. 6. Homogeneous void fraction estimation along the length of the feeding conduit of the nozzle.